Development and Implementation of a Flight Test Program for a Geometrically Scaled Joined Wing SensorCraft Remotely Piloted Vehicle

Tyler David Aarons

Thesis submitted to the Faculty of the
Virginia Polytechnic Institute and State University
in partial fulfillment of the requirements for the degree of

Master of Science
in
Aerospace Engineering

Robert A. Canfield, Chair
Craig A. Woolsey, Co-Char
Ned J. Lindsley

October 5, 2011
Blacksburg, Virginia

Keywords: Joined Wing, SensorCraft, Flight Test, Unmanned Aircraft, Unmanned Aerial Vehicle, UAV, UAS, Scaling, Remotely Piloted Vehicle, RPV

Development and Implementation of a Flight Test Program for a Geometrically Scaled Joined Wing SensorCraft Remotely Piloted Vehicle

Tyler David Aarons

Abstract

The development and implementation of a flight test program for an unmanned aircraft is a multidisciplinary challenge. This thesis presents the development and implementation of a rigorous test program for the flight test of a Geometrically Scaled Joined Wing SensorCraft Remotely Piloted Vehicle from concept through successful flight test. The design methodology utilized in the development of the test program is presented, along with the extensive formal review process required for the approval of the test plan by the Air Force Research Laboratory. The design, development and calibration of a custom instrumentation package is also presented along with the setup, procedure and results from all testing. Results are presented for a wind tunnel test for air data boom calibration, propulsion system static thrust testing, a bifilar pendulum test for experimental calculation of mass moments of inertia, a static structural loading test for structural design validation, a full taxi test and a successful first flight.

Acknowledgements

There are so many people who I would like to thank for helping me complete my thesis work.

First and foremost, I would like to thank my primary collaborator, Jenner Richards. Jenner's unwavering dedication to the project and unmatched work ethic has proven to be an invaluable asset to the effort. In several cases, Jenner's ingenuity and creativity have come up with solutions to problems that could have easily grounded the effort. From design to fabrication and modeling to simulation, Jenner's expertise and dedication were a key factor in the success of this flight test effort and will ensure the success of follow on efforts.

I would also like Jeff Garnand-Royo, my primary colleague at Virginia Tech. During the 6 months leading up the flight test, Jeff came on to the project to help with instrumentation system design as an Undergraduate Research Assistant working on strain gage system design. As his time on the project expanded, so did his influence. I am pleased to say that Jeff is taking over my role on this project, and I know he will do a fantastic job with the follow on test planning and instrumentation system design.

I would also like to thank my advisors, Dr. Bob Canfield and Dr. Craig Woolsey. I would like to thank Dr. Canfield for selecting me for this effort as well as supporting my and providing guidance every step of the way. His willingness to keep an open door afforded me the (nearly) daily ability to seek guidance and share ideas. I would like to thank Dr. Woolsey for supporting me throughout my time graduate school. From selecting me for undergraduate research, to putting my name forward for this project and finally to serving as my co-advisor on this project, Dr. Woolsey's support and guidance was an invaluable resource during my time at Virginia Tech.

I would also like to thank Dr. Afzal Suleman for his support during my time in Victoria, as well as during the trips to the test site in Foremost. Additionally, I would like to thank Dr. Chris Cotting for serving as my mentor during the early stages of my flight test planning effort. Chris provided advice and guidance based on his expansive industry experience, and he was an invaluable resource to me. I would also like to acknowledge the support and guidance of Virginia Tech/ Wright State Collaborative Center for Multidisciplinary Sciences under the direction of Dr. Rakesh Kapania.

I would also like to acknowledge AFRL funding and support. Specifically, I would like to thank the AFRL POC for this project, Dr. Ned Lindsley, for his unwavering dedication to and enthusiasm for this effort. I would also like to thank Dr. Max Blair and Pete Flick for their support and guidance based on years of work with the SensorCraft configurations. I would also like to acknowledge the suggestions and contributions made by the AFRL Technical Review

Board and Safety Review Board members, specifically Dr. Gary Hellman, during the Flight Test Plan formal review process. Their advice helped me correct many shortcomings and oversights in the flight test plan and promoted a successful testing effort.

I would also like to acknowledge the assistance of several collaborating students, both at Virginia Tech and at the University of Victoria. I would like to thank Virginia Tech students Eddie Hale and Grant Parrish for their help with the design, fabrication and testing of the Air Data Boom as well as Charles Eger for his support of the flight test effort and dedication to the project going forward. I would also like thank the University of Victoria students who worked at Quaternion Engineering during this effort. Specifically, I would like to thank Ryan Flagg, Willem Brussow, Peter Lu and Shayan for their help with the fabrication of the RPV, flight testing of the reduced complexity models and overall support of the effort.

I would also like to acknowledge the support of our two pilots, Jon Harwood and Kelly Williams. Jon served as the primary test pilot for all Mini SensorCraft flights as well as the backup pilot for the GSRPV flight test in addition to providing guidance during composite fabrication. His ideas and insight were an invaluable resource to the project. Kelly served as the primary pilot for the GSRPV flight test as well as provided guidance during all JetCat P200-SX turbine operation. He has been operating r/c scale turbine engines and flying turbine powered aircraft for many years, and his experience and expertise greatly helped the effort.

I would also like to acknowledge the Victoria Flying Club staff for their help and support of the bifilar pendulum test. General manager Gerry Mants was helpful and supportive every step of the way, allowing us to spend four days on site testing.

I would like to graciously acknowledge the support of my parents, grandparents, family and friends throughout my time at Virginia Tech and specifically while working on this project. To my friends, I wouldn't have been able to do this without you! You kept me level headed during the busy times, provided support and guidance when I was discouraged and shared in the celebrations in success. It has been a great ride! To my grandparents, your unconditional support and encouragement in all my endeavors is greatly appreciated. Thank you so much! To Pap, you are an inspiration and a role model. Your support from day one has proven to be invaluable in every endeavor in my life. Thank you so much.

To my parents, I can't thank you enough. You put up with me when I started taking apart appliances during elementary school "to see how they worked," you encouraged me as I formed an interest in aircraft design and turned the basement into a workshop, you supported me when chose to go to Virginia Tech to study Aerospace Engineering and you stood by me when I decided to stay another two years to get my Master's degree. You have been there to support me every step of the way, and I couldn't have done it without you!

Photograph Acknowledgements

All photographs presented in the body of this thesis were taken by the author, with the exception of the figures mentioned below.

Figure 26 - Custom Mount for Air Data Boom Testing (modified from Ref. 23)

Photographer: Grant Parrish

Figure 39 - Installed Static Thrust Test Rig

Photographer: Jenner Richards

Figure 48 - Bifilar Pendulum Orientation Required to Calculate Pitch Inertia

Figure 49 - Lift Into Pitch Orientation Showing Wing Scrape Cage and Lifting Ropes

Figure 57 - GSRPV on the Runway at the Foremost Airfield

Figure 58 - GSRPV High Speed Taxi Test

Figure 60 - GSRPV in Flight

Figure 61 - View from Tail Camera During First Flight

Figure 62 - GSRPV on Final Approach

Photographer: Unknown – These photographs were taken by unknown members of the flight test team during testing.

Attribution

Jenner Richards is the primary collaborator with the author. Jenner is a PhD candidate at the University of Victoria in Victoria, British Columbia as well as co-founder of Quaternion Aerospace. Jenner Richards also co-authored the Flight Test Plan presented in Appendix A.

Contents

Appendix A Contents

List of Figures

Appendix A List of Figures

List of Tables

Appendix A List of Tables

1 Introduction

The flight test of a modern aircraft requires a synthesis of disciplines. Aircraft structures, performance, stability and control, propulsion, aerodynamics and more are required to come together to determine if a particular aircraft can complete its intended mission.[1] The possible areas of investigation are extremely broad, ranging from proof of concept flights of completely new aircraft to routine maintenance and inspection of a design that has been in service for years. In all cases, the organization of a flight test effort, including the development and oversight of the flight test plan, is the responsibility of the Flight Test Engineer (FTE).

1.1 The Responsibilities of a Flight Test Engineer

According to the U.S. Naval Test Pilot School Flight Test Manuals for Fixed Wing Performance and Stability and Control, effective test program planning requires a sound theoretical background for the tests being performed.[2,3] This background will help establish the scope of tests, appropriate test techniques, data reduction methods and result presentation methods. The primary responsibilities of a FTE are as follows.

1.) Organizing and Implementing the Flight Test Program

A FTE is in the best position to coordinate and oversee all aspects of the program because he or she does not fly the aircraft, nor is he or she responsible for its fabrication. This allows the FTE to design and prepare the test plan, test cards and briefings objectively and maintain a high level perspective of the overall flight test effort.

2.) Establishing Instrumentation Requirements

A FTE determines the required test instrumentation based on the desired measurements and results. The FTE also oversees the design and implementation of the instrumentation system where appropriate.

3.) Data acquisition, reduction and presentation

A FTE coordinates experimental data acquisition during testing and oversees the post-processing required to extract the desired results from the raw data. This can also include the interpretation of the data and the application of theoretical principles to understand the results.

4.) Technical Report Writing

The FTE coordinates the documentation of the testing effort.

1.2 Flight Testing of the Joined Wing SensorCraft

This thesis presents the development and implementation of a flight test program for a next-generation unmanned aircraft, the Joined Wing SensorCraft. The Joined Wing SensorCraft is an aircraft with four lifting surfaces in a diamond configuration envisioned to incorporate conformal radar antennas in each wing. Due to the complex geometry and novel configuration, flight testing was determined to be the next step in understanding the unique aeroelastic characteristics of this configuration. This document will open with background information about the SensorCraft mission, the Joined Wing SensorCraft configuration and most importantly the source of the aeroelastic response being investigated. A description of the overall Flight Test Program in which this flight test was implemented will follow, as well as the motivation for the effort in the context of other computational and flight test efforts aimed at understanding the aeroelastic response of this configuration. Finally, the implementation of the aforementioned responsibilities of a flight test engineer will be outlined and explained, elaborating on the processes followed and lessons learned along the way.

2 Background Information

2.1 What is the SensorCraft?

The SensorCraft is a concept initiated by the Air Force Research Laboratory (AFRL) to serve as a next-generation, high-altitude, long-endurance (HALE) reconnaissance system. By incorporating the sensing capabilities of several current generation aircraft into a single, advanced unmanned aerial vehicle (UAV), the SensorCraft will provide intelligence, surveillance and reconnaissance (ISR) capabilities to contribute to persistent battle space awareness.[4] The SensorCraft mission calls for a rated endurance of 30 hours at a maximum range of 2000 nautical miles.[4] A nominal mission profile is shown in Figure 1.

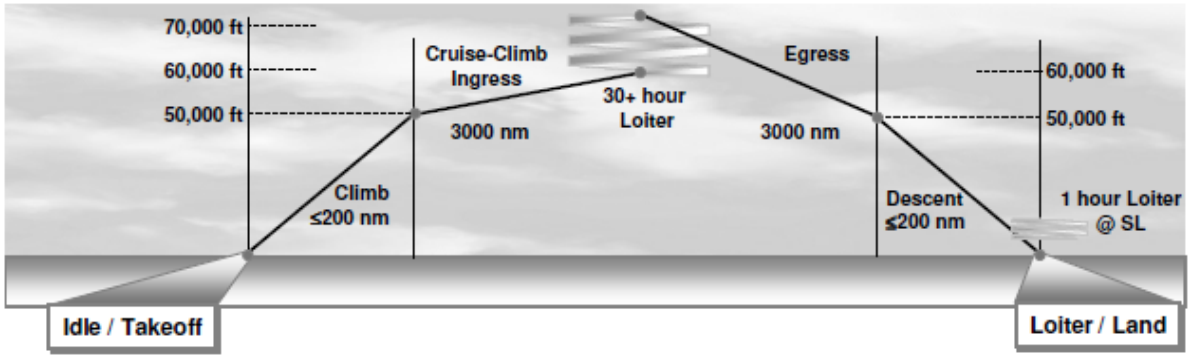

Figure 1 - Nominal SensorCraft Mission Profile[4]
Used under fair use guidelines, 2011.

Northrop Grumman, Lockheed Martin and Boeing each produced unique concept aircraft aimed at incorporating next generation sensing capabilities into a UAV capable of completing this challenging mission. Figure 2, Figure 3 and Figure 4 present conceptual sketches of a design from each airframer.

Figure 2 - Lockheed Martin Wing-Body-Tail SensorCraft[4]
Used under fair use guidelines, 2011.

Figure 3 - Northrup Grumman Flying Wing SensorCraft[4]
Used under fair use guidelines, 2011.

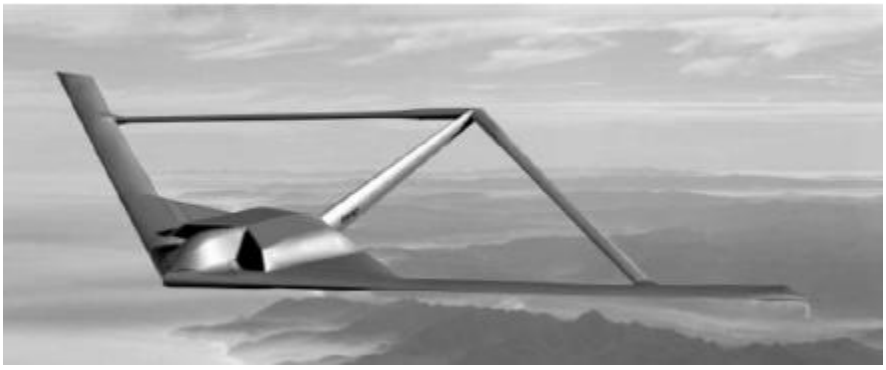

Figure 4 - Boeing Joined Wing SensorCraft[4]
Used under fair use guidelines, 2011.

The Boeing Joined Wing SensorCraft (JWSC) is the most unique design proposed to complete the SensorCraft mission. The flight test of a scaled model of this configuration is the topic of this thesis.

2.2 The Boeing Joined Wing SensorCraft

The Boeing JWSC, shown in Figure 4 and Figure 5, represents a substantial deviation from conventional aircraft configuration design. The primary driver behind the unique layout is the ability to incorporate advanced radar antennas into all four lifting surfaces. The SensorCraft mission requires these large antennas to provide advanced (high gain and foliage penetration) radar capability aimed at detecting extremely difficult targets.[6] By designing the JWSC to include conformal radar antennas embedded in each lifting surface, an unobstructed, real time,

360 degree sensor field of regard is attained. This is a capability unmatched by any existing aircraft today.

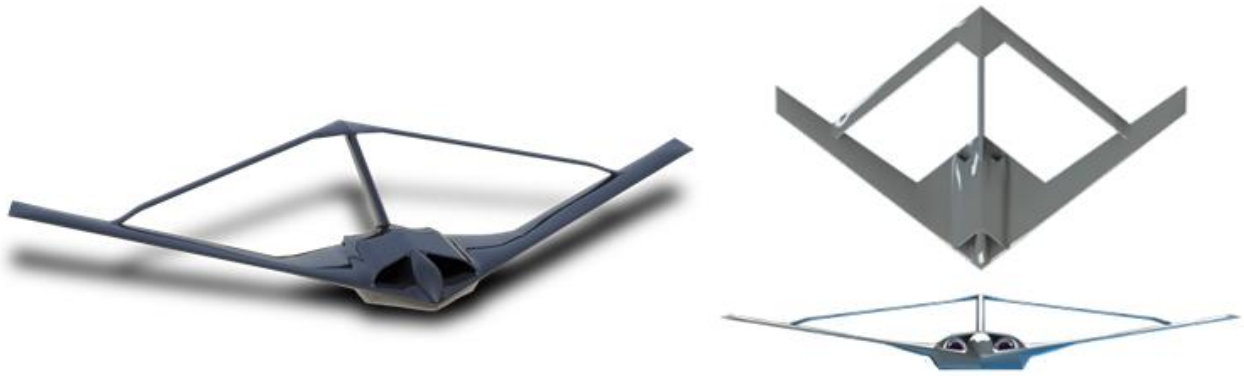

Figure 5 - CAD Renderings of the Boeing Joined Wing SensorCraft (adapted from Ref. 5) Used under fair use guidelines, 2011.

This ability is of great benefit to the ISR mission; however, it does come with a price. Previous computational studies of joined-wing aircraft configurations have shown the importance of the nonlinear aeroelastic response due to large deflections of the lifting surfaces and follower forces.[7,8,9] The source of this nonlinear aeroelastic response is the high flexibility of the structure relative to the large magnitude of the aerodynamic loading on the lifting surfaces in combination with the susceptibility of the aft wing to compression. This susceptibility is illustrated by decomposing the lift on each wing relative to a bending plane formed by the lifting surfaces. The in-plane lift component is well supported by the truss structure formed by the forward wing, aft wing and tail boom. The out-of-plane component, however, is resisted by weaker bending stiffness. This component causes compression in the upward forward portion of the wing box and tension in the lower rear portion.[10] The decomposition of the lift force, and the resulting load distribution in the wing box is shown in Figure 6.

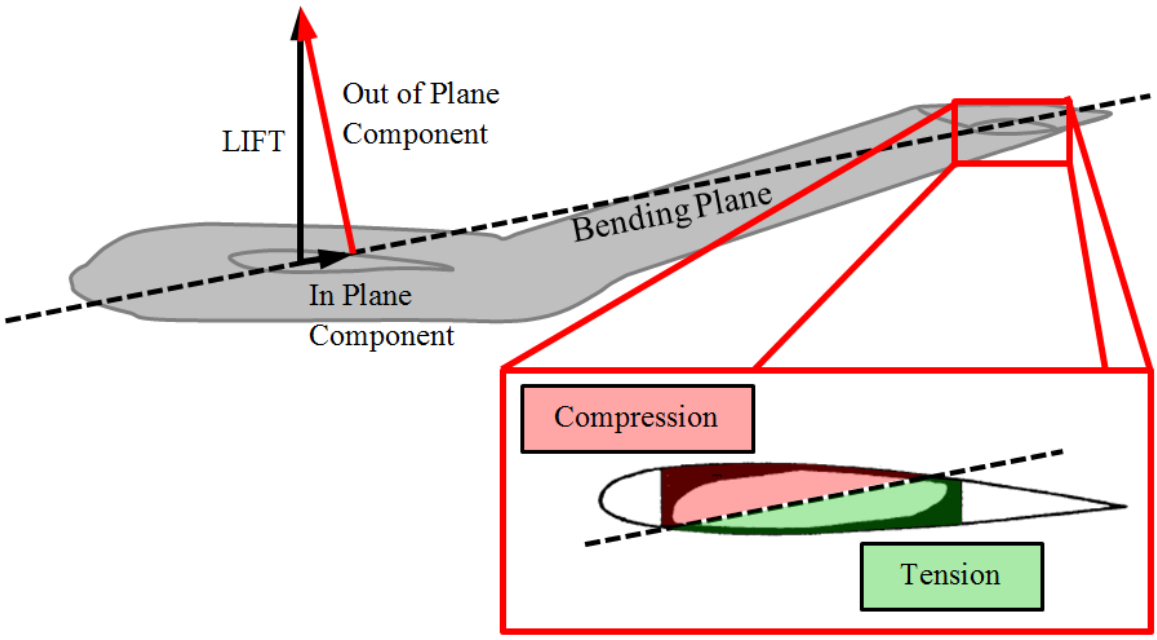

Figure 6 - Joined Wing SensorCraft Lift Decomposition (adapted from Ref. 10)
Used under fair use guidelines, 2011.

This loading distribution, under extreme loading scenarios such as a gust load immediately after takeoff, can lead to the buckling of the aft wing. This nonlinear behavior could be removed by strengthening the wing; however, this would result in large penalties in structural weight greatly reducing the performance of the aircraft. To avoid these penalties, nonlinear aeroelastic design, analysis and testing are required to ensure that the Joined Wing SensorCraft is able to sustain these nonlinear responses without structural failure.

2.3 Motivation

First introduced by Wolkovich in 1986, the joined wing concept was originally proposed to offer lower structural weight and less induced drag than a conventional wing and tail design.[10] These benefits were challenged in 1996, when Gallman and Kroo published a study which modeled a joined wing commercial transport concept using a fully stressed design method and nonlinear analysis. This study concluded that for the mission being studied, a joined wing design was actually heavier than a conventional design.[26] This result lessened interest in the joined wing as a next generation transport aircraft; however, recently there has been renewed interest in the joined wing as a next generation surveillance UAV. As mentioned previously, embedded radar antennas in all four lifting surfaces would provide unmatched ISR capability; however, in

order to realize this potential, nonlinear analysis and optimization of the joined wing design is required. In 2001, Livne published a survey paper highlighting the work to date in the structural and aerodynamic design of joined wing aircraft.[27]

In 2002, Blair and Canfield completed a weight modeling study for joined wing aircraft including examining the aeroelastic response of a joined wing model.[7] They noted that a correct joined-wing aeroelastic model may yield a design that leverages the nonlinear effects due to large deformations and geometric nonlinear response to the benefit of the vehicle, rather than a design that avoid these effects. They concluded that nonlinear analysis is required to accurately capture the aeroelastic response of joined-wing aircraft.

In a follow on paper in 2005, Roberts, Canfield and Blair expanded the study to include the structural and aerodynamic optimization of a nonlinearly scaled model, including buckling analysis. They concluded that a gust load condition is the critical load case in which the joined-wing configuration exhibits a large geometric nonlinearity in the form of aft wing buckling. Additionally, it was again noted that nonlinear analysis is essential to correctly capture the aerodynamic response of a joined wing configuration.[8]

In 2005, Blair, Canfield and Roberts also published a Journal of Aircraft article aimed at exploring joined-wing aircraft design incorporating the necessary nonlinear response. This study demonstrated the ability to converge on a successful design; however, the authors note that, "although we are confident in the theoretical integrity of the analysis tools used in this study, we conducted no experimental validation of the nonlinear structural mechanisms rendered in joined-wing configurations. This is highly recommended at this point in time." [9] The need for experimental validation was apparent.

In 2007, Bond completed her dissertation which included a wind tunnel study aimed at understanding the effect of aft wing twist on the Boeing Joined Wing SensorCraft.[11] This work was also presented in an AIAA paper. In this study, a 1:38 scale, half-span model was created with ±15° of aft wing twist with the goal of removing the aft wing control surfaces to maximize the usable wing area for the incorporation of sensors. The study found that pitch control through the use of a flexible aft wing is possible, but this result leads to a secondary conclusion. If pitch control is possible through the use of controlled aft wing twist, uncontrolled aft wing twist would be detrimental to the longitudinal stability of the aircraft in flight. Clearly, understanding and controlling the nonlinear aft wing response is critical to the success of the design.

In her dissertation, Bond also discusses the test of a 1/15 scale aluminum half-span model for static nonlinear response testing. In this test, the goal was to demonstrate and measure the nonlinear response through a static load test. This study showed that the application of follower forces (lift forces that remain perpendicular to the wing as the wing deflects) is critical to properly demonstrate the response of the joined wing. The necessity of modeling these follower forces was demonstrated by comparing linear results (follower forces were not included) to nonlinear results from both finite element analysis and experimental results.[11]

An additional effort completed by Pereira in 2007 documented the application of an aeroelastic scaling methodology to the fabrication of a Joined Wing model[30]. This study included a ground vibration test used to measure the natural frequencies of the model. The results of this test showed excellent correlation with the with the optimized computation model promoting the possibility of fabricating aeroelastically scaled test articles.

Finally, Boeing has completed an extensive wind tunnel study of an aeroelastically scaled Joined Wing SensorCraft model on a pitch plunge apparatus; however, this study was limited to longitudinal effects.[12] The marginal stability of the Dutch Roll Mode necessitates the experimental study of both longitudinal and lateral directional stability.

These previous efforts have greatly contributed to the understanding of the nonlinear response characteristic of the JWSC configuration; however, these effects have never been successfully tested in a flight test program. A previous flight test program of a JWSC configuration was completed at the AFRL; however, this study was limited to the design, analysis and flight test of a "rigid" model that incorporated no aeroelastic scaling, and the vehicle was not the Boeing JWSC configuration. This model was known as VA-1, was successfully flown in a single flight and then suffered a deep stall hard landing on the second flight. The model was significantly underpowered; however, it proved that a low-cost flight model was a practical and feasible method of investigating the performance and flying qualities of a joined wing model. The 2008 AFRL final report on this effort provides details on the complete effort and is approved for public release.[28] This work is also presented in a 2007 AIAA paper that details the lessons learned from the flight of the VA-1 as well as presents plans for going forward with a more advanced, low-cost, aeroelastically scaled flight demonstrator[31].

McClelland supported the analysis efforts of VA-1 by completing experimental inertia measurement of the VA-1 airframe in a bifilar pendulum test as part of his Master's thesis

work.[29] This work showed that a bifilar pendulum test is a viable means of experimentally determining the moments of inertia of a joined wing aircraft, despite the unique geometry and the challenges presented by hanging the aircraft in all three orientations required to measure the moments of inertia about the three principle axes.

With the aforementioned computational and experimental studies in mind, The AFRL determined that an aeroelastically scaled Remotely Piloted Vehicle (RPV) provides a low cost effective way to experimentally investigate the nonlinear aeroelastic responses characteristic of the Boeing JWSC configuration and and pave the way for future, more advanced aeroelastic demonstrators to investigate active gust load alleviation (GLA) and control of the aft wing response.

The first step in making this advanced JWSC RPV a reality was a feasibility study completed by Jenner Richards in 2009.[13] This study explored a method for scaling the aeroelastic response of the full scale SensorCraft down to a $1/9^{th}$ scale model. A preliminary design for the RPV is also presented. This paper was followed by a 2010 paper authored by Richards, Suleman, Aarons and Canfield that outlines the multidisciplinary approach to the first year of work on this program, including the early stages of fabrication of the RPV as well as the design of the flight test plan.[14] Finally, a 2011 paper by Richards, Aarons, Suleman, Canfield, Woolsey, Lindsley and Blair outlines the work on this program leading up to the first flight, including the detailed design and fabrication of the vehicle, the final development of the flight test plan, and the flight testing of numerous reduced complexity flight test models.[5]

Since the presentation of the aforementioned papers, this program has seen a successful flight test. This thesis presents the complete development and implementation of the rigorous flight test program for the flight test of a Geometrically Scaled Joined Wing SensorCraft RPV from concept through successful flight test.

3 Joined Wing SensorCraft Flight Test Program Overview

This chapter provides an overview of the Joined Wing SensorCraft Flight Test Program, beginning with the scaled test point selected for the flight test effort. This is followed by a description of the collaborating entities participating, as well as an explanation of the contributions of each. This chapter is closed with a description of the breakdown of the project and an explanation of how the work presented in this thesis fits into the overall effort.

3.1 Test Point of Interest

The AFRL required that the RPV be built and flown at 1/9th scale. The flight test point of interest corresponds to a full fuel take off condition at sea level. This worst case flight condition represents the most hazardous portion of the mission due to the slow flight speed (just above stall speed) and high wing loading due to the large volume of fuel on board. Table 1 summarizes both the full scale and the corresponding reduced scale test configurations.[13] Figure 7 presents a juxtaposition of the full scale JWSC, the 1/9th scale RPV and a 6 ft tall man to illustrate the relative size of the RPV.

Table 1 - Summary of full scale and RPV test configurations

	Full Scale JWSC	**RPV**
Span (ft)	150	16.4
Test Point Speed (kt)	168	56
Test Point Weight (lb)	155,337	204.5
Test Point Wing Loading (psf)	124.4	13.6
Altitude (ft)	Sea Level	Sea Level

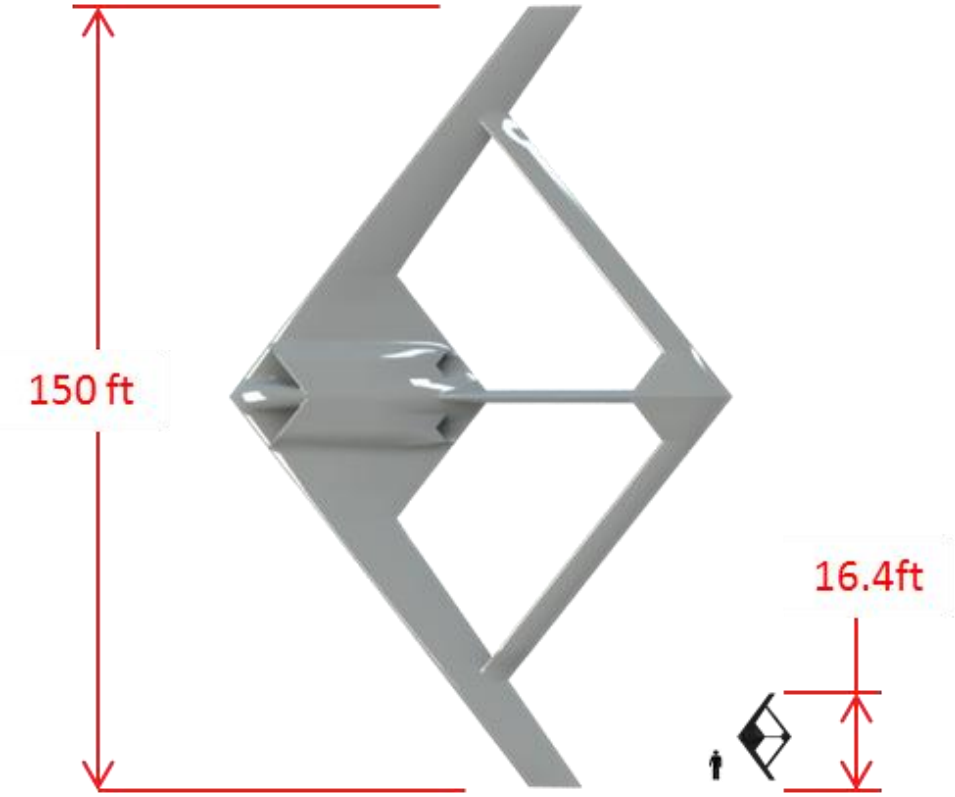

Figure 7 - Relative size of full scale Joined Wing SensorCraft, RPV and a 6 ft Man[14]
Used under fair use guidelines, 2011.

3.2 Collaborators and Contributions

The design, fabrication and flight testing of the JWSC RPV is the subject of an ongoing international collaboration between AFRL, Virginia Tech, the AFRL/Virginia Tech/Wright State/University of Maryland Collaborative Center for Multidisciplinary Sciences (CCMS), University of Victoria, Quaternion Engineering, the Canadian Center for Unmanned Vehicle Services (CCUVS) and Transport Canada. Figure 8 below presents a flowchart of the project organizational hierarchy.

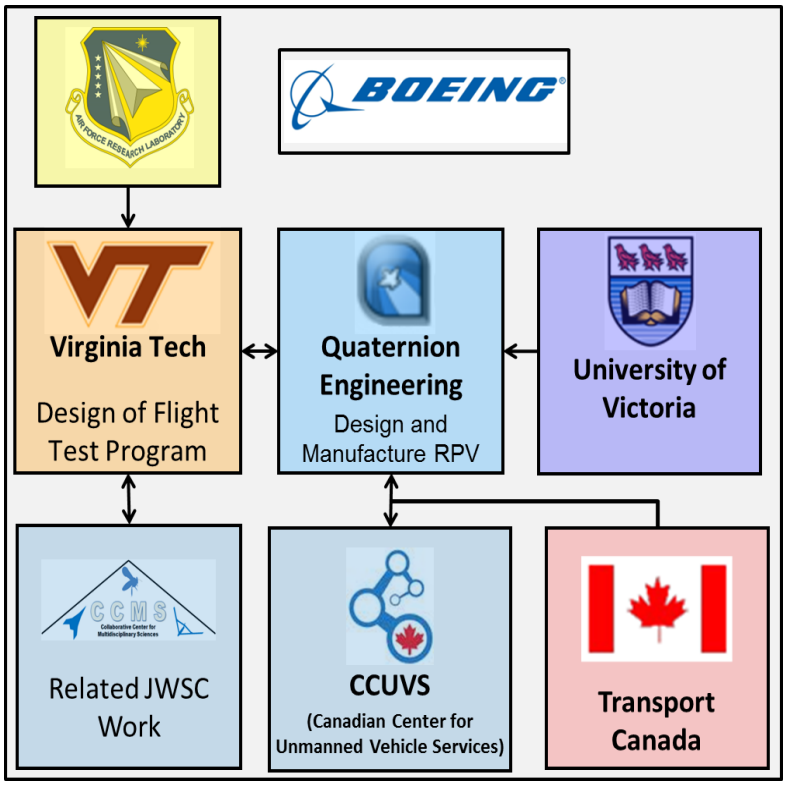

Figure 8 - Project Organizational Hierarchy

The JWSC is a Boeing concept, however, they are not directly involved with the project. The funding organization is the AFRL, who contracted Virginia Tech for the design, development and implementation of the flight test plan for the RPV. CCMS is a collaborative center with research groups at Virginia Tech, Wright State and the University of Maryland aimed at multidisciplinary design and development of air vehicles across a large regime of flight envelopes from micro air vehicles to HALE aircraft to long range, supersonic vehicles. A large component of the CCMS research taking place at Virginia Tech is focused on the JWSC concept. Several research projects, including the JWSC Flight Test Program, are aimed at the development and understanding of the JWSC and its associated aeroelastic phenomena.

Virginia Tech has contracted Quaternion Engineering, a Canadian Small to Medium Enterprise (SME) based in Victoria, BC, Canada for the design and fabrication of the RPVs. The subcontract involves the University of Victoria because the founders of Quaternion Engineering are Dr. Afzal Suleman and Mr. Jenner Richards, a Professor and PhD student at the university, respectively. Additionally, several co-op students from the university have worked at Quaternion and contributed to the fabrication of the RPV and associated activities.

Finally, in order to obtain flight approval in Canada, Quaternion Engineering worked with Transport Canada via the Canadian Centre for Unmanned Vehicle Services (CCUVS). CCUVS is a non-profit corporation whose purpose is to "facilitate sustained, profitable growth of the Canadian unmanned systems sector."[25]

3.3 Program Breakdown

Due to the unique JWSC geometry, the relative large scale of the RPV and the challenge of fabricating aeroelastically scaled, flight worthy components, the JWSC Flight Test Program was divided into two distinct phases: a Flight Worthiness Program and an Aeroelastic Response Program. The Flight Worthiness Program involves the conceptual design, fabrication and flight testing of a Geometrically Scaled Remotely Piloted Vehicle (GSRPV) with equivalent rigid body dynamics to that of the full scale aircraft. In other words, the GSRPV has scaled overall mass and moments of inertia, but no aeroelastic scaling. The Aeroelastic Response Program will build upon the success of the Flight Demonstration Program and expand it to include the design, fabrication and flight testing of the RPV re-winged with linear aeroelastically scaled lifting surfaces. A second flight test program will then be undertaken in an attempt to demonstrate the required nonlinear response with the linearly scaled surfaces. In the event that nonlinear response is not attained, a third set of wings will be fabricated and tested including nonlinear aeroelastic scaling.

The work presented in this thesis is part of the Flight Worthiness Program and accordingly applies to the design and implementation of a flight test program for the GSRPV. The Aeroelastic Response Program, including the design, fabrication and flight test of an aeroelastically scaled RPV represents follow on work.

4 Test Item Description

This chapter provides a high level description of the GSRPV, including overall dimensions and key performance parameters. A detailed elaboration on the subsystems of the aircraft is available in Appendix A, Section 3. More information on the design of the vehicle and supporting subsystems is available in References 5, 13 and 14.

4.1 General Description

The GSRPV is a 1/9th scale model of the Boeing JWSC concept. A photograph of the GSRPV on the tarmac at the flying site in Foremost, Alberta, Canada is presented in Figure 9.

Figure 9 – Geometrically Scaled RPV

The GSRPV is a joined-wing configuration consisting of a center body housing twin JetCat P200-SX turbine engines, a vertical tail boom and four lifting surfaces. The forward wings have positive dihedral and are swept aft. The aft wings have negative dihedral and are swept forward to join with the forward wings forming a diamond. Figure 10 presents a dimensioned 3-view drawing of the GSRPV highlighting key design parameters, and a summary of these parameters is presented below in Table 2.

Table 2 - Geometrically Scaled RPV Specifications

Geometrically Scaled RPV Specifications	
Wingspan	16.4 ft
Wing Area	15.0 ft^2
Length	10.58 ft
Aircraft Dry Weight	100.0 lbs
Fuel Capacity	6.75 gal
Test Point Weight	204.5 lbs
Total Thrust	104 lbs
Front Wing Sweep	37.9°
Front Wing Dihedral	6.2°
Aft Wing Sweep	-37.9°
Aft Wing Dihedral	-8.0°

Key performance parameters (KPP's) for the GSRPV are presented below in Table 3. Note that the stall speed presented uses an estimated C_{Lmax} = 1.90 (no flap deflection) from a CFD simulation completed at Quaternion Engineering.[5]

Table 3 - Key Performance Parameters

Stall Speed (Full Fuel)	40.6 kts
Stall Speed (Empty)	33.7 kts
Never Exceed Speed	152 kts
Cruise Speed Range	66-125 kts
Max Range	Visual
Max Endurance	40 min

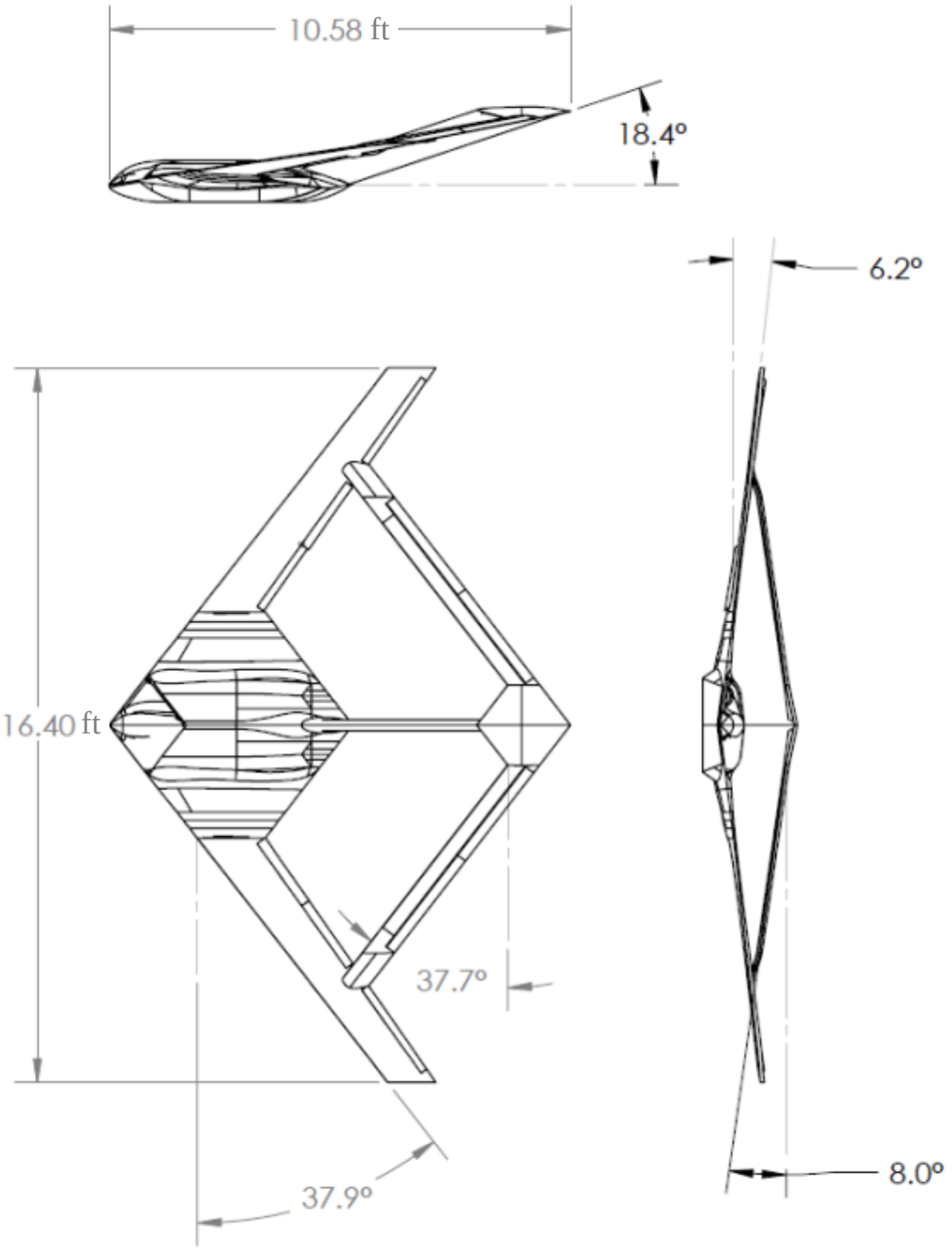

Figure 10 - Overall Dimensions of the Geometrically Scaled RPV (dimensions shown in ft)

5 Instrumentation System Design

As described in Section 1.1, a FTE is responsible for establishing instrumentation requirements. In the case of the GSRPV flight test program, this also included the design and fabrication of the instrumentation system. This section outlines the instrumentation system that was designed for the GSRPV. The GSRPV instrumentation package served as a low cost, low complexity means of testing several methods of wing deflection measurement and it also allowed flight test data logging and post processing operations to be designed and debugged with a smaller volume of data than will be required for the Aeroelastically Scaled RPV flights. Lessons learned from this instrumentation package will be used to optimize a more complex instrumentation package for the future Aeroelastically Scaled RPV flights. The entire instrumentation package was designed to be self-contained and powered by a single battery. By designing the instrumentation system to be a standalone system, independent from all flight critical components of the RPV, the risk of a flight critical malfunction is lessened.

The following sub-sections outline the components of the instrumentation package: the wing deflection measurement system consisting of accelerometers and strain gages, the instrumentation power system, the analog to digital conversion (ADC) and data logging systems and a custom air data boom.

5.1 Wing Deflection

Wing deflection measurement will be an integral part of the future flight test of the Aeroelastically Scaled RPV. The GSRPV served as a testing platform for wing deflection measurement systems. The overall wing deflections of the GSRPV are small (nowhere near the nonlinear range desired for the Aeroelastically Scaled RPV); however, testing the instrumentation in flight on the GSRPV will promote the success of the Aeroelastic Response Program by validating instrumentation system design.

There are two methods of measuring wing deflection that were tested on the GSRPV: strain gauges and accelerometers. Figure 11 shows the location of the strain gauges and accelerometers on the GSRPV.

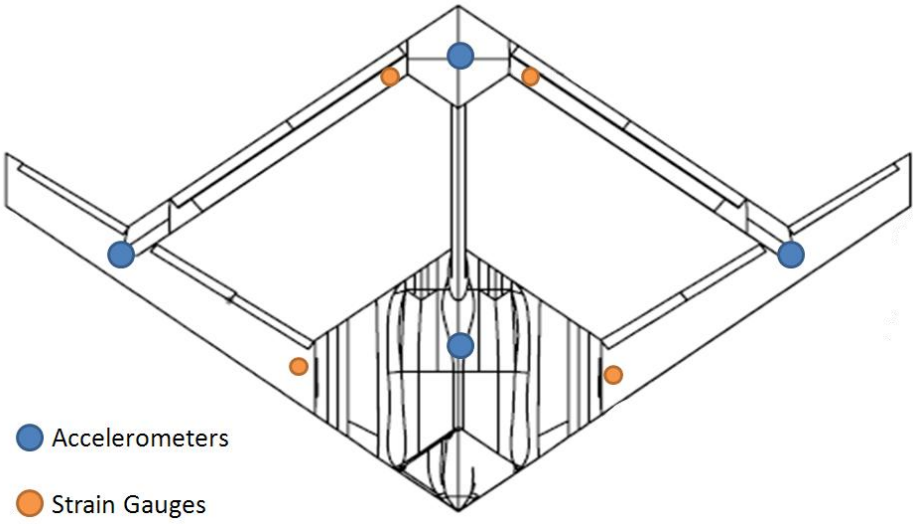

Figure 11. Accelerometer and Strain Gauge Locations

From this figure, it can be seen that strain gage arrays are located at the roots of both the forward and aft wings and accelerometers are located at the center of gravity, at each wing joint and at the top of the vertical tail boom. The strain gages on the front wing are located on the front spar. The use of two deflection measurement methods allows for redundant measurement of critical flight test data, and also allows for the comparison of the quality of the data. Each measurement method is presented in detail next, followed by a description of the analog to digital conversion (ADC) and data logging system designed for this system.

5.1.1 Accelerometers

Tri-axis accelerometers were selected as a wing deflection measurement option because they provide a large amount of data (three orthogonal accelerations at a single point), they are easy to implement and allow for post-processing the data to obtain wing deflection measurements. By integrating the local acceleration vs. time curves twice with respect to time, the displacement at the location of the accelerometers can be calculated. Aircraft attitude information from the onboard autopilot, a Cloud Cap Technology Piccolo II, can then be used to rotate the accelerometer displacements into the inertial reference frame (from the local reference frame set by the orientation of the installed accelerometers). Finally, the rotated displacements can be compared to the baseline un-deflected aircraft geometry to compute wing deflections.

The use of accelerometers has several advantages. Sensors within the scope of accuracy desired for this effort can be obtained relatively inexpensively and they are easy to calibrate and

install. Additionally, the raw data can be used to study the vibrations at each installation location. The primary drawback of the use of accelerometers is the noise and bias in the data.

To design the accelerometer system, level turn wing loading calculations were completed to show that the maximum planned load factor during the planned GSRPV flights is 2.89 g's (minimum radius turn at the never exceed speed). To account for all planned flight maneuvers, Analog Devices ADXL335 3-axis, ±3g accelerometers were selected. The accelerometers were mounted on Sparkfun breakout boards, as shown in Figure 12. This breakout board provides 0.1µF capacitors on each analog output (x,y and z-axes) giving the ADXL335 a functional bandwidth of 50Hz on each axis.

Figure 12 – ADXL335 Accelerometer on Sparkfun Breakout Board

Scaling and biasing of the output from the accelerometers was required to correlate the analog voltage to an acceleration measurement, as well as account for any small bias introduced by the instrumentation wiring, connectors, or small differences in the manufacture of each accelerometer. To accomplish this, a reading of 0g and 1g was required on each axis. These readings could then be used to establish a 1g scale for each accelerometer, as well as quantify the 0g "center point" for each axis. To accomplish this, each accelerometer was attached to a square box, and 30 second readings were taken for each axis perpendicular to and parallel to the direction of gravity; perpendicular readings provided the 0g level and parallel readings provided the 1g level. Figure 13 presents a picture of the accelerometers in the level calibration setup, measuring 1g on the x-axis.

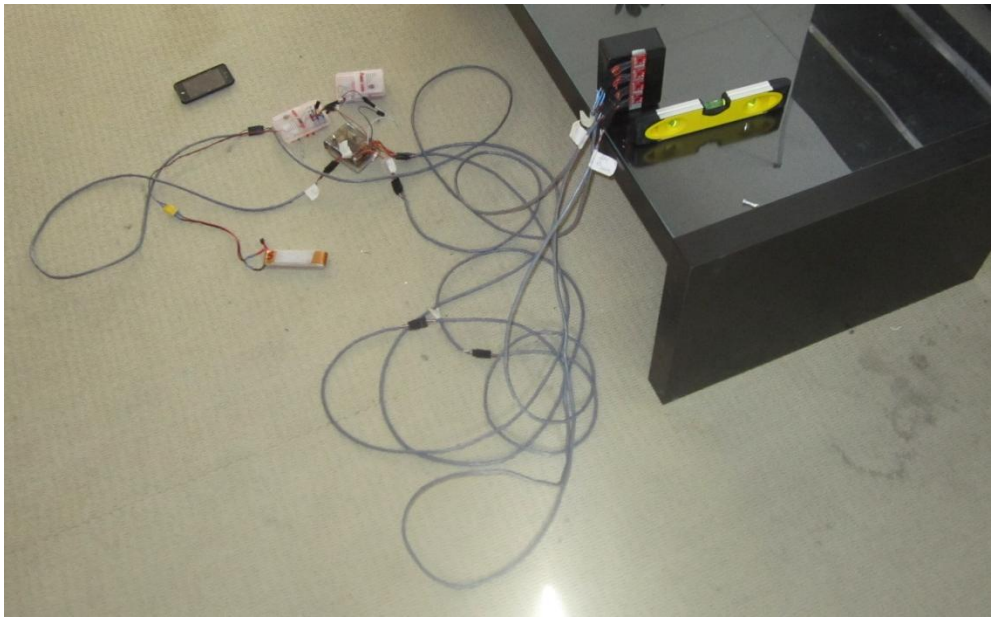

Figure 13 – Calibration of the Accelerometer System

5.1.2 Strain gages

Strain gages were selected as a wing deflection measurement option because they provide accurate, localized strain information which can be integrated to compute the wing deflection. The primary drawback of a strain gage system is the installation and maintenance of the gages. Strain gages are sensitive and fragile, and damage to the gages can provide large errors in the strain measurements.

The strain gage system for the JWSC GSRPV was designed and fabricated by Jeff Garnand-Royo as part of an undergraduate research project in support of the JWSC Flight Test Program.[15] To design the strain gage system, three separate components are required to be implemented: the strain gage, the bridge and the amplification system.

5.1.2.1 Strain Gage Selection

For the JWSC GSRPV, finite element structural analysis from Quaternion Engineering was used to calculated the expected strain at the desired location of the strain gages for a "worst case" flight condition corresponding to a 3g maneuver. This calculated strain was used to select a strain gage. Micro-Measurements CEA-06-250UW-350 Linear Pattern General Purpose Strain Gages, as shown in Figure 14, were selected due to their relatively large size (for ease of installation) as well as strain measurement range. These strain gages have a nominal gage resistance of 350 Ω ± 0.3% and a gage factor of 2.115 ± 0.05%.

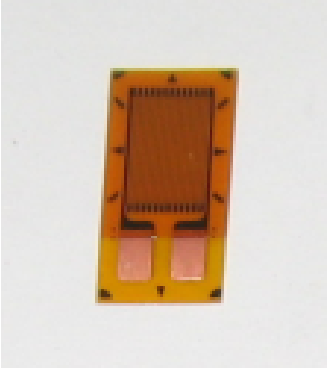

Figure 14 - Strain Gauge System Components

5.1.2.2 Bridge Implementation

The strain gages were implemented in a quarter Wheatstone Bridge system, as is shown in Figure 15.

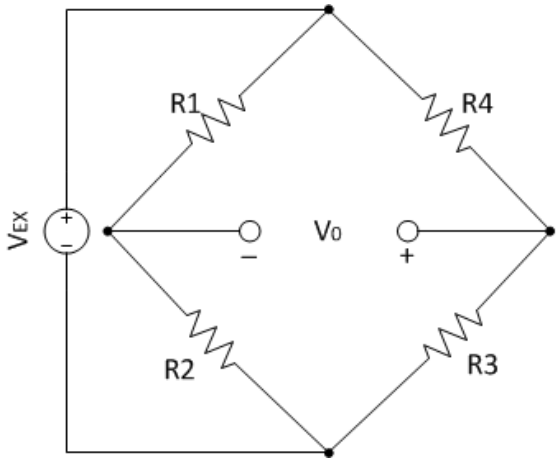

Figure 15 - Wheatstone Bridge Circuit

The Wheatstone Bridge allows for the measurement of very small changes in resistance through difference measurement, or the measurement of the change from steady state of an initially balanced system. The Wheatstone Bridge consists of 4 resistors, labeled above as R_1, R_2, R_3, R_4, and is powered by an excitation voltage, V_{EX}. The output voltage of the bridge, V_0, which is the difference between the positive and negative legs, becomes[16]:

$$\boldsymbol{V_0 = V_{0+} - V_{0-} = \left[\frac{R_1}{R_1 + R_2} - \frac{R_4}{R_3 + R_4}\right] V_{EX}} \qquad (\mathbf{1})$$

From this equation, it can be seen that the voltage output of the bridge will be zero if the proportion $R_1/R_2 = R_4/R_3$ remains true. In this condition, the bridge is "balanced." To register strain within this system, one, two, three, or all four of the resistors may be replaced with a strain

gage. When this is done, any change in resistance due to the strain gage will unbalance the bridge resulting in a nonzero voltage output. This voltage output can be used to calculate the strain by using the gage factor equation,

$$\varepsilon = \frac{\Delta R / R_G}{GF} \tag{2}$$

where the strain present in the strain gage, ε, is equated to the change in resistance, ΔR, divided by the nominal strain gage resistance, R_G all divided by the gage factor, a property of the strain gage provided by the manufacturer, *GF*.[16]

If resistor R_1 is replaced with an active strain gage, a quarter Wheatstone Bridge is formed. Assuming that the resistance of each half of the bridge is equal, ($R_1 = R_2$ and $R_3 = R_4$) this equation can be substituted into the Wheatstone Bridge in Equation (1) to calculate the bridge output voltage as a function of strain, the excitation voltage and the gage factor:

$$V_0 = \frac{GF\ \varepsilon}{4}\left(\frac{1}{1 + GF\ \frac{\varepsilon}{2}}\right) V_{ex} \tag{3}$$

Thus, by knowing the gage factor, the output voltage of the quarter bridge can be used to calculate the strain present in the strain gage. The result presented in Equation (3) only applies to a strain gage in position R_1. Gages in other locations will produce different equations, as is shown in Table 4.

Table 4 –Output Voltage as a Function of Strain for Each Position in a Wheatstone Quarter Bridge

Gage Position	Output Voltage
$\boldsymbol{R_1}$	$V_0 = \frac{GF\ \varepsilon}{4}\left(\frac{1}{1+GF\ \frac{\varepsilon}{2}}\right)V_{EX}$
$\boldsymbol{R_2}$	$V_0 = -\frac{GF\ \varepsilon}{4}\left(\frac{1}{1+GF\ \frac{\varepsilon}{2}}\right)V_{EX}$
$\boldsymbol{R_3}$	$V_0 = \frac{GF\ \varepsilon}{4}\left(\frac{1}{1+GF\ \frac{\varepsilon}{2}}\right)V_{EX}$
$\boldsymbol{R_4}$	$V_0 = -\frac{GF\ \varepsilon}{4}\left(\frac{1}{1+GF\ \frac{\varepsilon}{2}}\right)V_{EX}$

Note that a bridge with the bridge output polarity as shown in Figure 15, a negative bridge output voltage will result from a decrease in resistance in R_1 or R_3. Similarly, a positive bridge output voltage will result from a decrease in resistance in R_2 or R_4. Using the standard convention, that positive strain is tensile and negative strain is compressive, it follows that tensile strains will produce a positive output voltage if a strain gage is substituted for R_1 or R_3 and a negative output voltage if substituted for R_2 or R_4. Similarly, compressive strains will produce a negative output if a strain gage is substituted for R_1 or R_3 and a positive output voltage if substituted for R_2 or R_4.[16] This can be verified by substituting positive and negative values for strain, ε, for tensile and compressive strains respectively in Table 4 and verifying the sign on the output voltage.

One final improvement can be made by accounting for temperature effects on the strain gage. This is required because the active grid on the strain gage is composed of a metallic foil and temperature changes (such as those experienced by an aircraft in flight) could cause the gage to change resistance due to expansion or compression of the foil, leading to false strain reading.[15] Temperature compensation can be accomplished by replacing the second resistor on the side of the bridge containing the primary strain gage with a "dummy gage." This "dummy gage" is installed such that it experiences the same temperature effects as the primary gage, but does not

experience the strain. By placing the primary and dummy gages on the same side of the bridge, the required relationships $R_1 = R_2$ and $R_3 = R_4$ are maintained as both of the gages experience the same change in resistance due to temperature. Accordingly, the output of the Wheatstone bridge represents only the change in resistance due to the deformation of the active gage. For the JWSC strain gage system, the dummy gages were mounted on a small piece of carbon fiber and an anti-vibration foam mount was used to mount the gage to the aircraft. Both gages were placed under a custom fiberglass protective cover on the surface of the aircraft. The dummy gage mount is shown in Figure 16 without the cover and in Figure 17 with the cover.

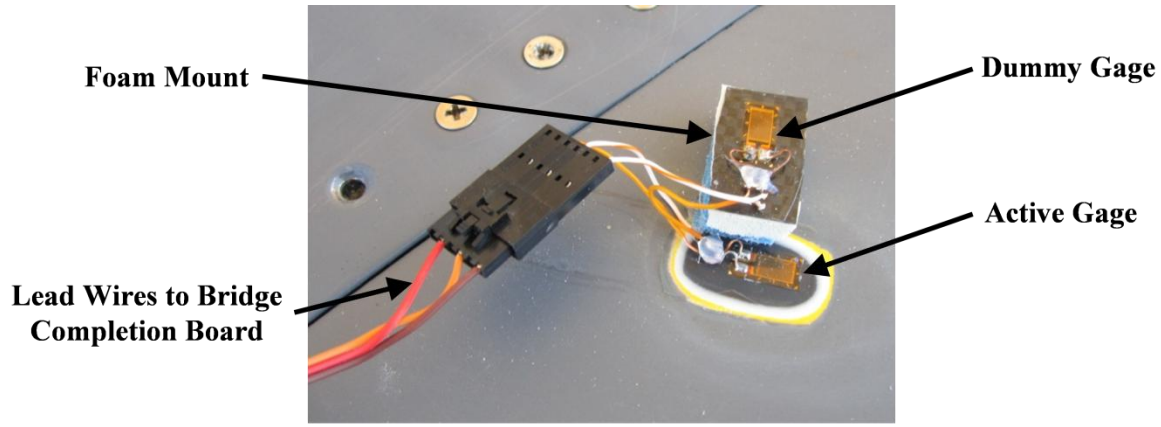

Figure 16 - Strain Gage Layout on Wing without Cover

Figure 17 - Strain Gage Cover

5.1.2.3 Amplification

With a properly configured quarter bridge setup, the voltage output from the bridge is very small, usually on the order of millivolts. A change in voltage of this magnitude is difficult to accurately capture without amplification. In order to accurately capture this change, scaling and biasing of the output is required to bring it into a range where the data logging system can read small changes and capture all strain activity.

For the JWSC strain gage system, the required scaling and biasing was accomplished via an INA 125 instrumentation amplifier. The INA 125 provides complete bridge excitation with regulated voltage from selectable pin references of 2.5V, 5V or 10V and a single external resistor can set a gain from 4 to 10,000. [17] For the JWSC system, the INA125 was powered with a regulated 5V supply and the 2.5V regulated pin was used to excite the bridge. The use of this pin incorporates a +2.5V bias, shifting the output of the INA125 from -2.5V to 2.5V to 0V to 5V which is able to be recorded by the data logging system. The positive and negative output legs of the bridge are wired to the INA125 and, incorporating a scaling gain, the output of the INA125 is represented by,

$$V_{out} = 2.5 + G_{IA}\, V_0 \tag{4}$$

where the 2.5 represents the 2.5V bias, G_{IA} is the gain for the INA125 which is described as

$$G_{IA} = 4 + \frac{60000}{R_{TP}} \tag{5}$$

In this equation, R_{TP} is the variable trim pot resistance set via a trim pot incorporated into the bridge completion circuit.[15,17]

5.1.2.4 Final JWSC Strain Gage System

For the JWSC strain gage system, R_1 and R_2were replaced with CEA-06-250UW-350 linear pattern general purpose strain gages; R_1 was replaced with the active gage and $R_2$was replaced with the dummy gage and R_3 and R_4were replaced with 350 Ω precision resistors to complete the bridge. Two 10kΩ trim pots (variable potentiometers) were used in parallel with the precision resistors to balance the bridge at the desired equilibrium point prior to each test. A schematic of the quarter bridge setup used is presented in Figure 18 and a labeled picture of a bridge completion circuit board is presented in Figure 19. Four identical boards were fabricated,

one for each of the onboard strain gage arrays. These boards contain the INA 125 instrumentation amplifiers as well as the trim pots and precision resistors required to complete the bridge.

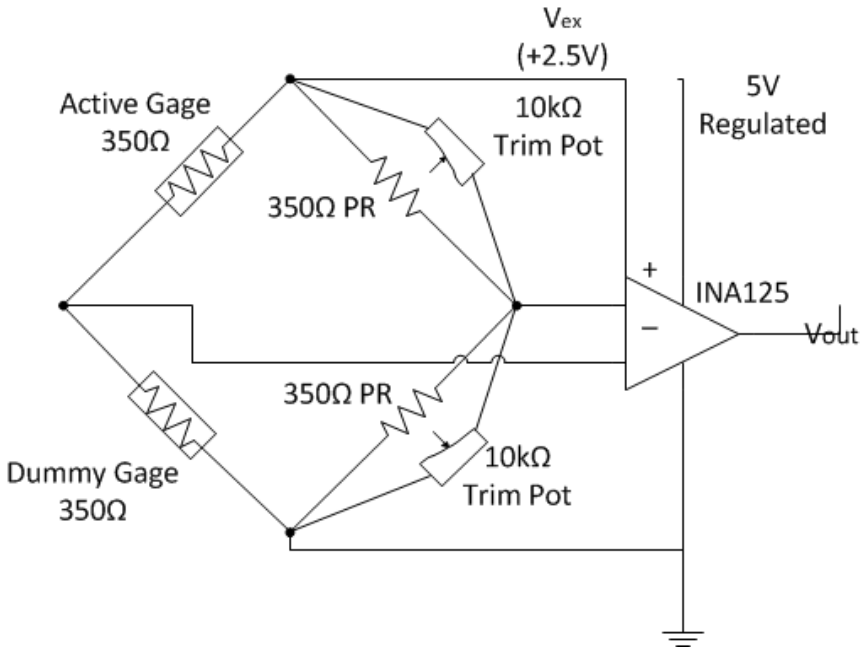

Figure 18 - JWSC Quarter Wheatstone Bridge Schematic

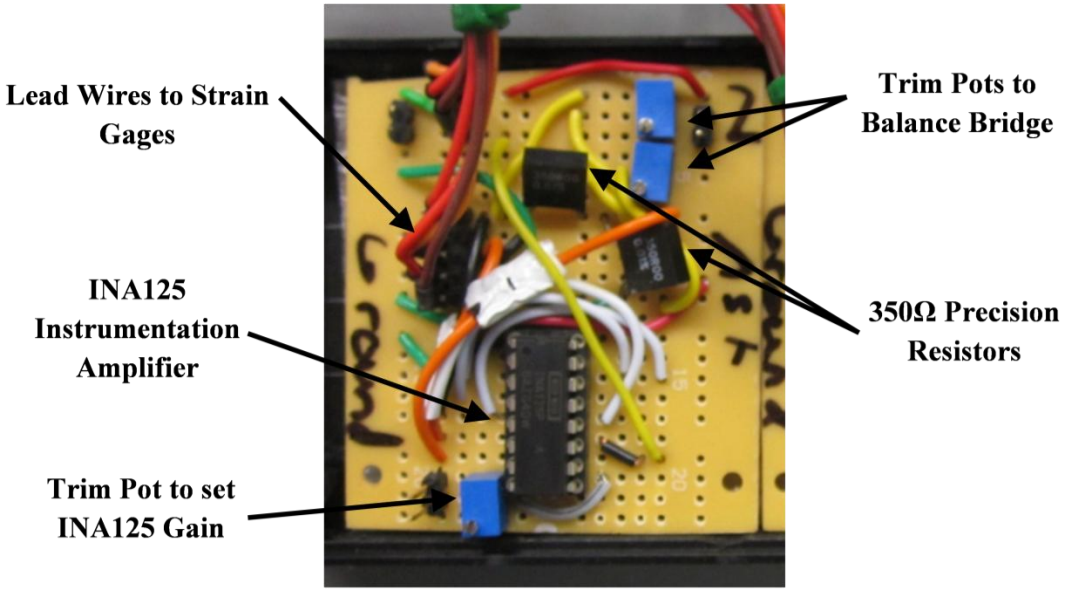

Figure 19 – Two Bridge Completion Circuit Boards

5.2 Analog to Digital Conversion and Data Logging

In order to store the voltage outputs from both the strain gages and accelerometers in real time, analog to digital conversion of the signals was required. Two MicroChip PIC18LF4553 microcontrollers were used for analog to digital conversion, one for the strain gage system and one for the accelerometer system. MicroChip PIC18LF4553 microcontrollers are 40 pin, plastic dual-in-line package (PDIP) chips that provide up to 13 channels of 12-bit ADC capability. For the JWSC instrumentation package, 12 channels were required for the accelerometer system (three channels per accelerometer, four accelerometers) and four were required for the strain gage system (one for each strain gage). The PIC18LF4553 also compiles the digital data into a single serial output and sends this output to the datalogging system. Figure 20 present a picture of the strain gage microcontroller board and Figure 21 presents a schematic of the PIC18LF4553 microcontroller as configured for the JWSC instrumentation system.

All programming of the PIC18LF4553 was accomplished using C-code generated and compiled in the MicroChip MPLAB Integrated Development Environment (IDE) and then the PICkit 2 Development Programmer/Debugger was used to program the flash memory on the chip itself.

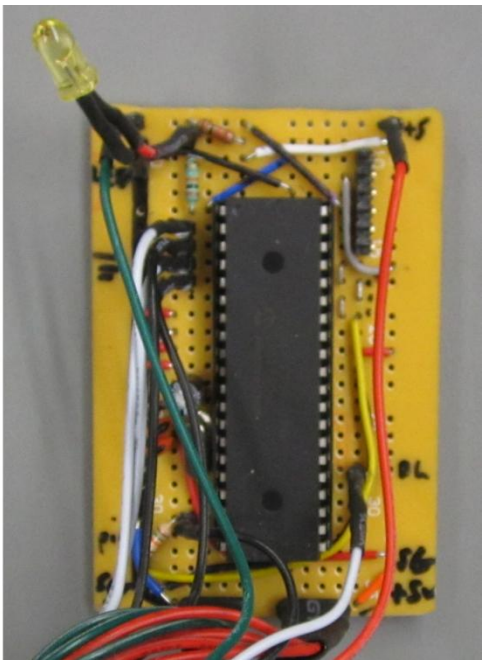

Figure 20 - Complete Microcontroller Systems for the Strain Gages

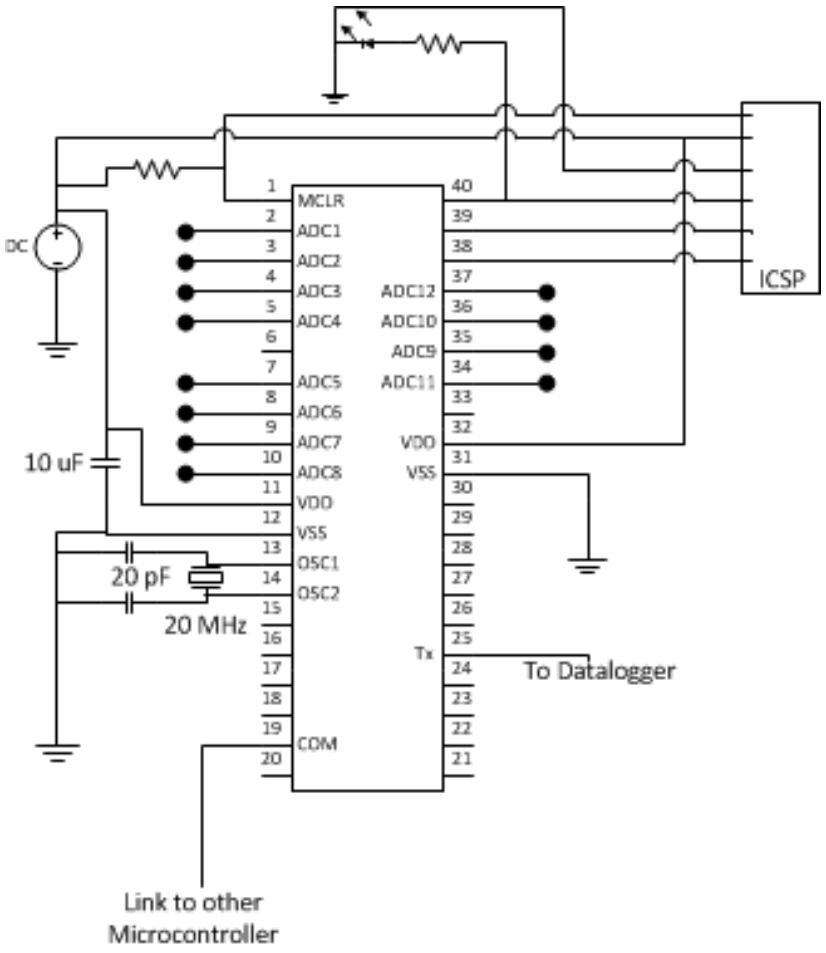

Figure 21 - PIC18LF4553 Microcontroller Schematic

The PIC18LF4553 was powered using pins 11, 12, 31 and 32 and a 10 uF power decoupling capacitor was included between pins 11 and 12. The microcontroller was run at 20MHz, as controlled by a 20MHz crystal and two 20 pF stabilizing capacitors placed between pins 13 and 14. The In Circuit Serial Programming (ICSP) capability was incorporated using an external bus and pins 1, 40, 39 and 38. This provided the required hardware for all serial programming of the microcontroller. Pin 40 was also used to display a "heartbeat." This was a small code that flashed a light emitting diode (LED) when the microcontroller is operating properly. All pins labeled as ADC (2,3,4,5,7,8,9,10, 34, 35, 36 and 37) were used for analog to digital conversion for the output from either the strain gages or accelerometers. For the strain gage system, only four channels were required, so the remaining pins were grounded. This provided a continuous low voltage output, which made post processing the data much easier. Pin 25 was used as the serial data output channel, and this pin was wired to the LogoMatic V2 data

logger to record the data. Two LogoMatic V2 data loggers receive the serial output from the microcontrollers, and store the data stream as a text file on a micro SD memory card. Figure 22 presents a picture of both LogoMatic V2 Dataloggers.

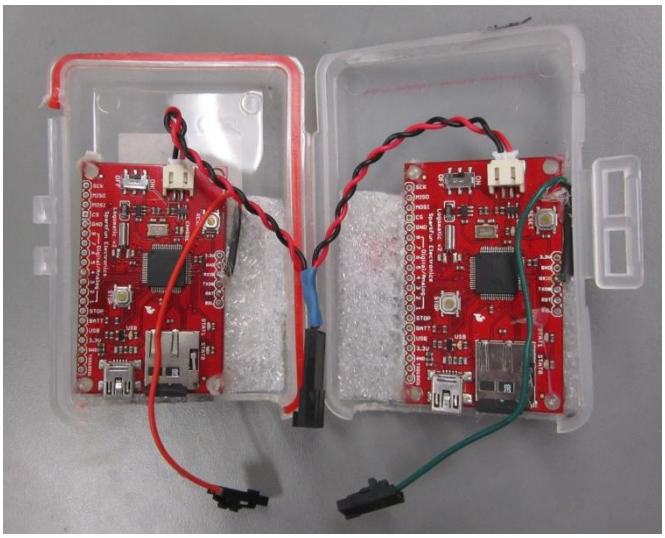

Figure 22 - LogoMatic V2 MicroSD Data Loggers

In order to synchronize and timestamp the data, an overflow timer was employed on the microcontroller providing ADC capability for the accelerometer package, and pin 19 was used on both microcontrollers to establish communication between them. The timer was set to operate the system at 40Hz. This provides a measurement every 0.025 seconds. The overflow timer was run on the microcontroller operating the accelerometer system, and when the overflow timer was reached, the accelerometer microcontroller restarts the timer, sends a "start logging" command to the strain gage microcontroller and starts logging data itself. Both microcontrollers then complete all required ADC processes for a single data point, compile the serial data stream, and send that serial output to the dataloggers.

Communication wire was used as a means to transfer the signal between all components of the instrumentation system. Molex connectors were used to make the wiring modular in places where connections were required (wing joints, boom joint, etc.). Communication wire provides a number of wires (four for the strain gages, six for the accelerometers) wrapped in conductive, aluminum foil, layering and then further wrapped inside an outer plastic layering. The conductive foil layer was wired in with the ground wire to provide shielding. This shielding allows the outer conductive layer to act as a Faraday cage, reducing the risk of electrical noise and electromagnetic interference (EMI) with other devices on board the aircraft.

5.3 Instrumentation Power System

The entire instrumentation system is powered by a 2-cell 7.4V lithium polyer (LiPo) battery pack. A Sparkfun LM7850 5V voltage regulator was used to provide a regulated 5V to the INA125 instrumentation amplifiers (which excite the strain gages), the Logomatic v2 data loggers and the strain gage microcontroller. A Sparkfun LD1117V33 3.3V voltage regulator was used to provide a regulated 3.3V to the accelerometers and the accelerometer microcontroller. A switch was incorporated to manually isolate the entire system from the battery, and two LEDs were incorporated to visually show confirmation of both 5V and 3.3V output.

5.4 Complete System Schematic

A complete system is schematic is provided in Figure 23. This schematic shows all components of the instrumentation package as described in the previous sections.

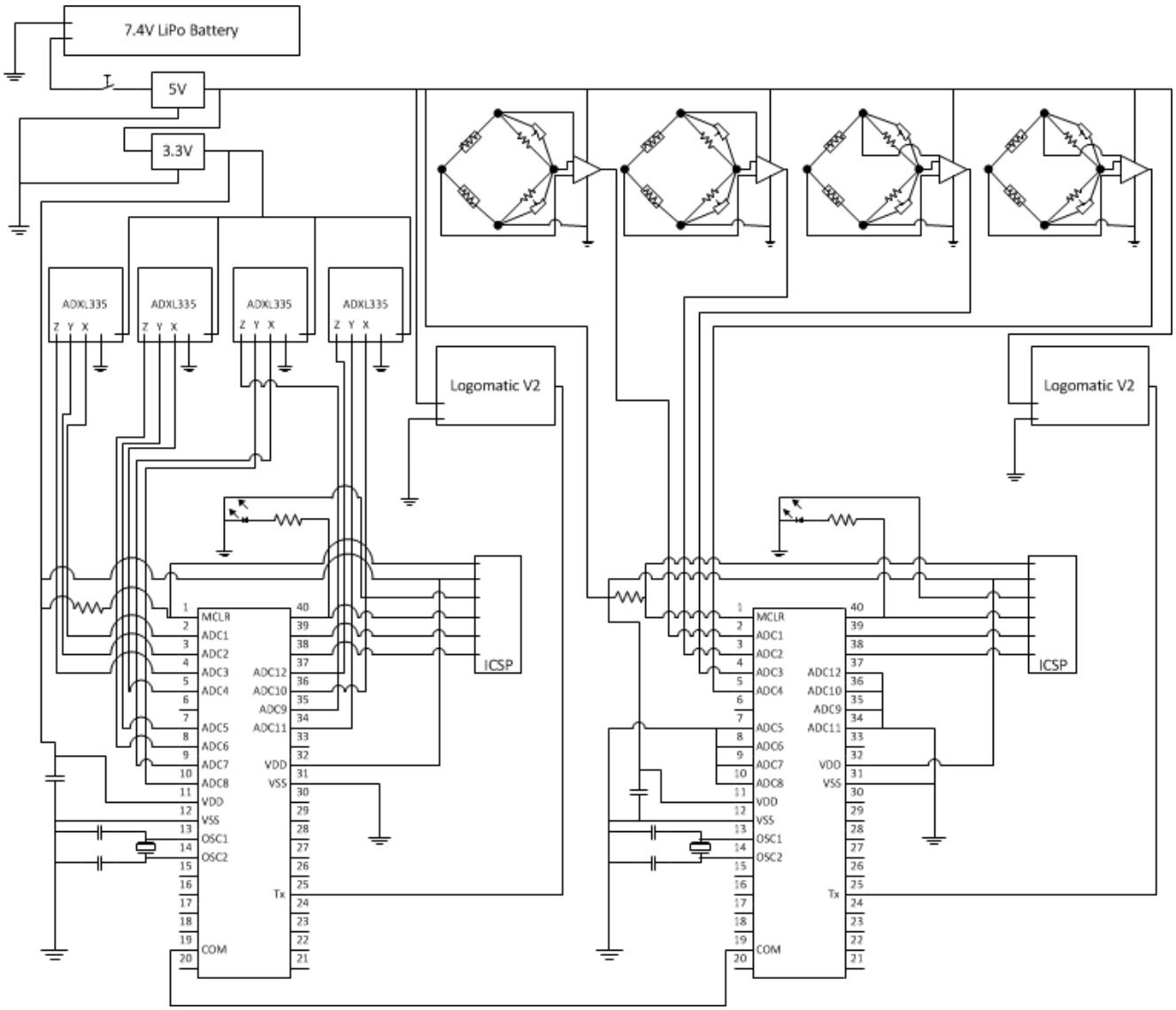

Figure 23 - Total Instrumentation System Schematic

5.5 Air Data Boom

An air data boom can be used to provide accurate angle of attack and sideslip angle measurements during all flight test operations. These measurements are advantageous over inertial measurement unit (IMU) readings from the autopilot because air data boom measurements incorporate wind speed and direction, which gives the true attitude of the aircraft relative to the free stream.

At the onset of the project, commercial air data booms were considered; however, they are too expensive to fit within the instrumentation budget of this project. Accordingly, a custom air data boom was designed and fabricated at Virginia Tech. This boom consists of a 40 in long, 0.75 in inner diameter aluminum rod and two custom CNC machined, dynamically balanced vanes. The vanes were fabricated using fiberglass-basswood-fiberglass sandwich panels, and zinc-steel counterweight was used to balance the vanes at the hinge line, to reduce the change of flutter during operation. A picture of a complete air data boom is presented in Figure 24.

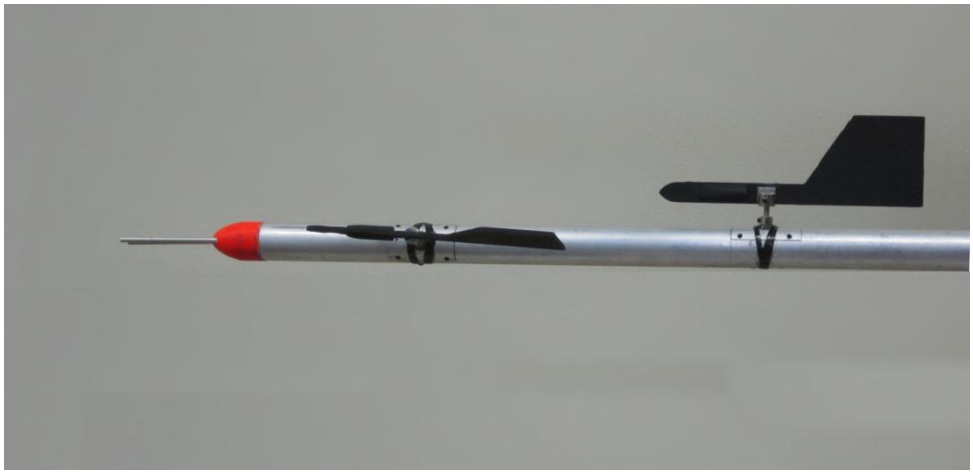

Figure 24 - Custom Air Data Boom

Angular measurements are provided by two Spectrum Sensors 6909-1003-030 low friction rotational potentiometers mounted on custom machined aluminum inserts. These potentiometers provide a 320 degree measurement range with minimal friction. The wipers for the potentiometers are mounted on the rotational shaft of each vane, and this shaft passes through the center of the potentiometer body. The analog output from each potentiometer can be processed in a similar manner to the analog output from the strain gages and accelerometers. Complete ADC requirements can be met with only two channels on a microcontroller. Figure 25 presents and exploded view of the vane assembly.

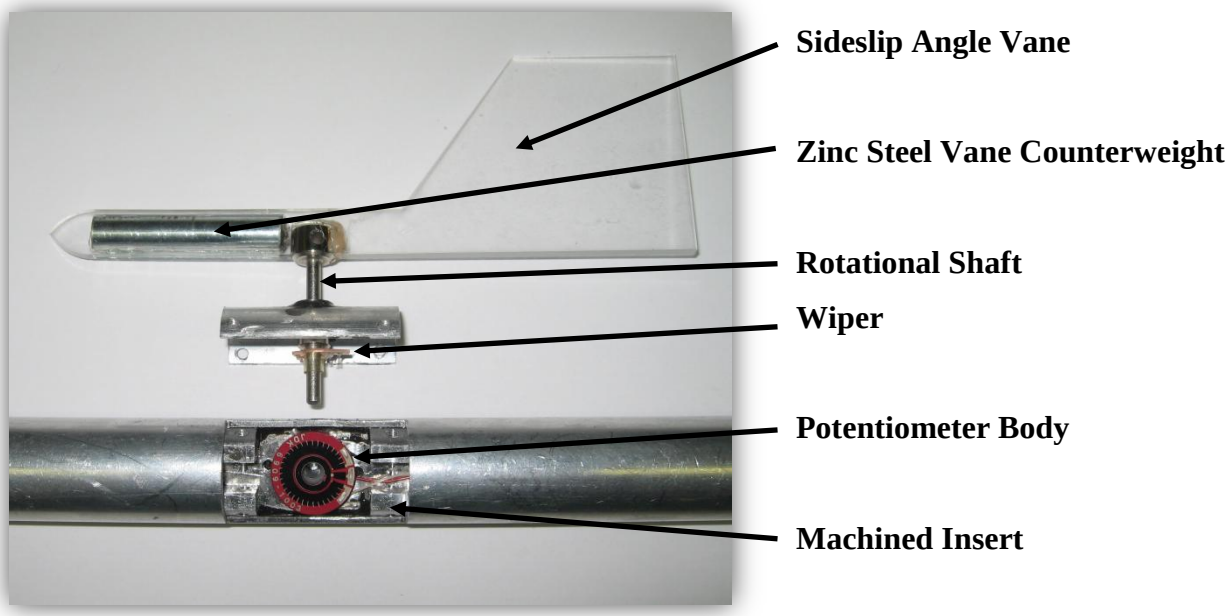

Figure 25. Exploded View of Air Data Boom Vane Assembly

Three identical air data booms were fabricated and subsequently calibrated in Virginia Tech's Open Jet Wind Tunnel. The calibration procedure and results are presented in Section 7.1.

6 Flight Test Plan

As described in Section 1.1, a FTE is responsible for organizing and implementing the flight test program, which includes organizing and preparing the test plan, test cards and briefings. This section summarizes the methodology and design of the rigorous flight test plan document that was created and implemented for the GSRPV, including the formal review process required with the AFRL, culminating with the receipt of a Military Flight Release (MFR). This section is aimed at describing the development of the test plan. Details on the testing procedures and results are available in Section 7 and the complete, Flight Test Plan is available for review in Appendix A.

6.1 Design Methodology

At the onset of the program, a flight test methodology was accepted based on that suggested by Kimberlin.[1] Using this as a guide, the following process was followed:

1. Define the Overall Program Goals.
2. Define a series of Flight Testing Objectives aimed at meeting the overall Program Goals.
3. Categorize these as primary, secondary and tertiary objectives based on the relative importance of the objective to the Overall Program Goal.
4. Develop a test (or series of tests) for each objective.
5. Establish metrics for success of the flight test program.
6. Organize these tests into an order that incrementally increases risk and minimizes redundancy, extracting the maximum amount of useful information from each test.
7. Ensure that all requirements (federal, international, project management, flying site, etc.) are met and followed.

The following sections will elaborate on this process as it was applied to the flight test of the GSRPV.

6.2 Program Goals

The overall program goals of the GSRPV flight test were to validate the scaling of the overall mass and mass moments of inertia of the full scale aircraft to the reduced scale RPV and subsequently demonstrate the airworthiness of the vehicle through safe, controlled flight. These goals were designed such that successful completion of the GSRPV flight test paves the way for the future planned flight test of the more complex Aeroelastically Scaled RPV and the measurement of geometrically nonlinear aeroelastic responses in flight.

6.3 Program Objectives

Guided by the aforementioned goals, a series of primary, secondary and tertiary objectives were developed. With these objectives defined, a test (or series of tests) was designed to meet each objective. These objectives, along with the tests that correspond to each shown after in parentheses, are listed below. One important concept represented is that the Primary Objectives correspond directly to the overall program goals. The three-phase testing schedule that was developed is presented in Section 6.5, results from testing to date is presented in Section 7 and the formal test plan is located in Appendix A.

1. **Primary Objectives:**
   - Validate scaled overall mass and center of gravity (CG) location *(Center of Gravity Test)*
   - Validate scaled rigid body mass moments of inertia *(Bifilar Pendulum Test)*
   - Demonstrate airworthiness and successful control of the GSRPV *(Phasing Flight Test)*
2. **Secondary Objectives**
   - Demonstrate successful data acquisition and logging of flight test data through the custom instrumentation system *(Ground Tests, Phasing Flight Test)*
   - Experimentally determine key turbine parameters, including static thrust, installed static thrust and fuel consumption *(Turbine Tests)*
   - Validate control surface deflections and mixing *(Servo Response Test, Control Surface Scheduling Test)*
   - Validate structural design *(Static Structural Loading Test)*

- Investigate feasibility of safely reaching 204 lb weight test point *(Incremental Weight Increase Test)*

3. Tertiary Objectives

- Obtain dynamic model parameters (*Dynamic Mode Flight Tests*)
- Investigate flight maneuvers to achieve required loading for nonlinear aeroelastic response *(Aeroelastic Response Preparation Test)*

6.4 Metrics for Success

After defining the hierarchy of objectives, metrics for success were defined in order to facilitate reporting after the completion of testing as well as assist in the justification of continued testing with the Aeroelastic Response Program. In order for the flight test program to be considered a success, all primary objectives had to be met, along with a majority of the secondary objectives. Tertiary objectives had no bearing on whether or not the test was declared a success, but successful completion of these objectives promotes the success of the Aeroelastically Scaled RPV flight test program. The successful completion of the tests associated with each objective, as described in the test plan, were used to quantify meeting that objective.

6.5 Testing Breakdown

The GSRPV flight test was divided into three distinct phases, with the complexity and scope of the tests increasing within each phase. This approach was taken to incrementally increase risk and minimizes redundancy, while still extracting the maximum amount of useful information from each test.

This section is intended to give a high level overview of the testing order, as well as the overall aim of each phase of testing. The following sub-sections explain the goals of each phase of testing. Specific details on each test are provided as well as the current status of that test (complete or pending). For preliminary tests, results are presented in this section; however, for the majority of the tests, detailed procedural explanations, along with the results of testing completed to date are provided in Section 7. Additionally, a further explanation of each of the tests is available in Appendix A, Section 3.3.

6.5.1 Phase 1 - System Tests

Phase 1, System Tests, included the integration and testing of all onboard systems. The aim of this phase of testing was to individually test each system, including instrumentation, to ensure that all were functioning properly prior to traveling to the flight test site. The tests included in this phase included a servo response test, control surface scheduling test, backup control test, instrumentation system tests, propulsion tests and a landing gear drop test.

6.5.1.1 Servo Response Testing

For the servo response test, the onboard autopilot is used, along with a control surface deflection meter, to establish an experimental correlation between commanded servo pulse width and control surface deflection for each surface. In other words, this test allows the commanded output from the autopilot to be equated to a control surface deflection, in degrees, for each control surface on the aircraft. These correlations can then be used to monitor control surface deflection during flight as the autopilot logs and telemeters servo commands to the ground station. Additionally, the results of this test are a required input to the autopilot to calibrate stability augmentation for the GSRPV. This test was completed at Quaternion Engineering prior to traveling to the flying site.

6.5.1.2 Control Surface Scheduling Test

The control surface scheduling test verifies that control surface schedule developed for the GSRPV was successfully implemented. In other words, all onboard servos and control surfaces move as expected given a particular flight command, and all control mixing had been properly implemented. Details on this control surface schedule are presented in Appendix A Section 2.3 and details on the control system itself are presented in Appendix A Section 2.8.

This test is critical to ensure that the pair of servos on each control surface are properly matched and deflect synchronously. If the servos were not exactly matched, they would "flight" one another, providing resistive force to the other's movement. This would cause unnecessary stress on the internal mechanics of each servo as well as demand high current loads from the batteries powering the system, consume the capacity of the packs far too quickly.

To complete this test, Willem Brussow and Peter Lu utilized the onboard Power Box Royales (a modular servo control and power system) to individually center and trim each servo to ensure smooth travel of each surface individually. Once complete, the properly tuned Power

Box Royales were incorporated into the complete control system to employ the control surface schedule and provide redundant power and reliable control of the onboard servos.

6.5.1.3 Instrumentation System Testing

The instrumentation system tests check the ADC capabilities, data logging synchronization, storage reliability all onboard instrumentation systems. All instrumentation was fabricated as described in Section 5, including custom enclosures to ensure that the components would not be damaged during flight.

During bench testing, each microcontroller was programmed individually and then the complete system was tested. Testing was first completed using a mockup of the instrumentation system on a bread board. This was followed by fabrication of the final microcontroller boards and testing of the final, flight-ready system.

Preliminary testing was used to ensure that each microcontroller was capable of logging data, as designed, on the Logomatic V2 Data Loggers independently. With both systems independently functional, the synchronization system was tested by including the onboard timing on the accelerometer microcontroller. A final test investigated the consistency in the regulated voltage output by the power system developed for the instrumentation system with changing voltage of the battery powering the system. The results of these tests, including a more detailed look at the procedures followed is presented in Section 7.2.

6.5.1.4 Propulsion Tests

The propulsion tests are used to evaluate the performance of the JetCat P200-SX turbines. These tests include both the bench top static thrust testing of the individual turbines, including a comparison to AFRL reference data, as well as a static installed thrust test of the full GSRPV. The bench testing validates the stand-alone performance of each turbine while the installed static thrust testing investigated the effects of inlet and exhaust ducting design. These tests also serve the purpose of allowing the test team to become familiar with the operation of the JetCat turbines, including the operation of two turbines simultaneously. The full procedural explanation and results of these tests as completed are presented in Section 7.3 and 7.4 for the static thrust and installed static thrust tests, respectively.

6.5.1.5 Landing Gear Drop Test

The landing gear drop as designed in the test plan test is used to evaluate the as-built design of the landing gear to see whether or not it can withstand the required loads upon landing. For the JWSC, this test was designed in accordance with MIL-T-6053C and MIL-A-8863C. To complete testing, the landing gear is mounted to a solid plywood board in the exact geometric configuration required for the Geometrically Scaled RPV. Weights are added to the board and distributed such that the CG of the system corresponds to the CG of the overall RPV. A total of five planned drops, as outlined in Table 5 below, complete the test.

Table 5 – Landing Gear Loads Test Matrix

Drop Number	Weight (lbs)	Descent Rate (FPS)	Drop Height (ft)	Attitude
1	131.8	10	1.55	Level
2	131.8	10	1.55	Tail Down
3	204.5	6	0.559	Level
4	204.5	6	0.559	Level
5	204.5	6	0.559	Tail Down

The descent rates used are specified in MIL-T-6053C, and the drop heights were calculated such that the gear would be at the required descent rate at the point of impact with the ground. The attitudes specified correspond to the two required test conditions, wheels level and tail down. For the level attitude, the aircraft will be dropped such that all landing gear wheels contact the ground at the same time (this corresponds to the nose strut fully extended). For the tail-down landing, MIL-T-6053 requires that the pitch angle needs to correspond an attitude corresponding to 90 percent of the maximum lift coefficient in level flight for the powered approach configuration. For the GSRPV, this corresponds to $C_L = 1.685$ (assuming a flap $\Delta C_L = 0.24$) at an angle of attack of $\alpha = 9.4°$. After each drop, the fully extended height of the strut is measured along with the height of and width of the rear gear. This will test for any permanent deformation that occurs.

Prior to the flight of the GSRPV, Quaternion Engineering completed a landing gear drop test similar to the test described above. It was decided to not proceed with the aforementioned test due to its requirement to test at the full test point weight of 204.5 lbs. The first flight of the

GSRPV was completed at 140 lbs, so testing completed at Quaternion Engineering took place at the 140lb test weight. The test that was completed prior to the first flight was based on FAR requirements, however, and the aforementioned test will be completed for future flights when sustaining a landing at the full 204.5 lbs is required.

6.5.2 Phase 2 - Flight Readiness Tests

Phase 2, Flight Readiness Tests, included ground testing of the complete RPV system. With all systems tested individually in Phase 1 testing, Phase 2 testing verified the functionality of the complete, flight ready RPV. This phase includes a center of gravity test, a bifilar pendulum test and a static structural loading test.

6.5.2.1 Center of Gravity Test

For the center of gravity test, two electronic scales were used to calculate overall mass and center of gravity (CG) of the aircraft. With the aircraft at zero degrees angle of attack, summing the readings on the two scales gives the overall mass and, knowing the overall mass, the distribution between the two scales can be used to compute the longitudinal CG. Placing the aircraft at an angle of attack allows the vertical CG to be calculated, once the longitudinal CG is known.

This test was completed as described for the GSRPV prior to first flight; however, discrepancies in the measurements of the CG location caused by the resolution and accuracy of the electronic scales available to the test team led to the development of a second test. To accurately measure the CG of the aircraft, two large, plastic boxes were placed on the ground and a 1.5 in diameter dowel rod was placed on top of the boxes. The aircraft was placed with the dowel rod spanwise between the forward and aft landing gear. The aircraft was then rolled on the dowel rod until the aircraft balanced. The location of the dowel rod then represented the CG location of the aircraft. This test was completed for both full fuel and empty. Results are summarized in Table 6.

Table 6 - GSRPV First Flight Mass, CG and Static Margin

	mass (kg)	CG (m aft of nose)	Static Margin
Empty	51.00	0.95	40.0%
Full	68.85	0.94	41.8%

6.5.2.2 Bifilar Pendulum Test

The bifilar pendulum test serves to experimentally determine the overall mass moments of inertia of the RPV about the principle axes. This test is required to generate experimental inertias to validate the mass modeling of the aircraft, as well as pave the way for future iterations of this test where the inertias will be tuned using ballast weights (for aeroelastic scaling).

A Bifilar Pendulum test involves hanging the aircraft from a bifilar (two parallel support wires) pendulum system in three separate orientations. The dynamical equations of motion governing the general case of a rigid body suspended by a bifilar pendulum are nonlinear; however, ensuring that several fundamental assumptions are met, these equations can be greatly simplified.[18] The simplified model assumes that in each orientation (roll, pitch and yaw), the CG of the aircraft lies directly in between each support filament (equidistant from each filament) and the vertical axis of the aircraft in that orientation is parallel to the wires. Finally, using small angle oscillations, the period of the rotational oscillations of the system about the vertical axis can then be used to compute the moment of inertia about that axis in terms of measurable quantities as follows,

$$I_{vertical} = \frac{WD^2\tau^2}{16\pi^2 L} \tag{6}$$

where W is the weight of the aircraft, D is the distance between the filaments, τ is the rotational period of oscillation of the system and L is the length of the support filaments.

The above model assumes that the support filaments themselves have no effect on the system. Accordingly, improvement can be made by accounting for the torsional properties of the suspension filaments[18]. If an object of known inertia is suspended from one of the support filaments, a string torsional spring constant can be calculated as follows,

$$k_{eff} = \left(\frac{2\pi}{\tau_1}\right) I_{known} \tag{7}$$

where τ_1 is the period of oscillation of the single filament system and I_{known} is the known moment of inertia of the object being tested. This correction can be included in the calculation of the mass moment of inertia about the vertical axis as follows,

$$I_{VC} = \frac{WD^2\tau^2}{16\pi^2 L} + \frac{k_{eff}\tau^2}{2\pi^2} \tag{8}$$

where I_{VC} represents the corrected mass moment of inertia about the vertical axis.

Finally, in order to successfully suspend the aircraft about each axis, a support carriage is required. The support carriage must be fabricated (or ballasted) such that the CG lies in the same position as the aircraft in order to ensure that the above mentioned assumptions are still met. Once complete, the inertia of the support carriage alone (without the aircraft in it) must be measured such that this value can be subtracted from the inertia of the aircraft/carriage system resulting in a moment of inertia for the aircraft itself[19].

Incorporating all corrections and measurements, the final mass moment of inertia about the each axis can be computed as follows,

$$I_{V\,FINAL} = \left(\frac{WD^2\tau^2}{16\pi^2 L} + \frac{k_{eff}\tau^2}{2\pi^2}\right)_{AC+Carriage} - \left(\frac{WD^2\tau^2}{16\pi^2 L} + \frac{k_{eff}\tau^2}{2\pi^2}\right)_{Carriage} \tag{9}$$

This equation computes the final mass moment of inertia of the aircraft about the vertical axis by computing the inertia of the aircraft/carriage system and subtracting the inertia of the carriage itslef, incorporating the torsional string constant in both calculations.

A Bifilar Pendulum Test has been successfully used to calculate the mass moments of inertia of the JWSC GSRPV. The complete experimental procedure and the final results, incorporating the theoretical setup explained above, is presented in Section 7.5.

6.5.2.3 Static Structural Loading Test

A static structural loading is used to experimentally validate the structural design and fabrication of the GSRPV and ensure that the as-built structure was capable of withstanding the predicted aerodynamic loading required to complete all planned flight maneuvers. To complete this test, the aircraft was inverted in a custom designed support rig and sand bags were distributed along the wings to simulate aerodynamic loading. The aircraft was designed to withstand a 3g max loading, with a factor of safety of 1.5, at the test point weight of 204.5 lbs. For safety, the GSRPV static loading test includes testing up to a 3g loading at the first flight weight of 140 lbs. Follow on testing beyond 140 lbs will be completed before subsequent flights. The autopilot incorporates a g-load limiter, so no loading greater than 3g will be

experienced in flight. A full description of this test as completed, including the selected test point spanwise lift distribution is presented in Section 7.6.

6.5.3 Phase 3 - Flight Tests

The third phase of testing includes all flight test operations of the RPV, or all operations where the RPV is moving under its own power. To mitigate risk, a low-speed handling test and a high-speed taxi test open this phase. This is followed by the most important test in the entire program, the first flight of the GSRPV, known as a phasing flight test. Follow on flight testing, which is planned for future flight tests, includes more advanced flight tests such as dynamic mode evaluation testing, incremental weight increase test and aeroelastic response preparation testing.

6.5.3.1 Low Speed Taxi Test

The low speed handling test involves taxiing the aircraft and testing its handling qualities using figure-8 maneuvers at speeds up to 10 knots. This test allows the turning radius of the aircraft to be set by adjusting the travel of the nose wheel to meet the pilots expectations. Additionally, this test evaluates the stability of the aircraft during low speed operations on the runway and tests the performance of the braking system. This test was completed prior to the first flight of the GSRPV.

6.5.3.2 High Speed Taxi Test

The high-speed taxi test consists of straight line, mock takeoff runs down the runway with a gradual increase in speed up to a maximum of 85% of the takeoff speed. This test serves to validate the high speed handling qualities and braking capabilities of the aircraft at speeds approaching the takeoff speed. Takeoff and landing are the two most dangerous parts of any RPV flight, and accordingly, testing the high speed handling characteristics of the RPV on the runway can go a long way to reduce the overall risk of the flight.

As with the low speed taxi test, testing completed to date includes all of these maneuvers with the aircraft in manual mode (no stability augmentation provided by the autopilot). Future testing includes completing these maneuvers with stability augmentation active. Further details on the taxi testing, including the results of testing completed to date is presented in Section 7.7.

6.5.3.3 Phasing Flight Test

The final test in phase three testing is the maiden flight of the GSRPV. This test, known as a phasing flight test, is aimed at verifying the link between input, measurement and response. In other words, the pilot provides an input to the aircraft, the aircraft responds accordingly and the onboard instrumentation system measures that response. Establishing this correlation is the first step in an instrumentation system that can capture the required nonlinear response. This test was successfully completed on October 15th, 2011 and a description of the first flight is presented in Section 7.8.

The phasing flight test is a simple flight test; however, for completeness, the flight is decomposed into seven segments, as explained next, to illustrate the flow of this test as well as special considerations during each phase. During each phase of this test, aircraft attitude and control surface deflection data are be compared to pilot input to ensure that the aircraft is responding as expected to pilot input and the resulting control surface deflection. This test is considered a success if the aircraft achieves successful takeoff, climb, trim, descent and landing. The in-flight maneuvering tests are attempted only after the aircraft is trimmed, if the remaining fuel allows. The seven segments of the phasing flight test are presented below:

1. Takeoff

The pilot will accelerate the aircraft down the runway. The ground station operator will communicate current airspeed measurements to the pilot, and once takeoff speed (120% stall) is reached, the pilot will provide pitch-up input and the GSRPV will become airborne. The GSRPV, in the first flight configuration, had theoretical stall speed of 21.4 m/s and a takeoff speed of 25.6 m/s.

2. Climb

During the first flight of any RPV, the time immediately after the first takeoff is the riskiest portion of the flight, because the aircraft is not trimmed and the pilot is not familiar with the handling qualities. Accordingly, the pilot will gain altitude as quickly as possible to the test altitude to avoid problems caused by unexpected aircraft response at low altitude. The nominal test altitude is 550 ft to allow ample time for recovery in the event of unanticipated control response, but to stay within comfortable visual range for the pilot. The pilot will be free to climb at a comfortable rate of his choosing and the test altitude will be selected by the pilot during this

test as a "comfortable" altitude where visibility and aircraft referencing (assessing aircraft attitude) is acceptable, as long as the aircraft stays below the 700 ft ceiling for the flying site.

3. Trim

Once at altitude, the pilot will trim the aircraft to attain stable, controlled flight. The assistance of the backup pilot may be used, if necessary. Only after the aircraft is fully trimmed will the maneuvering tests begin.

4. Racetrack

The first pattern completed will be a level racetrack pattern. This test will evaluate the ability of the aircraft to make coordinated turns as well as fly "hands off" straight and level. The racetrack pattern will consist of the following 4 legs:

1. 1,500 ft straight line*
2. 180°, 750 ft constant radius turn
3. 1,500 ft straight line*
4. 180°, 750 ft constant radius turn

*A 1,500 ft. leg will take approximately 16 seconds at the test point speed of 56 knots and 9.3 seconds at an average cruise speed of 95 knots and 7.1 seconds at a fast cruise speed of 125 knots.

5. Figure 8

The Figure 8 maneuver will consist of a 750 ft constant radius turn to the left immediately followed by a 750 ft constant radius turn to the right. This test will evaluate the ability of the aircraft to smoothly transition from one turn immediately into another.

6. Landing Configuration Handling Evaluation

With all required maneuvering tests complete, if flight time remains for additional testing, the pilot will fly the aircraft on a "mock" approach to test the handling with the flaps extended. This will require the pilot to line up the GSRPV for landing, reduce power and apply the flaps. Approximately 50% of the way through the approach, the pilot will apply power, retract the flaps and climb back to the test altitude out. At no time during this test will the aircraft come lower than 250 ft above the ground, and earlier tests will take place at higher altitudes.

7. Landing

With all required testing complete, the pilot will safely land the aircraft on the runway. Care will be taken to keep the airspeed well above the stall speed throughout the entire approach and landing to avoid poor handling at low flight speeds. The aircraft is designed with tricycle landing gear with a steerable nose gear, which is controlled via the yaw control channel while on the ground. The brakes will be applied after touchdown to slow the aircraft to a stop.

6.5.3.4 Planned Advanced Flight Tests

This final subsection outlines three advanced flight maneuvers that are planned for follow on flight efforts, paving the way for the success of the Aeroelastic Response Program and the flight test of the Aeroelastically Scaled RPV.

The first advanced flight test will investigate the dynamic stability of the aircraft with the primary focus on the Phugoid Mode and the Dutch Roll Mode. Vortex lattice analysis completed at Quaternion Engineering has shown that both the Phugoid Mode and the Dutch Roll Mode are marginally stable, and this test will serve to verify these results. This test will include using control doublets to excite the Phugoid Mode and the Dutch Roll mode and measuring the period of the resulting oscillations. The period can then be used to calculate the natural frequency. The Piccolo II has the capability to execute pre-programmed doublets of user defined lag times; however, preliminary tests will use manual doublet inputs for safety. The magnitude of the inputs and the dwell time of the doublets will start with half deflection and a dwell time of 1 second.

The second advanced flight test will aim to demonstrate safe flight at the scaled test point. Preliminary testing, as described above, will take place at a takeoff weight significantly below the test point. This flight will mirror that of the Phasing Test, but trimming weights will be added to the trimming weight bays in the wings and fuselage to gradually increase the weight of the aircraft to the test point. The final goal of this test is to achieve a safe flight at the scaled test point weight. Ballast weight will be added incrementally, while still maintaining the appropriate CG location and moments of inertia. The increments in which the weight will be added will be determined during a second bifilar pendulum test aimed at tuning the moments of inertia to match the full scale aircraft. During each flight, the overall performance of the aircraft will be evaluated by the pilot. Prior to adding more ballast weight, the pilot, test director and

ground controller will evaluate the performance of the aircraft and determine whether it is safe to continue adding ballast weight. If at any time during these flights the aircraft displays unexpected or undesired flight handling characteristics or is unable to climb at the desired gradient due to the added weight, the pilot will land the aircraft as quickly as safely possible and discontinue this test.

The final advanced flight test in the Flight Demonstration FTP will lay the groundwork for the Aeroelastic Response Program and the flight test of the Aeroelastically Scaled RPVby determining the flight test maneuver (or maneuvers) which achieve the required loading on the aft wing to excite the nonlinear aeroelastic response while minimizing risk. This test allows the pilot to try three maneuvers that can generate the required loading: an upwind turn, a push-over pull-up and a windup turn. These maneuvers each present a unique method of reaching the required wing loading. An upwind turn is a simple maneuver where the pilot will fly the aircraft into the wind and then complete a 180° turn. The turn, coupled with the wind speed will produce a high wing loading. This is the simplest maneuver, but it can only be completed once during each flight "lap" and it only accomplishes positive loadings. The push-over pull-up requires the pilot to put the aircraft into a controlled dive and then pull-up, causing the aircraft to encounter positive loading at the bottom of the maneuver and negative loading at the top of the maneuver. The ability to achieve negative loading is useful, but putting the aircraft in a dive at the low altitudes required by a remotely controlled pilot (for visual reference) is a risky maneuver. Finally, the windup turn is when the pilot maintains constant speed and flys the aircraft through a spiral pattern. As the radius of the turn decreases, the wing loading increases. This approach allows for a gradual increase in wing loading, but again it can only accomplish positive loadings. Initial testing will take place unballasted, but follow in tests will gradually increase the weight to the scaled test point.

6.6 Formal Review Process

The final step in the flight test plan design methodology that is presented in Section 6.1 is to ensure that all formal requirements (federal, international, project management, flying site, etc.) are met and followed. To accomplish this for the JWSC, there was a five step process that was required by the AFRL to receive full clearance to fly the JWSC GSRPV. These steps included an internal/external flight test document self-review, a technical review board (TRB), a

safety review board (SRB), application for and receipt of a special flight operations certificate (SFOC) and finally application for and receipt of a military flight release (MFR). The governing document for this process is ARLFMAN 99-103 Flight Test and Evaluation, the AFRL document governing planning and conducting flight test and associated ground tests as part of AFRL programs[20]. This manual was used as the governing document for the development and formal review of the JWSC flight test plan.

The first step required to receive full clearance to fly the GSRPV was to finish the formal flight test documentation, including a description of all testing described previously as well as a detailed overview of all test logistics (flying site, airspace, personnel, go/no-go criteria, etc.), test procedures and safety protocols. Details on these items are presented in Appendix A Sections 4, 5 and 6 respectively. The first draft of the Flight Test Plan was complete on December 21st, 2010.

Upon the completion of the formal Flight Test Plan document, the first formal review board, the TRB, was scheduled for March 24th, 2011. AFRLMAN 99-103 states that the technical review process is:

> The formal review and documentation to ensure a thorough assessment of the test plan for technical soundness and adequacy. The technical review will verify the overall method of test is adequate to evaluate the requirements and verify that objectives can be met with acceptable technical risk.

The technical review process is to be completed by, "an independent group of knowledgeable individuals convened to ensure a thorough assessment of the test plan for technical soundness at adequacy."[20]

The TRB meeting consisted of a two and a half hour presentation, followed by 90 minutes of questions. These questions led to an extensive review of the flight test plan, incorporating large changes in technical scope and approach. Following the completion of all required modifications, a follow-up TRB meeting was scheduled to address these questions. The follow up TRB meeting was completed on May 10th, 2011. This meeting consisted of a 90 minute presentation and an accompanying question and answer session. After the completion of this meeting, a second round of changes was made to the document. After nearly six months formal review and extensive modifications to the test plan, TRB approval was received on June 15th, 2011.

With the TRB complete, the second formal review board, the SRB, was scheduled for July 5th, 2011. AFRLMAN 99-103 states that the safety review process is:

> The formal review and documentation of test safety planning of a flight test and associated ground test by the independent safety reviewing authority. The outcome of the safety review is an approved test plan and assessment of the overall test risk. The process consists of two parts – the safety review and the test approval.

The safety review process is to be completed by "an independent group of knowledgeable individuals convened to review the test plan, ensure test hazards are identified, eliminated, or minimized, and recommend the overall risk level to the TAA," where TAA is the test approval authority. [20]

Analagous to the TRB meeting, the SRB meetings consisted of a two and a half hour presentation, followed by 90 minutes of questions which covered all aspects of the flight test program from a safety perspective. Again, these questions led to an extensive review process for the flight test plan; however, the scope of the TRB already completed incorporated many changes that would normally be covered by the SRB. Accordingly, the SRB review process did not take nearly as long. At the completion of the SRB process, the JWSC GSRPV Flight Test was given a Low-Medium Risk Level, and the test plan was sent to Dr. Kenneth Barker, the ARFL designated technical authority and TAA for the JWSC GSRPV flight test.

The final step required before Dr. Barker would issue final approval was the application for and receipt of the Transport Canada Special Flight Operations Certificate (SFOC). An SFOC is the documentation required to legally operate an unmanned aircraft in Canadian airspace. Transport Canada notes that, "Section 602.41 of the CARs* states, no person shall operate an unmanned air vehicle in flight except in accordance with a Special Flight Operation Certificate (SFOC)." Furthermore, an "SFOC is intended to ensure the safety of the public and protection of other users of the airspace during the operation of the unmanned air vehicle.[21]" Jenner Richards of Quaternion Engineering completed the required documentation, applied for and received an SFOC dated June 16th, 2011. The complete SFOC is available for reference in Appendix O of the Flight Test Plan presented in Appendix A.

---

* Canadian Aviation Regulations

Following the completion of the TRB, SRB and receipt of the SFOC, AFRL program manager Ned Lindsley met with Dr. Kenneth Barker and final approval, including the presentation of the formal MFR was complete on July 29th, 2011. The formal MFR document is presented in Appendix B for reference. The receipt of this document gave the JWSC flight test team full clearance to complete flight operations and represented the culmination of nearly seven and a half months of formal review.

7 Testing Procedures and Results

This section presents detailed procedural explanations and results of all testing complete at the time this thesis was written. Each subsection presents a separate testing effort.

7.1 Air Data Boom Calibration

As described in Section 5.5, three custom air data boom fabricated at Virginia Tech and calibrated at in Virginia Tech's Open Jet Wind Tunnel. This section describes the experimental procedure and presents the results of the calibration.

7.1.1 Test Apparatus

The open-jet wind tunnel is a blower type, open circuit design powered by a 30hp BC-SW Size 365 Twin City centrifugal fan. Flow speed is controlled by a General Electric AF-600 variable frequency drive which commands fan speeds up to 1180RPM. Coupled with the 5.5:1 contraction ratio to the test section, this produces a maximum test section flow speed of 30 m/s. Once exiting the test section, the flow encounters a stack diffuser 1.2m aft of the nozzle which diffuses the air into the room.[22]

To complete testing, Grant Parrish designed and fabricated a custom mount to support each air data boom within the test section and allow simultaneous variation of the angle of attack, α, and sideslip angle, β. Figure 26 presents the mount, both alone and as mounted in the tunnel.

Figure 26 - Custom Mount for Air Data Boom Testing (modified from Ref. 23)
Used under fair use guidelines, 2011.

The custom mount featured a circular board that was free to rotate on top of a second board that was rigidly mounted to a steel cross member in the test section of the open-jet wing tunnel. The cross member was supported in the wind tunnel by two aluminum clamps that could be loosened, allowing variation in angle of attack. The circular board on which the air data boom was mounted featured locking pins that could be used to rotate the circular board in 5° increments from -25° to +25°. This setup allowed simultaneous variation in angle of attack and sideslip angle.

Angle of attack measurements were made prior to each test run using a Mitotoyo Pro 360 digital inclinometer. The Mitotoyo Pro has a resolution of 0.1° and an accuracy of ±0.1°.[24] The sideslip angle measurements were calibrated using the custom mount prior to testing. To calibrate, the mount was placed in a vertical orientation and the Mitotoyo Pro 360 was used to measure the exact sideslip angle that corresponded to each locking pin location. Table 7 presents the results of the mount calibration for sideslip angle. Analog to digital conversion of the analog output from each potentiometer was completed using an ArduPilot Mega which provides 10-bit ADC capability.

Table 7 - Sideslip Measurement Calibration

Nominal Angle	Measurement 1	Measurement 2	Average
20.0°	20.3°	20.2°	**20.25**°
15.0°	15.6°	15.4°	**15.50**°
10.0°	10.4°	10.4°	**10.40**°
5.0°	5.4°	5.6°	**5.50**°
0.0°	0.2°	0.1°	**0.15**°
-5.0°	-4.8°	-5.0°	**-4.90**°
-10.0°	-10.1°	-9.9°	**-10.00**°
-15.0°	-14.6°	-15.1°	**-14.85**°
-20.0°	-19.7°	-19.8°	**-19.75**°

7.1.2 Test Procedure

The full test procedure involved the calibration of three air data booms over four days of wind tunnel testing. Each air data unit was individually calibrated at 36 test point combinations of angle of attack and sideslip angle, at four flow speeds for each combination. The flow speeds tested corresponded to 200 RPM increments over the full range of the tunnel. Figure 27 presents a visual representation of all angle combinations tested, where the green blocks represents angle combinations tested and the white blocks represent angle combinations not tested. Table 8 presents the average flow speeds tested, calculated using dynamic pressure measurements from a Pitot-static tube built into the Open Jet Wind Tunnel Traverse averaged over two days of testing.

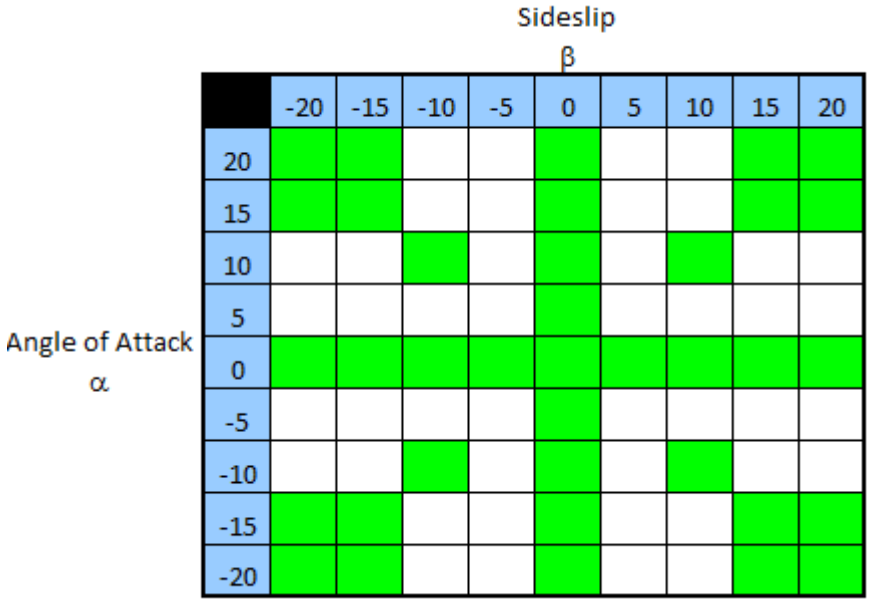

Figure 27 - Air Data Boom Calibration Angles

Table 8 – Average Flow Speed Range Tested

RPM	**600**	**800**	**1000**	**1180**
Flow Speed (m/s)	12.6	17.1	21.3	25.2
Flow Speed (knots)	24.5	33.2	41.5	49.0

For each test point, 10 seconds of continuous data was recorded at 10 Hz, and the average measurement from the 100 resulting data for each speed points was taken as the final

measurement. Testing was completed in three "sweeps" for each boom. The first sweep held sideslip angle constant at 0° and varied angle of attack. The second sweep held angle of attack constant at 0° and varied sideslip angle. The third and final sweep contained the other data points, starting at +20° angle of attack, hitting all of the required sideslip angles and then decreasing 5° in angle of attack, until all required angle combinations were tested. Over the course of four days of testing, 43,200 measurements were post processed to produce 144 calibration points for each of the three air data booms.

7.1.3 Results

Figure 28, Figure 29 and Figure 30 present plots of the potentiometer reading for each vane angle, across the range of flight speeds for Boom 1. The plots for Boom 2 and Boom 3 are nearly identical, so they are not presented here. Each plot corresponds to one of the sweeps explained above, and all flow speeds are represented.

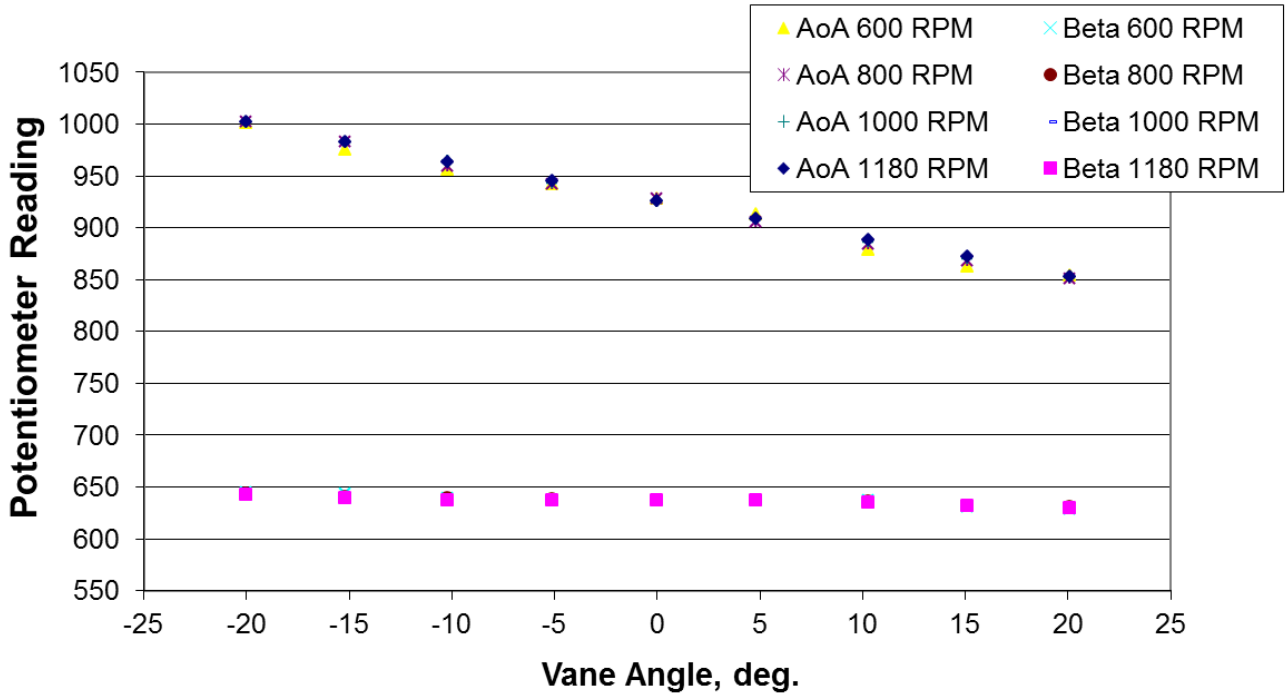

Figure 28 – Boom 1, Sweep1: Variation in Angle of Attack with Constant Sideslip Angle

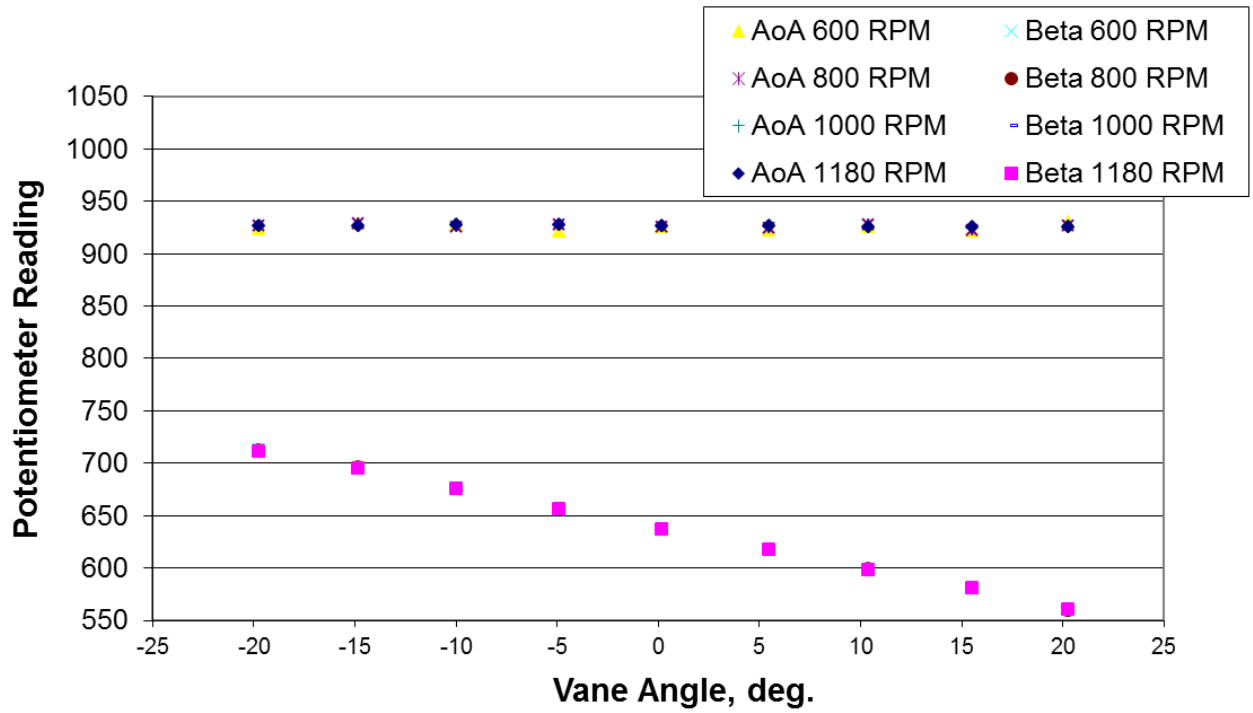

Figure 29 - Boom 1, Sweep2: Variation in Sideslip with Constant Angle Angle of Attack

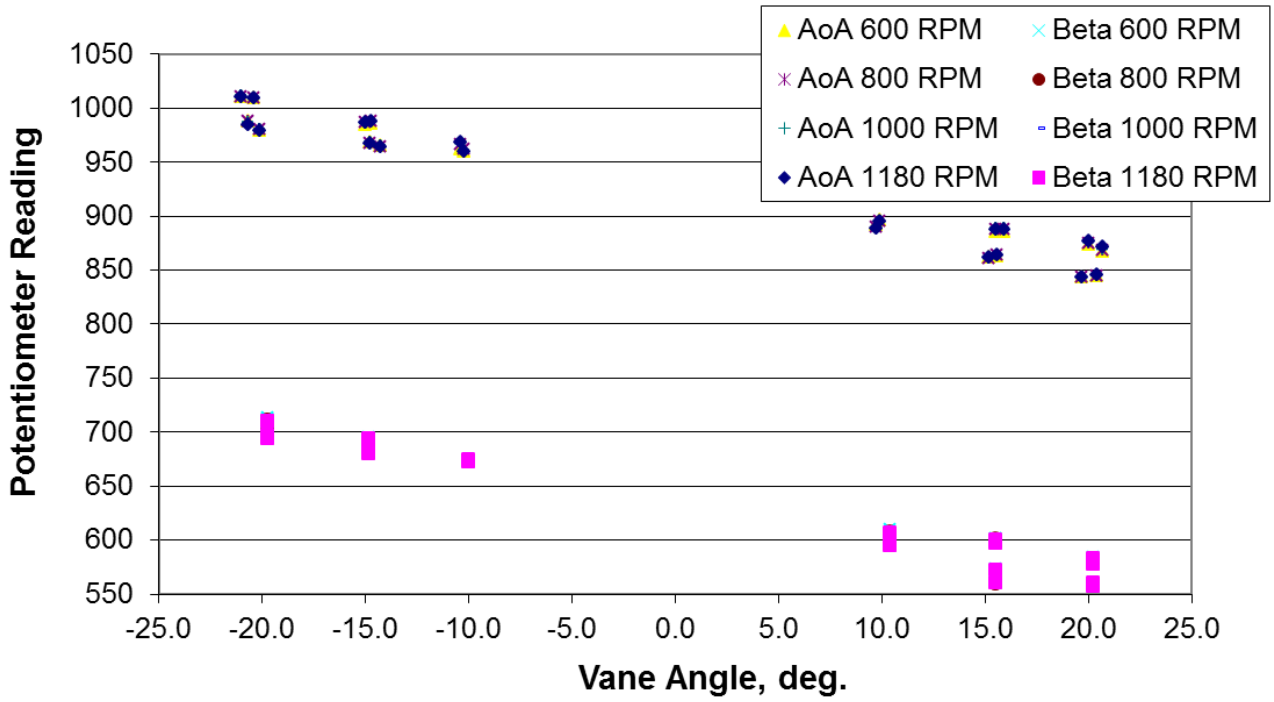

Figure 30 - Boom 1, Sweep3: Remaining Calibration Angles

From Figure 28, Figure 29 and Figure 30, it can be seen that the readings are nearly constant with variation in flow speed. This is an important result and characteristic of any air data boom. The small variation that is present occurs at the slowest flow speed, and this is acceptable as 24.5 knots is well below the stall speed of the JWSC GSRPV.

Combining the data from all three sweeps into a single plot forms a full calibration curve for each air data boom. Figure 31 presents the calibration curve for Boom 1, along with a linear regression fit through each data series.

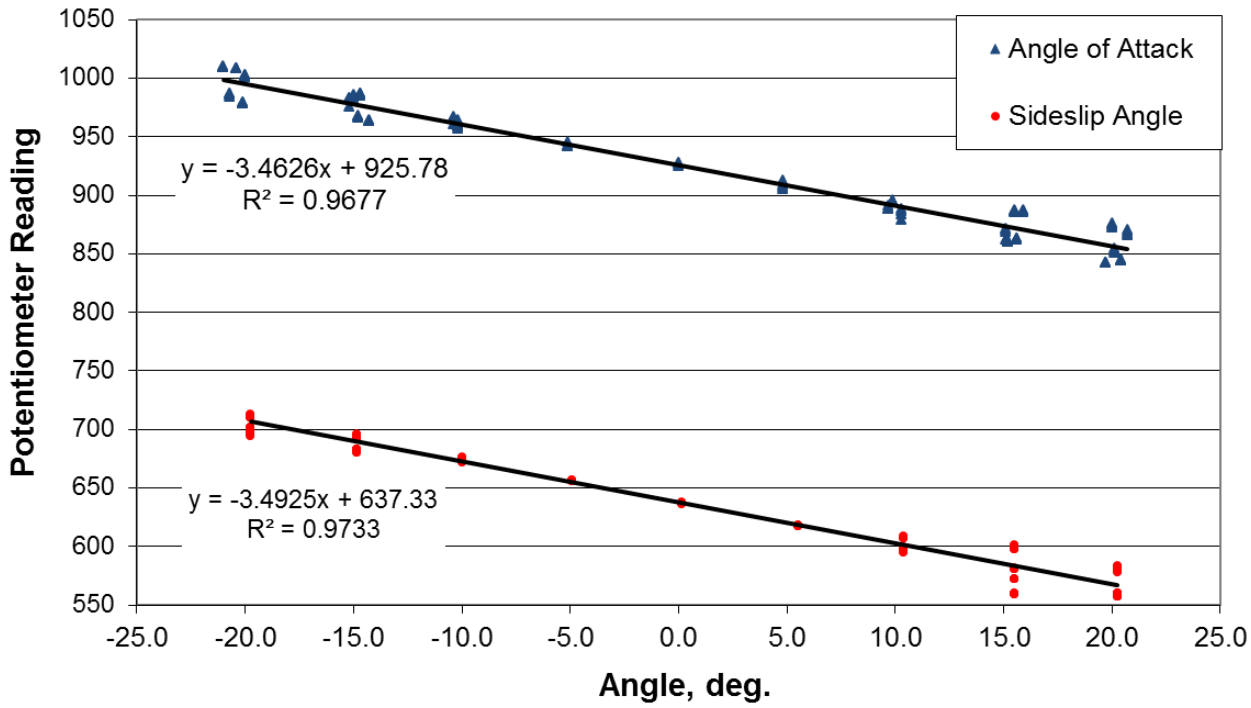

Figure 31 - Full Calibration Curve, Boom 1

From Figure 31, it can be seen that for both angle of attack and sideslip angle, the largest spread in the data occurs at ±15° and ±20° for both the sideslip angle and angle of attack. This spread in the data is most likely caused by flow effects due to the boom itself (separated flow in the wake of the boom) or due to the proximity of the vanes to the edges of the open test section at the larger angles. Much like flow around a circular cylinder, the wake behind the boom could be causing turbulent flow which is causing variations in the measurement at large angles. Within -10° to 10° the data shows excellent linearity with nearly no appreciable spread.

This full calibration curve could be used to correlate in-flight potentiometer measurements to angle of attack and sideslip angle measurements. In the opinion of the author,

this calibration curve is sufficient for preliminary flight testing and validation of the air data boom design; however, further calibration is required to more accurately capture the effects at larger angles of attack and sideslip angles. Preliminary analysis has shown that the spread of the data is not random, but rather the spread above or below the linear trend line can be predicted. Four calibration curves could be generated to capture the nature of the data within each quadrant of the matrix presented in Figure 27. This calibration was not completed at the time this thesis was written because it was decided not to fly the air data boom on the JWSC GSRPV, and accordingly, this calibration is left for future work.

The same conclusions apply to the calibration curves for Boom 2 and Boom 3, presented in Figure 32 and Figure 33, respectively.

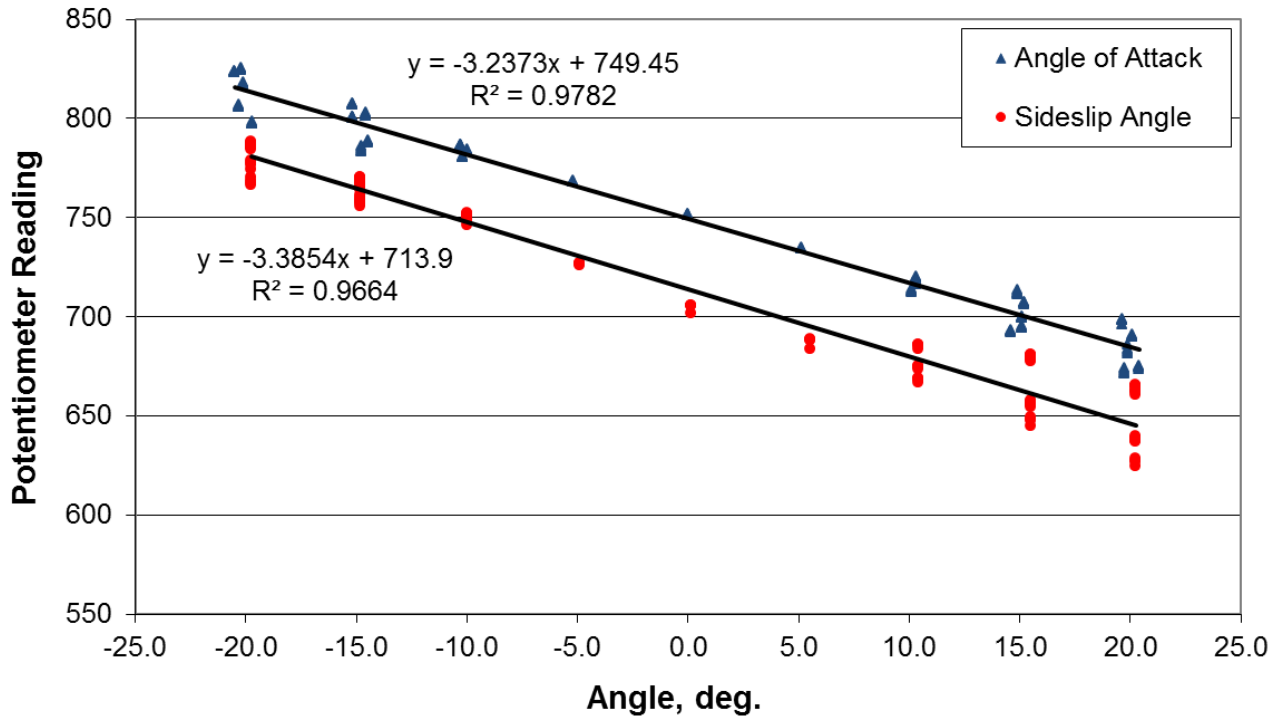

Figure 32 - Full Calibration Curve, Boom 2

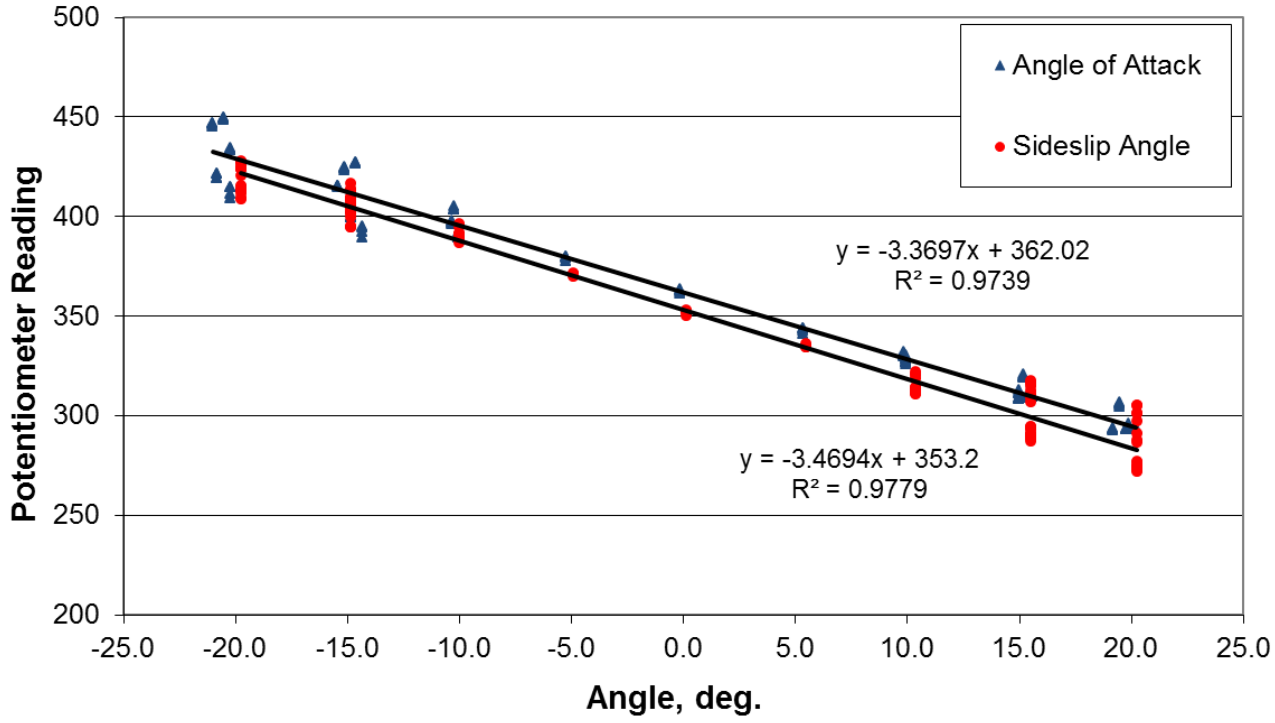

Figure 33 - Full Calibration Curve, Boom 3

7.1.4 Conclusions

In summary, a series of three low-cost air data booms have been developed, fabricated and calibrated at Virginia Tech for use on JWSC RPVs. Post processing of the wind tunnel data has shown that between angles of attack and side slip angles of -10° to 10° the data shows excellent linearity with nearly no appreciable spread; however, at larger angles, spread was introduced into the data reducing the accuracy of a linear calibration. Preliminary analysis into the sources of these errors have shown that the spread at larger angles is not random, but rather can be predicted to fall above or below the linear calibration line if the angle of attack and sideslip angle are known. Further calibration is required to fully capture these effects, but no further calibration testing is required due to the large volume of calibration data available and the acceptable R^2 values.

7.2 Instrumentation System Bench Testing

This section details the bench testing of both the accelerometer and strain gage systems. During bench testing, each microcontroller was programmed individually and then the complete system was tested. Preliminary testing was used to ensure that each microcontroller was capable

of logging data, as designed, on the Logomatic V2 Data Loggers. The complete accelerometer system was tested; however, for ease of testing, rotational potentiometers were used in place of the strain gages. A required success criteria of 30 seconds (1200 independent data points) of continuous data without any data logging errors was met.

With both systems independently functional, the synchronization system was tested by including the onboard timing on the accelerometer microcontroller and linking the two microcontrollers together. This test verified that the strain gage system was dependent on the timing on board of the accelerometer microcontroller if the link between the two microcontrollers was broken, the strain gage microcontroller stopped logging data. Additionally, this test verified that the data from both microcontrollers was synchronized. Several data logging test runs of 30 minutes (72,000 independent data points) produced data streams with a maximum discrepancy of less than 0.5 seconds (20 data points), which was deemed acceptable for a low-cost exploratory system. This corresponds to a relative error of 0.028% between both data streams.

A final test investigated the consistency in the regulated voltage output by the power system developed for the instrumentation system. The aim of this test was to investigate the voltage output from the 3.3V and 5V voltage regulators as the instrumentation system battery voltage and capacity was decreased. A HobbyKing battery tester was used to measure the remaining battery capacity and a multimeter was used to measure the voltage output from each voltage regulator. In between collection of each data point, a small DC motor was used to drain the battery. Figure 34 presents the results of this test, with a smooth line fit through the data to make it easier to see the trends in the data.

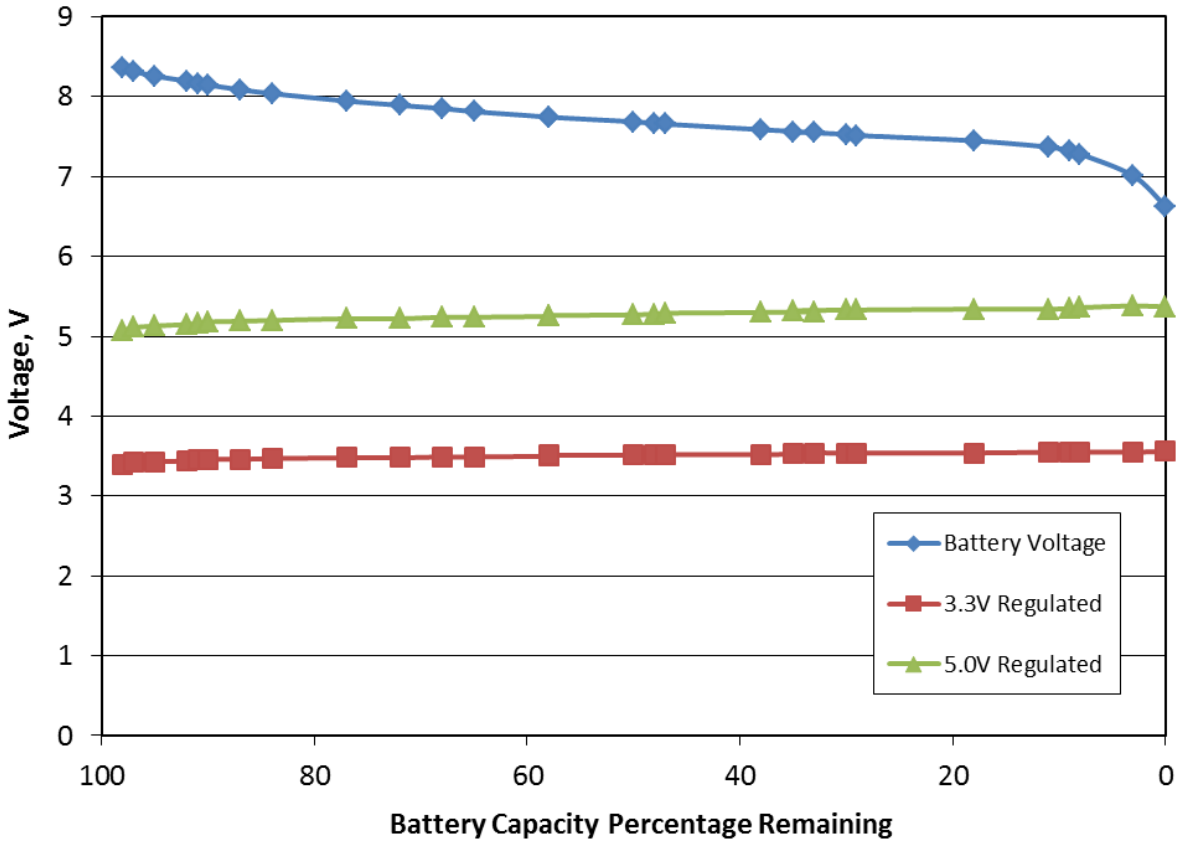

Figure 34 - Regulated Voltage Output Test Results

From this test, it can be seen that the voltage from the 5V and 3.3V voltage regulators actually increases slightly as the supply battery is discharged. The voltage output from the 5V voltage regulator varies from 5.07V to 5.37V, a relative change of 6% and the voltage output from the 3.3V voltage regulator varied from 3.39V to 3.56V, a relative change of 5.15%.

These changes in output introduce error into the final output from the microcontroller for both the strain gages and accelerometers. For the accelerometers, the ADC procedure completed by the microcontroller includes the discretization of the supply voltage of the microcontroller into 4096 steps (for 12-bit conversion). The voltage output from each accelerometer (on each axis) is then correlated to one of the steps within this range. The calibration of the accelerometer system, as described above in Section 5.1.1, established a 0g center point and a 1g level for each accelerometer as relative positions within this range. If the supply voltage to the microcontroller changes, the magnitude of each step within the 4096 step range changes, and as such, the accuracy of the calibration is diminished. Similarly, the accuracy of strain gage system is

dependent on a highly accurate excitation voltage. If the supply voltage to the INA125 changes during a test, the bridge is taken slightly out of balance introducing error into the output. In order to remove these errors, future instrumentation systems could use higher accuracy voltage converters to ensure smaller supply voltage fluctuation to each microcontroller providing more consistent results.

7.3 Static Thrust Test

In order to verify the manufacturer's specified performance parameters for the JetCat P-200SX turbine engines, bench top static thrust testing of the engines was performed. This section presents the test apparatus, test procedure and results of this test as performed for both of the GSRPV JetCat P-200SX engines.

7.3.1 Test Apparatus

To complete static thrust testing, a custom test apparatus was fabricated to measure the thrust. Figure 35 presents a picture of the apparatus before testing.

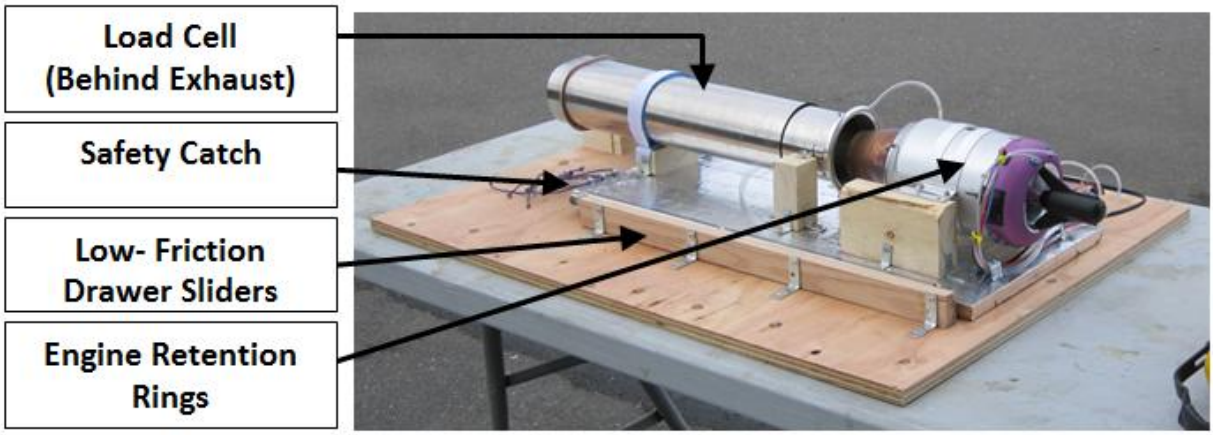

Figure 35 - Static Thrust Test Apparatus

The static thrust test apparatus consisted of a plywood board on which the engine and exhaust tube were mounted. The turbine was held in place by the manufacturer provided aluminum engine retention rings on sections of 2x4 mounted to the plywood board. The exhaust tube was supported by wood blocks at the forward mounting points and by a Velcro strap at the rear to prevent vibration. Two heavy duty filing cabinet drawer sliders were used to provide a sliding, low-friction connection to the large base. Thrust was measured by Chatillon DFIS-50

load cell mounted to the sliding board and the stationary base. The DFIS-50 features a maximum rated load of 50lbs and has a resolution of 0.05lbs. The drawer sliders featured a hard stop at the forward end and a safety catch was made by looping high tensile strength cord through eye hooks on the sliding board and on the base. Both of these provided a measure of safety in the event that the load cell failed, to prevent the plywood board from being propelled forward by the engine. All fuel lines and electrical power lines were secured to the sliding board using u-shaped, screw down retainers. Finally, the entire sliding board was covered in foil tape to prevent thermal damage.

The engine was controlled by a standard radio controlled transmitter and receiver to provide the throttle command to the turbine. The JetCat P200-SX Electronic Control Unit (ECU) and the Ground Support Unit (GSU) were used to ensure reliable operation of the turbine engine. The JetCat Jet-tronic ECU provides real-time closed-loop control of the turbine, resulting in better starts, smoother idle and more reliable performance. The ECU, which features a Hitachi H8 16-bit microcontroller, has a fully automatic starting sequence, which promotes safe, reliable starts. The ECU also monitors turbine RPM and exhaust gas temperature (EGT) during operation via sensors in the turbine. The GSU was used for monitoring key parameters such as maximum RPM and minimum RPM, in real time, during startup and ground testing. To provide more robust measurement (and a better graphical user interface), the GSU was connected to a laptop running JetCat Jet-tronic software via a manufacturer provided connection USB cable.

7.3.2 Test Procedure

Testing was completed by two operators. The first operator controlled the functionality of the engine and took thrust readings from the load cell. The second operator took readings of throttle position, throttle pulse width, EGT and fuel consumption from the laptop computer. Testing took place over the course of three days, with the majority of testing taking place on the third day. For each engine, four throttle sweeps were completed by varying the throttle from either 0% to 100% or from 100% to 0%. Both directions were included for each engine to capture the effects of thermal soaking of the exhaust tube. All data was compared to benchmark data from an AFRL test, independent of this effort, that took place on October 26th and 29th, 2009.

7.3.3 Results

Results are presented below with the data from all static thrust testing. These results represent a summary of the testing of three different turbines on five different days. This includes two AFRL runs and nine JWSC runs. All data is presented together to show the excellent correlation of the data.

Figure 36 presents a plot of thrust vs. turbine RPM, including a third order polynomial curve fit through the data.

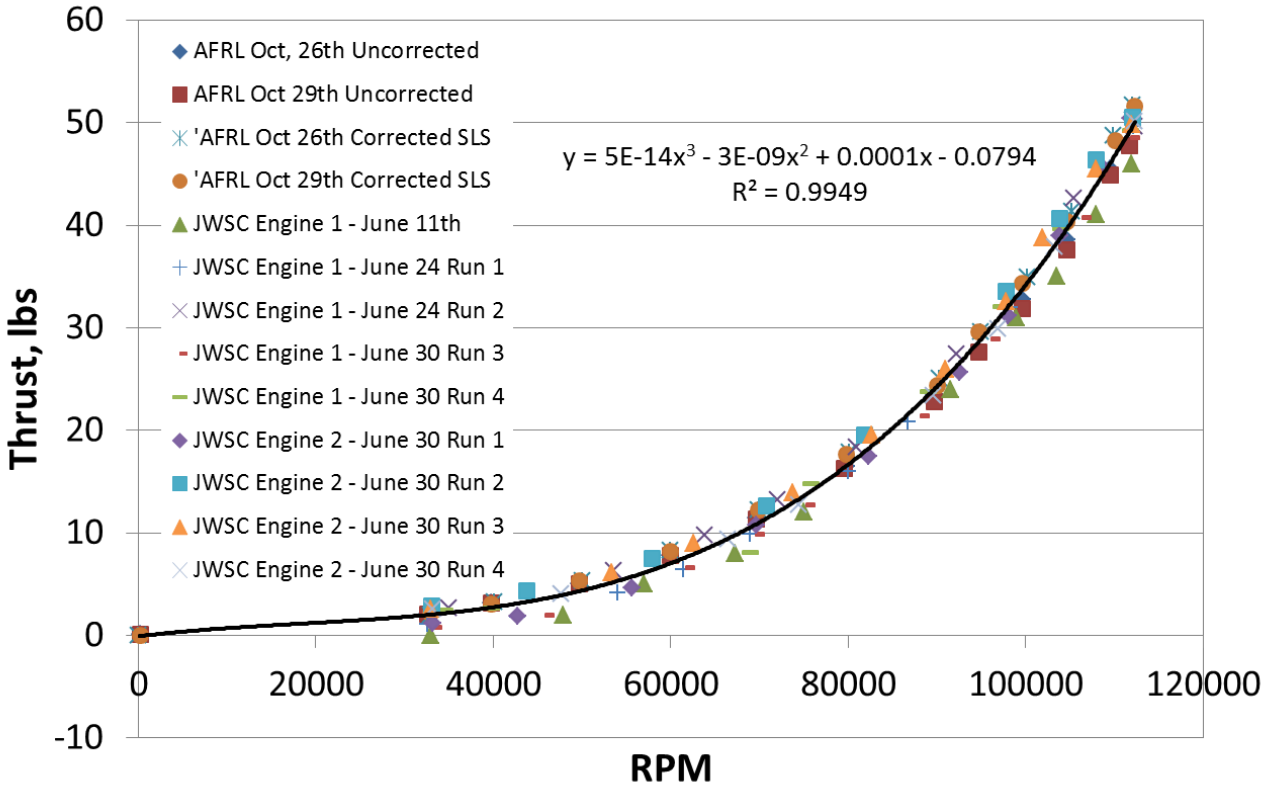

Figure 36 - JetCat P200-SX Thrust vs. RPM

One key takeaway from Figure 36 is that the manufacturer specified maximum thrust of 50 lbs is nearly met. The average maximum thrust from all nine JWSC runs was 49.3 lbs with a maximum recorded thrust of 50.5 lbs. The most important result from this plot is the repeatability of the data. Above approximately 15 lbs thrust, the data points lie nearly on top of one another, promoting both the reliability of the JetCat ECUs, as well as the performance of the turbine engines. Despite testing three separate engines on different test days in different locations, the thrust vs. RPM curves for all of the engines are nearly identical. The small spread

present at the lower end of the curve was most likely caused by the small amount of friction present in the test apparatus.

Figure 37 presents a plot of exhaust gas temperature vs engine RPM as measured by a thermocouple embedded in the exhaust cone on the turbine, along with a third order polynomial curve fit through the data.

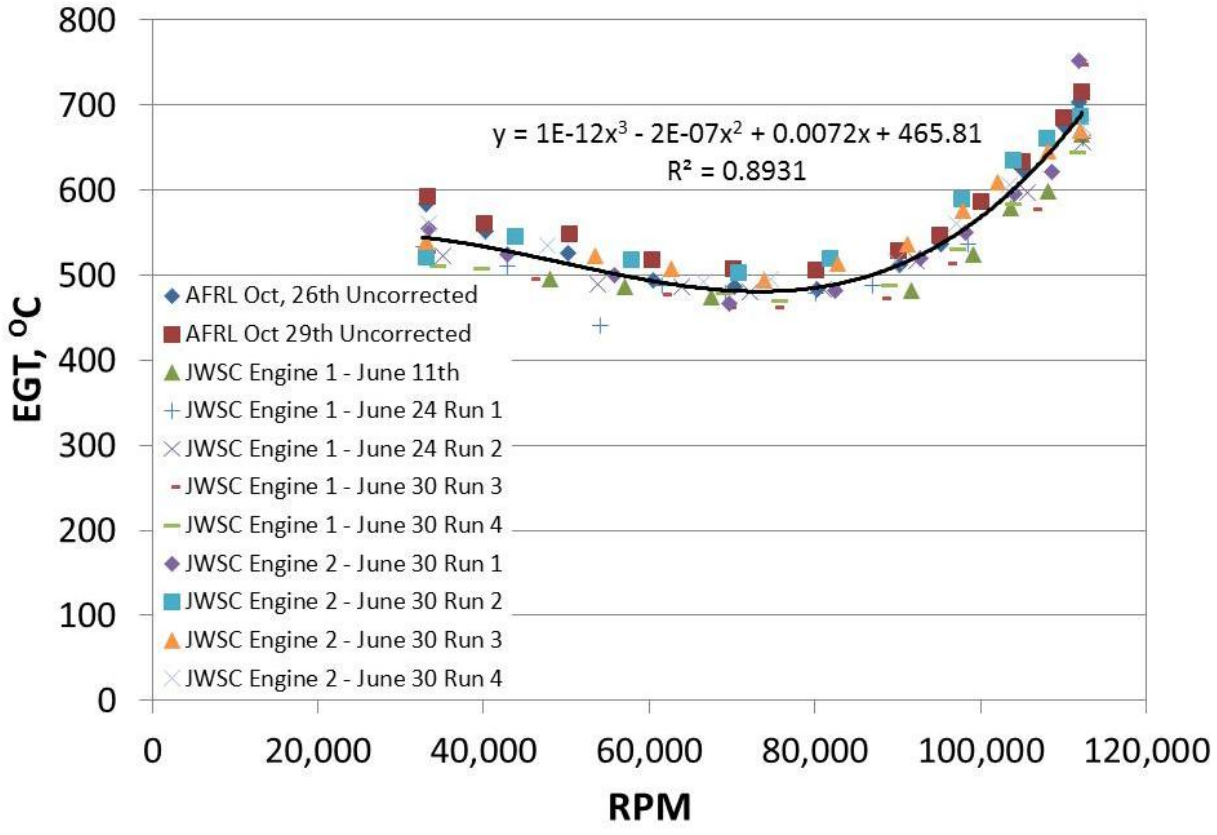

Figure 37 - JetCat P200-SX Exhaust Gas Temperature vs. RPM

The data in Figure 37 shows that from approximately 25,000 RPM to approximately 75,000 RPM, the exhaust gas temperature actually decreases with increasing RPM. Upon initial inspection, this result may seem surprising; however, the JWSC GSRPV Pilot, Kelly Williams, who has over 15 years of experience flying and operating small scale turbine engines, explained that the parabolic shape is due to the increasing effect of convective cooling as the RPM (and corresponding exhaust gas speed) increases. As the engine starts operating, the exhaust gas temperature decreases with increasing RPM because the flow speed is increasing, causing convective cooling of the exhaust cone. At approximately 75,000 RPM, the exhaust gas

temperature is at the minimum point. From here, the exhaust gas temperature increases as RPM increases because the large amounts of fuel being burned generates too much thermal energy for the convective cooling of the exhaust cone to overcome. This parabolic shape is a design property of the small scale turbine engines and is beneficial as the majority of turbine operation during flight takes place in the mid RPM band where exhaust gas temperature is the lowest.

As with the thrust vs. RPM plot, the data in the EGT vs. RPM is extremely repeatable; however, a bit more spread is present. This spread was caused by the alternating direction of throttle travel during turbine runs. On runs where the throttle was increased, the high RPM temperature is higher because the exhaust cone is being heated during the entire run. Similarly, on runs where the throttle was decreased, the low RPM temperature is higher. In summary, the temperature was always highest at the end of each perspective run relative to a similar run in the opposite direction of throttle travel.

The final results from the static thrust test, fuel consumption vs. RPM, is presented in Figure 38. This data represents a statistical computation completed by the JetCat Jet-tronic ECU based on empirical data and measured fuel pump voltage (RPM).

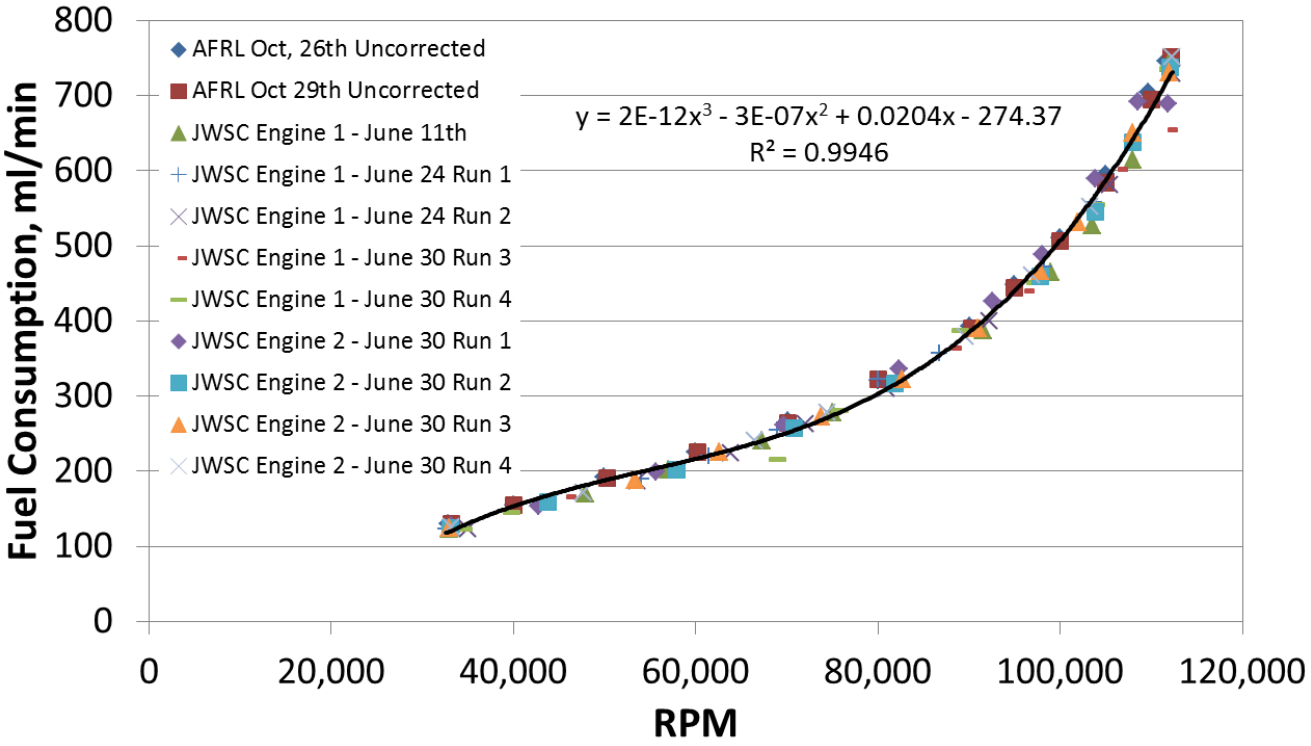

Figure 38 - JetCat P200-SX Fuel Consumption vs. RPM

This plot shows that for turbine rotational speeds up to approximately 90,000 RPM, fuel consumption is nearly linearly dependent on RPM. From there, an exponential trend takes over with the fuel consumption nearly doubling during the last approximately 25,000 RPM.

7.3.4 Conclusions

The static thrust testing of the JetCat P200-SX engines provided insight into the performance of the turbine engines. Testing was completed over three days on two separate turbine engines. The data collected was compared to AFRL reference data from an independent effort. All data showed excellent correlation across the entire operational range of the engine. Additionally, the manufacturer's specified maximum thrust performance was matched. This testing promoted the safety and reliability of the JetCat P-200SX turbine engines. This reliability is primarily afforded by the closed-loop control of the turbine by the Jet-tronic ECU.

7.4 Installed Static Thrust Test

As a follow on to the static thrust test, an installed static thrust test was completed by Quaternion Engineering to verify the performance of the engines as installed in the aircraft. All data and pictures presented in this section are reproduced with permission of Jenner Richards of Quaternion Engineering.

7.4.1 Test Apparatus

In order to complete installed static thrust testing, a custom apparatus needed to be built to reduce the magnitude of the measured thrust by 50%. The reason for this required reduction is that the load cell used for the static thrust testing is only rated up to a maximum load of 50lbs and installed static thrust testing required the measurement of thrust up to a theoretical maximum of 100 lbs. To accomplish this aim, a hinged test apparatus was constructed. Figure 39 presents a picture of the installed static thrust test apparatus fabricated by Jenner Richards of Quaternion Engineering.

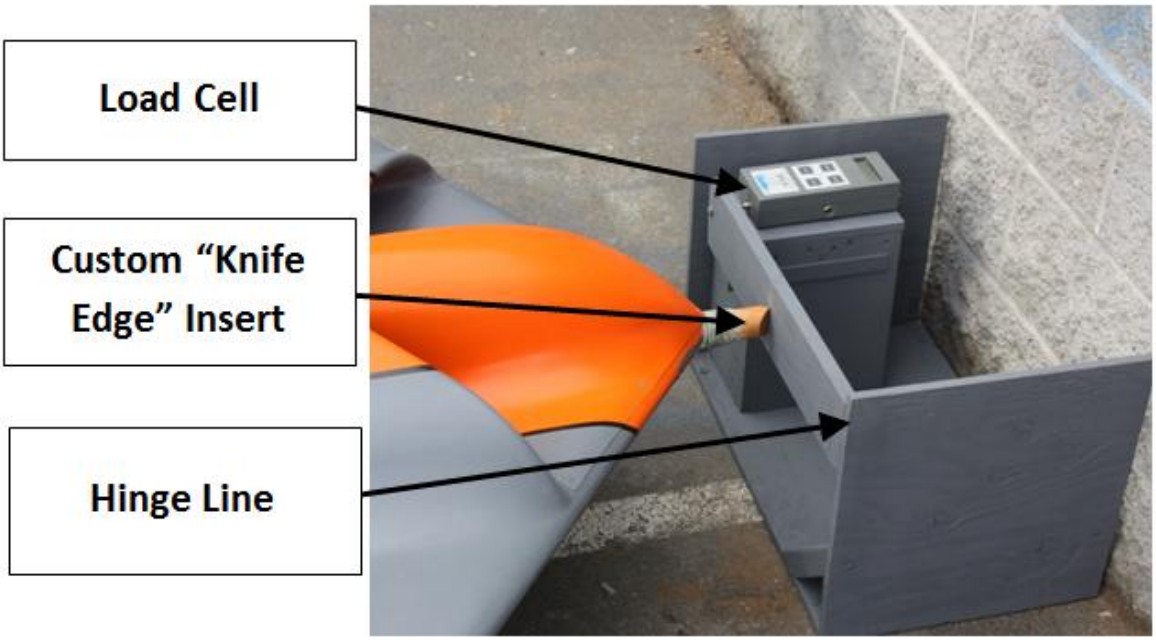

Figure 39 - Installed Static Thrust Test Rig

This apparatus consists of a wooden frame with a hinged beam across the front. The beam is supported on one end by the hinge and on the other by the load cell. If a load is placed on the midspan centerline of the beam, this dual support mechanism evenly distributes the load between the hinge line and the load cell. As such, a 100lb force applied at the midspan centerline of the beam results in a 50lb force on the load cell. To verify the design, the apparatus was inverted and nine loads ranging from 2.00kg to 20.50kg were applied, and the resulting measurements were compared to the expected 50% value. The maximum error for all of the runs was 2.13%, which was deemed acceptable for this effort. The data from these tests is presented below in Table 9.

Table 9 – Installed Static Thrust Test Apparatus Design Validation Test Data

Load (Kg)	Reading (Kg)	Expected (Kg)	Error (%)
2.00	1.02	1.00	2.00%
4.70	2.30	2.35	2.13%
6.70	3.32	3.35	0.90%
9.35	4.62	4.675	1.18%
11.35	5.64	5.675	0.62%
13.50	6.74	6.75	0.15%
15.50	7.72	7.75	0.39%
18.50	9.12	9.25	1.41%
20.50	10.10	10.25	1.46%

To complete testing, a custom "knife edge" insert was made for the front of the JWSC GSRPV to concentrate the thrust force on the centerline of the beam.

7.4.2 Test Procedure

The installed static thrust testing procedure mirrored that of the static thrust test with the exception that only two runs were completed. Throttle percentage, throttle command (pulse width), EGT, fuel flow rate, and RPM were all recorded for each engine during each test run. Additionally, the thrust reading from the load cell was recorded.

7.4.3 Results

Results are presented in Figure 40 for thrust vs. right engine throttle percentage for both engine runs. The right and left engine throttle percentages were nearly identical for both runs as the throttle input to the ECUs for each engine is provided by the same channel on the receiver (through a Y-split servo connection). The maximum discrepancy in throttle during all testing was 0.4%. Data from the performance of each engine individually is not presented because it is identical to the data presented above for the single engine static thrust testing.

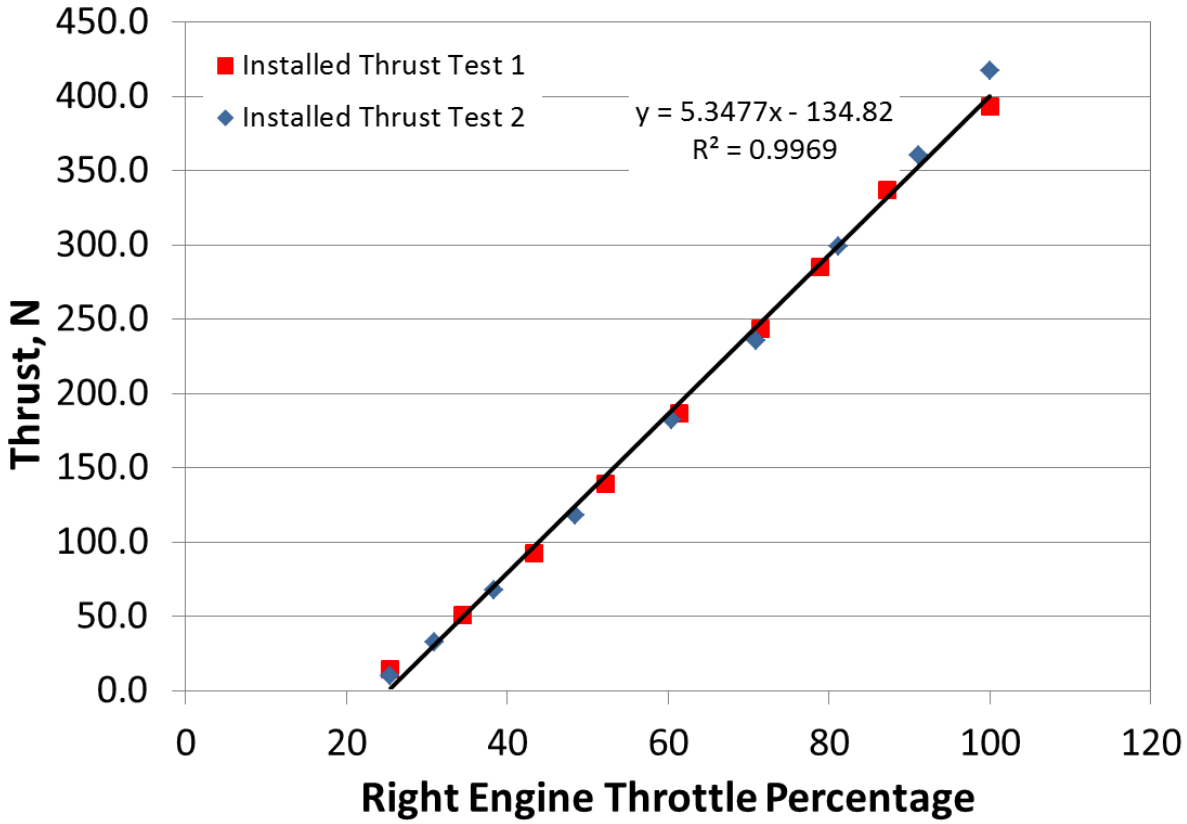

Figure 40- Installed Static Thrust Test Results for Thrust vs. Right Engine Throttle Percentage

Figure 40 shows that thrust is approximately linearly dependent on throttle percentage. More importantly, the maximum thrust from each test run was 393N (88.3 lbs) and 417.5N (93.8 lbs). These maximum values represent 10.4% and 4.8% losses in total thrust respectively when compared to double the average maximum thrust from all static thrust testing. These losses are most likely due to the inlet design of the JWSC GSRPV. Another potential source of the losses could be the modified shape of the exhaust tube required to fit it in the exhaust port of the JWSC outer mold line.

These results show that the GSRPV will have a thrust to weight ratio of 63.1% to 67.0% at the unballasted weight of 140 lbs. This is more than adequate for the safe operation of a RPV, as long as care is taken to avoid adverse attitudes where excess thrust is required to recover. For the scaled test point of 204.5 lbs, this corresponds to 43.2% to 45.9%. A good rule of thumb for RPVs is a minimum thrust to weight ratio of 50%. This thrust to weight ratio is lower than ideal

for the operation of an RPV; however, safe flight may be possible. Future simulation is required to test the handling qualities of the GSRPV at these lower thrust to weight ratios.

7.4.4 Conclusions

The completion of installed static thrust testing has proven that the single engine performance validated through the static thrust test can be extended to the full aircraft with losses of approximately 4.8%-10.4% due to the inlet and exhaust geometry of the GSRPV. These losses are of small enough magnitude to not negatively affect the performance of the GSRPV at the unballasted weight; however, follow on testing at the scaled test point could prove risky because of the reduction in maximum thrust-to-weight ratio.

7.5 Bifilar Pendulum Test

A Bifilar Pendulum test was completed in order to experimentally determine the mass moments of inertia of the GSRPV and compare them to the as-modeled results generated by Quaternion Engineering's mass model. The Bifilar Pendulum test presented here was used only to determine the mass moments of inertia about the principle axes; however, future testing will be aimed at tuning the moments of inertia to match those of the full scale aircraft for aeroelastic scaling.

7.5.1 Test Apparatus

In order to hang the GSRPV in all three required orientations, a custom cage was fabricated. Enclosing the fuselage in the cage during testing not only protected the aircraft, but also provided hard points for hanging the aircraft. Figure 41 presents the custom cage designed for this test.

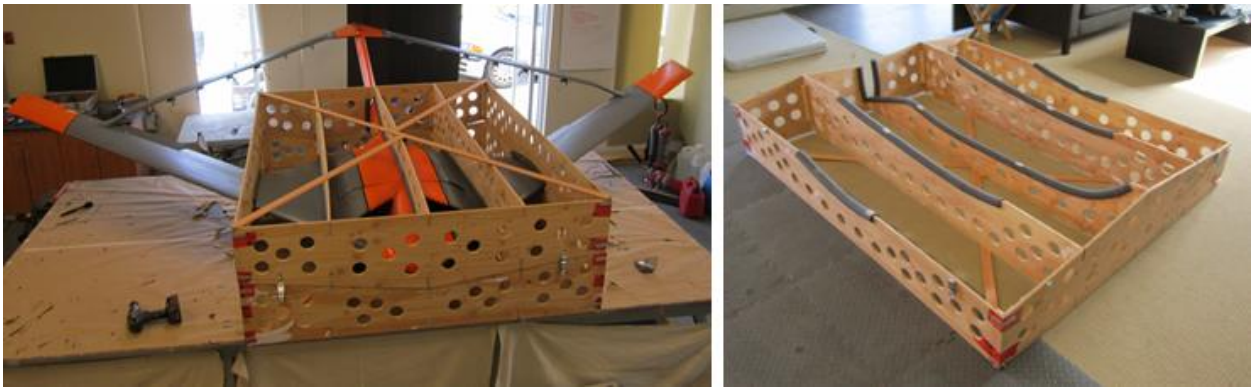

Figure 41 - Bifilar Pendulum Cage Assembled (Left) and the Top Half (Right)

The cage was fabricated in two halves using sheets of 3/8 in plywood. Three internal vertical supports were incorporated to support the aircraft within the cage. A CAD model of the GSRPV was used to create templates for all of the required components of the cage. Each of the 14 pieces was then hand traced, cut out and assembled to complete the final cage. Foam pipe insulation was incorporated in all places where the cage contacts the aircraft to provide a snug fit as well as prevent damage to the aircraft. The cage was held closed by a series of eight snap latches, two on each side.

The cage was required to support the aircraft in all three orientations with the CG of the aircraft directly between the support filaments. To allow balancing during testing, threaded rods were installed in all required mounting locations. Additionally, sand bags were used to ballast the cage such that the CG of the cage and aircraft were in the same location. Figure 42 highlights the mounting locations as well as the ballast weight and Figure 43 presents a close up view of one of the threaded rod mounting locations. Additional ballast weight not shown in Figure 42 was used to ballast the aircraft and cage vertically. This weight was attached to the lower side of the cage on the centerline, vertically below the longitudinal center of gravity. High strength carabiners were used as clips to provide a robust but removable attachment method for the filaments to the cage. For each filament, $1/8^{th}$ inch aircraft cable was used due to its high tensile strength and relatively low cost.

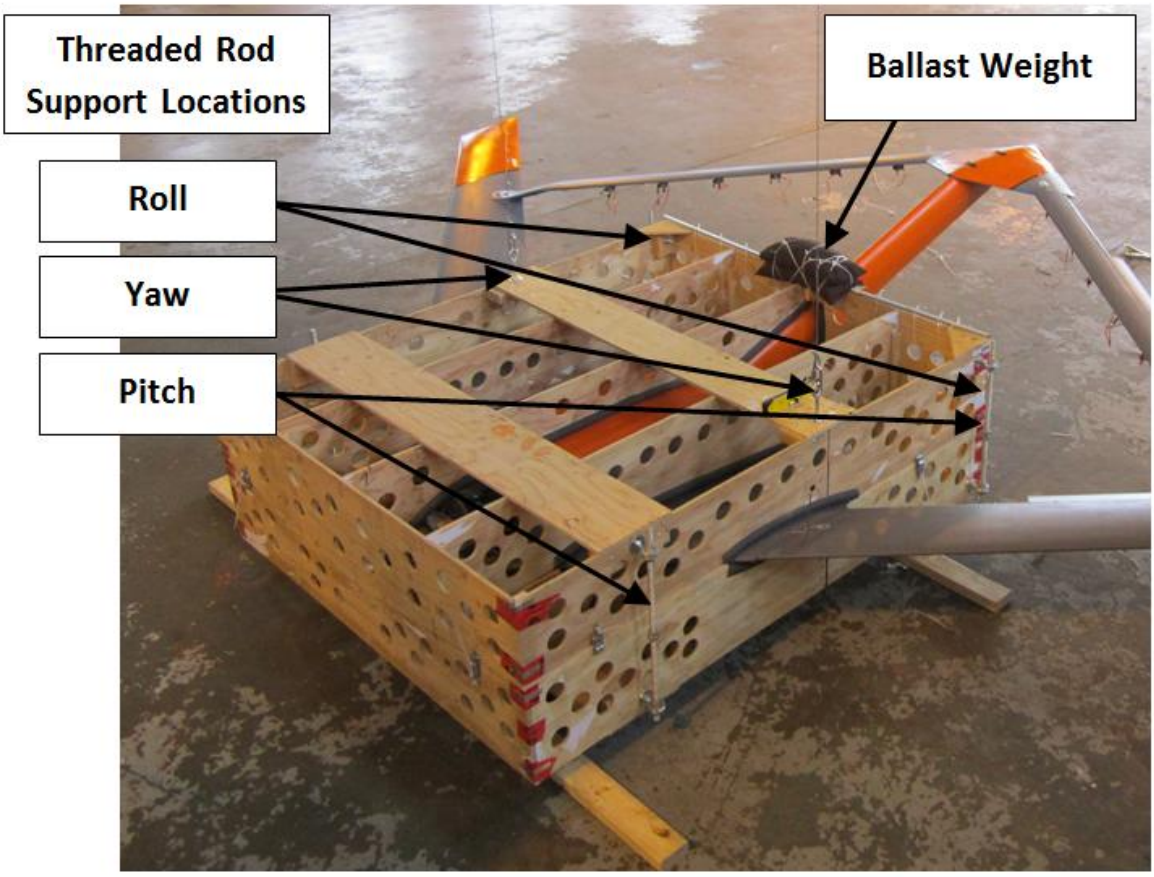

Figure 42 – Bifilar Pendulum Hanging Locations and Ballast Weight Location

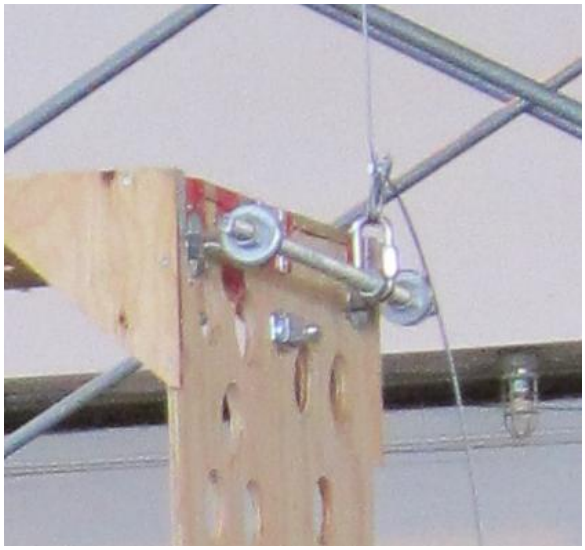

Figure 43 - Close Up View of Threaded Rod Mounting Location

Testing was completed in the Victoria Flying Club hangar at the Victoria International Airport. The hangar features open rafters 18ft from the hangar floor. These hangers provided

the perfect structure from which to hang the bifilar pendulum cage. To accomplish this, custom clamps were fabricated to suspend the wires and included adjustable guy wires for additional support of the weight. Figure 44 presents a picture of one of the clamps. Table 10 presents a summary of key design dimensions and masses for reference.

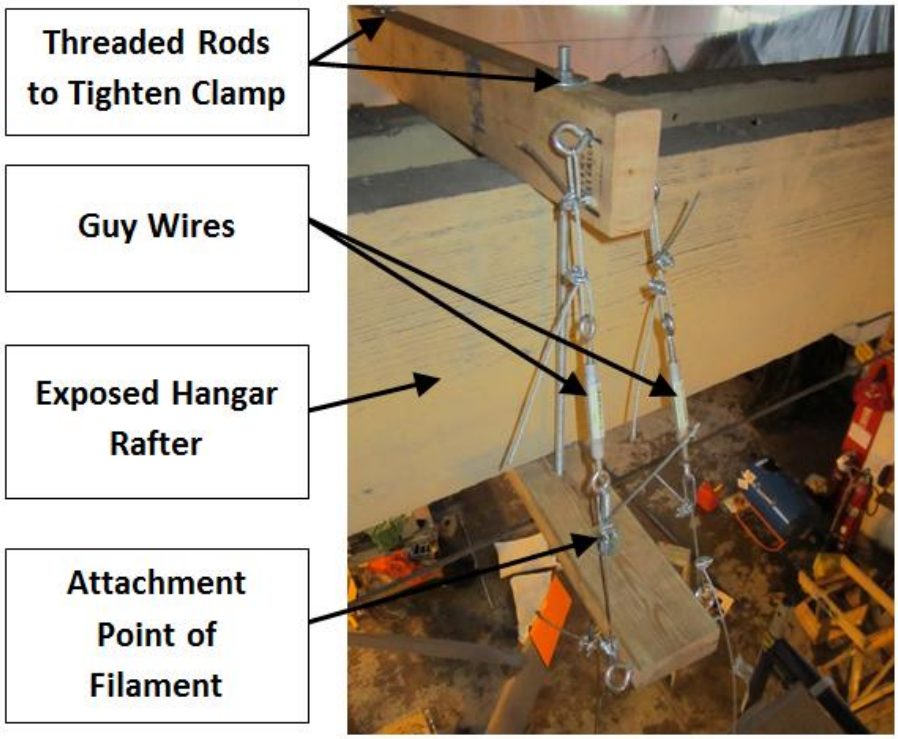

Figure 44 - Bifilar Pendulum Support Clamp

Table 10 – Key Design Dimensions and Masses

	Roll	**Pitch**	**Yaw**
Length of Filaments, L (cm)	369.9	196.9	486.2
Distance Between Filaments, D (cm)	167.6	145.1	147.3
Ballasted Cage Mass (kg)	80.6	80.6	69.2
Aircraft Mass (kg)	45.3	45.3	45.3

7.5.2 Test Procedure

The most difficult part of any Bifilar Pendulum Test is the setup. Testing took place over the course of four days; however, the total data measurements required took less than 30 minutes total! Testing was first completed on a small aluminum rod of known inertia suspended from a single filament for the calculation of the string torsional spring constant, k_{eff}. This procedure was repeated for all three required filament lengths (roll, pitch and yaw) because k_{eff} is dependent on filament length. Figure 45 presents a picture of the aluminum rod suspended from one of the filaments during testing and Table 11 presents the calculated values for k_{eff}. For these measurements, single oscillation times were recorded.

Figure 45 – Inertia Measurement of Aluminum Rod for Calculation of k_{eff}

Table 11 - Calculated Values of k_{eff}

	k_{eff} (kg m^2/s^2)
Roll	0.003955
Pitch	0.003436
Yaw	0.002326

With k_{eff} calculated, testing began on the bifilar pendulum cage. The inertia of the cage was calculated about each axis by suspending the cage in the required orientation and introducing a small rotational oscillation. Three to four full oscillations were allowed to pass to allow preliminary damping to occur, and then the total time for ten oscillations was recorded. To compute the period of oscillation, the total was divided by ten. By recording a longer period of time, the error present in each measurement of a single oscillation is reduced. A total of five measurements were made on each principle axis. This entire procedure was then repeated for the cage with the aircraft in it. Figure 46, Figure 47 and Figure 48 present pictures of the aircraft hanging in the required orientation to calculate the inertia about the yaw, roll and pitch axes, respectively.

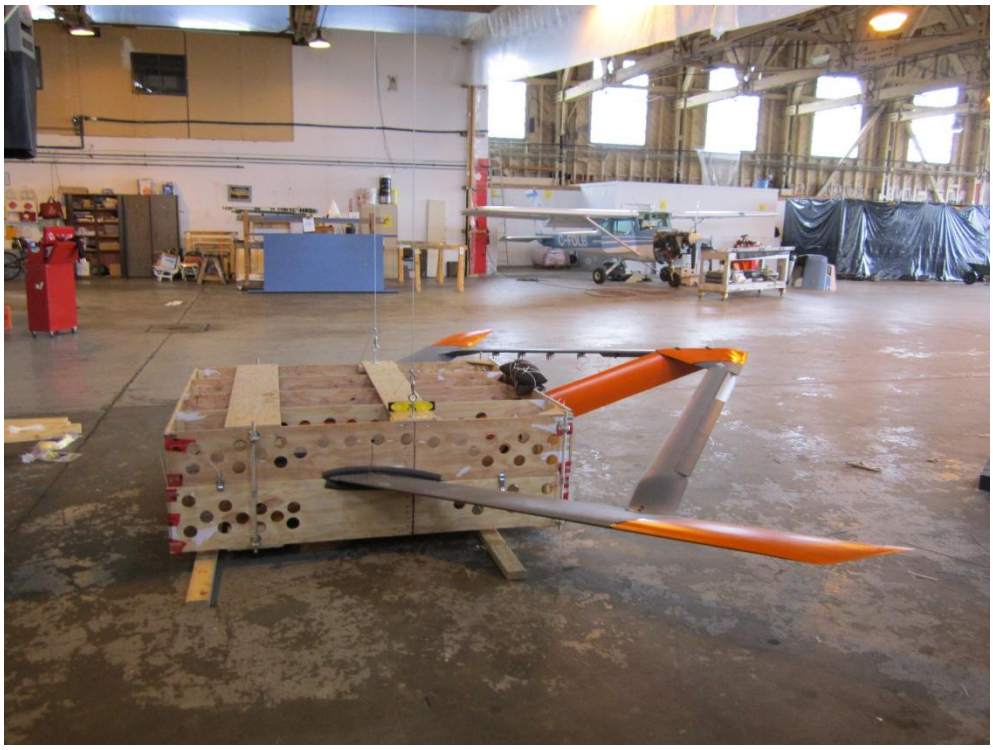

Figure 46 - Bifilar Pendulum Orientation Required to Calculate Yaw Inertia

Figure 47 - Bifilar Pendulum Orientation Required to Calculate Roll Inertia

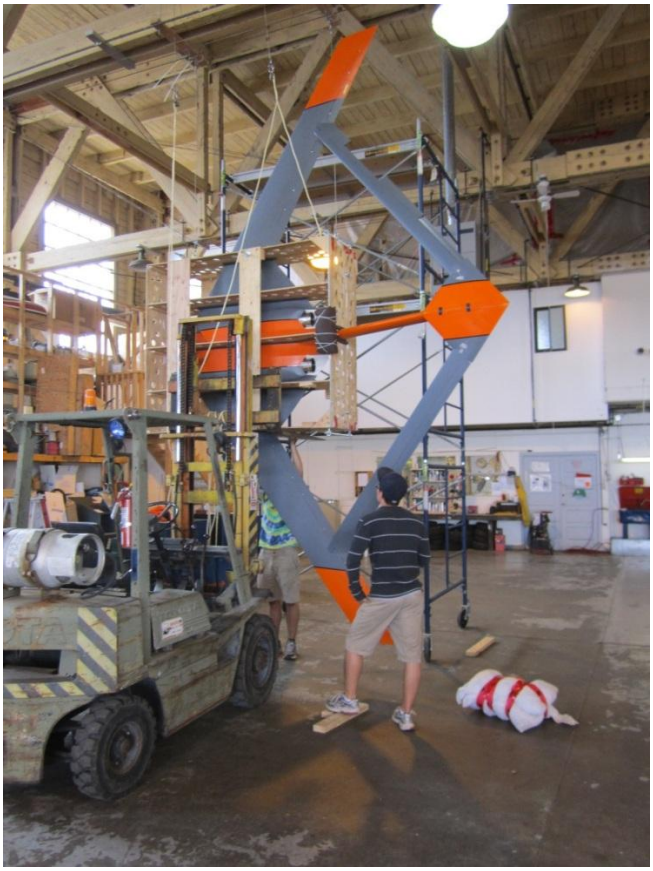

Figure 48 - Bifilar Pendulum Orientation Required to Calculate Pitch Inertia

The fork lift seen in Figure 48 was required because in the pitch orientation, the aircraft is hanging with a wingtip in close proximity to the ground, and manually placing the aircraft in this orientation was impossible. To accomplish the lift, a pulley system was utilized and a wing scrape cage was built around the left wing (the wing closest to the ground). The aircraft was then lifted into the proper orientation by pulling vertically upward with the pulley system, allowing the wing scrape cage to slide the wing into position. Once in the proper orientation, the bifilar filaments were attached, the wing scrap cage was removed, the lifting ropes were slackened and testing was commenced. To lower the aircraft, the entire process was reversed. Figure 49 presents a picture of the lift in progress.

Figure 49 – Lift Into Pitch Orientation Showing Wing Scrape Cage and Lifting Ropes.

The final test completed was the experimental determination of the mass moment of inertia of a steel square rod, known as the benchmark rod, for validation of the method used. The 12 ft long, 25.9 lb steel rod was hung from the yaw orientation filaments (without the cage) and the procedure described above was repeated. Figure 50 presents a picture of the benchmark rod during testing, suspended above the bifilar pendulum cage in the yaw orientation.

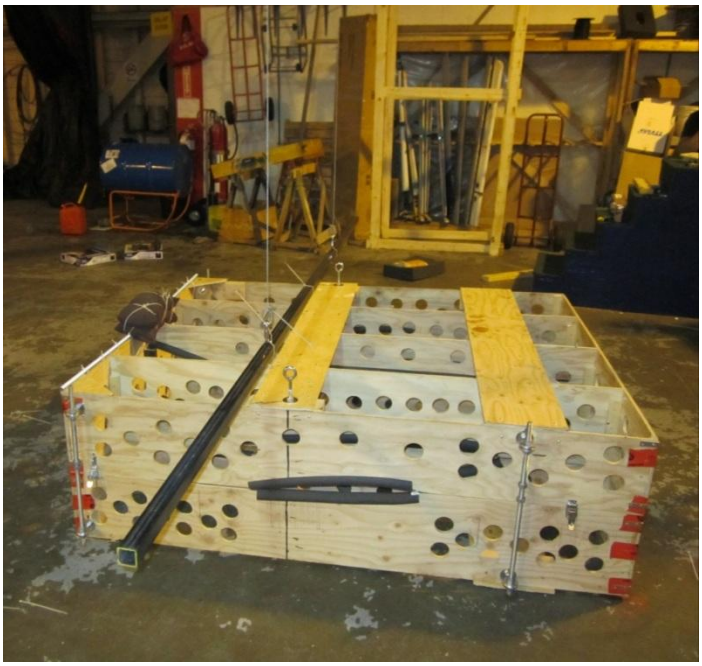

Figure 50 – Testing of the Benchmark Rod

7.5.3 Results

Once all testing was complete, the calculations described in Section 6.5.2.2 were completed to calculate experimental mass moments of inertia for the GSRPV as well as the benchmark square rod, accounting for the torsional effects of the suspension filaments. These results were compared to the predicted inertia values computed using Quaternion Engineering's SolidWorks CAD model of both the as built GSRPV and the benchmark rod.

Table 12 presents the experimental and predicted (as modeled) mass moment of inertia for the benchmark rod as well as the percent difference. Table 13 presents the as tested mass and CG location for the aircraft as well as testing results. For the calculation of the percent difference, the predicted mass moment of inertia was taken to be the true value.

Table 12 – Bifilar Pendulum Test Results for the Benchmark Square Rod

Experimental	13.10	kg m^2
Predicted	13.35	kg m^2
Difference	1.85	%

Table 13 - Summary of Bifilar Pendulum Test Results for the GSRPV

Mass		45.3	kg
CG Location (aft of nose)		100.7	cm
Roll	**Experimental**	29.25	kg m^2
	Predicted	28.64	kg m^2
	Difference	2.13	%
Pitch	**Experimental**	25.59	kg m^2
	Predicted	33.53	kg m^2
	Difference	23.68	%
Yaw	**Experimental**	56.08	kg m^2
	Predicted	59.99	kg m^2
	Difference	6.52	%

These results illustrate the accuracy of the method employed. The small error present in the benchmark rod validates the method used and provides confidence going forward with future, more advanced bifilar pendulum tests in which the mass moments of inertia must be tuned.

For the measurements made on the GSRPV, the results are very satisfactory. Roll and yaw, the two most critical inertias due to Dutch Roll Mode marginal stability, show excellent correlation to predicted values. This provides confidence in both the model and the experimental method. The largest error present was in pitch; however, there are several possible sources of error that have been identified and can be corrected going forward with future testing. First, the support cables for the pitch orientation were the shortest, resulting in the shortest oscillatory period. This shortened period corresponds to a higher rotational velocity and accordingly increased effects of air resistance (damping of the rotational motion). This will shorten the total time to measure 10 oscillations, giving the appearance of less inertia due to a smaller period of oscillation. This error could be lessened by lengthening the oscillatory period by reducing the distance between the filaments. A second source of error present during testing was the presence of the lifting ropes. Though slackened, the ropes were still attached to the cage providing a small

resistive force, again shortening the total time to measure 10 oscillations. Finally, the model shifted slightly when suspended in the pitch orientation. This shift was caused by large tolerances in the support cage introduced by hand fabrication. Future iterations (where inertias will be tuned) will include a machined aluminum support cage to reduce the effects of these errors.

7.5.4 Conclusions

The Bifilar Pendulum Test provided accurate experimental mass moments of inertia for the GSRPV. An object of known inertia was tested, and a small 1.85% error validated the method used. Testing of the GSRPV provided excellent correlation with the as-modeled, predicted data for the roll and yaw orientations. The pitch orientation had the largest error between the modeled and measured values; however, several potential sources of this error have been identified and can be corrected for future iterations of this test.

7.6 Static Structural Loading Test

A static structural loading was completed to experimentally validate the structural design and fabrication of the GSRPV and ensure that the as-built structure was capable of withstanding the predicted aerodynamic loading required to complete all planned flight maneuvers. The aircraft was designed to withstand a 3g max loading, with a factor of safety of 1.5, at the test point weight of 204.5 lbs. For safety, the GSRPV static loading tested up to a 3g loading at the first flight weight of 140 lbs. The autopilot incorporates a g-load limiter, so no loading greater than 3g will be experienced in flight.

Before testing could commence, a test speed and corresponding trim condition for spanwise lift distribution had to be selected for the test. The static structural loading test point speed was selected as 36 m/s, because this is the slowest speed at which that aircraft could attain a 3g loading. This case was selected because, at higher speeds, the forward wing tips produce negative lift due to the large "wash in" angle there. Additionally, due to the large static margin of the GSRPV (forward CG location) compared to the full scale design, the aft wing is actually producing negative lift in most cases. During a static loading test, negative lift and positive lift are impossible to simulate at the same time because weight can only be used to push down on the wing. Therefore, trim condition had to be selected that did not have negative lift on any lifting

surface. The 36m/s trim case corresponded to positive lift on the entire forward wing and no lift on the aft wing. Accordingly, only the forward wing had to be loaded for the static structural loading test.

Once the test point and trim condition were selected, the spanwise lift distribution calculated using the Athena Vortex Lattice (AVL) code was discretized into three segments. Discretization was required to create an experimental loading case that is representative of the computed spanwise loading. The experimental loading case consisted of point loads equivalent to the numerical integral of the spanwise lift curve within each segment applied at the spanwise centroid location of trapezoids formed by connecting the endpoints of each segment. Figure 51 presents a graphical representation of these calculations. It is important to note that for this test, the spanwise lift distribution does not include the lift generated by the fuselage, and accordingly, the curve starts at a spanwise location of 0.4m.

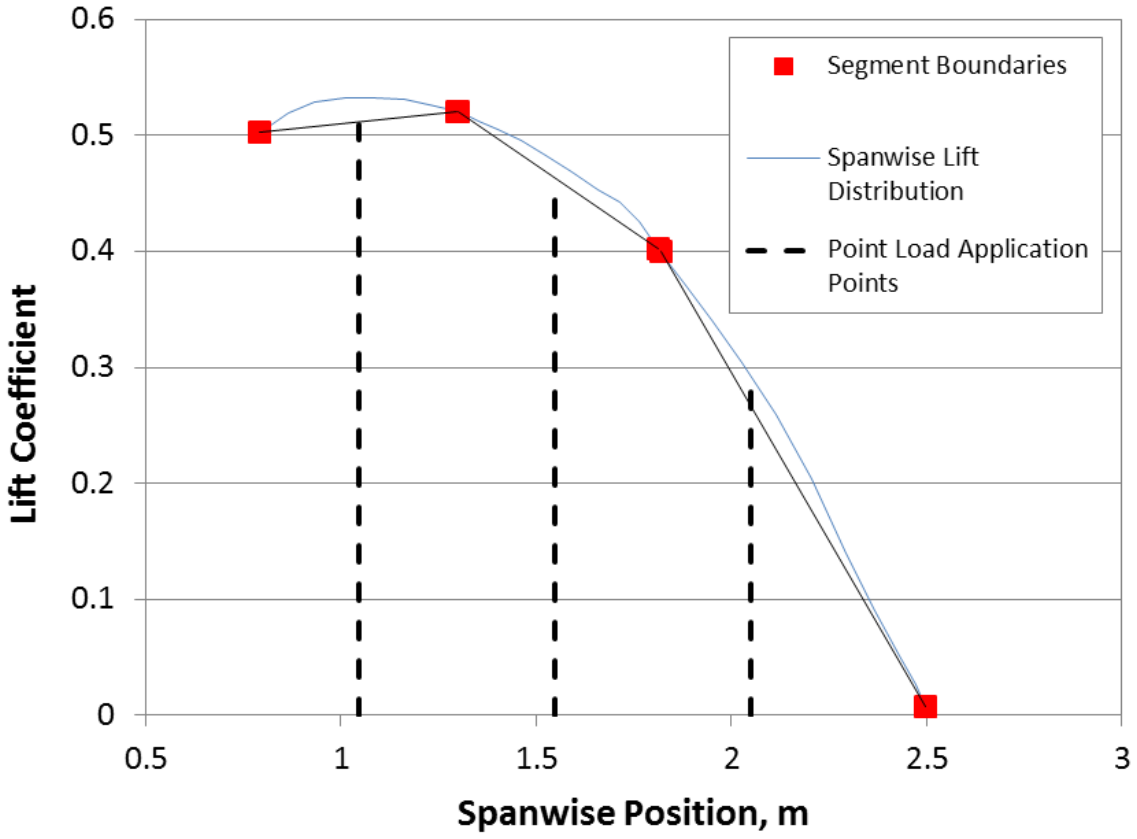

Figure 51 – Graphical Depiction of Static Structural Loading Test Case

The point loads were generated using custom sand bags applied at the locations described. Sand bags were created for loadings from 0g to 3g in 0.5g increments. Table 14 summarizes the point loads required at each location to achieve the desired loading increments.

Table 14 – Summary of Required Loading

	Required Point Loads (kg)		
Desired Loading	**1.05 m**	**1.55m**	**2.05m**
0.5g	4.59	3.74	2.08
1.0g	9.18	7.49	4.17
1.5g	13.78	11.23	6.25
2.0g	18.37	14.97	8.33
2.5g	22.96	18.71	10.42
3.0g	27.55	22.46	12.50

7.6.1 Test Apparatus

The bifilar pendulum cage was carefully designed such that the top half of the cage can double as the test apparatus for the static structural loading test. The top half of the cage, presented in the Figure 41, features a flat top so that it can be inverted on a flat surface. The GSRPV can be inverted, allowing sand bags to be placed in the required locations on the under-side of the wings to simulate the required wing loadings. Figure 52 presents a picture of the GSRPV inverted in the structural loading test apparatus.

Custom sand bags were fabricated in the required sizes. For each required loading point, three 1g bags and a single 0.5g bag were fabricated. This combination of sand bags for each location is capable of simulating all required loadings. Additionally, three wooden yard sticks were mounted to boxes and placed at the tip of each wing and at the tip of the boom for measurement of the deflections at each test point, as shown in Figure 53. The strain gage system was completely installed in the aircraft and operational during testing.

Figure 52 – GSRPV in the Static Structural Loading Test Apparatus

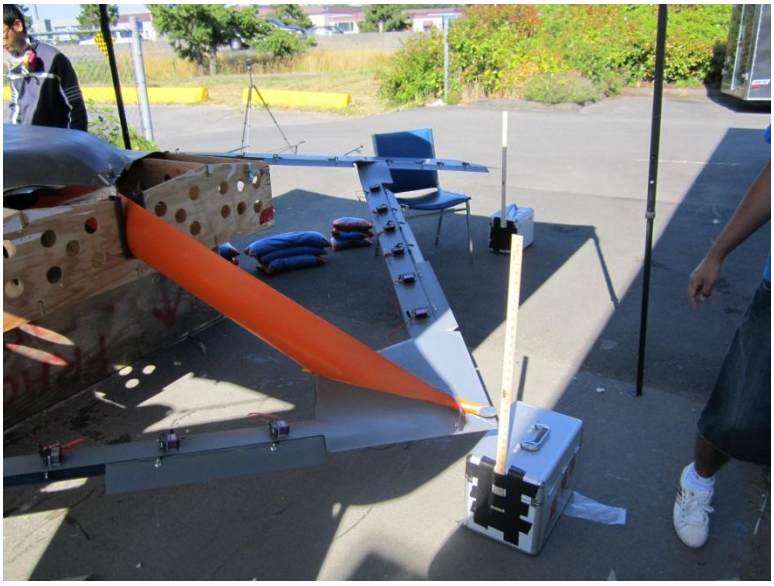

Figure 53 – Vertically Mounted Yard Sticks for Deflection Measurement

7.6.2 Test Procedure

To complete testing, sand bags were incrementally placed at the required loading in 0.5g increments. Testing was completed as quickly as safely possible to reduce fatigue on the structure and care was taken to symmetrically load the aircraft to avoid movement within the test apparatus. At each test point, the wings were examined for structural damage and panel buckling. At each test point, the maximum deflection was marked on the yard sticks at the tips

of the wings and boom. The magnitude of the deflection was measured and after the completion of the entire test.

7.6.3 Results

The GSRPV successfully withstood loading up to a 3g load at the flying weight of 140 lbs without permanent structural damage. Figure 54 presents a picture of the right forward wing loaded with a 3g loading.

Figure 54 – 3g Load on the Right Forward Wing

Figure 55 presents a plot of deflection of the tip of both wings and the boom for all applied load cases with a smooth line fit through all of the data points to clearly illustrate the trends in the data.

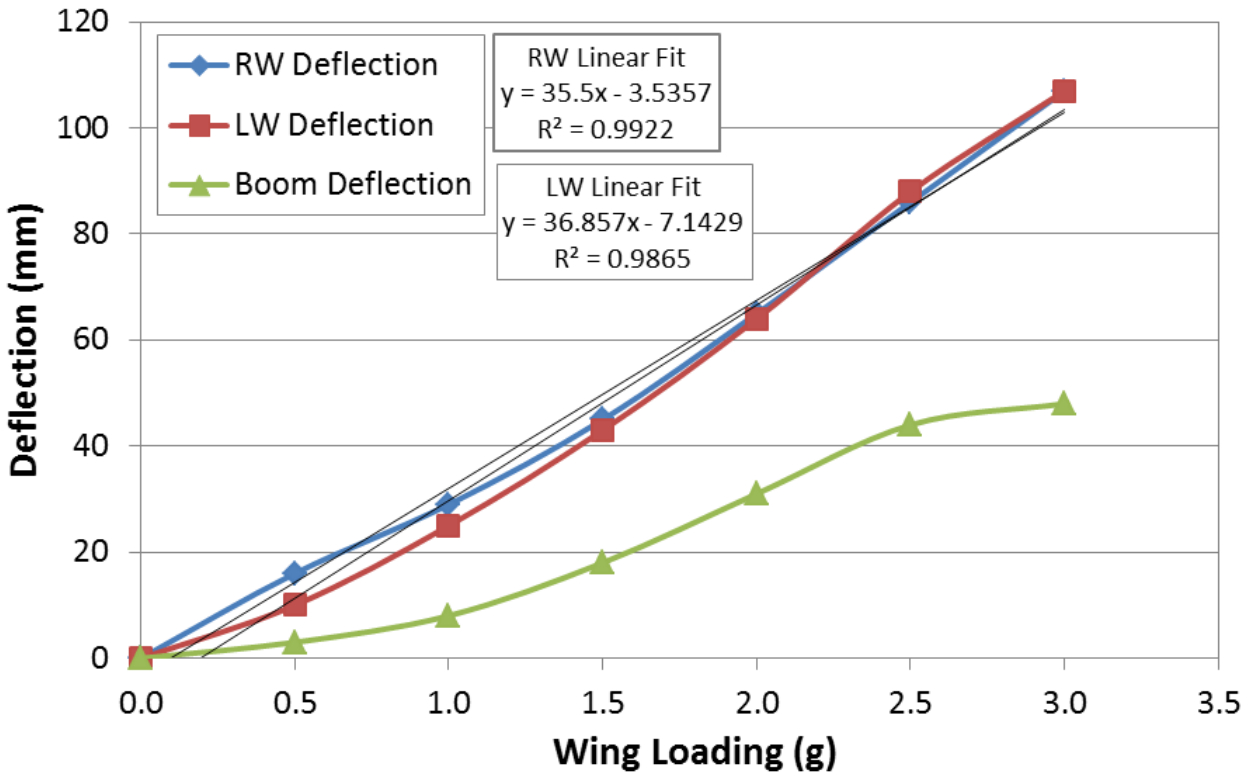

Figure 55 - Static Structural Loading Wing Deflection Data with Smooth Line to Illustrate Trends

From these plots, it can be seen that the forward wings exhibit nearly identical, linear increase in deflection with applied load up to a symmetric maximum deflection of 107mm at 3g. This is an expected result, and the small discrepancy present between at the lower loadings was due to discrepancies in the readings at 0.5g and 1g as illustrated in Figure 55. These discrepancies were most likely introduced by small asymmetries in the loading or error in the recording of the deflection on the vertical yard sticks. For future iterations of this test, it is recommended to measure the deflection at the mid-span of each wing to further characterize the deflections.

The aft wing, however, exhibited a very interesting trend, and in the opinion of the author, ***the most important result in testing completed to date.*** The critical section of the curve is represented by loading above 2g where the slope of the curve decreases as the loading increases. Extrapolating this curvature to higher loadings approaching the limit load of 4.5g leads to a theoretical negative slope on the load deflection curve. While this extrapolation is only based on three data points, this lends support to the theory that the boom would actually begin to deflect downward under extreme loading, leading to potential aft wing buckling! No

other test result completed to date more completely or succinctly supports the aim of this project of demonstrating the nonlinear aft wing response. This result provides increased confidence that nonlinear response will be able to be attained when increased flexibility is introduced into the structure. Future, follow on static loading tests at higher wing loadings will be aimed at repeating this result and providing validation to the theoretical extrapolation discussed earlier with additional aft wing measurements.

The results from the strain gage system showed significant amounts of noise, but potentially produced some useful data. Current work is aimed at post-processing the data to obtain strain measurements; however, Figure 56 provides a sample plot of some of the raw experimental data.

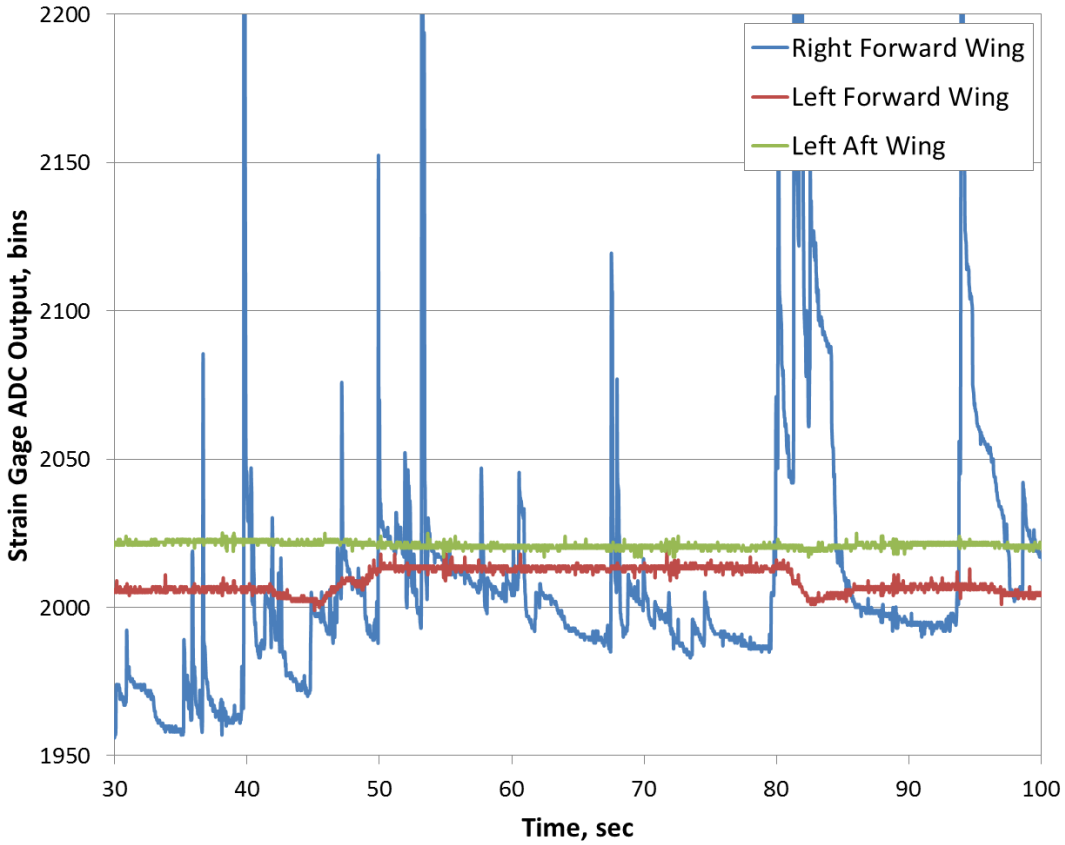

Figure 56 –Raw Strain Gage Data for 1g Static Loading

The two most useful data curves presented above are for the left forward wing and left aft wing strain gage measurements. These strain gages are mounted on the upper surface of each wing where compression is expected. The data from these gages appear to be clean; however,

the full extent of the usefulness of the data is not yet understood. The left forward wing shows a segmented, step-like trend, with is to be expected as sand bags were applied and removed to reach the desired 1g loading during this test; however, the left aft wing does not exhibit the same trend. The maximum reading on the forward and aft wing strain gages is 2013 and 2020 respectively. Noting that the midpoint of a 12-bit ADC spectrum (which corresponds to a balanced bridge) is 2048, both of these readings represent a negative bridge output voltage. The polarity convention presented in Section 5.1.2.2 notes that a negative output voltage corresponds to a compressive strain on a strain gage substituted in the R_1 bridge resistor. In other words, both of the strain gages on the left wing were experiencing compression during testing, and the forward wing was experiencing a compressive force of larger magnitude. The test data for the higher load cases shows a similar trend, and current work is aimed at post processing this data to determine the relative magnitude of the readings when compared to the applied load cases.

The right aft wing strain gage quarter bridge system had a short circuit, and accordingly the data is not presented. The large amount of noise in the right forward wing data was likely due to damage to the strain gages after installation, but prior to testing.

7.6.4 Conclusions

A static structural loading test was completed for load cases ranging from 0g to 3g in 0.5g increments at the 140lb, un-ballasted flying weight. The structure suffered no permanent damage from testing. The measured deflection of the forward wing tips increased linearly with increasing load, as expected; however, the tip of the boom did not. At high wing loadings (above 2g) the slope of the boom deflection curve decreases as the loading increases. Extrapolating this curvature to higher loadings approaching the limit load leads to a theoretical negative slope on the load deflection curve which, under extreme loading, could lead to potential buckling of the aft wing. This test result supports the feasibility of the aim of this project in demonstrating the nonlinear aft wing response and provides confidence going forward that nonlinear response will be able to be attained when increased flexibility is introduced into the structure.

7.7 Taxi Testing

The final test completed prior to the first flight was the taxi testing of the flight ready GSRPV.

7.7.1 Test Location

Testing took place at the flying site at the Foremost Airfield in Foremost, Alberta, Canada. The Foremost Airfield is a low-traffic civilian airfield at which the JWSC flight test team has obtained an SFOC for flight test operations. Figure 57 presents a picture of the GSRPV on the runway at the Foremost Airfield.

Figure 57 - GSRPV on the Runway at the Foremost Airfield

Taxi testing was completed on August 10th, 2011, wrapping up over a week of ground testing and preparation.

7.7.2 Test Procedure

Taxi testing of the GSRPV was divided into two separate tests, the Low Speed Handling Test and the High Speed Taxi Test. The full instrumentation system was operational during all testing to record experimental data, as well as to verify the proper operation of the system with all other onboard systems running (including both turbine engines).

7.7.2.1 Low Speed Handing Test

The Low Speed Handing Test was completed first. This test validated the handling qualities of the aircraft at low speed maneuvers with a maximum speed of 10 knots. For this test, the pilot started both turbine engines and completed several straight line passes and figure 8 maneuvers on the runway apron. Completing this test on the apron provided a large, flat space within which the aircraft was able to turn in either direction. During this test, the pilot trimmed the nose wheel and tested the braking system. Once the pilot was satisfied with the trim state and performance of the GSRPV braking system, he taxied the GSRPV to the runway for the High Speed Taxi Test.

7.7.2.2 High Speed Taxi Test

The High Speed Taxi Test was completed with a series of straight line runs down the runway at increasing speeds. At the end of each run, the brakes were applied to slow the aircraft to a speed at which a 180 degree turn could be successfully completed. Runs were completed in both directions on the runway because there was no wind present at the time of testing.

During testing, the ground station operator monitored the airspeed measurement of the Piccolo II autopilot and radioed this reading to the pilot. The pilot was informed of the nominal maximum speed of each run, and reduced power when the nominal speed was reached.

7.7.3 Results

Testing was completed with approximately 33% fuel, as reported by the pilot who fueled the aircraft prior to testing. Table 15 presents a summary of the nominal test speeds and the corresponding percentage of stall speed for both the fully fueled configuration and the as-tested configuration, as well as the maximum speed achieved during the test. Note that the nominal speeds presented for the first four runs were the speeds at which the pilot reduced power and applied the brakes. The maximum achieved speed is the maximum recorded speed for all testing.

Table 15 - Summary of High Speed Taxi Test Speeds

Configuration	**Full Fuel**	**As Tested**
% Fuel	**100%**	**33%**
Weight (lbs)	**140.0**	**115.7**
Run 1 Nominal - 9.7 knots	23.9%	26.8%
Run 2 Nominal - 18.0 knots	44.3%	49.7%
Run 3 Nominal - 25.3 knots	62.2%	69.8%
Run 4 Nominal - 32.1 knots	79.0%	88.6%
Max Achieved- 32.3 knots	**79.5%**	**89.1%**

During high speed taxi testing, the GSRPV performed well, achieving the desired maximum speed of 32.1 knots and exceeding it with a maximum speed of 32.3 knots. Fully fueled, this corresponds to 79.5% of the stall speed. As tested (at approximately 33% fuel), this corresponds to 89% of the stall speed. Figure 58 presents the GSRPV traveling at a speed of 32.3 knots.

Figure 58 – GSRPV High Speed Taxi Test

Both the strain gage and accelerometer systems were fully operational during high speed taxi testing and recorded data as planned. At the time of writing this thesis, the strain gage data has not yet been examined; however, preliminary analysis of the accelerometer data provides

positive results. Figure 59 presents an excerpt from the raw accelerometer data from the high speed taxi test. As labeled, accelerometer 1 (ax1, ay1 and az1) was located on top of the fuel tank at the center of gravity with the y axis pointing out the nose and the z-axis vertically upward. Accelerometer 2 (ax2, ay2 and az2) was located on the underside of the left wing, with the y-axis parallel to the free stream flow and pointing forward and the x-axis pointing away from the fuselage. Accelerometer 3 (ax3, ay3 and az3) was located on the underside of the right wing in the same fashion with the y-axis pointing parallel to the free stream flow and pointing forward but the x-axis was pointing towards the fuselage. Finally, accelerometer 4 (ax4, ay4 and az4) was located at the tip of the boom with the y-axis pointing forward and the x-axis pointing horizontally to the right.

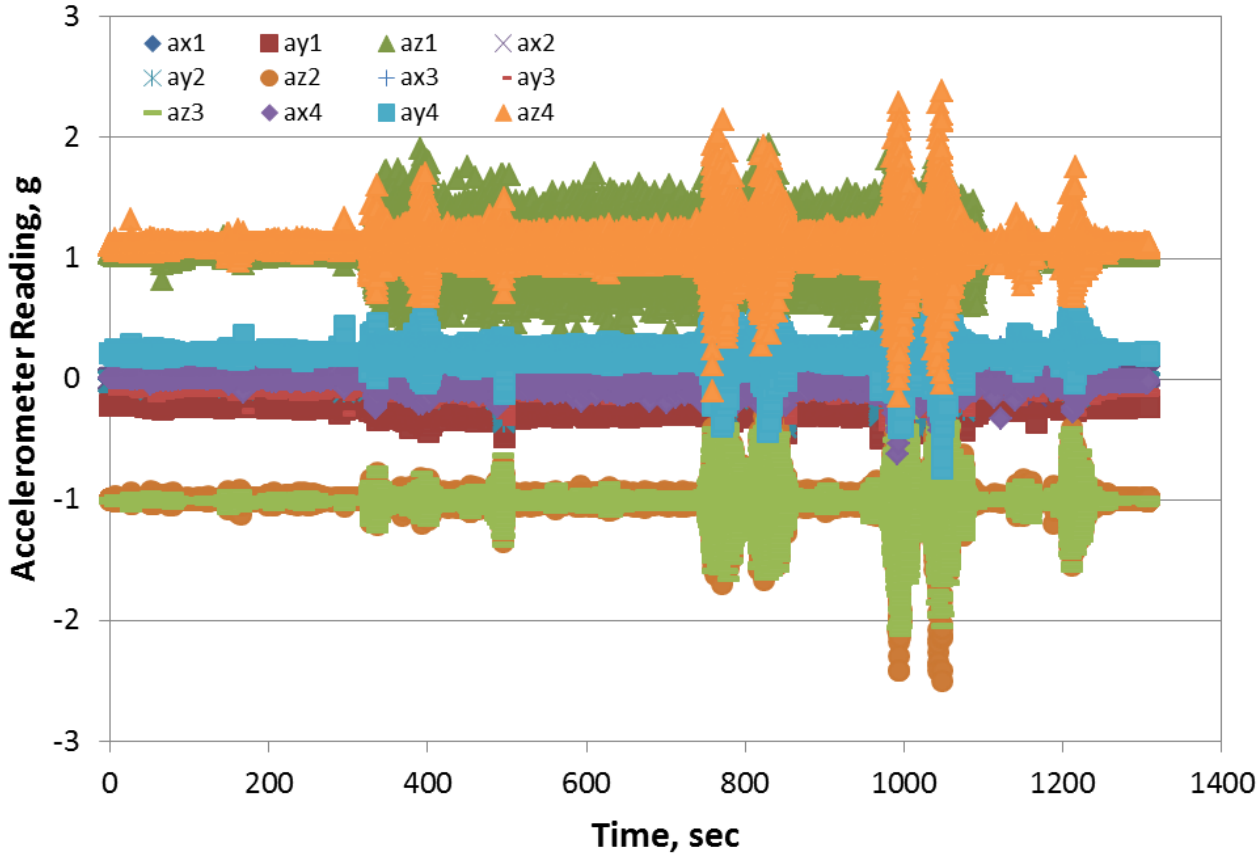

Figure 59 – Accelerometer Data from High Speed Taxi Testing

Analysis of this figure illustrates several key results. First, the data is very clean, with no outliers or errors in the data log for the entire data stream, which includes over 1300 seconds of continuous data logging for all 12 accelerometers at 40Hz. This corresponds to 624,000 measurements without a single error. This validates the design of the system, including the

logging rate. Second, the peaks present in the data stream are clearly represented in the measurement of all of the accelerometers. This means that the accelerometers are functioning properly. Current efforts are aimed at understanding what events during the high speed taxi test caused these peaks, and correlating the accelerometer measurements to these events.

Analysis of this figure also illustrates one key required improvement prior to continued testing. The az1 reading, which corresponds to the z-acceleration reading of the accelerometer located at the center of gravity, shows a large amount of noise during the majority of testing. This means that the accelerometer mounted on the fuel tank either came loose, introducing vibration into the data or he tank itself was vibrating. Prior to the first flight, the accelerometers were more securely mounted with hot melt glue to lessen the possibility of them breaking loose during flight.

7.7.4 Conclusions

Taxi testing of GSRPV, including both a low speed handing test and a high speed taxi test was completed culminating in a high speed taxi run at 89.1% stall speed. The pilot commented that the aircraft displayed favorable handling characteristics on the ground and the brakes performed well. All testing was completed in manual mode (without stability augmentation provided by the autopilot), and the full instrumentation system was operational during testing. Future work planned is aimed at more extensive post-processing of strain gage and accelerometer data, including new data generated during the first flight.

7.8 Phasing Flight Test – GSRPV First Flight

The first flight of the GSRPV, the Phasing Flight Test, was completed on October 15th, 2011. This thesis was defended prior to the completion of this flight; however, preliminary results and a description of the flight are presented here for completeness. Post processing and analysis of flight performance is left for future work.

7.8.1 Test Procedures

For the Phasing Flight Test, the test team returned to the flying site at the Foremost Airfield in Foremost, Alberta, Canada. After the successful completion of the high speed taxi test in August, the sole goal of this trip to Foremost was to achieve a successful first flight.

Testing was divided into two parts, a high speed taxi test in fly-by-wire mode followed by the first flight.

The high speed taxi test consisted of a repeat of the test completed in August; however, this time, the test was completed in fly-by-wire mode. This allowed the pilot to trim and tune the nose wheel to achieve the desired steering performance during the takeoff run. After the completion of the high speed taxi test, the first flight attempt was made. The first flight was aimed at safely demonstrating the ability to perform figure-8 and racetrack patterns, as well as test instrumentation system performance in flight.

During all testing, the essential personnel consisted of a primary pilot, a backup pilot, two ground station operators, a test director, a range safety officer and a camera man. The primary pilot was in control of the aircraft at all times in fly-by-wire mode through the Piccolo II autopilot. The backup pilot was responsible for "spotting" for the primary pilot as well as providing assistance with trim settings and navigation. The backup pilot was also capable of taking control of the aircraft at any time through a backup transmitter. The two ground station operators each served separate key roles. The primary ground station operator monitoring aircraft attitude and autopilot status, as well as navigational (GPS) status and handling any alarms or warnings that would sound. The second ground station operator monitored altitude and airspeed and relayed this information to the pilot when prompted. The test director stood next to the pilots during the flight and was responsible for guiding the pilot through the planned maneuvers. The range safety officer was responsible for monitoring and controlling the airspace around the Foremost flying site through a handheld VHF, radio as well as providing guidance to all personnel to avoid any hazardous situations. Finally, the camera man was responsible for documenting the entire flight.

Prior to the flight, all simulation data, mission analysis and scaled Mini SensorCraft performance parameters were consolidated into a final set of KPPs for the GSRPV in the first flight configuration. Table 16 below summarizes these parameters.

Table 16 - GSRPV First Flight Configuration and KPPs

	mass (kg)	CG (m aft of nose)	Static Margin
Empty	51.00	0.95	40.0%
Full	68.85	0.94	41.8%
Key Performance Parameters			
Stall Speed:		21.4 m/s	
Takeoff Speed:		25.6 m/s	
Nominal Cruise Speeds:		35-45 m/s	
Approach Speed:		25.6 m/s	

7.8.2 Results

The high speed taxi test in fly by wire mode was completed first; however, the pilot did not have sufficient control of the nose wheel and the aircraft veered off the runway. The pitot tube was broken; however, no other damage was caused. To correct this problem, the gain on the nose wheel servo was increased. With the increased gain, the pilot was confident in the controllability of the aircraft during the takeoff roll, so a takeoff attempt was made. Unfortunately, during taxi out to the end of the runway, the aircraft entered failsafe mode due to poor signal. To correct this problem two additional remote receivers were added to the rear of the aircraft to improve reception. With this problem fixed, a second takeoff attempt was made. During the takeoff run, the nose wheel exhibited a strong degree of hysteresis and the pilot shut down the engines during the takeoff roll because he was unsure of his ability to maintain control. After the engine shut down, the aircraft once again veered off the runway and broke the pitot tube.

After repairing the pitot tube again, a third takeoff attempt was made and this time the attempt was successful! The first flight of the GSRPV consisted of a 7 minute 58 second flight completed entirely in fly-by-wire mode. Figure 60 presents a picture of the aircraft in flight and Figure 61 presents a shot taken from the tail camera on board of the aircraft.

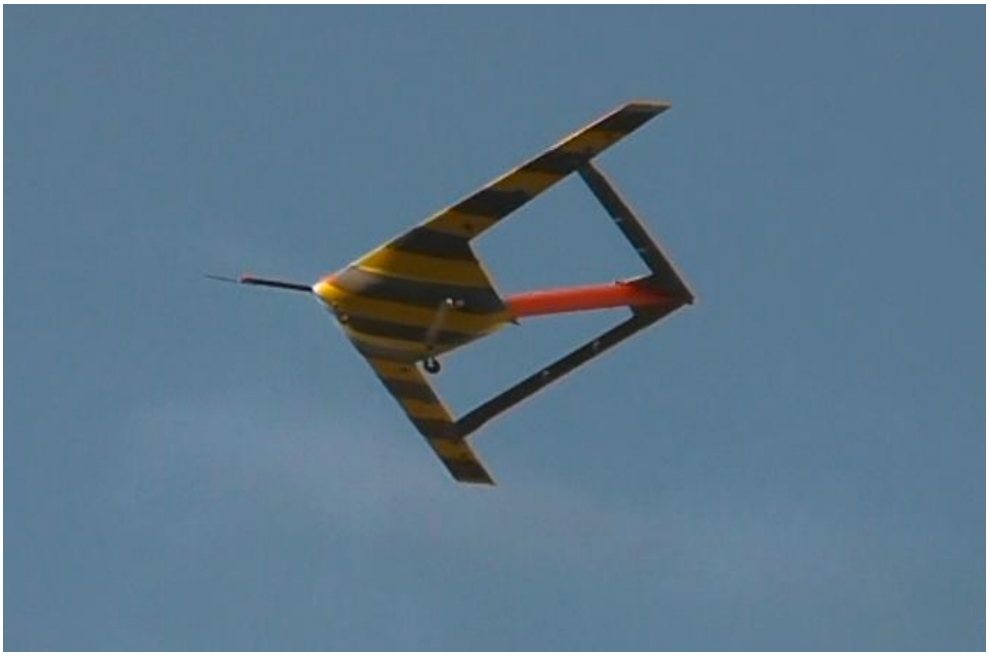

Figure 60 - GSRPV in Flight

Figure 61 - View from Tail Camera During First Flight

The pilot was able to successfully complete both figure 8 and racetrack patterns, well within the airspace allotted for the flight. The nominal cruise speed range of 35-45 m/s provided an ample speed range to complete all flight maneuvers in a slow, controlled manner while still avoiding stall. During the flight, dutch roll oscillations were noticeable, but the fly-by-wire

mode was able to dampen them to the point where they did not negatively affect the flight. After the flight, the pilot commented that the aircraft performed extremely well and, despite the complexity of the system and inherent nervousness present when flying any aircraft for the first time, he rated the flight as only a 5-6/10 for effort required.

After completing several racetrack patterns and figure 8s, a mock approach was successfully completed. Satisfied with the performance during the mock approach, a landing attempt was made. After completing the down leg, the aircraft was brought parallel to the runway. A gentle glide slope was maintained during the entire approach and a soft touchdown was made completing a successful flight. Figure 62 presents a picture of the GSRPV on final approach.

Figure 62 - GSRPV on Final Approach

After touchdown, the aircraft veered towards the near side of the runway. The pilot attempted to control the aircraft; however, he was unable to correct the lateral movement. He called for the backup pilot to take control. The backup pilot immediately took control, corrected the rollout and shut down the engines. During final roll out, the left rear tire blew due to the large side forces experienced, but no damage was caused to the aircraft. The aircraft rolled to a stop, bringing the GSRPV flight test program to a successful completion.

The one major disappointment of the first flight was that the instrumentation power wire pulled out of the retaining clip, and as a result, the strain gages and accelerometers recorded no data. The instrumentation system was able to successfully record data during the high speed taxi test and the first takeoff run, however, no data was recorded during the flight due to the failure.

7.8.3 Conclusions

With the completion of the first flight of the GSRPV, the Flight Demonstration program came to a successful close. Over two years of preliminary and preparatory work by personnel at Quaternion Engineering, the University of Victoria and Virginia Tech resulted in a successful flight. This flight provided validation of several key design choices, as well as success going forward with more advanced flights and flight maneuvers. Future work is aimed at post-processing of flight data recorded by the Piccolo II autopilot as well as identifying the cause of the failure of the instrumentation system wiring and correcting this failure during future testing.

8 Reduced Complexity Flight Tests

At the onset of the project, final approval from AFRL had not yet been received to put the JWSC Flight Test Program under contract. As such, internal research and development (IRAD) work was completed both at Virginia Tech and at Quaternion Engineering. The IRAD work completed at Virginia Tech included the fabrication and subsequent flight test of a reduced complexity model of the JWSC to investigate the two areas of primary concern, an unstable dutch roll mode and yaw control authority. Additionally, the first flight of a novel configuration is guaranteed to result in some unexpected handling characteristics, so it was deemed better to experience and investigate these characteristics using reduced complexity flight models rather than with the full, $1/9^{th}$ scale RPV.

The successful flight test of this aircraft formed the foundation for an ongoing flight test program for reduced complexity flight test models. During the last two years, nine reduced complexity flight models (of three different design iterations) have been successfully designed, built and flight tested, each providing invaluable insight into the control surface effectiveness, handling qualities, stability, control and required pilot workload of the JWSC configuration. Between Virginia Tech and Quaternion Engineering, there have been over 60 successful flights of reduced complexity JWSC models. The following sections, adapted from Reference 14, outlines each of the three design iterations, including its important design characteristics and lessons learned from the flight test of the model.

8.1 Flat Plate Foamie

The first reduced complexity JWSC flight model created was a 66 in wingspan flat plate foam aircraft with a flying weight of 2.2 lbs named the "Flat Plate Foamie." This aircraft is designed to serve as an experimental platform to test and validate proposed control schemes as well as address the yaw stability and control authority questions. The model, shown being flown by the author in flight in Figure 63, was constructed of 0.25 inch flat extruded polystyrene fanfold insulation underlayment board with carbon fiber arrow shaft spars. The streamer shown in Figure 63 was added to aid the pilot in referencing the aircraft during flight, because the unique, diamond shape of the JWSC proved to be difficult to track during flight.

Figure 63. Flat Plate Foamie in flight during a flight test (adapted from Ref. 14) Used under fair use guidelines, 2011.

When designing the model, a balance was struck between the simplicity and operability of the model and the desired accuracy of the representation of the flight dynamics of the full scale RPV. The model features dihedral, anhedral and sweep angles representative of the full scale geometry; however, the camber and complex spanwise twist distribution present in lifting surfaces was omitted. Additionally, a simple, high thrust-to-weight ratio propeller propulsion system was used for ease of operation and maintenance. Finally, the laminar flow airfoils selected for the full scale RPV are replaced by flat plates due to the small scale of the model and the chosen materials.

A series of flight tests were completed to first establish an acceptable CG location for the model and trim the aircraft. Once this was completed, remaining flight tests were used to test various control surface schedules for the aircraft, assess control authority, investigate yaw stability and gain pilot experience flying a joined-wing aircraft.

These flight tests yielded several results. The first and most important result was that the aircraft was able to maintain stable, controlled flight despite minimal yaw control authority. One

major problem encountered was the sensitivity of the aircraft to the thrust line of the motor. Approximately eight degrees of declination of the thrust line was required for stable, level flight. A second major problem encountered was the large angle of attack required to maintain level flight and the tendency of the aircraft to tip stall in sharp turns. This problem was primarily caused by the low flight speed afforded by the propulsion setup chosen for this model; however, the absence of the spanwise twist distribution could have contributed to the tip-stalling tendencies.

In summary, the Flat Plate Foamie provided a simple yet successful first attempt at flying a JWSC model. The lessons learned and the problems encountered were used to design and test the second model, the EDF Twist Corrected Foamie.

8.2 EDF Twist Corrected Foamie

The second sub-scale model created was designed and built to correct the shortcomings of the Flat Plate Foamie. The model, shown in flight in Figure 64, was constructed of extruded polystyrene foam wrapped in fiberglass with inlaid uni-carbon strips to provide stiffness to the lifting surfaces. In an effort to remove the tip stall tendency, increase flight speed and remove the thrust line issues, custom wing jigs were created to incorporate the spanwise twist distribution, and the propeller propulsion system was replaced with an electric ducted fan (EDF) propulsion system. These two design improvements contributed to the name, the "EDF Twist Corrected Foamie."

Figure 64. EDF Twist Corrected Foamie in flight during a flight test (adapted from Ref 14) Used under fair use guidelines, 2011.

Flight testing of the EDF Twist Corrected Foamie showed marked improvement over the Flat Plate Foamie. The higher flight speeds reduced the danger of tip stalling in turns and greatly improved the flight performance. The pilot commented that as long as the aircraft maintains

speed through turns and long shallow turns were taken as opposed to abrupt high bank angle maneuvers, the aircraft behaves favorably with predictable behavior. Follow on stall testing showed that the aircraft has docile, level stall tendencies as long as tip stalls are avoided. The EDF Twist Corrected Foamie was flown with both a single EDF, as well as with a twin EDF propulsion system to more closely match the thrust to weight ratio of the GSRPV, and both systems performed well. The twin EDF propulsion system increased the wing loading, and accordingly higher flight speeds were required, but this did not cause a problem. Overall, the EDF Twist Corrected Foamie performed well for a large range of flight tests; however, before proceeding to the flight test of the GSRPV, a closer representation of the complete geometry was required.

8.3 Mini SensorCraft

The final iteration of the reduced complexity flight tests consists of a directly scaled, 37.5% model of the JWSC RPV (73 in wingspan) powered by twin 2.75 in diameter EDFs named the "Mini SensorCraft." This model was designed, fabricated and flight tested by Quaternion Engineering; however, the aim and scope of flight testing is presented here for completeness.

To create this model, the female molds created for the full scale GSRPV were scaled to 37.5% of the RPV mold size. By using these molds to fabricate the aircraft, the outer mold line of the Mini SensorCraft is identical to that of the full scale RPV, thus providing the best reduced-scale model possible. Figure 65 presents a picture of the MiniSensorCraft in flight.

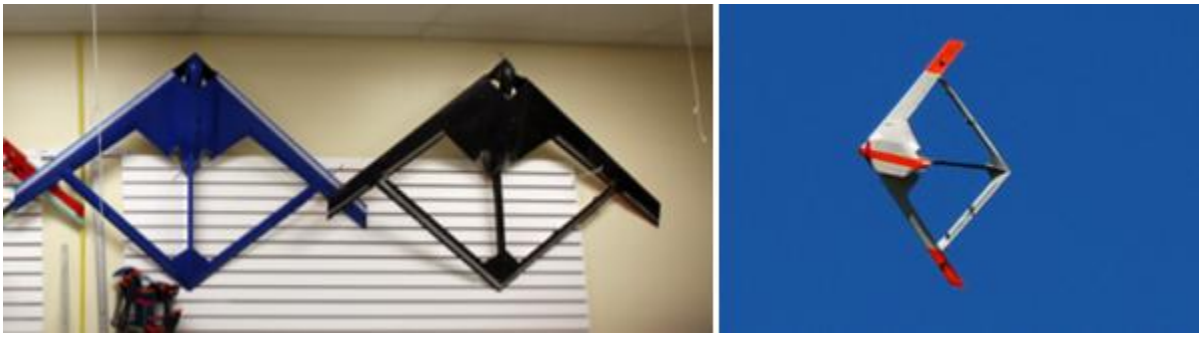

Figure 65 – Mini SensorCraft Reduced Complexity Flight Models (adapted from Ref 5)
Used under fair use guidelines, 2011

Over the course of nearly 12 months of fabrication and testing, five Mini SensorCraft airframes were built and tested in over 40 successful flights. The scope of the tests performed

ranged from initial proof of concept flights to fully autonomous flights with an incorporated ArduPilot open source autopilot. Additionally, a large number of control surface schedules were tested, including the unsuccessful incorporation of split flaps, in an effort to generate yaw control authority. Stall speed tests, handling qualities evaluation tests and practice flight tests of all planned flight maneuvers have also been completed. The primary problem with the flight of the Mini SensorCraft has been controlling dutch roll oscillations that are characteristic of the configuration. The most successful method found to control these oscilations has been the incorporation of stability augmentation through the ArduPilot autopilot which utilizes a roll damper

8.4 Summary of Reduced Complexity JWSC Models

Overall, the Reduced Complexity Flight Models have provided invaluable insight into the flight performance and handling qualities of the JWSC configuration. Additionally, the incremental increase in complexity of each of the models allowed the lessons learned from each preliminary model to be incorporated into the follow on, more advanced models. The Flight Testing of the Mini SensorCraft is ongoing at the time of writing this thesis, and the ability to practice flight maneuvers with this aircraft has proven to be a critical asset to the program.

9 Conclusions and Future Work

This thesis has presented the development and implementation of a rigorous flight test program for the flight test of a Geometrically Scaled Joined Wing SensorCraft Remotely Piloted Vehicle. It has presented and explained the development of the flight test plan, including the development of testing procedures and requirements from initial concept to successful flight test. By using the flight test plan presented here as a model, the follow on Joined Wing SensorCraft flight test program (as well as other, planned UAV flight test programs) can benefit from the experiences, lessons learned, successes and failures documented herein. The following presents a summary of key conclusions, recommendations and planned future work.

An incremental approach in complexity of all tests and testing requirements was used, and this proved to be critical to the success of the program. By incrementally increasing both the complexity of the aircraft being tested, as well as the complexity of the tests being performed with all vehicles, the inherent risk involved with testing was minimized. Additionally, the need for ground testing was shown. By attaining the maximum amount of ground test data possible, simulators and computational performance models were tuned to closely match the flight performance of the aircraft. These simulators and models provided invaluable insight into the performance of the vehicle prior to flight and important for developing control gains for the autopilot.

The iterative review process required by the AFRL was long and involved; however, the feedback and guidance provided by the members of the Technical Review Board and Safety Review Board proved to be extremely beneficial going forward with the flight test program. The flight test plan presented in Appendix A presents the results of nearly seven and a half months of formal review. By using the format and structure of this document as a guide, future programs required to complete the same (or similar) review process can benefit from the process elaborated on in this document.

In addition to developing the flight test program, this thesis also presented the development of a low-cost, low-complexity instrumentation system for the GSRPV, including the development of a strain gage and accelerometer based system for wing deflection measurement as well as the development and calibration of a custom air data boom. This system performed well during all preliminary testing, including taxi testing; however, a critical

failure occurred when the data logger power wire failed during flight testing and no data was recovered. When developing the instrumentation system, a balance was struck between fidelity, simplicity and cost, and unfortunately, the system failed at the most critical time due to a failed power wire. Going forward with future testing, it will be important to improve the robustness of the system by incorporating using more robust wiring and connecting clips as well as externally visible indicators (possibly LED lights) of active data logging. Commercially available data acquisition systems may also be investigated to improve data quality and to lessen the risk of a failure.

The results of all testing completed during the flight test program was also presented, from calibration of the air data boom through the flight test. Results presented included the calibration of the air data booms, instrumentation bench testing, propulsion system testing, a bifilar pendulum test, a static structural loading test and a complete RPV taxi test and a successful flight test.

The calibration of the custom air data boom has shown that between angles of attack and side slip angles of -10° to 10° the data shows excellent linearity with nearly no appreciable spread; however, at larger angles, spread was introduced into the data reducing the accuracy of a linear calibration. Preliminary analysis into the sources of these errors has shown that the spread at larger angles is not random, but rather can be predicted to fall above or below the linear calibration line if the angle of attack and sideslip angle are known. Further calibration is required to fully capture these effects, and this is left to future work.

The static thrust testing of the JetCat P200-SX engines provided insight into the performance of the turbine engines. Testing was completed over three days on two separate turbine engines. The data collected was compared to AFRL reference data from an independent effort. All data showed excellent correlation across the entire operational range of the engine. Additionally, the manufacturer's specified maximum thrust performance was matched. This testing promoted the safety and reliability of the JetCat P-200SX turbine engines. This reliability is primarily afforded by the closed-loop control of the turbine by the Jet-tronic ECU.

The completion of installed static thrust testing has proven that the single engine performance validated through the static thrust test can be extended to the full aircraft with losses of approximately 4.8%-10.4% due to the inlet and exhaust geometry of the GSRPV. These losses are of small enough magnitude to not negatively affect the performance of the GSRPV at

the un-ballasted weight; however, follow on testing at the scaled test point could prove risky because of the reduction in maximum thrust-to-weight ratio.

The Bifilar Pendulum Test provided accurate experimental mass moments of inertia for the GSRPV. An object of known inertia was tested, and a small 1.85% error validated the method used. Testing of the GSRPV provided excellent correlation with the as-modeled, predicted data for the roll and yaw orientations. The pitch orientation had the largest error between the modeled and measured values. Future work should be aimed at reducing the weight of the test cage, more securely constraining the model within the cage to reduce shifting and decreasing the effect of the cables in the pitch orientation.

A static structural loading test was completed for load cases ranging from 0g to 3g in 0.5g increments at a 140lb, un-ballasted flying weight. The measured deflection of the forward wing tips increased linearly with increasing load, as expected; however, the tip of the boom did not. At high wing loadings (above 2g) the slope of the boom deflection curve decreases as the loading increases. Extrapolating this curvature to higher loadings, approaching the limit load, leads to a theoretical negative slope on the load deflection curve which, under extreme loading, could lead to potential buckling of the aft wing. This test result supports the feasibility of the aim of this project in demonstrating the nonlinear aft wing response and provides confidence going forward that nonlinear response will be able to be attained when increased flexibility is introduced into the structure. Unfortunately, this nonlinear trend is only based on the last three data points taken during the test. Future work is aimed at repeating this test and taking more measurements at high wing loadings to confirm the nonlinear behavior experienced by the tail boom and the aft wing.

Taxi testing of GSRPV, including both a low speed handing test and a high speed taxi test was completed in manual mode, culminating in a high speed taxi run at 89.1% stall speed. The pilot commented that the aircraft displayed favorable handling characteristics on the ground and the brakes performed well. The full instrumentation system was operational during testing. This test was repeated in fly-by-wire mode prior to the first flight.

This program culminated with the successful first flight of the GSRPV. The success of the flight provided validation of several key design choices, including structural design and control system design, as well as provided confidence going forward with more advanced flights

and flight maneuvers. Future work is aimed at post-processing of flight data recorded by the Piccolo II autopilot, as well as planning for and completing planned follow on testing.

In summary, this thesis has presented the work of the author over approximately 24 months, and was designed to present the author's contribution to the project and frame it within the overall scope of the project. This thesis outlines the development and implementation of the flight test plan and program for the GSRPV from concept to successful flight test. The successful completion of the flight test has provided experience and confidence going forward with the more complex Aeroelastic Response program and the Aeroelastically Scaled RPV.

Appendices

A. Flight Test Plan

This appendix presents the formal flight test plan developed for this effort. This document is presented as a ***stand-alone document***. Page numbers have been updated to fit into this thesis, but for the complete presentation of the document, all sections and references presented herein are independent of those presented in this thesis.

Fair Use of Figures

All figures contained in this document were created by the authors, or were used under fair use guidelines, 2011. Four figures were taken from websites to illustrate hardware being incorporated into the aircraft. The sources for those figures are presented below.

Figure 39 - GoPro HD Hero 960 Camera in Ruggedized Case

Source:

"GoPro HD Hero 960." Tech Tilt. 3 October 2010.
http://www.techtilt.com/2010/10/03/gopro-hd-hero-960/

Figure 40 - 3D Hero Camera System in Ruggedized Case

Source:

"GoPro - 3D HERO System." technologyihub. 8 April 2011
http://www.technologyihub.com/gopro-3d-hero-system/

Figure 41 – Oracle Video Diversity Controller

Source:

"Oracle Video Diversity Controller." New Generation Hobbies. 2010
http://www.nghobbies.com/cart/index.php?main_page=product_info&cPath=1_5_95&products_id=106

Figure 42 - Control surface deflection meter

Source:

"AccuThrow Control Surface Deflection Meter." Hobbico, Inc. 2010
http://www.greatplanes.com/accys/gpmr2405.html

Joined Wing SensorCraft
Flight Demonstration Program Flight Test Plan
Geometrically Scaled RPV

Blacksburg, VA — Victoria, BC — Foremost, AB

Co-Authors:

Tyler Aarons – Virginia Tech

Jenner Richards – The University of Victoria

Security Classification: Unclassified

AFRL Program Manager: Ned Lindsley

Virginia Tech POC: Robert Canfield

University of Victoria/ Quaternion Engineering POC: Afzal Suleman

CCUVS POC: Sterling Cripps

Version 10: Updated 6 July, 2011

Executive Summary

The aeroelastic scaling of the Boeing Joined Wing SensorCraft (JWSC) and flight testing of the scaled model is the topic of an ongoing international collaboration between Virginia Tech and The University of Victoria (Canada). The program leverages the resources of Quaternion Engineering Inc. (Victoria, Canada), the Canadian Centre for Unmanned Vehicle Systems (CCUVS), and the AFRL/ Virginia Tech/ Wright State Collaborative Center for Multidisciplinary Sciences (CCMS) at Virginia Tech. This ambitious program has two primary objectives. The first is to develop a cost-effective, aeroelastically scaled, remotely piloted vehicle (RPV) to investigate the known geometrically nonlinear behavior associated with the JWSC configuration. The second objective is to design and perform flight test experiments to demonstrate, measure and characterize the nonlinear behavior in flight.

The JWSC is a high aspect ratio, joined wing aircraft. It features four lifting surfaces forming a diamond shape with a fuselage and vertical tail along the longitudinal axis of symmetry. The JWSC RPV has a 16.4ft span (5m) and is powered by twin JetCat P200-SX turbine engines. The airframe total flying weight at the scaled test point will be 204.5 lbs. Cruise speed range is approximately 66-125 kts and control is accomplished through the use of 10 control surfaces.

The JWSC Flight Test Program (FTP) is divided into two distinct phases: the Flight Demonstration Program and the Aeroelastic Response Program. The Flight Demonstration Program involves the design and flight testing of the Geometrically Scaled RPV with equivalent rigid body dynamics, but with no aeroelastic scaling. The program extends to include construction methods, flight test instrumentation selection and integration, control system tuning and flight test program development and execution. The Flight Demonstration Program, including development of the Geometrically Scaled RPV, is the subject of this report. Once the Geometrically Scaled RPV flight tests are completed, the Aeroelastic Response FTP will begin. This program includes the re-winging of the Geometrically Scaled RPV to include aeroelastically scaled lifting surfaces. The Flight Test Program for this new, re-winged RPV, known as the Aeroelastically Scaled RPV, will be the subject of a second, follow on test plan. This document supports the approval process for the Flight Demonstration Program, including all ground and flight tests related to the Geometrically Scaled RPV. A separate test plan will be filed for the Aeroelastic Response FTP.

The Flight Demonstration FTP is divided into three phases, with the complexity and scope of the tests increasing with each phase.

Phase 1: **System Tests -** This phase includes the Integration and testing of all onboard systems, including instrumentation and data logging capabilities, static thrust testing, verification of control surface mixing and experimentally finding the center of gravity.

Phase 2: **Flight Readiness Tests -** This phase includes ground testing of the complete Geometrically Scaled RPV. A bifilar pendulum will be used to experimentally determine the overall mass moments of inertia, static structural loadings to validate structural design.

Phase 3: **Flight Tests -** This phase includes all flight test operations of the RPV. Taxi tests, phasing tests and maneuvering tests are all included in this phase. Test planning is also included for parameter identification tests as well as an incremental increase in weight to the test point.

Table of Contents

List of Tables

List of Figures

1 Introduction

1.1 Motivation

High altitude, long endurance (HALE) unmanned aerial vehicles (UAVs) are capable of providing revolutionary intelligence, surveillance and reconnaissance (ISR) capabilities over vast geographic areas when equipped with advanced sensor packages. The aeroelastic responses, specifically aft wing buckling and gust load response, associated with the Joined Wing SensorCraft (JWSC) have been demonstrated and investigated in numerous computational and wind tunnel studies[1-3]; however, these phenomena have never been successfully tested in a flight test program. The Air Force has determined that an aeroelastically scaled Remotely Piloted Vehicle (RPV) provides a low cost and effective way to investigate these non-linear aeroelastic responses. By experimentally demonstrating, investigating and measuring these responses, future flight test programs will be able to test active aeroelastic control and gust load alleviation systems to reduce the structural and aerodynamic effects of the nonlinear responses. In addition, the testing of the RPV will serve to validate the aeroelastic scaling methods employed and support management planning for future tests of SensorCraft technologies.

1.2 Background Information

The SensorCraft is a concept initiated by the Air Force Research Laboratory (AFRL) to serve as a next-generation, HALE reconnaissance system. The SensorCraft is envisioned to fill the role of the next generation HALE ISR platform to contribute to persistent battlespace awareness capabilities in the 2015 time frame.[4] The full scale JWSC mission profile is shown in Figure 1.

The Boeing Joined Wing Concept, shown in Figure 2, represents the topic of this flight test plan.

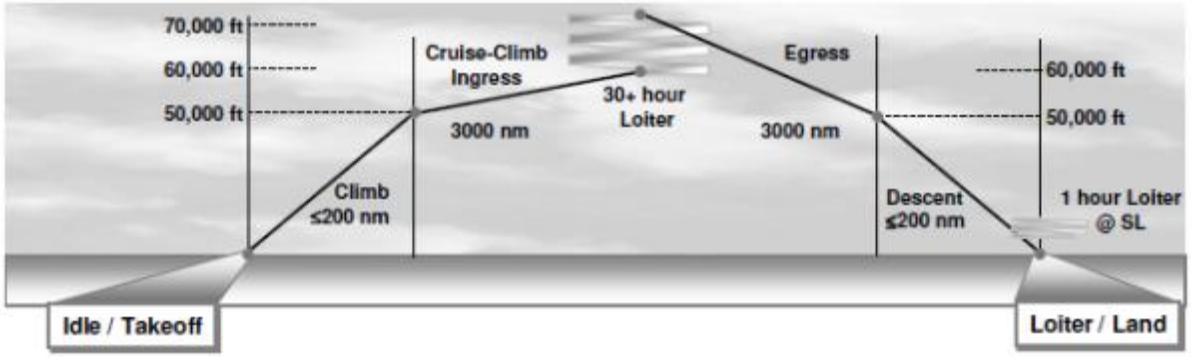

Figure 1 – Full Scale SensorCraft mission profile[4]

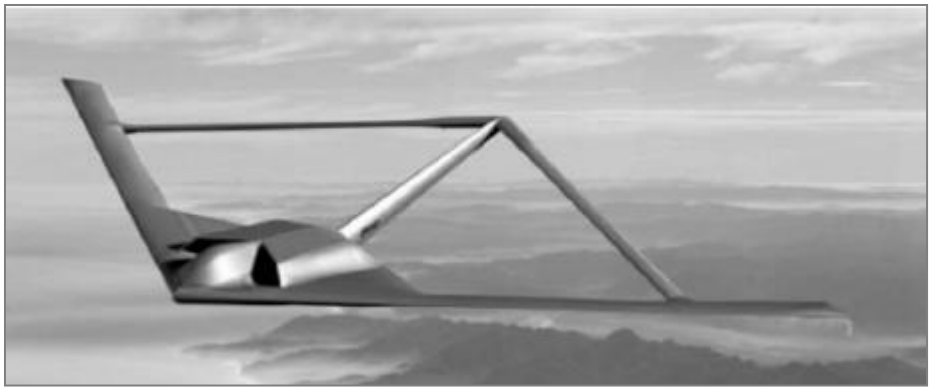

Figure 2. Joined wing SensorCraft Concept[4]

The primary driver behind this departure from conventional aircraft design is the ability to incorporate conformal radar antennas in the fore and aft wings to provide persistent 360 degree, foliage penetrating surveillance. This ability is of great benefit to the ISR mission; however, it does come with a price. Previous computational studies of joined-wing aircraft configurations have shown the importance of geometric nonlinearity due to large deflections and follower forces that may lead to buckling of the aft wing[1,5]. This potential buckling represents a unique and challenging aeroelastic design problem. The non-linear behavior, which is a result of the joined wing configuration and advanced, lightweight structural design, could be removed by strengthening the wing to a point where these non-linear behaviors vanish; however, this would result in large penalties in aspect ratio and structural weight, greatly reducing the performance of the aircraft. To avoid these penalties, nonlinear aeroelastic design, analysis and testing are required to ensure that the JWSC is able to sustain the nonlinear responses required to complete the proposed ISR mission. An aeroelastically scaled RPV provides a low cost and effective way to investigate these non-linear aeroelastic responses.

The full scale flight point of interest corresponds to a fully fueled take off condition at sea level. This "worst case" flight condition represents the most hazardous portion of the mission due to high wing loading and low thrust-to-weight ratio due to the high volume of onboard fuel necessitated by the HALE ISR mission; see Figure 1. The Air Force requests that a 1/9th scale RPV be built with equivalent scaled physics. Table 1 summarizes both the full scale and the corresponding reduced scale test configurations while Figure 3 illustrates the size of the full scale and RPV airframes.

Table 1. Summary of full scale and RPV test configurations

	Full Scale JWSC	RPV
Span (ft)	150	16.4
Test Point Speed (kt)	168	56
Test Point Weight (lb)	155,337	204.5
Test Point Wing Loading (psf)	124.4	13.6
Altitude (ft)	Sea Level	Sea Level

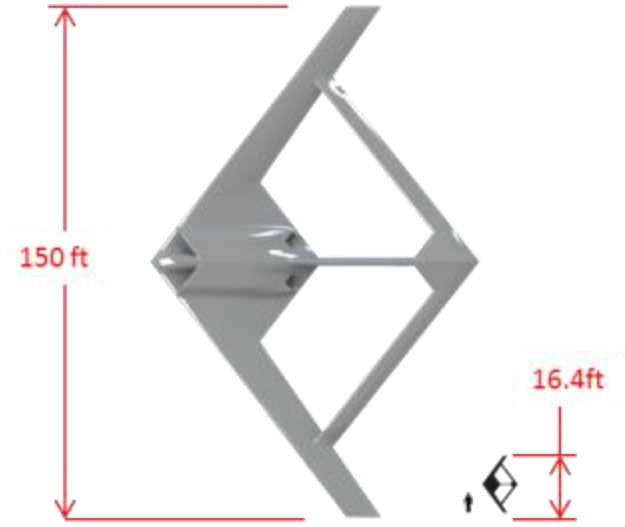

Figure 3 - Relative size of full scale JWSC and RPV[6]

1.3 Program Overview

The aeroelastic scaling of the JWSC and flight testing of the scaled model is the topic of an ongoing international collaboration between Virginia Tech and The University of Victoria (Canada). The program leverages the resources of Quaternion Engineering Inc. (Victoria, Canada), the Canadian Centre for Unmanned Vehicle Systems, and the AFRL/ Virginia Tech/ Wright State Collaborative Center for Multidisciplinary Sciences (CCMS) at Virginia Tech.

1.3.1 Program Breakdown

Due to the unique JWSC geometry, the relative large scale of the RPV and the challenge of fabricating aeroelastically scaled, flight worthy components, the JWSC Flight Test Program (FTP) is divided into two distinct phases: a Flight Demonstration Program and an Aeroelastic Response Program. The Flight Demonstration Program involves the design of a Geometrically Scaled RPV (one with equivalent rigid body dynamics, i.e. preserved aerodynamics, overall mass and moments of inertia, but no aeroelastic scaling) including construction methods, flight test instrumentation selection and integration, control system tuning and flight test program development. This also includes the construction and flight testing of several preliminary models to determine flying qualities and trim requirements[*]. During this program, preliminary aeroelastic scaling, which represents the beginning of the Aeroelastic Response Program, will also be performed. The Flight Demonstration Program will conclude with the successful completion of the tests described in Section 3.3.

Once the Geometrically Scaled RPV flight tests are completed, construction will begin on the aeroelastically scaled RPV and a second flight test program will be developed. The project will culminate in the completion of the flight test program of the aeroelastically scaled RPV. The Aeroelastic Response

[*] All preliminary, reduced complexity flight models were designed, tested and flown using private funding from Quaternion Engineering as internal research and development (IRAD) to promote the success of this program.

Program and the Aeroelastically Scaled RPV are not covered in this test plan. They will be the subject of a follow-on test plan.

1.3.2 Participating Organizations

The major organizations playing roles in this project are Virginia Tech, The University of Victoria, Quaternion Engineering Inc., the Canadian Centre for Unmanned Vehicle Systems (CCUVS), and the AFRL/ Virginia Tech/ Wright State Collaborative Center for Multidisciplinary Sciences (CCMS) at Virginia Tech. Virginia Tech is the primary contractor. Quaternion Engineering is the subcontractor, and also the owner of the test articles. The University of Victoria employs the founders and employees of Quaternion Engineering, Inc. AFRL is the lead test organization (LTO) and provides funding and guidance for the project. CCUVS is a participating test organization (PTO), and provides support for the execution of all planned tests.

2 Test Item Description

This section provides a description of the Geometrically Scaled RPV. A general description of the vehicle, including overall dimensions will be presented first. This will be followed by descriptions of the control surface layout, structural design and propulsion system. A description of the internal layout of the fuselage and the location of all trimming weights will close this section.

2.1 General Description

The test item for the Flight Demonstration Program is the Geometrically Scaled RPV and the tests will include the first flight of a prototype airframe. To reduce risk, four reduced complexity models have been used as a gradual increase in complexity to the final Geometrically Scaled RPV. For more information on the reduced complexity models, see Appendix A. The Geometrically Scaled RPV is a 1/9th scale model of the Boeing JWSC concept, and the RPV has been designed and manufactured by Jenner Richards of the University of Victoria. A CAD rendering of the Geometrically Scaled RPV is presented in Figure 4.

Figure 4 - CAD Renderings of the Geometrically Scaled RPV[7]

The Geometrically Scaled RPV is a joined wing configuration consisting of a center body housing twin JetCat P200-SX turbine engines, a vertical tail boom and four lifting surfaces. The forward wings have positive dihedral and are swept aft. The aft wings have negative dihedral and are swept forward to join with the forward wings at approximately 56% span (measured from the centerline) forming a diamond. Figure 5 presents a dimensioned 3-view drawing of the Geometrically Scaled RPV highlighting key design parameters. A summary of these parameters is presented below in Table 2.

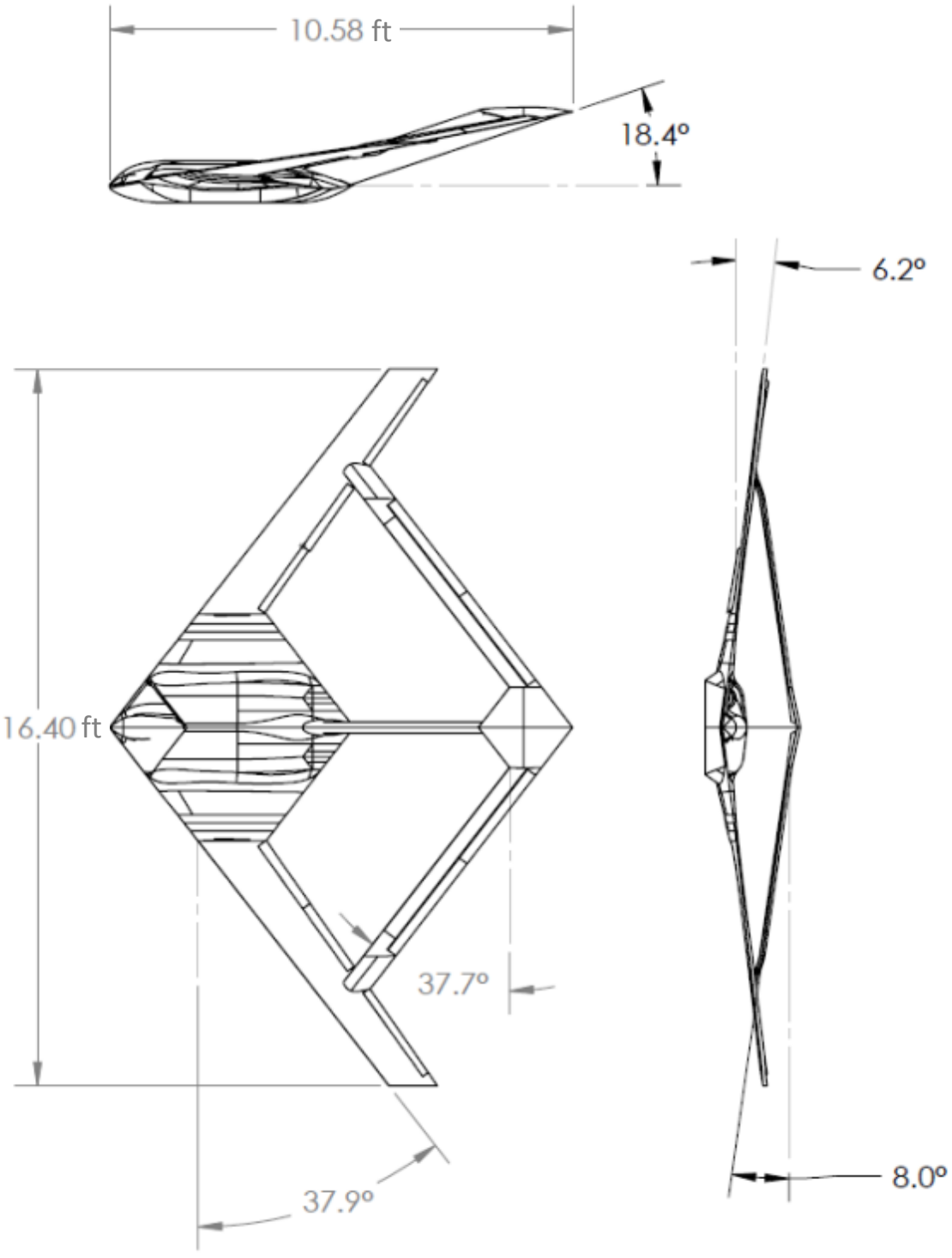

Figure 5 - Overall Dimensions of the Geometrically Scaled RPV (dimensions shown in ft)[13]

Table 2 - Geometrically Scaled RPV Specifications

Geometrically Scaled RPV Specifications	
Wingspan	16.4 ft
Wing Area	15.0 ft^2
Length	10.58 ft
Aircraft Weight	131.8 lbs
Test Point Weight	204.5 lbs
Total Thrust	104 lbs
Test Point Speed	56 kts
Front Wing Sweep	37.9°
Front Wing Dihedral	6.2°
Aft Wing Sweep	-37.9°
Aft Wing Dihedral	-8.0°

2.2 Performance

Key performance parameters (KPP's) for the Geometrically Scaled RPV are presented below in Table 3 and a typical mission profile is presented in Figure 6. Note that all KPP's are estimates based on Fluent CFD analysis of the JWSC configuration in free stream conditions. The stall speed that is presented below is for the maximum weight in free stream conditions.

Table 3 - Key Performance Parameters

Stall Speed	46.3 kts
Never Exceed Speed	152 kts
Cruise Speeds	66-125 kts
Max Range	Visual Range
Max Endurance	40 min

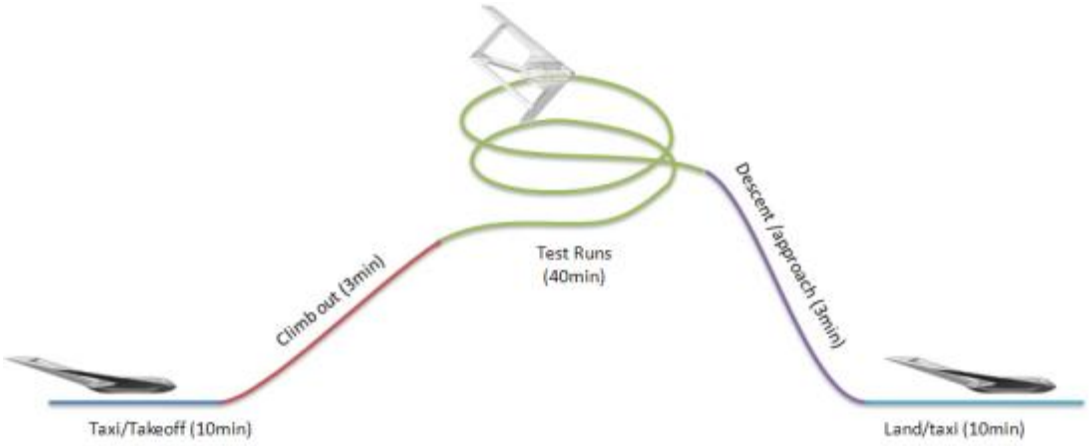

Figure 6 - Geometrically Scaled RPV Mission profile[6]

2.3 Control Surface Layout

2.3.1 Control Surface Scheduling

The control surface locations are specified in the supplied full size aircraft geometry. Surface sizing and locations are unchanged with the exception of splitting the outboard ailerons into two separate surfaces due to a complex hinge line as the wing twists towards the tip. Figure 7 shows the control surface layout.

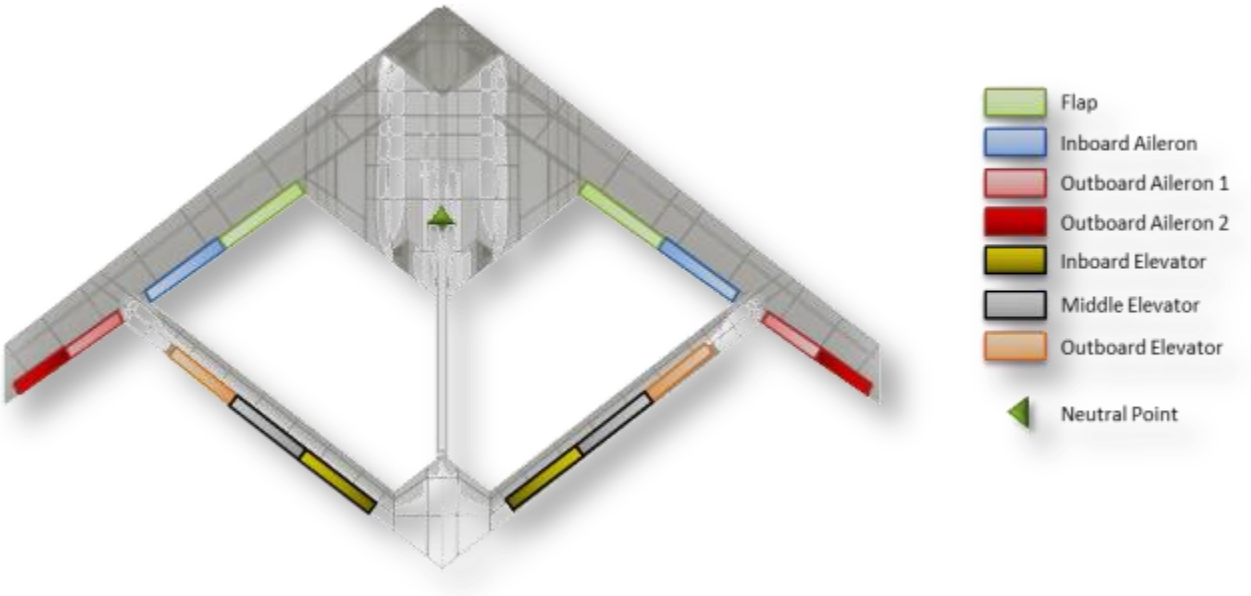

Figure 7 – Control Surface Layout[7]

Several control surface scheduling schemes have been both simulated and tested using reduced scale aircraft. The scheduling that will be used in the initial flight test of the rigid aircraft is summarized in Table 4.

Table 4 - Control Surface Scheduling

Surface	Function
Flap	Flaps
Inboard Aileron	Flaps or Aileron
Outboard Aileron 1	Primary Aileron
Outboard Aileron 2	Primary Aileron
Inboard Elevator	Primary Elevator
Middle Elevator	Secondary Elevator
Outboard Elevator	Drag rudder for yaw control (Split flap)

Multiple surfaces are used to control the aircraft in each axis to provide redundancy for all critical control modes in case of in-flight failure of any surface. For the primary control surface schedule, roll command uses the inboard and outboard ailerons deflecting together as one pseudo surface, a pitch command uses the inboard and middle elevators as one pseudo surface, and yaw commands uses the outboard elevator as a split flap. Preliminary testing with reduced complexity models and in simulation has shown that the outboard aileron alone provides sufficient control authority in roll. Accordingly, the inboard aileron can be used as a flap (if more flap area is desired by the pilot) or as an aileron for additional roll control. This change is accomplished via mixing in the transmitter, and it has no effect on the placement of servos or the use of the Power Box Royals. A final potential modification uses the inboard ailerons and outboard elevators deflecting in opposite directions as a pseudo split flap/drag rudder for yaw control. This option avoids the modification of a single surface into a split flap. All three options presented above have been tested thoroughly through the use of the Mini SensorCraft, the most advanced of the reduced complexity models.

2.3.2 Servo Selection and Control Surface Flutter Reduction.

In order to reduce the possibility of control surface flutter, each surface is actuated using two servos. An aluminum rib at each hinge point acts both as the hinge attachment and also as a hard point for attaching the control horn. This reduces any flex to mitigate the possibility of flutter. Each control surface is hinged in two locations using a spherical joint. This ensures that minimal loading is transferred to the control surface and prevents binding due to excessive wing bending.

In order to size servos for the Geometrically Scaled RPV, hinge moments were calculated using VLM analysis for ±30° control surface deflections at the never exceed speed (worst case calculations). Computed hinge moments were compared with the rated torque of candidate servos (as specified in kg-cm). The final servo selected, the Turnigy HV-767 servo has a servo rating of 31 kg-cm. The results of the servo sizing calculations are presented below in Table 5.

Table 5 – Servo Sizing Analysis

Turnigy HV-767 Servo Torque = 31 kg-cm

Surface	Cmhinge	Moment (N-m)	# of Servos	Req Torque (N-m)	Req Torque (kg-cm)	FOS
Flaps+	-1.89E-03	3.94	2	1.968	20	1.57
Flaps-	8.64E-04	1.80	2	0.900	9	3.44
Inboard Aileron +	-2.13E-03	4.44	2	2.219	22	1.40
Inboard Aileron -	9.65E-04	2.01	2	1.005	10	3.08
Outboard Aileron +	-1.77E-03	3.68	4	0.921	9	3.37
Outboard Aileron -	9.84E-04	2.05	2	1.025	10	3.02
Inboard Elevator +	-2.46E-03	5.12	2	2.5603	26	1.21
Inboard Elevator -	1.55E-03	3.23	2	1.616	16	1.92
Outboard Elevator +	-2.22E-03	4.62	2	2.310	23	1.34
Outboard Elevator -	1.82E-03	3.79	2	1.894	19	1.64

From these calculations, it can be seen that the minimum factor of safety present is 1.21, and this is at an absolute worst case flight condition of maximum positive elevator deflection at the never exceed speed. By maintaining a minimum factor of safety of 1.21, the risk of control surface flutter is greatly reduced. Servos operate using a high-gain feedback controller to monitor and maintain the commanded position. Additionally, the HV-767 has a manufacturer specified operating frequency of 333 Hz. As long as the servo is not pushed beyond its maximum torque rating, the servo is able to maintain the commanded position with little variation due to loading. This, coupled with two servos per control surface (two points of contact with the main wing) minimizes the risk of control surface flutter.

2.3.3 Control Surface Center of Gravity Location

Table 6 presents the center of gravity locations for all of the control surfaces as a percentage of the mean geometric chord.

Table 6 - Center of Gravity Locations for Geometrically Scaled RPV Control Surfaces

Surface	Mean Geometric Chord (in)	CG Loc. Aft of Hinge Line (% MGC)
Flap	2.99	38.5%
Inboard Aileron	2.80	38.4%
Outboard Aileron (Inner)	2.60	38.1%
Outboard Aileron (Outer)	2.40	37.9%
Elevators (inboard, mid, outer)	2.48	31.7%

2.3.4 Control Surface Stiffness Testing

In order to calculate the control surface stiffness (as built, including linkages), a static structural loading test was completed by Jenner Richards at Quaternion Engineering. The inner outboard aileron was tested because this surface produces the most rolling moment and was therefore deemed the most critical control surface. The elevator control surfaces are equally critical from a control standpoint; however, the elevators are much thicker (and stiffer) due to the geometry of the aft wing. To test, the control surface was mounted to a steel cross member, as shown in Figure 8, to produce a solid foundation.

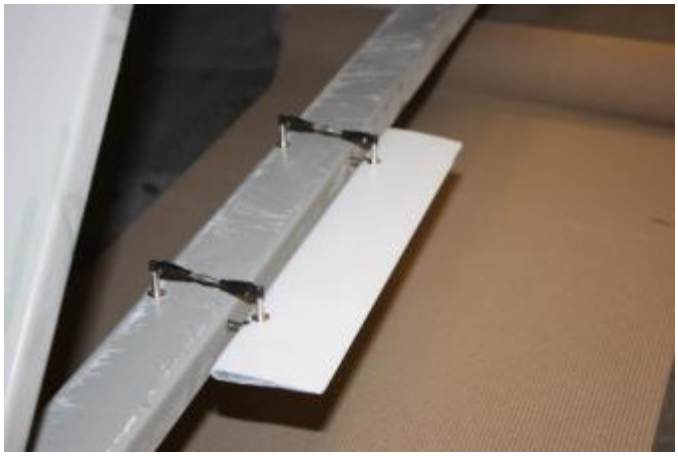

Figure 8 - Experimental Setup for Control Surface Stiffness Testing

A spring gage was used to apply a force at a known distance from the hinge line to apply a moment to the aileron at the location where the linkage was attached. The second linkage was removed during testing, so the results presented are for a single linkage (this is a very conservative test). Digital calipers were used to measure the tip displacement relative to the mounting fixture (to account for any twist in steel base). This process is shown in Figure 9.

Figure 9 - Measurement Process for Control Surface Stiffness

The measurements were converted into an angular displacement. This conversion used the linear displacement of the tip (as measured) and the location from the hinge line. Four load cases were tested, and four measurements were taken for each load case. Table 7 presents the results of these calculations and Figure 10 presents a plot of angular displacement vs. applied torque. From these calculations, it can be seen that the inner outboard aileron has an average stiffness (average taken across all 4 load cases) of **0.82 N-m/degree or 7.3 lb-in/degree**. It is important to note that these are very large torques relative to those expected during flight, and the load is applied at the tip. In flight, the load is distributed across the control surface. Accordingly, the results presented are conservative.

Table 7 - Control Surface Stiffness Testing Results

	Load Case 1	Load Case 2	Load Case 3	Load Case 4
Applied Torque (N-m)	3.12	3.75	4.37	4.99
Test 1 Rotation (rad)	0.063	0.082	0.089	0.107
Test 2 Rotation (rad)	0.064	0.079	0.089	0.112
Test 3 Rotation (rad)	0.061	0.085	0.096	0.111
Test 4 Rotation (rad)	0.067	0.084	0.095	0.109
Average Rotation (Radians)	0.064	0.082	0.092	0.110
Average Rotation (Degrees)	**3.653**	**4.712**	**5.277**	**6.297**
Average Stiffness (N-m/degree)	**0.85**	**0.79**	**0.83**	**0.79**

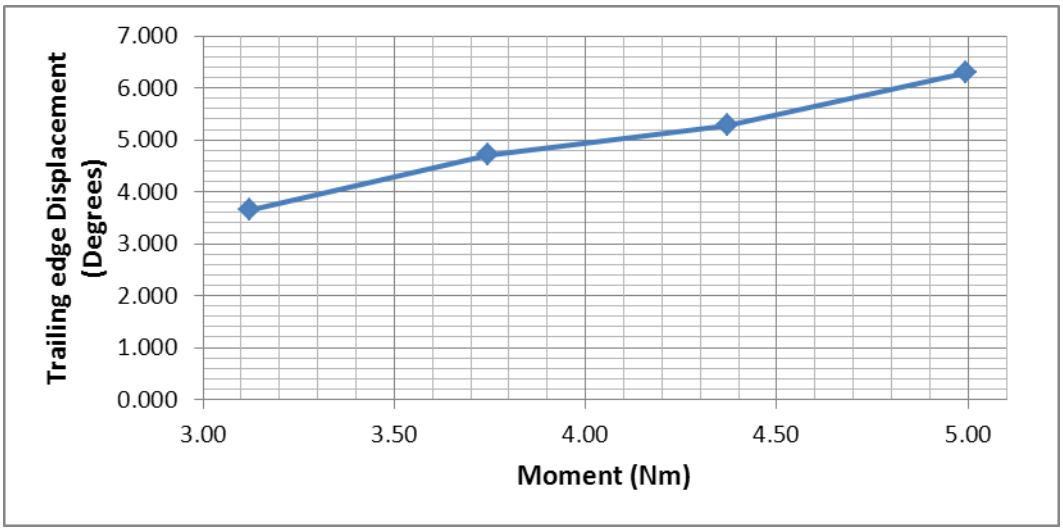

Figure 10 - Trailing Edge Displacement vs. Applied Moment

2.3.5 Control Surface Derivatives

Appendix N presents a complete list of control surface derivatives, given per degree of deflection, for all control surfaces for a range of angles of attack from -2° to 10°.

2.4 Structure

2.4.1 General Arrangement

The overall structural design of the RPV was driven by several factors including sufficient structural strength, component space reservations and modularity/reuse of the aircraft for future aeroelastic tests.

The structure, shown in Figure 11, uses conventional rib/spar construction with composite skins bearing the main loading paths. Both the front and rear wings have a forward and aft shear web which ties into integral spar caps in the wing skin to make conformal spar-boxes. The forward wing employs an additional shear web that also acts as a trailing edge closeout spar at control surface locations. Ribs are located at various stations along the span to take torsional loads and prevent wing panel buckling and flutter. The fuselage employs a similar construction with conformal spar caps running across the span. All bulkheads, spars and ribs are designed to interlock to ensure accurate location and simple assembly, as shown in Figure 12.

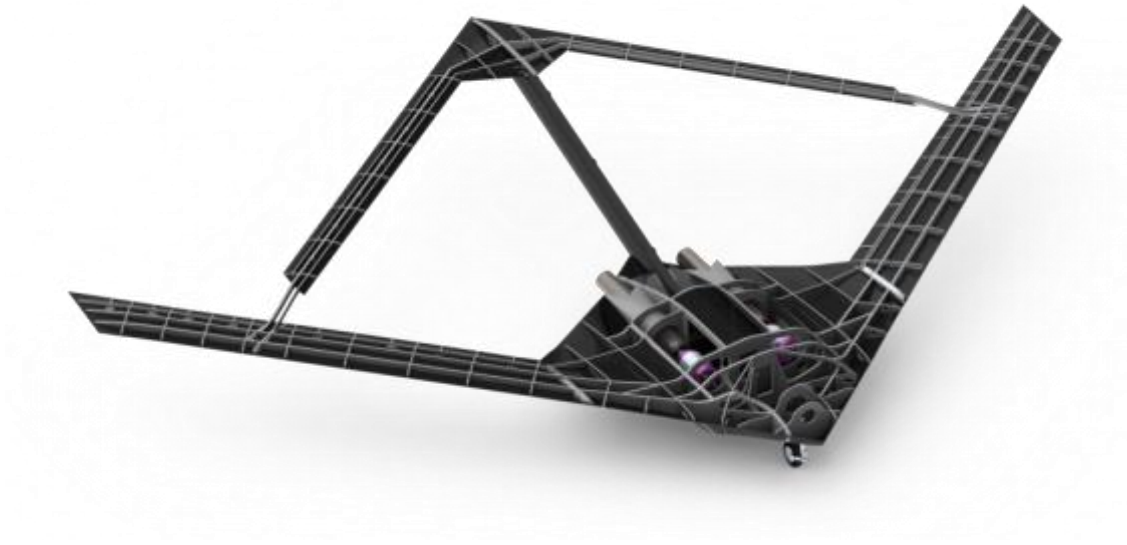

Figure 11 - General Arrangement of the Geometrically Scaled RPV[7]

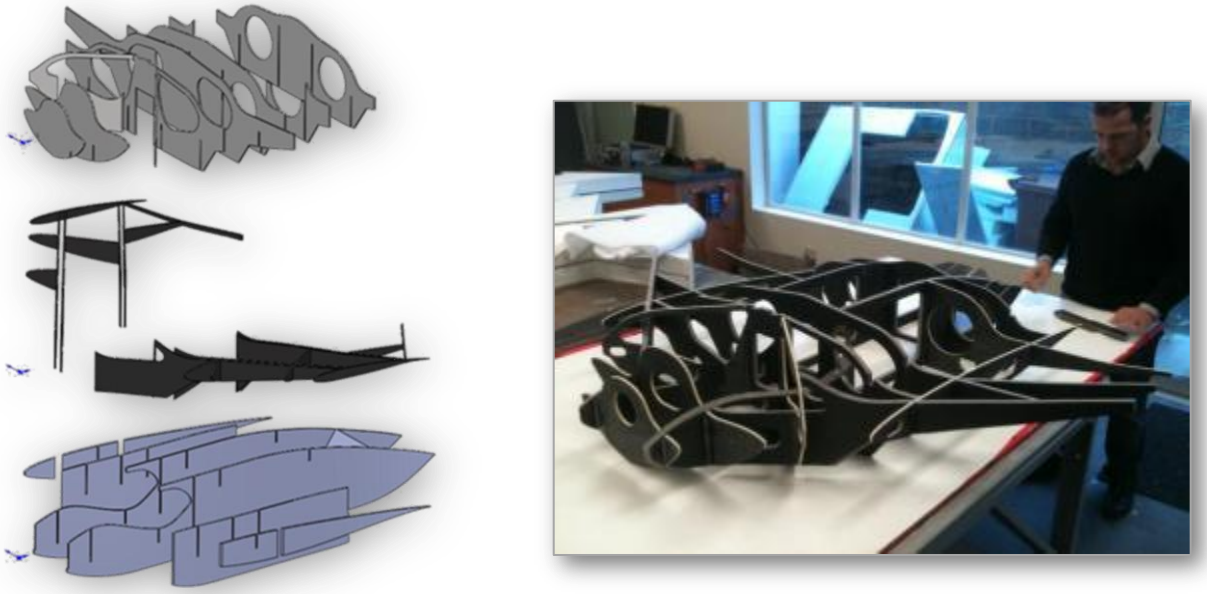

Figure 12 - Exploded View Showing Interlocking Components of the Fuselage Design (Left) Final Product (Right)[7]

The aircraft breaks down for transport and this modularity also allows quick refitting in the case of damage during flight testing. The forward wing attaches to the fuselage with a series of aircraft fasteners that transfer load from the wing spar caps into the fuselage skins. The rear wings attach to the

forward wings using a single aircraft grade fastener. The aft wing spars terminate with a partial main wing airfoil cross section. This allows the rear wing to mate into the forward wing between two aluminum ribs. A gusset plate is employed on the underside of the wing to anchor the fastener and tie joint loads into the aluminum ribs. The rear wings attach to the vertical boom using four aircraft grade fasteners. Finally the boom attaches to the fuselage by means of main boom spar passing through into a receiving compartment in the fuselage. A torque wrench will be used to ensure that all bolts are properly secured during aircraft assembly.

2.4.2 Finite Element Analysis and Validation

A Finite Element Analysis (FEA) was performed to size the aircraft's structure for a predetermined set of loading cases. The following section outlines some of the considerations, assumptions and results of this study. The results of the FEA analysis were used to develop the composite stacking sequence used for the Geometrically Scaled RPV.

2.4.2.1 Load Cases Considered

Several load cases were considered in sizing the Geometrically Scaled RPV. The aircraft mission and flight test regime called for a maximum positive-g maneuver load of three g's, a negative one g maneuver, a one g taxiing load, and loads induced by a 30^{o} aileron deflection at the maximum flight speed. Load distributions were calculated based on a vortex lattice model, shown in Figure 13, for the aerodynamic loading cases.

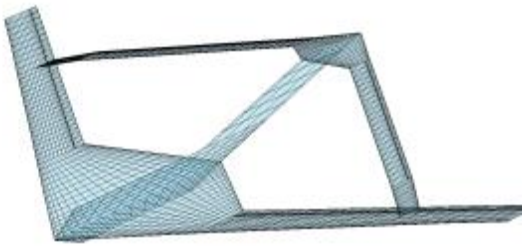

Figure 13. Vortex Lattice Model used to Generate Aerodynamic Loads[7]

For the positive and negative g cases, the aircraft was trimmed for each condition and the loads along the surfaces were transferred to the FEA model as constant equivalent loads at various panels throughout the model. Figure 14 shows the vortex lattice loads together with the assumed constant averaged load at forward wing inboard, forward wing outboard, and fuselage stations.

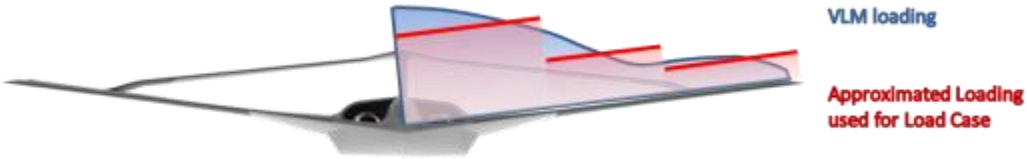

Figure 14. Aerodynamic Loads Calculated from VLM Analysis (in blue) and Approximated Loads (in red) Transferred to the FEA Model[7]

Mass properties were assigned to elements to accurately model structural weight and aircraft components such as fuel, engines and other supported systems, modeled as point masses. Inertial relief (inertial forces due to system acceleration) was then calculated to balance the applied loads to more accurately simulate a free flight condition.

2.4.2.2 Materials

Properties for the various materials were sourced from supplier's data sheets and included carbon fiber, fiberglass, laminating resin, PVC foam core, and 6061 aluminum. The orthotropic properties were calculated for carbon/epoxy and glass/epoxy laminates, including uni-directional and woven materials. Test laminates were laid up and measured to accurately determine the fiber volume fraction that could be expected using available composite fabrication techniques.

2.4.2.3 FEA Model

The FEA involved the simulation of the aircraft using layered shell elements representing the skins and internal structures. The bulkheads were modeled as foam core laminates and skins were sectioned into different zones where the type, number, thickness, and orientation of plys could be varied. Figure 15 shows the FEA model. Then, failure criteria were used to relate the material strength to the general stress-strain state due to multi-axial loads. The failure criteria employed here were the max stress, max strain, Tsai-Wu failure criterion and core shear failure criterion.

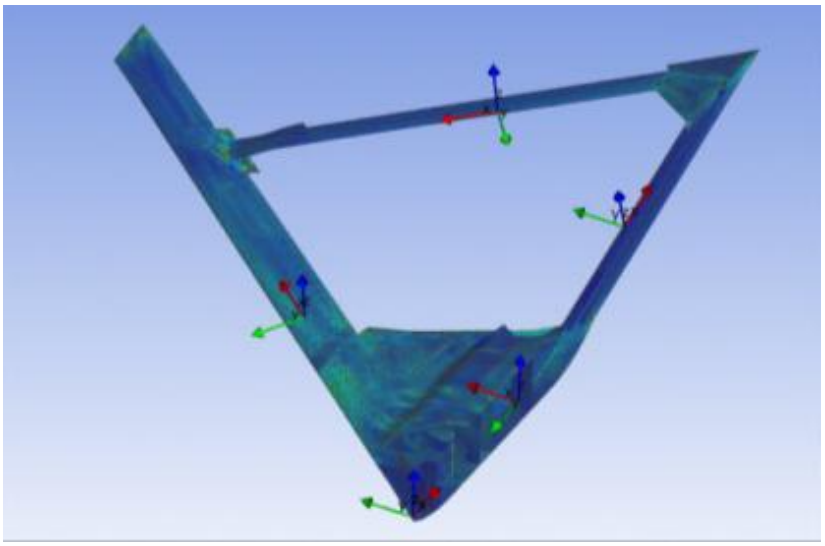

Figure 15. FEA Model of Rigid Sensorcraft Showing Primary Coordinate Systems[7]

2.4.2.4 Final Ply Layup

Several iterations were required to define a structure with a factor of safety greater than 1.5. The number, type and direction of plies in the skins, conformal spar caps and doublers were varied throughout the structure. The final ply build up for the fuselage, wings and boom are shown in Figure 16-Figure 19.

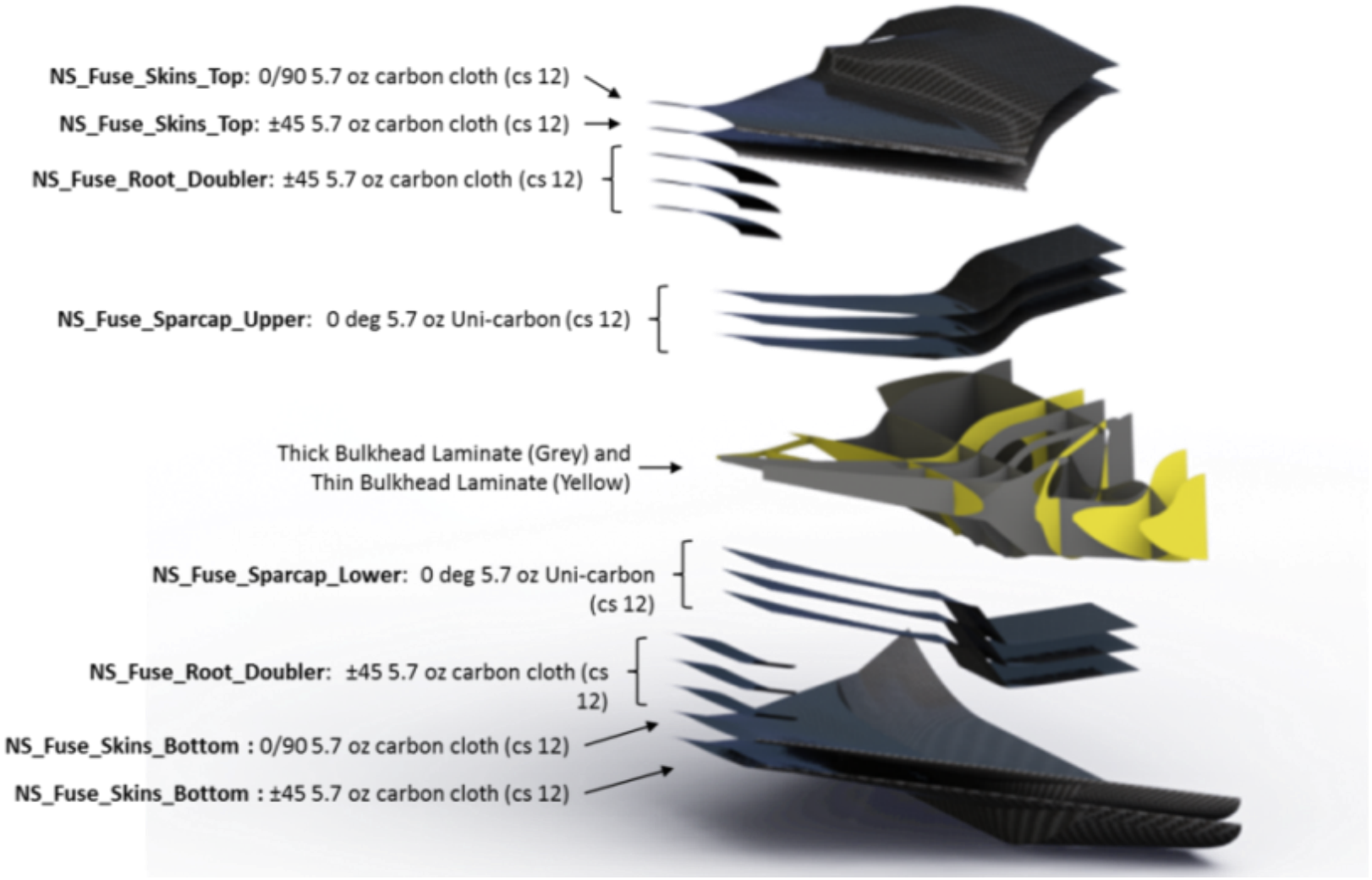

Figure 16 – Fuselage Stacking Sequence[7]

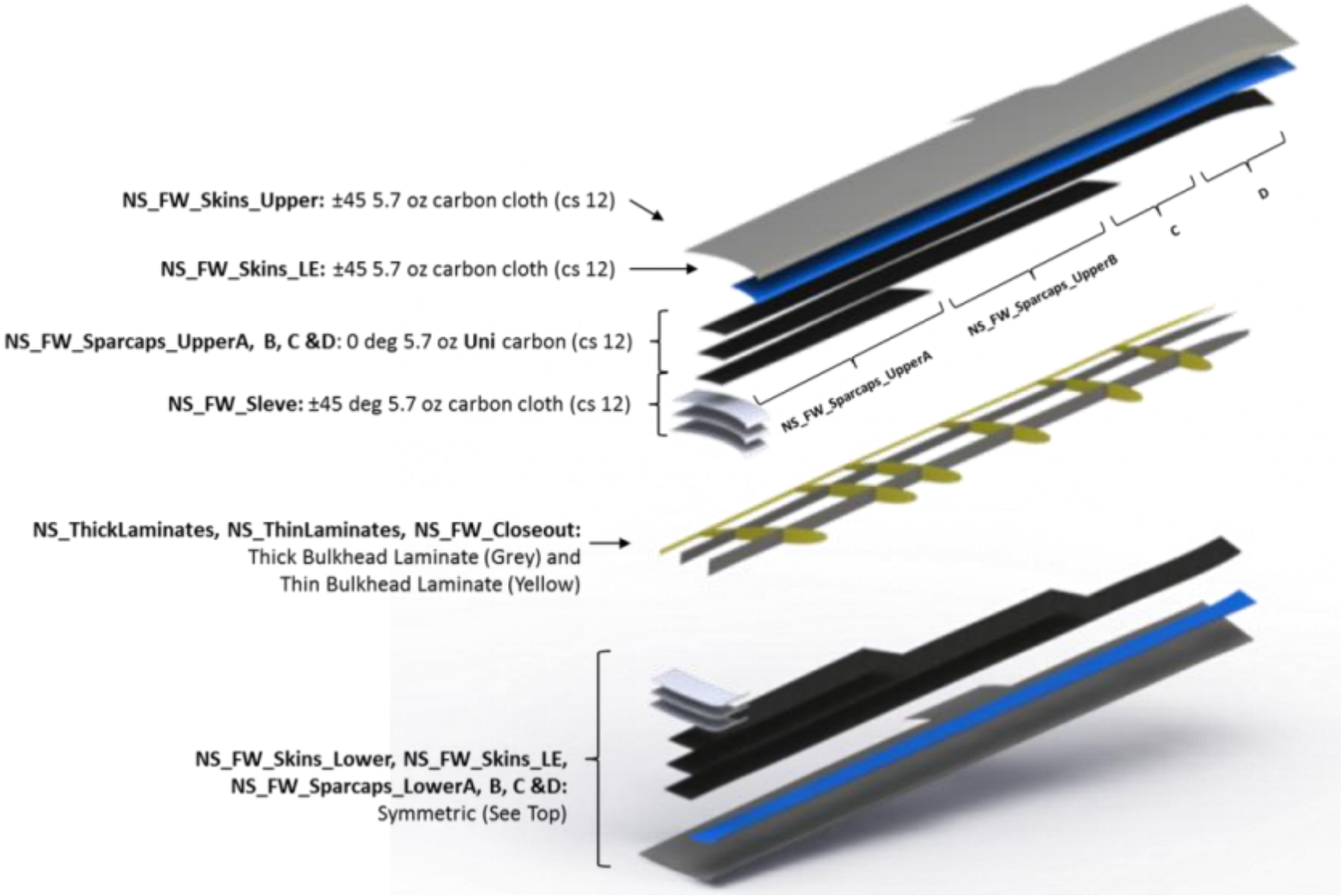

Figure 17 - Forward Wing Stacking Sequence[7]

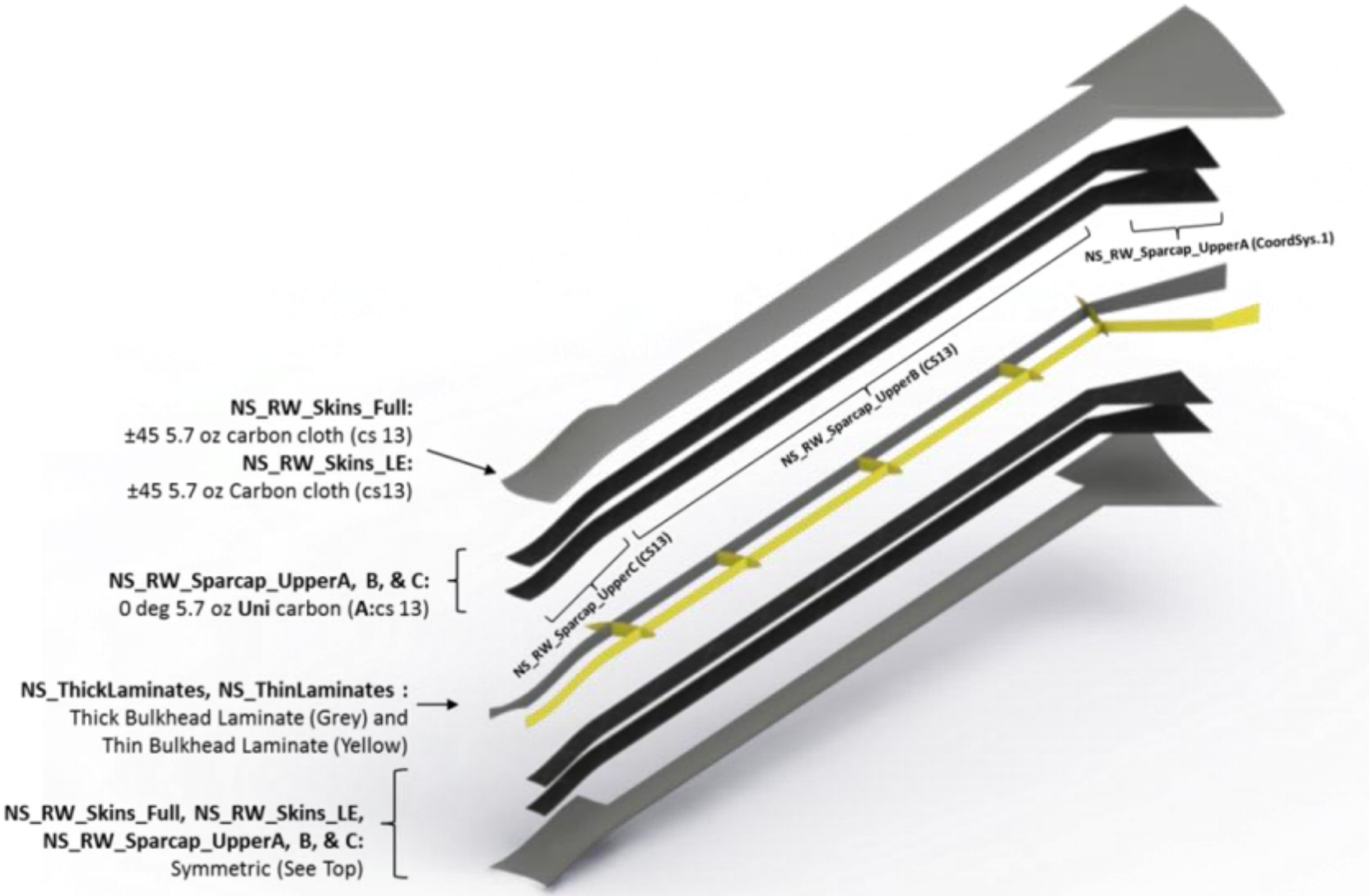

Figure 18 - Aft Wing Stacking Sequence[7]

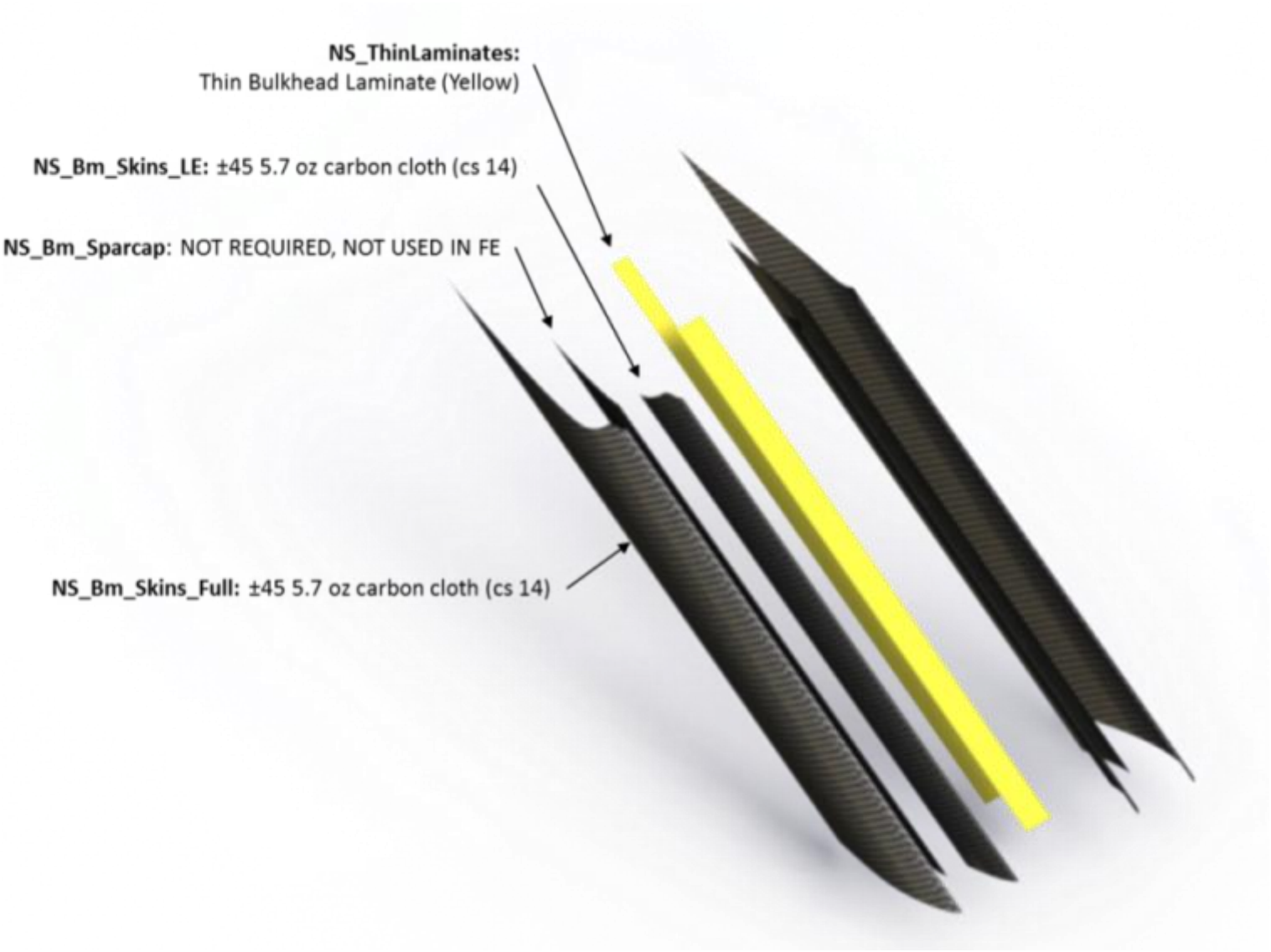

Figure 19 - Vertical Boom Stacking Sequence[7]

2.5 Propulsion

Two JetCat P200-SX turbine engines, located within the fuselage as shown in Figure 20, power the Geometrically Scaled RPV.

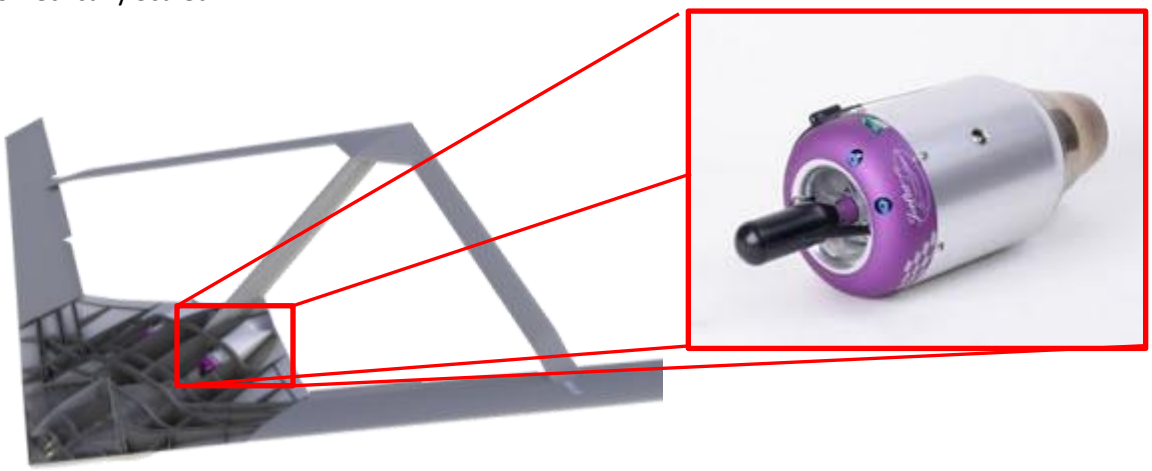

Figure 20 - Location of JetCat P200-SX Turbines in the Fuselage

The P200-SX is the largest turbine available from JetCat turbines. Table 8, shown below, provides the manufactures specified performance parameters for a single JetCat P200-SX turbine.

Table 8 - JetCat P200-SX Specifications[9]

Thrust	52 lbs @ 112,000 RPM
Weight	5 lbs
Diameter	5.12 in
RPM Range	32,000 - 112,000 RPM
Exhaust gas temperature	580°C-690°C
Fuel consumption	24 oz per/min at full power
Fuel	Jet A1 or 1-K kerosene
Lubrication	5% synthetic Oil in the fuel
Maintenance interval	25 hours

The JetCat P200-SX has many features which make it a safe and reliable choice for powering the JWSC RPV including a heavy duty starter, onboard RPM and exhaust gas temperature sensors and JetCat's industry leading customer service; however, two of the most important features are the Electronic Control Unit (ECU) and the Ground Support Unit (GSU). Below is a description of these features:

1. **JetCat Electronic Control Unit (ECU)** - The JetCat Jet-tronic ECU provides real-time closed loop control of the turbine, resulting in better starts, smoother idle and more reliable performance. The ECU, which features a Hitachi H8 16 bit microcontroller, has a fully automatic starting sequence which promotes safe, reliable starts. The ECU also monitors turbine RPM and exhaust gas temperature during flight via sensors in the turbine. Additionally, the ECU monitors fuel

pump voltage, battery voltage and calculates statistical data including total fuel consumption, total turbine time, maximum RPM, run time. The ECU also monitors total turbine runtime. This is especially useful as JetCat requires each turbine to be sent in for maintenance every 25 hours of runtime. The total engine time will be checked before each start of the engine.

2. **Ground Support Unit (GSU):** Used for monitoring or prescribing (within operational limits) key parameters such as maximum RPM and minimum RPM, in real time, during startup and ground testing. The GSU may be connected or disconnected from the ECU at any time.

The inlet and hot gas passages within the fuselage have been directly scaled for the RPV with the exception of a slight narrowing of the section around the turbines. This portion has been narrowed to create the required 0.75 inch clearance around the perimeter of each turbine to allow air passage for cooling. Figure 21 shows a cross section of the modified fuselage ducting.

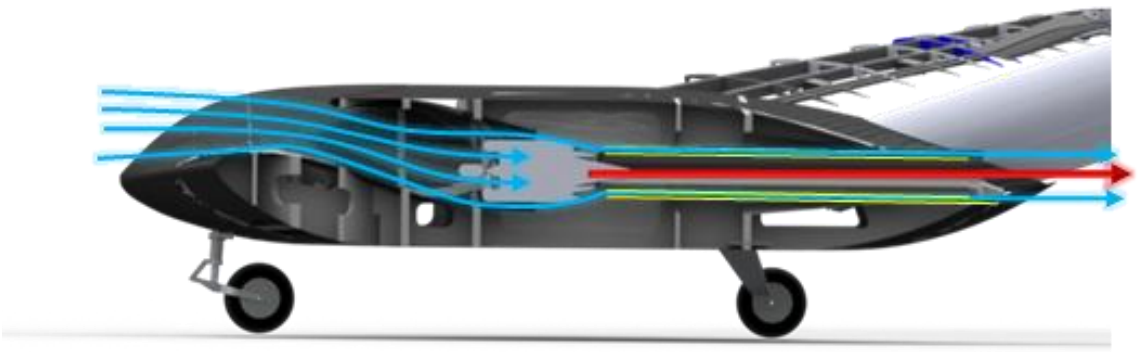

Figure 21 - Fuselage Cross-section Showing Inlet and Exhaust Routing[7]

The engines are placed near the rear of each pass-through for two reasons. The first is to directly route the hot exhaust out the fuselage, minimizing heat transfer, and the other reason is to increase the cooling airflow around the engine. Placing the engine at the point where the duct begins to constrict sets up a venturi effect which helps to draw cooling air around the outside of the engine. This is especially important when the aircraft is stationary, as in taxi and startup. Due to the danger posed by ingesting foreign objects into the turbine, mesh strainer screen is placed across the inlet to the fan opening as shown in Figure **22**.

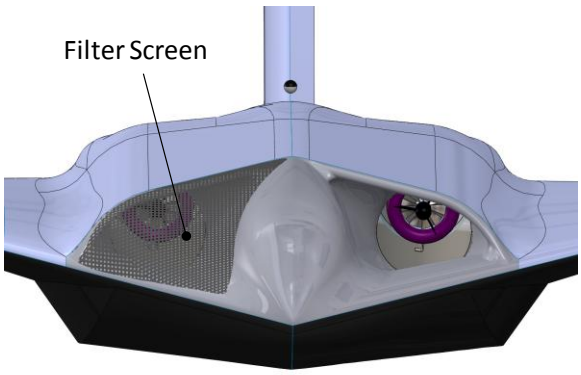

Figure 22 - Strainer Screen to Prevent Ingestion of Debris[6]

2.6 Payload

Due to the nature of the Geometrically Scaled RPV flight tests, the required payload consists of fuel, avionics (instrumentation) and trimming weights (used to ballast to the test point weight as well as provide the proper moments of inertia about each axis). In order to simplify future re-winging of the Geometrically Scaled RPV to include aeroelastically scaled lifting surfaces, no fuel is stored in the wings. Variance in the weight of the wings due to fuel burn would result in aeroelastic scaling that was only valid for a short period of time. Accordingly, the majority of the fuel is stored in a large tank on the centerline of the aircraft near the center of gravity. This location minimizes CG shift when fuel is burned. Figure 23 below shows the layout of the fuselage.

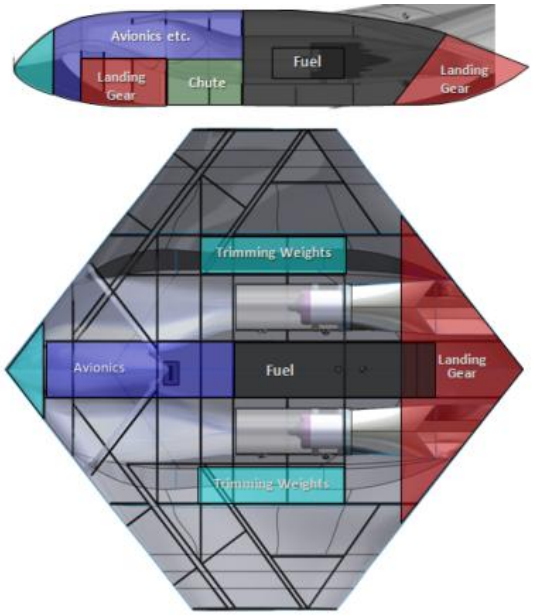

Figure 23 - Fuselage Layout

As mentioned previously, the overall mass and moments of inertia are matched through the addition of trimming masses. Careful attention is paid to the location of these trimming masses so that both overall mass and inertias are matched. In order to achieve this, four areas are chosen as locations

for the trimming weights such that their effects on the principle moments of inertia (I_{xx}, I_{yy}, and I_{zz}) are uncoupled. The locations of the trimming masses are depicted in Figure 24.

The first location is chosen within the fuselage. Since it is nearer the center of gravity, weight added here has little effect on any of the principle moments of inertia, and is only used to augment the takeoff gross weight (TOGW) of the aircraft. Next, a compartment is chosen within the wing near the joint. Addition of weight here has the greatest effect on the rolling and yawing moment, while largely uncoupling the pitching moment of inertia. (This location is also desirable structurally since the main wing is supported here by the aft wing). A compartment is chosen in the aft wing/tail boom intersection due to its larger volume and large effect on the yaw and pitch moments with the final location in the nose of the aircraft to help trim the aircraft longitudinally.

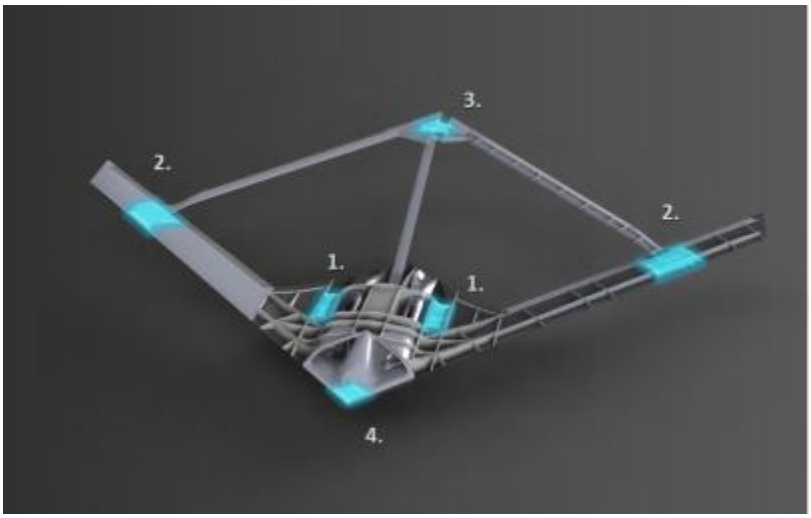

Figure 24 - Location of Trimming Weight Bays (1 in fuselage, 2 in wings, 3 in tail and 4 in nose)[7]

Table 9 presents the moments of inertia and overall aircraft mass both before and after tuning masses are placed in the payload bays. Table 9 also presents the predicted trimming mass that is required in each bay.

Table 9 - Moments of Inertia and Masses Before and After Tuning

	Payload (kg) Bays 1/2/3/4	Mass (kg)	Ixx (kg-m^2)	Iyy (kg-m^2)	Izz (kg-m^2)
Aircraft Before Trimming Weights Added	0/0/0/0	59.8	10.46	12.69	20.29
Aircraft After Adding Trimming Weights	10/11.9/8.2/3.1	93	62.22	42.45	99.09
Scaled Baseline SensorCraft	-	93	61.52	43.72	100.81

*Moments of inertia about the nose of the aircraft

2.7 Tricycle Landing Gear

Takeoff of the Geometrically Scaled RPV is accomplished via a tricycle style landing gear with steerable nose gear. The use of a tricycle arrangement of wheels gives stability during taxi testing and during the takeoff roll. Figure 25 shows the landing gear for the Geometrically Scaled RPV, including the custom designed oleo strut for the steerable nose gear. Figure **26** presents the custom designed oleo strut.

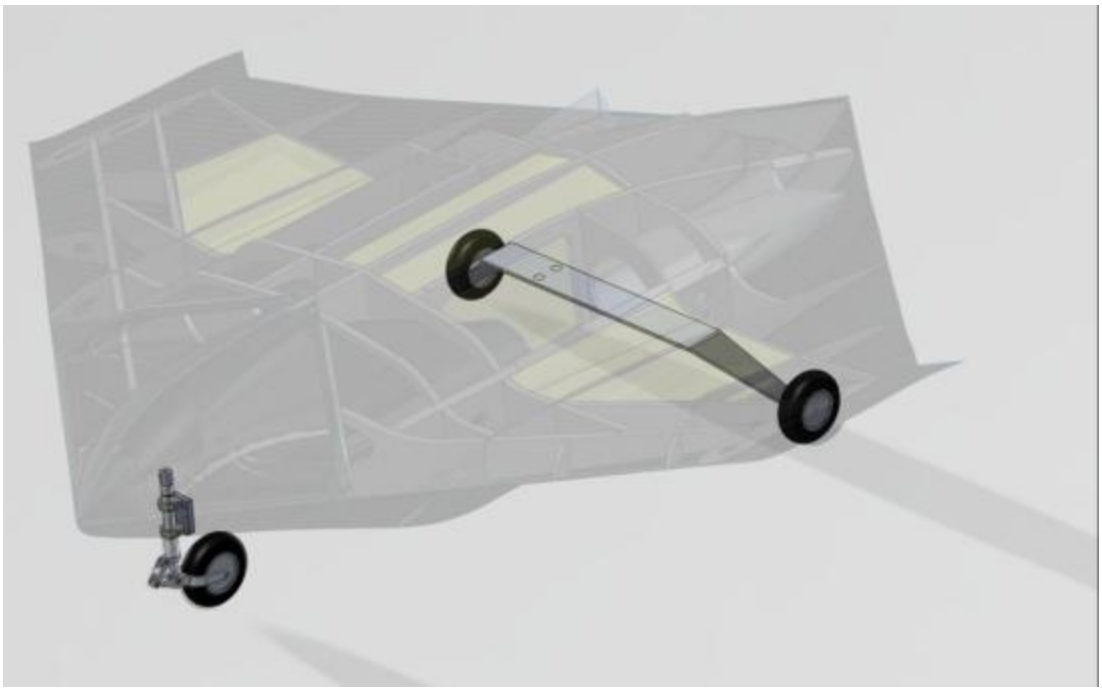

Figure 25 – Geometrically Scaled RPV Tricycle Landing Gear[13]

Figure 26 - Custom Designed Oleo Strut for Nose Gear

2.7.1 Sizing of the Landing Gear

Sizing of the landing gear was accomplished using the method described in *Airplane Design* by Jan Roskam[10,11]. The gear is designed to allow the rear gear to move forward and aft to accommodate CG shift for various takeoff weights. The rear gear can be located at 5 places, equally spaced between the forward and aft CG limits of 910mm and 1107 mm aft of the nose, respectively. The gear is attached to the fuselage by 4 bolts, and the bolt holes for the gear are pre-installed for all 5 rear gear locations. The bolts will be tightened using a torque wrench to ensure consistent attachment.

Figure 27 presents the results of the Gear Sizing calculations for the Geometrically Scaled RPV for the aft most CG location and Figure 28 presents the results for the forward most CG location. All required criteria are satisfied for both configurations and Table 10 presents a summary of key design specifications for the landing gear. Table 10 shows that all angular requirements are satisfied for both the forward and aft CG limits (and correspondingly the forward and aft limits of the rear gear placement), and accordingly, all intermediate locations will also satisfy these requirements.

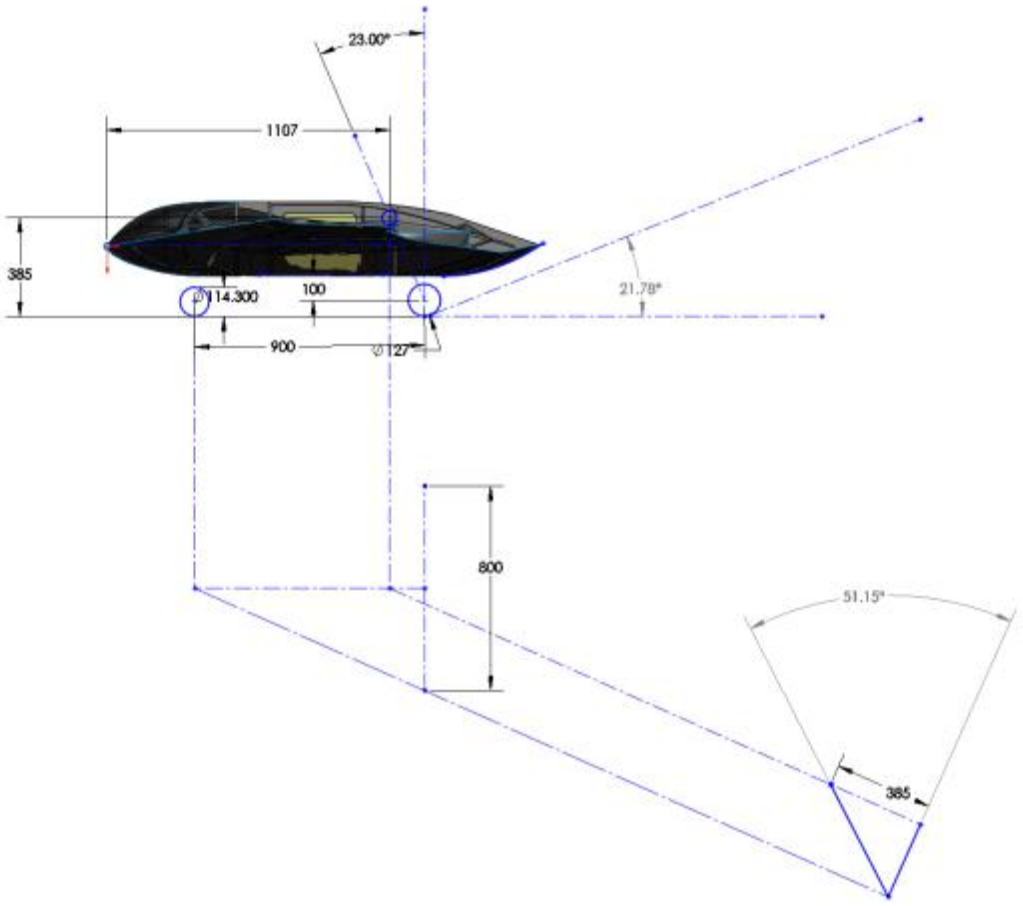

Figure 27 – Gear Sizing for the Geometrically Scaled RPV (dimensions in mm) for Aft Most CG Location[13]

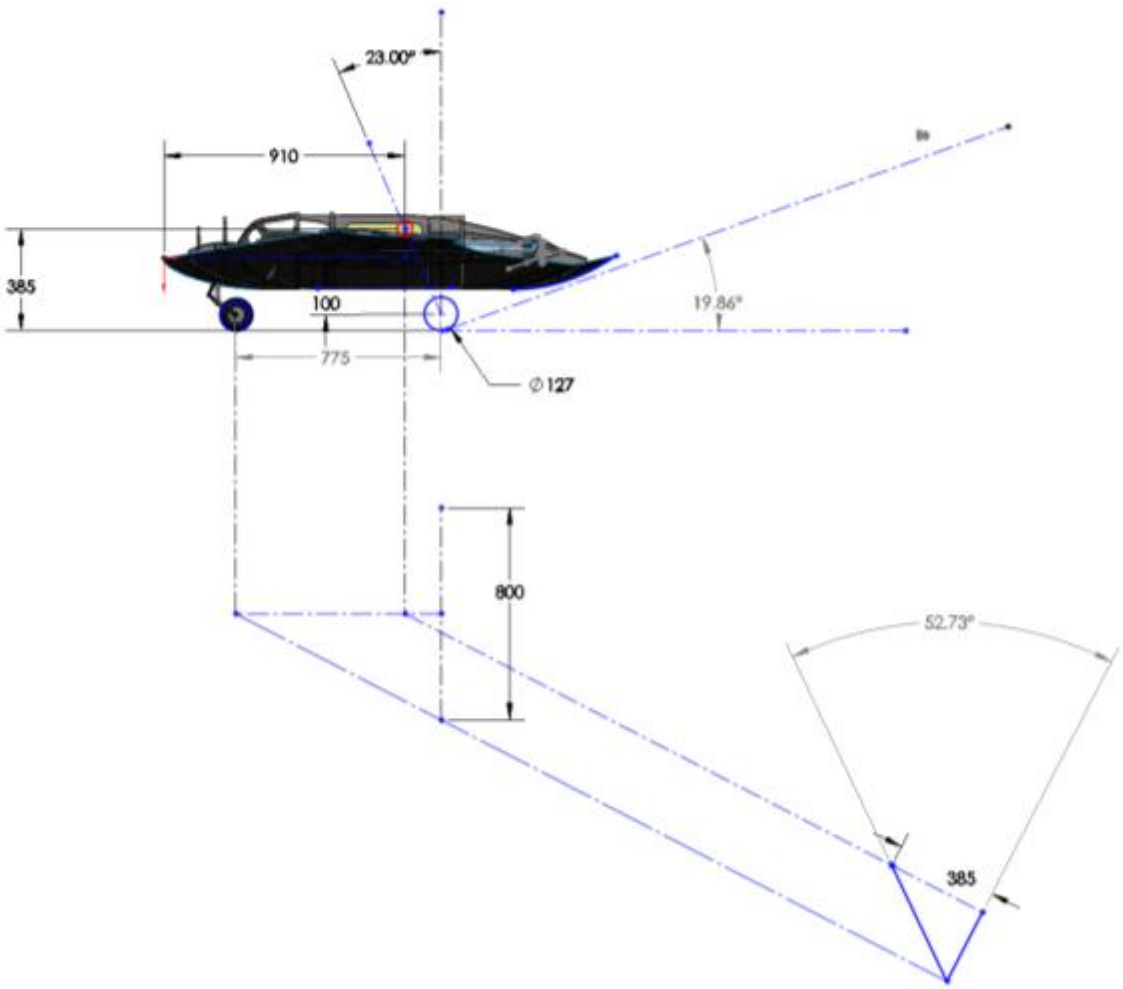

Figure 28 - Gear Sizing for the Forward Most CG Location[13]

Table 10 - Preliminary Design Specifications for Geometrically Scaled RPV Landing Gear

	Aft Most CG	Forward Most CG	Requirement
Length	900 mm	775 mm	-
Width	800 mm	800 mm	-
CG Height	385 mm	385 mm	-
Tip Back Angle	21.78°	19.86°	> 15°
Lateral Separation	46.09°	46.09°	> 25°
Tip-Over Angle	51.15°	52.73°	< 63°

This tricycle landing gear configuration has been successfully tested on a Mini SensorCraft airframe. This airframe is presented in Figure 29.

Figure 29 - Tricycle Landing Gear on Mini SensorCraft

2.7.2 Structural Design Validation using ANSYS Finite Element Analysis

In order to validate the structural design of the landing gear, a simulated worst case landing load was analyzed by Jenner Richards of Quaternion Engineering using FEA in ANSYS. The loading tested was a 4.5 g landing load (which corresponds to a 3g landing load with a factor of safety of 1.5) at both the forward CG and aft CG limits. Figure 30 and Figure 31 present the meshed models of the nose gear and rear gear, respectively. These models and all connection points with the main fuselage structure were analyzed. Figure 32 and Figure 33 present the results of the landing analysis for the nose gear and rear gear respectively. These figures show the location and magnitude of the maximum and minimum factor of safety (calculated based on a 4.5g loading). Table 11 summarizes the results of these calculations.

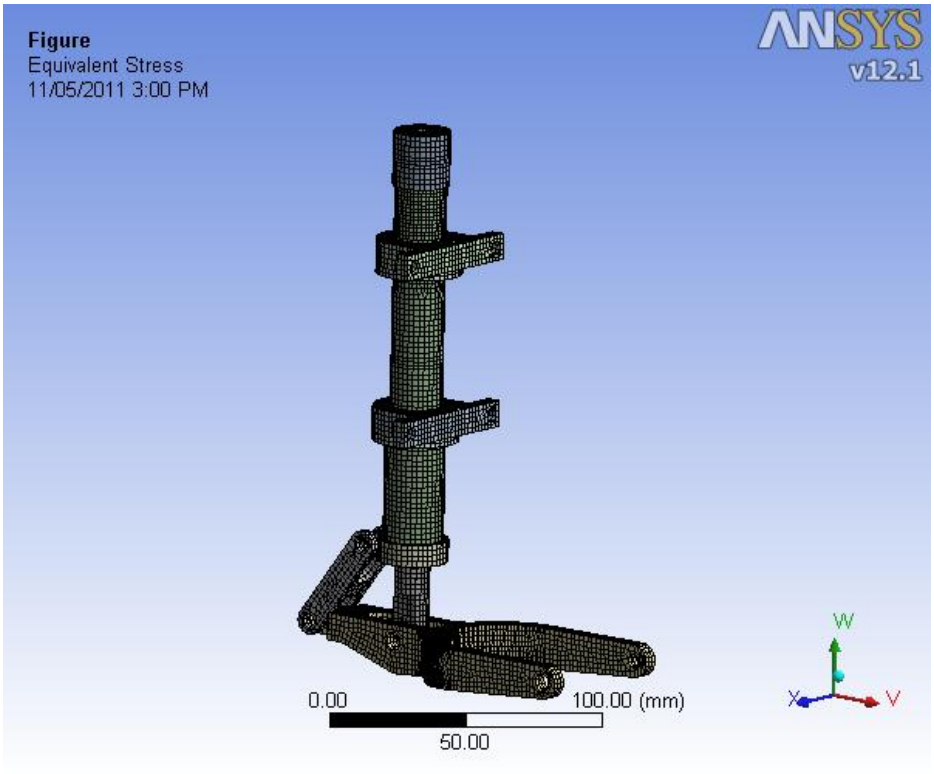

Figure 30 - Meshed Model of Nose Gear for Testing in ANSYS

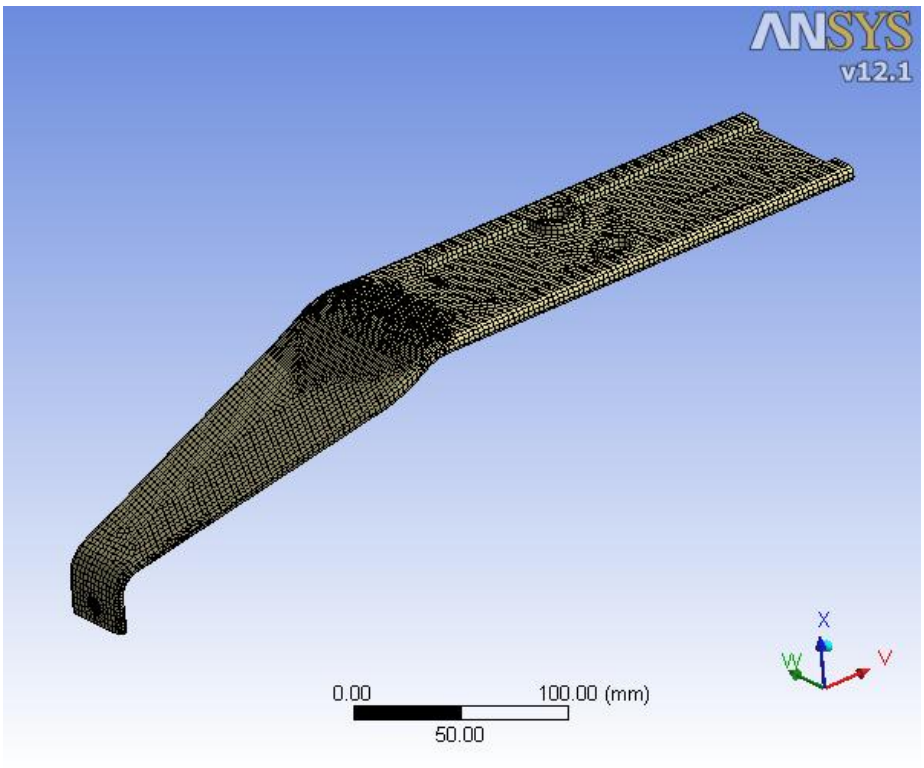

Figure 31 - Meshed Model of Rear Gear (half gear) for Testing in ANSYS

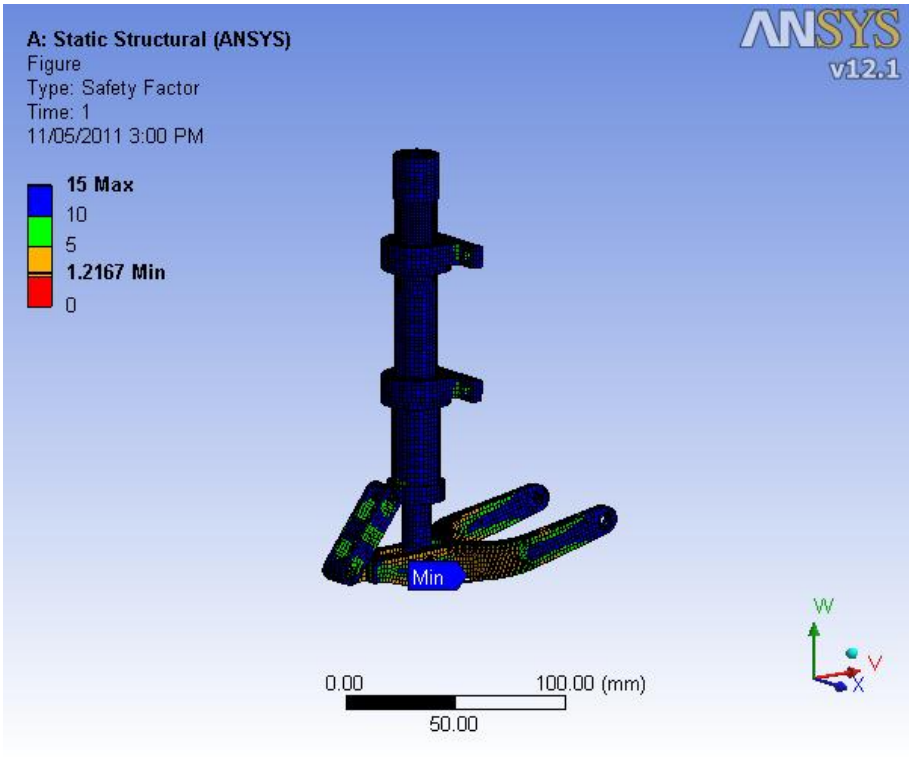

Figure 32 - Nose Gear Landing Analysis Results

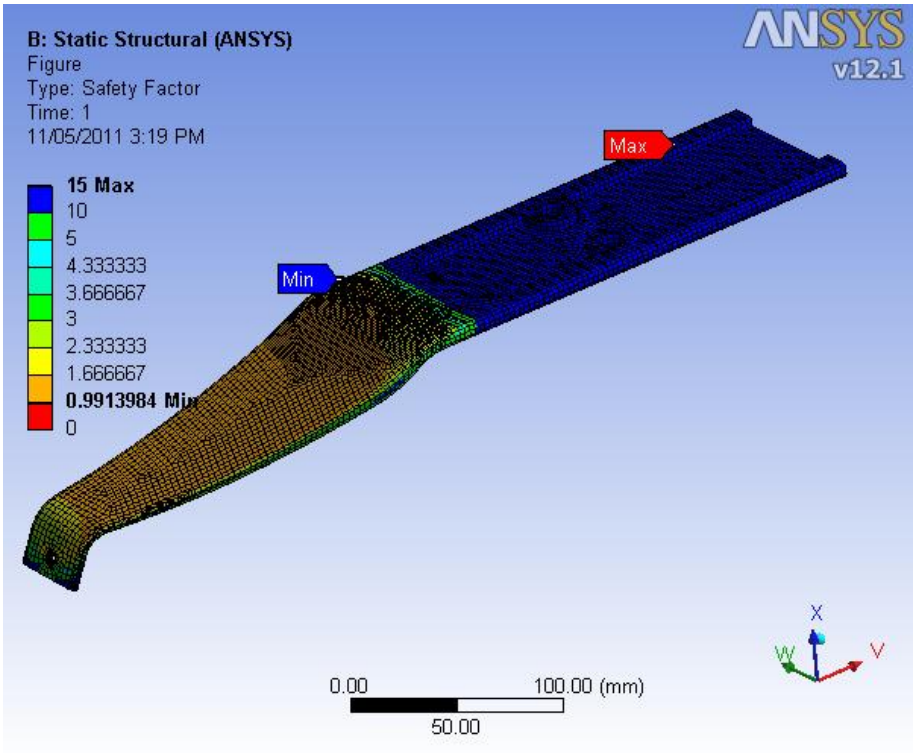

Figure 33 - Rear Gear Landing Analysis Results

Table 11 – Landing Gear FEA Analysis Results Summary

	Calculated 4.5g FOS	Corresponding 3g FOS
Nose Gear	1.22	1.83
Rear Gear	0.99	1.49

From these results, it can be seen that the Geometrically Scaled RPV has a minimum factor of safety of 1.83 for the nose gear and 1.49 for the rear gear, assuming a 3g landing load. This is acceptable for the flight test of an unmanned aircraft. All connection points with the fuselage were tested as well, and the resulting factor of safeties were higher than those presented above, indicating that the fuselage structure is capable of handling this worst case landing load.

2.8 Control

Control of the Geometrically Scaled RPV is accomplished via the onboard Cloud Cap Technology Piccolo II Autopilot coupled with an Acroname Robotics RxMux receiver multiplexer . Note that the Geometrically Scaled RPV will be under ***manual control*** at all times, with a backup pilot in place for all tests in which the RPV will be moving. The Piccolo II is used primarily as a data acquisition system and as a means of establishing reliable control of the RPV. The Acroname Robotics RxMux provides the ability to incorporate a backup, redundant receiver for use in the event that primary control is lost. A schematic of the control system used for the Geometrically Scaled RPV is shown in Figure 34.

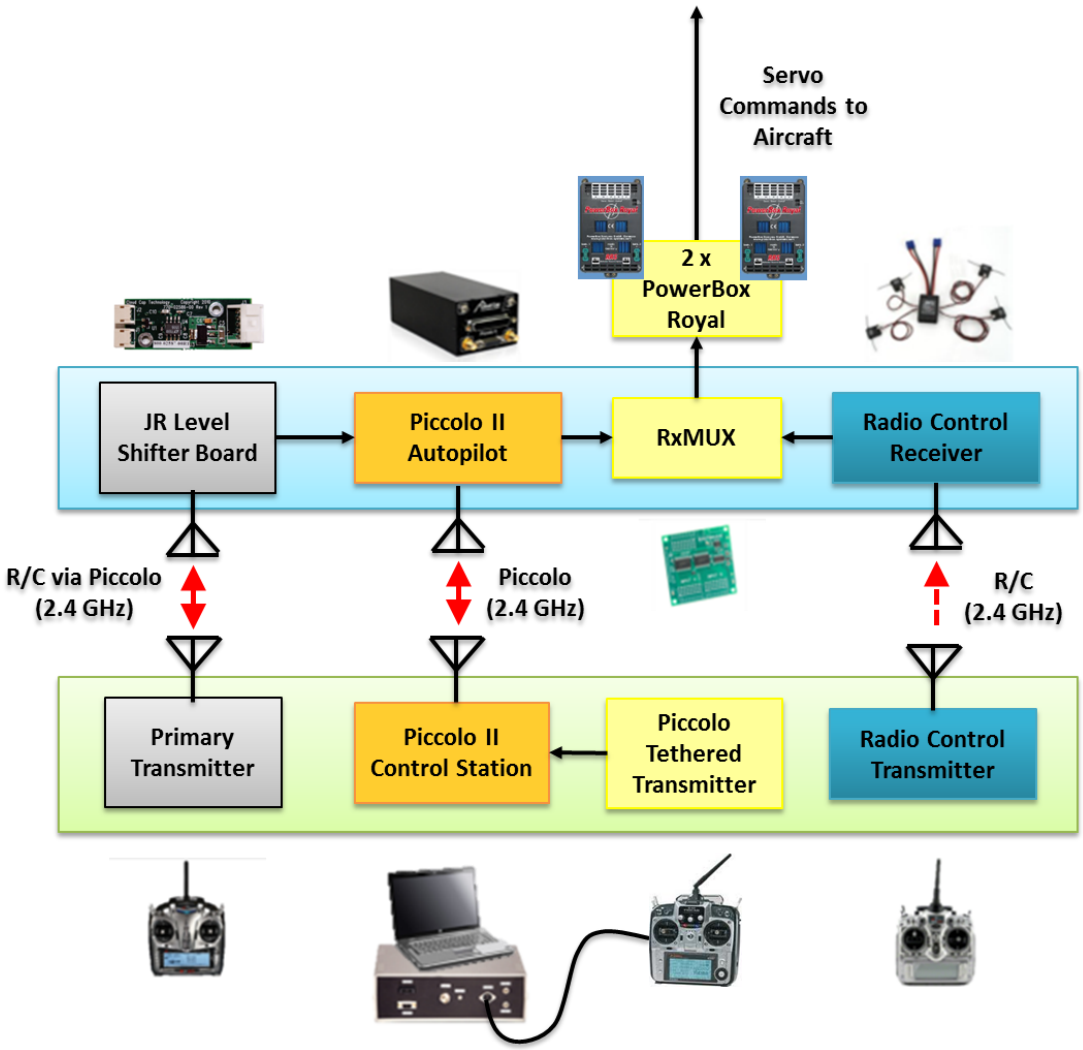

Figure 34 – Piccolo II/ RxMUX System Concept

Primary control of the RPV is provided through a JR 12X 2.4 GHz transmitter labeled above as the Primary Transmitter. Control signals are then sent to the RPV via a 2.4 GHz RF link, received using the JR Level Shifter Board, and processed by the onboard Piccolo II autopilot. The use of the JR Level shifter board allows the incorporation of two satellite receivers, improving RF communication to the aircraft. A backup transmitter, a JR 11X (labeled above as the Radio Control Transmitter), provides an entirely independent 2.4 GHz backup RF system in the event of total link loss with the primary transmitter. This backup link can be activated at any time during the flight by simply flipping a switch on the backup transmitter. Flipping this switch changes the active channel on the RxMUX, changing the source of the servo commands to the aircraft. The RxMUX functions by having two inputs and a single output, with the output controlled by a switch on the backup transmitter. The system is designed such that the backup controller can take control of the aircraft at any time, especially in the event of signal loss with the primary controller. The final transmitter, labeled Piccolo Tethered Transmitter, will be used only in the event that the aircraft travels out of visual range and neither the primary nor the backup pilot can see the aircraft well enough to fly it. The use of several 2.4 GHz RF links will not cause

interference because of the “binding” process between the transmitter and the receiver. Each transmitter has a unique identifying code, and when the receiver is bound to the transmitter, it will only receive signal from that transmitter. For more information about the backup control hierarchy, see Section 6.4.1. For a Frequency Usage Chart see Section 4.3.2.1.

Stability augmentation provided by the autopilot will be used to enhance yaw stability; however, the RPV will always be under manual control. The JWSC exhibits strong roll-yaw coupling, and preliminary flight tests with reduced complexity models have shown that a “fly by wire” system, such as that provided by the Piccolo II, can greatly assist in removing pilot workload during the flight by improving undesired coupling and reducing pilot workload. Stability augmentation does not take any control authority away from the pilot, it simply uses the built in instrumentation in the autopilot to correct undesired coupling. The stability augmentation provided by the autopilot can be switched off via a switch on the transmitter at any point during the flight, and the pilot can regain full, unassisted control. In order to create a completely independent backup system, the JR 11X system used by the backup pilot does not use the Piccolo II autopilot at all, and therefore does not have stability augmentation.

NOTE: Follow on flight test efforts may call for flights to take place at the backup test location in Portugal. In the event that ITAR clearance is not received to travel internationally with the Piccolo II, the MicroPilot2128^{LRC} autopilot will be used. This switch will cause ***no loss in functionality*** as the MicroPilot2128^{LRC} has the same key features as the Piccolo II and all flight key test personnel have experience operating with both systems. Additionally, the switch will not change any of the procedure presented in this test plan. More details on the MicroPilot2128^{LRC} are provided in Appendix L.

2.9 Instrumentation

2.9.1 Piccolo II

The Piccolo II serves as the primary data logging and data acquisition system on board of the aircraft. Aircraft altitude, attitude, airspeed, groundspeed and servo commands (which can be correlated, for a given mixing scheme, to control surface deflections) are all recorded and transmitted to the ground station in real time during the flight, along with GPS position. The Piccolo II also has built in gyros/accelerometers which allow for the incorporation of stability augmentation, if this is deemed necessary.

2.9.2 JetCat P200-SX

The JetCat P200-SX turbines contain built in sensors for engine RPM, exhaust gas temperature and fuel pump voltage. This data is continuously monitored by the JetCat Engine Control Unit (ECU), and this data can be viewed in real time by using the Ground Support Unit (GSU) while the aircraft is on the ground. Current work is aimed at incorporating real-time transmission of these parameters to the ground station during flight operations by reading them using the ECU’s RS232 serial connection. JetCat has provided the team with an internal white paper explaining how to transmit this data to the ground station during flight. The goal of the transmission system is to ensure that the data that is recorded with

the custom RS232 connection will match the data recorded with the GCU during ground testing of the system.

2.9.3 Air Data Boom

An air data boom is used to provide accurate angle of attack and sideslip angle measurements during all flight test operations. These measurements will be used for flight data purposes only. Commercial air data booms are too expensive to fit within the instrumentation budget of this project, so a custom air data boom was designed and fabricated. This boom consists of a 40 in long, 0.75 in inner diameter aluminum rod and two custom, laser cut acrylic vanes. Counterweight to balance the vanes at the hinge line is provided by 0.70 in long, 0.3125 inch diameter zinc steel inserts. The angular measurements are provided by two Spectrum Sensors 6909-1003-030 low friction rotational potentiometers mounted on custom machined aluminum inserts. The wipers for the potentiometers are mounted on the rotational shaft of each vane. Figure 35 presents an exploded view of the vane assembly. The air data boom has been calibrated in Virginia Tech's Open Jet Wind Tunnel.

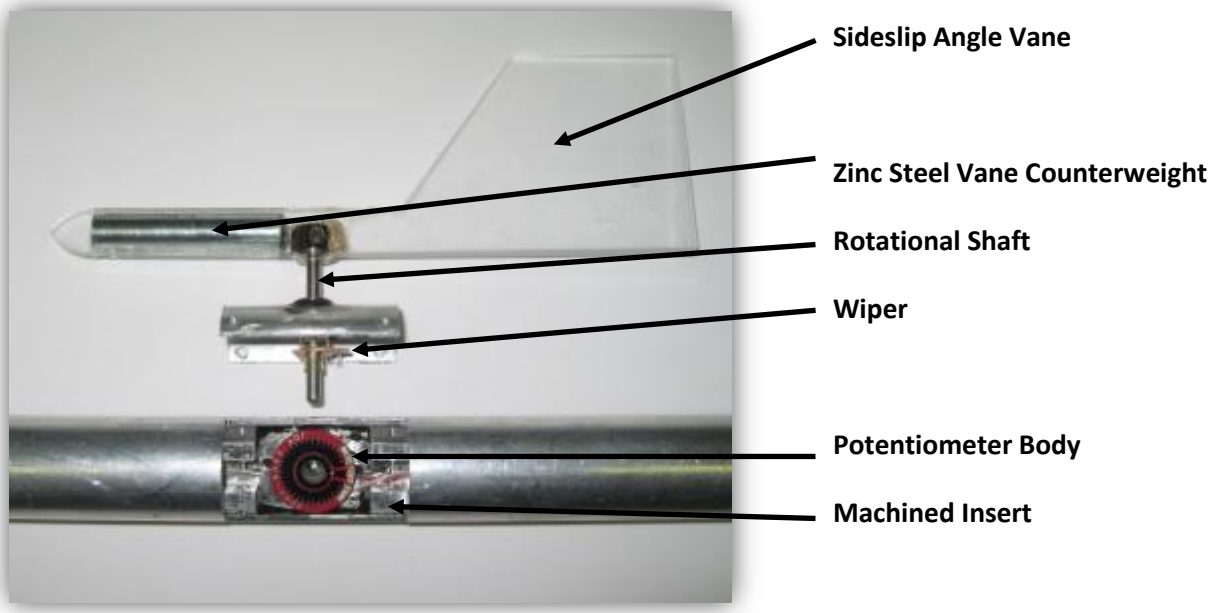

Figure 35. Exploded View of Air Data Boom Vane Assembly

2.9.4 Control Surface Deflection Measurement

The Piccolo II records all commanded servo deflections. An experimental correlation between this commanded deflection and control surface deflection will be created during the early stages of ground testing (see Section 3.3.1.2), and this will be used as a real-time measurement of control surface deflections during flight.

2.9.5 Wing Deflection

There are three methods of measuring wing deflection that will be tested on the Geometrically Scaled RPV: strain gauges, accelerometers and stereoscopic imagery. Figure 36 shows the location of the strain gauges and accelerometers on the Geometrically Scaled RPV.

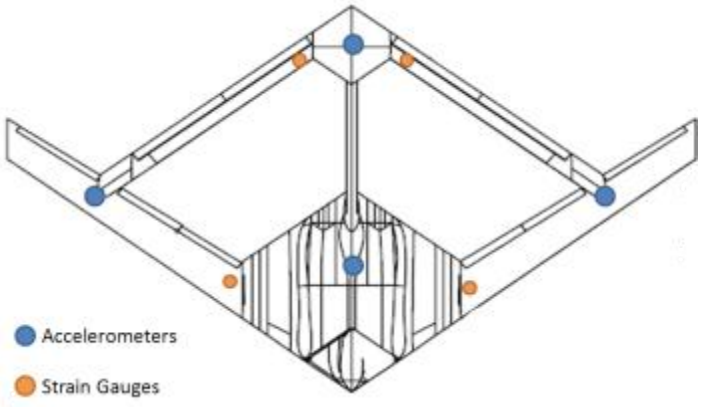

Figure 36. Accelerometer and Strain Gauge Locations

The use of all three deflection measurement methods allows for redundant measurement of critical flight test data, and also allow for the comparison of the quality of the data. These three measurement methods are presented in detail next.

2.9.5.1 Strain gages

Quarter-bridge strain gauge arrays were placed at root of both the forward and aft wings. By measuring the strain on each of these strain gages, and integrating these strains, wing deflection can be computed and recorded. The strain gauges used are Micro-Measurements CEA-06-250UW-350 General Purpose Strain Gages. These strain gauges were selected based on the maximum expected strain at each strain gauge location, computed using FEA. Three Micro-Measurements S-350-01 350 Ohm Bridge Completion Precision Resistors were used to complete each strain gauge array. The analog output from each quarter bridge is connected to one of the 12-bit analog to digital conversion (ADC) channels on a MicroChip PIC18LF4553 microcontroller. The PIC18LF4553 was programmed to take the analog input from each of the four strain gauge arrays and convert them into a single digital output. This digital signal was then sent to a Sparkfun Logomatic v2 Serial SD Datalogger, which stores the data onboard on a 1GB micro-SD memory card. 1GB of storage provides enough memory to store 20+ hours of continuous data logging with this system. The entire system is powered by a 7.2V Lithium Polymer (LiPo) battery pack fed through a Sparkfun LM7805 5V voltage regulator. Figure 37 shows each of the components used to complete this strain gauge system.

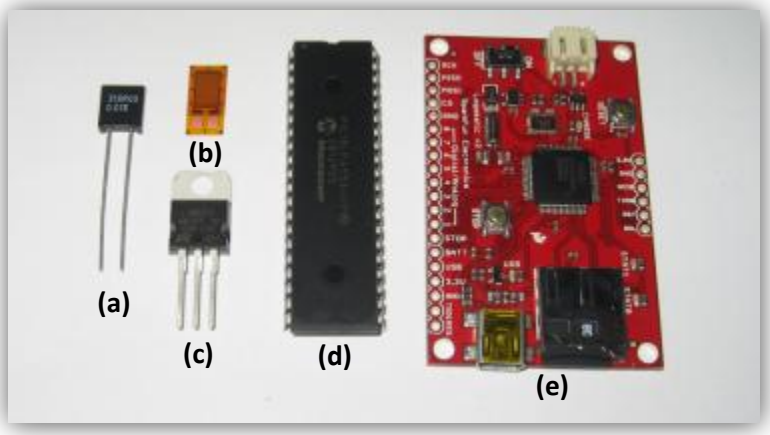

(a) 350Ω Bridge Completion Precision Resistors
(b) Strain Gauge
(c) 5V Voltage Regulator
(d) PIC18F4553 Microcontroller
(e) Logomatic v2 Datalogger

Figure 37. Strain Gauge System Components[7]

2.9.5.2 Accelerometers

Tri-axial accelerometers were placed at the CG, the top of the vertical tail boom and at each wing joint. By integrating the accelerations at these locations twice with respect to time, the displacement of these locations can be calculated. Aircraft attitude information from the Piccolo II autopilot can then be used to rotate the accelerometer displacements into the inertial reference frame. Finally, the rotated displacements can be compared to the baseline un-deflected aircraft geometry to compute wing deflections.

Level turn wing loading calculations show that the maximum planned load factor during the Geometrically Scaled RPV flights is 2.1 g's. To account for all planned flight maneuvers, the accelerometers selected are Analog Devices ADXL335 3-axis, ±3g accelerometers. The accelerometers were mounted on Sparkfun breakout boards providing 0.1µF capacitors on each analog output (x,y and z-axes) giving the ADXL335 a functional bandwidth of 50Hz on each axis. The three analog outputs from each accelerometer were connected to one of the 12-bit ADC channels on a MicroChip PIC18LF4553 microcontroller, and just as in the strain gauge system, the PIC18LF4553 converts the 12 analog inputs into a single, digital output. This output is then sent to a second onboard Logomatic v2 Serial SD datalogger. The included 1GB of storage provides enough memory to store 20+ hours of continuous data logging. The system is powered by a 7.2V LiPo battery pack fed through a Sparkfun LM7850 5V voltage regulator to power the Logomatic v2 and a Sparkfun LD1117V33 3.3V voltage regulator to power the accelerometers. Figure 38 shows each of the components used to complete this accelerometer system.

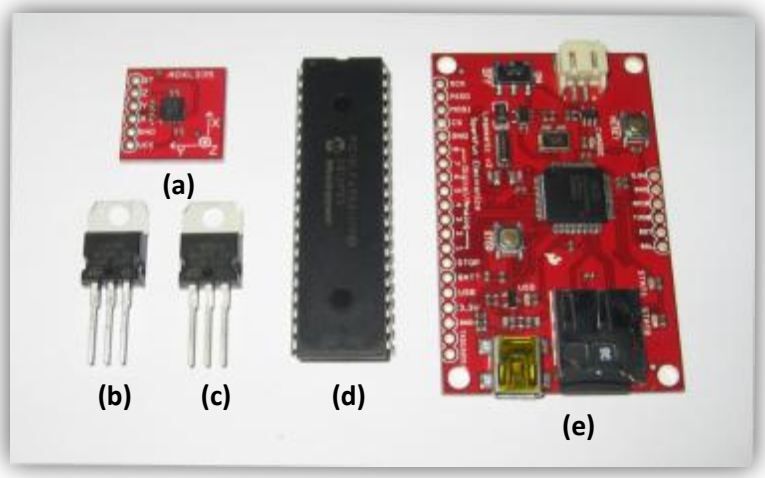

(a) ADXL335 Accelerometer
(b) 3.3V Voltage Regulator
(c) 5V Voltage Regulator
(d) PIC18F4553 Microcontroller
(e) Logomatic v2 Datalogger

Figure 38 - Accelerometer System Components[7]

2.9.5.3 Stereoscopic imagery

Stereoscopic imagery involves the use of two cameras placed at a known distance and angle from one another, each focused on the same object (in this case a wing). By combining these images through post processing software, a single, composite, three-dimensional image can be created. Fixed points of reference on the wings can then be used to back out wing deflections.

A stereoscopic system is advantageous because it allows for the deflected shape of the entire wing to be determined from two cameras. With strain gauges and accelerometers, each instrument only gives information about a single point on the wing, and thus many accelerometers and/or strain gauges are required in each wing to determine the deflected shape of the entire wing. Installing and calibrating a large number of instruments in each wing is not only time consuming, but it also requires the modification of the aircraft structure and skin. For the future planned flight tests of the Aeroelastically Scaled RPV, the aeroelastically scaled lifting surfaces will be designed with specific mass and stiffness distributions to match the required aeroelastic response. Incorporating strain gauges and accelerometers without changing the required mass and stiffness distribution will be difficult, so stereoscopic imagery is being investigated as a less structurally invasive measurement system.

GoPro HD Hero 960 cameras, such as the one shown in Figure 39, will be used for stereoscopic imagery. The GoPro HD Hero 960 provides a self-contained (battery and memory are internal) camera solution in a ruggedized shock and weatherproof housing.

Figure 39 - GoPro HD Hero 960 Camera in Ruggedized Case

The HD Hero 960 is capable powered by an internal, rechargeable 1100 mAh lithium-ion battery and is capable of records up to 2.5 hours on one charge and up to 9 hours total on a 32GB SD memory card. It is compact, with dimensions of 1.6" x 2.4" x 1.2" (H x W x D) and lightweight. The total system weighs only 3.3 oz including battery and 5.9 oz including the shock/weatherproof housing.

An extension of this system is the 3D Hero System, which synchronizes two HD Hero cameras into a 3D capable system. The 3D Hero System, shown in Figure 40, provides a double camera shock/weatherproof housing, a synchronizing cable to allow recording on bother cameras to begin with the push of a single button. Each camera records a 2D video file and post-processing software included with the 3D Hero System (GoPro CineForm Studio) creates a composite 3D video from the two 2D video files.

Figure 40 - 3D Hero Camera System in Ruggedized Case

Several methods of post processing the images for measurement have been identified and are being investigated, but the best option currently is the PhotoModeler photogrammetry software. PhotoModeler provides image-based modeling, for accurate measurement and 3D models and is

compatible with the HD Hero 960 camera. The PhotoModeler software assists in the calibration of the camera system to produce accurate measurements.

2.9.6 Emergency Navigation Camera

The Geometrically Scaled RPV will be equipped with a camera pointing out the nose to provide emergency first person view (FPV) navigation in the event that the RPV inadvertently travels out of visual range. This camera will transmit real-time video feed to the ground station at all times during the flight. The forward facing camera is a GoPro HD Hero digital camera. The camera offers a 127^{o} field of view and will record to flash memory (1080p at 30fps). This camera will also output a standard definition video stream to dual onboard video transmitters. Due to shape of the aircraft and carbon fabrication, two transmitters are used in order to ensure signal and antenna diversity.

The first video transmission link employs a 1 watt, FM analog unit broadcasting at a user selectable frequency (CH1: 5.745GHz or CH4: 5.765GHz) with an omni directional cloverleaf antenna. The receiver unit uses a 24dbi high gain directional dish antenna and the combination has a specified operating range of 25 miles. The second video link uses a 1.5 watt FM analog transmitter broadcasting in the 900 MHz spectrum (CH1: 0.9GHz CH2: 0.910GHz CH3: 0.980GHz CH4:1.010G CH5: 1.040GHz). The airside antenna is an end feed dipole, omni-directional antenna linked to a receiver unit with a unity gain omni-directional antenna. The rated range for this system is 5 miles.

At the ground station, each receiver is fed into an Oracle Video Diversity Controller (shown below in Figure 41) to provide redundant video reception. The Oracle measures the video signal strength from each receiver, selects the video and audio stream with the strongest signal and forwards that signal to the output. This provides the best possible video quality and lessens the risk of a lost signal, which is key for emergency navigation purposes. Additionally, the switching process happens so fast that no video or audio noise is generated.

Figure 41 – Oracle Video Diversity Controller

3 Test and Evaluation

This section opens with a discussion of the hierarchy of program objectives and success criteria that will be used to assess the success of the flight test. This is followed by a detailed description of all three phases of tests proposed for the Geometrically Scaled RPV FTP, including descriptions of all of the tests that make up each phase. This section closes with a table summarizing all proposed tests, their respective location and objective level.

3.1 Needs, Goals and Objectives

The aeroelastic responses, specifically aft wing buckling and gust load response, associated with the JWSC have been demonstrated and investigated in numerous computational and wind tunnel studies[1-3,5]; however, these phenomena have never been successfully tested in a flight test program. **The Air Force has determined that an aeroelastically scaled Remotely Piloted Vehicle (RPV) is needed to serve as a low cost and effective way to experimentally investigate these non-linear aeroelastic responses.** By demonstrating, investigating and measuring these responses, future aeroelastically scaled flight test programs will be able to test active aeroelastic control and gust load alleviation systems to reduce the structural and aerodynamic effects of the nonlinear responses.

3.1.1 Overall Program Goal

The overall program goals of the Flight Demonstration FTP are to validate the scaling of the overall mass and moments of inertia of the Geometrically Scaled RPV and subsequently demonstrate the airworthiness of the vehicle through safe, controlled flight.

3.1.2 Program Objectives

Using the aforementioned goals as a driver, a series of primary, secondary and tertiary objectives are listed below. Each planned phase (Integration and Ground Tests, Flight Readiness Tests and Flight Tests) is aimed at meeting one of the objectives listed below. The test (or series of tests) that corresponds to each objective listed below is shown after that objective in parentheses. For more information about these tests, see Section 3.3.

3.1.3 Primary Objectives

1. Validate scaled overall mass and center of gravity (CG) location ***(Center of Gravity Test)***.
2. Validate scaled rigid body mass moments of inertia ***(Bifilar Pendulum Test)***.
3. Demonstrate airworthiness and successful control of the Geometrically Scaled RPV ***(Phasing Flight Test 1)***.

3.1.4 Secondary Objectives

1. Demonstrate successful data acquisition and data logging of flight test data ***(Ground Tests)***.
2. Experimentally determine key turbine parameters, including static thrust, installed static thrust and fuel consumption ***(Turbine Tests)***
3. Validate control surface deflections and mixing ***(Servo Response Test, Control Surface Scheduling Test)***
4. Validate structural design ***(Static Structural Loading Test).***

5. Investigate feasibility of (safely) reaching 204 lb weight test point ***(Incremental Weight Increase Test)***.

3.1.5 Tertiary Objectives

1. Obtain dynamic model parameters(***Dynamic Mode Flight Tests***)
2. Investigate flight maneuvers to achieve required loading for nonlinear AE response ***(Required Loading Test)***

3.2 Success Criteria

In order to be considered a success, all primary objectives must be met, along with a majority of the secondary objectives. Below is a list explaining the relative importance of the secondary objectives. The tests are listed from most to least important, and this hierarchy will be used when evaluating the completion of "a majority" of the secondary objectives.

1.) Ground tests, turbine tests and the control surface scheduling test are all critical to ensure the success of follow on flight testing in Phase III. Accordingly, these are the tests that are the most important.
2.) The Static Structural Loading Test is the next in order of importance. Verifying that the structure is built as designed is incredibly important, but it is not critical to test all the way to the maximum possible wing loading of 2.89 as described in the test plan. Wing loadings of 1.12 and 2.1 will be tested, but 2.89 may not be tested due to safety concerns (2.89 requires 591 lbs to be placed on the wings).
3.) The Servo Response Test, which includes testing for dynamic actuator properties as well as mapping the control surface deflection angles using the autopilot commands, is the third most important. The real-time knowledge of control surface deflection angles is important, but not flight critical. Additionally, the knowledge of dynamic actuator properties is important to reduce the risk of Pilot Induced Oscillations, but again, this is not flight critical if the pilot is satisfied with the control surface response prior to flight.
4.) Finally, the Incremental Weight Increase test is the least important. It is unlikely that this test will even be attempted due to time constraints and complexity. Additionally, if it is attempted, it may not reach the full 204.5 test point due to the strict performance requirements (including pilot input) required to increase in weight.

Tertiary objectives have no bearing on whether or not the test is declared a success. Each test presented in Section 3.3 is labeled with a (P), (S), or (T) corresponding to a primary, secondary or tertiary objective, respectively. The successful completion of these tests will be used to quantify meeting the objectives.

3.3 Test Breakdown (3 Phases)

The Flight Demonstration FTP is divided into three phases, with the complexity and scope of the tests increasing with each phase. Phase 1, System Tests, includes the integration and testing of all onboard systems. This phase includes testing of instrumentation and data logging capabilities, static thrust testing, verifying control surface deflections and mixing and experimentally finding the center of gravity. Phase 2, Flight Readiness Tests, includes ground testing of the overall RPV system. This phase

includes a bifilar pendulum test to experimentally determine the overall moments of inertia and static structural loadings to validate the structural design. Phase 3, Flight Tests, includes all flight test operation of the RPV. Taxi tests, phasing tests, parameter identifications tests maneuvering tests are all included in this phase, as well as an incremental increase in weight to the test point. For more information about test logistics, including scheduling and locations for each phase of testing, see Section 4.

3.3.1 Phase 1 –System Tests

The following tests will be performed prior to shipping the aircraft to Foremost for Phase 2 and Phase 3 tests. The successful completion of these tests will ensure that all onboard systems, including instrumentation, are functioning properly prior to traveling to the flight test site.

3.3.1.1 System Readiness Test (S)

The aircraft will be assembled into a complete RPV and all systems will be tested for functionality. This test serves as a preliminary troubleshooting forum for all integration issues which may arise when combining the RPV structure, propulsion, landing gear and instrumentation. The aim of this test is to boost confidence that when the RPV arrives at the flight test site, assembly and integration will proceed smoothly.

3.3.1.2 Servo Response Test (S)

A full range of control input will be provided for each servo and the resulting deflections will be recorded using a standard control surface deflection meter, such as the one shown in Figure 42. A servo tester, which allows for the accurate generation of servo pulse width commands, will be used to establish a correlation between servo pulse width and control surface deflection for each control surface. The Piccolo II, which records commanded servo pulse, will be used as a low fidelity in-flight measurement of control surface deflection through the experimental correlation developed in this test.

Figure 42 - Control surface deflection meter

This test will also serve to identify dynamic actuator parameters including the lag time between command and response and the variation in these parameters with control mode (primary control vs. backup control). In order to be successful, there should be no “pilot perceivable” difference between pure 2.4 GHz control using the backup transmitter (the best possible link, avoids autopilot entirely) and control using the two redundant (900MHz and 2.4GHz) RF links through the Piccolo II. The measurement of the exact delay is not required as the RPV will be under manual control at all times (no

autopilot control); however, the pilot should not be able to notice a difference in control response between the primary and backup controls.

3.3.1.3 Control Surface Scheduling Test (S)

A full range of control input will be provided for each receiver channel to verify that the desired control surface scheduling is achieved. The unique and complex control surface layout of the JWSC has been investigated computationally, as well as in flight tests of reduced complexity models, and these tests have resulted in a desired control surface scheduling (i.e. which surfaces are used to command roll, pitch and yaw). This test serves to ensure that this control surface schedule is able to be scaled to the full scale RPV where there are multiple servos per control surface. This test will allow the use of multiple receivers to be tested, as well as the use of multiple servos per control surface. Additionally, this test will ensure that all control surfaces sharing receiver channels (i.e. those surfaces being controlled via a Y-splitter) experience equal deflections for a given commanded deflection. Finally, the two servos actuating each surface will be checked to ensure that they are not fighting each other and causing binding throughout the entire deflection range of the surface. Care will be taken to test for servo heating (potential servo motor burnout) and servo binding during these ground tests.

3.3.1.4 Back Up Control Test (S)

The RPV will be prepared for flight, including the propulsion system. With the aircraft firmly secured to the ground via padded posts in front of the wings and straps overtop of the fuselage staked into the ground, all onboard systems will be running (including instrumentation and propulsion) and control will be passed between the primary controller, the tethered controller and the backup controller via the RxMUX. In addition, loss of link will be simulated for both the primary and backup controllers to ensure that the "failsafe" condition is operational and that the loss of link hierarchy is operating as planned. This includes the pre-programmed autonomous flight path in the event of primary link loss. For more information about the autonomous flight path, see Section 6.8.4. The failsafe condition is executed during full loss of link, and corresponds to a controlled crash: full up elevator, full right rudder, full right aileron, turbines at idle or shutdown if possible. The failsafe condition is designed to minimize residual damage in the event of total loss of link. For more information about the failsafe procedure, see Section 6.8.2.

3.3.1.5 Data Collection and Storage (S)

The ground station operator will send a signal to the Geometrically Scaled RPV to begin data sampling from all onboard sensors and instrumentation. Data collection and on-board storage will be continued for a minimum of 30 seconds. Upon completion, the data will be downloaded and analyzed to ensure that there are no gaps in the data. This test will ensure that all onboard instrumentation is functioning and compatible.

3.3.1.6 Data Transmission (S)

The ground station operator will send a signal to the Geometrically Scaled RPV to begin data sampling from all onboard sensors and instrumentation. The real-time data transmission from the aircraft to the ground station will be monitored to ensure that there are no gaps in the data. Upon the completion of the data transmission period, the data received will be compared to the data that was

recorded on-board for similitude. Range will also be a consideration during this test, but the Piccolo II has a functional range of several miles, so it will be impossible to test the full range.

3.3.1.7 Camera Transmission (S)

The ground station operator will send a signal to the Geometrically Scaled RPV to begin recording and transmitting onboard video. The video streams as viewed on the ground station will be checked for signal loss or gaps in the transmission. For more information about camera placement and purpose, see Section 2.9.6.

3.3.1.8 Turbine Tests

These tests will be used to ensure that the JetCat P200-SX turbines are running properly both before and after installation into the RPV. Bench testing will allow test operators to become familiar with the required setup as well as the process required to operate the turbines. Installed thrust testing will serve to validate the internal inlet and exhaust paths, as well as verify that the turbines are able to produce the required static thrust for safe operability at all scheduled test points.

Notes:

1. The JetCat P200-SX turbines used in the Geometrically Scaled RPV are mechanically complex and require an understanding of turbine engines as well as a disciplined approach to their operation. All tests will be conducted in accordance with JetCat safety and operational protocol. JetCats manufacturer specified safety protocol is located in Appendix J.
2. The JetCat P200-SX is equipped with onboard sensors (RPM, exhaust gas temperature, fuel pump voltage) and the data is continuously monitored through the ECU. This capability will be extended to transmission while in the air.
3. The JetCat P200-SX has a manufacturer's specified 25 hour maintenance interval. Analysis has shown that all planned testing can be completed within the manufacturer's specified maintenance interval. Table 12 below presents an engine management schedule that details engine usage throughout all planned tests. This analysis assumes 3 hours for assembly of the engines and troubleshooting of all associated systems. Planned ground tests then take an additional 12 hours, leaving 10 hours for planned flight maneuvers. Predicted fuel consumption gives a maximum endurance of 40 minutes and a total mission time of 66 minutes. This means that 10 hours of testing would allow for 9 full missions with 6 minutes of run time to spare. This is more than satisfactory, given the planned flight tests.

Table 12 – Engine Management Schedule

Engine Usage	Hours
Preliminary Testing	
Assembly/ Troubleshooting	3
Static Thrust Testing	3
Installed Static Thrust Testing	3
Vehicle Testing	
Ground Testing/EMI Tests	3
Low Speed Handling Test	1
High Speed Taxi Testing	2
Flight Testing	10
TOTAL	25

3.3.1.8.1 Bench Testing (S)

Bench testing of each JetCat P200SX will be used to familiarize the operators with the operation of the turbine engines as well as test their performance. Figure 43 below presents a bench test setup for a JetCat P200SX turbine. A setup similar to this will be used for this test; however, the picture depicts an indoor setup with exhaust gas ventilation. The Geometrically Scaled RPV tests will be conducted outdoors. Figure 44 below shows the bench test setup used for the Mini SensorCraft EDF testing.

Figure 43 - Bench test setup for JetCat turbine (Geometrically Scaled RPV Tests will be outdoors)

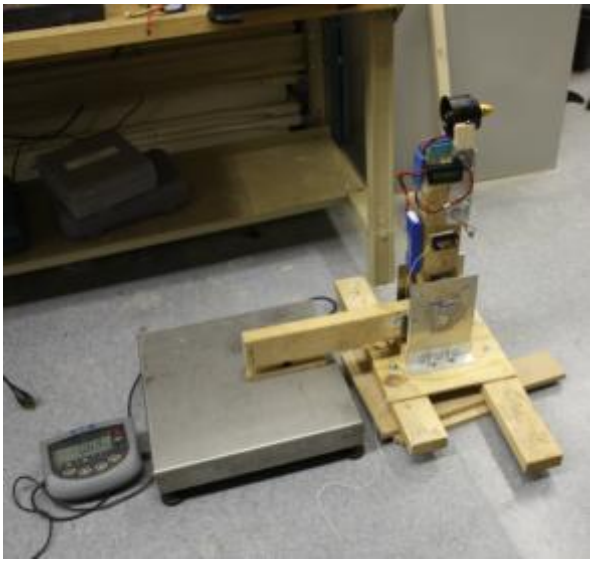

Figure 44 - Bench test setup used for Mini SensorCraft EDF testing

Turbine tests will begin with a bench test of each turbine to ensure the proper operation. This will include learning to properly use the ECU to start and monitor the turbine. All startup, runtime and cool down procedures will follow JetCat safety and operational protocol. Once the turbine operation is fully understood and the turbine has been fully broken in, static thrust and fuel consumption testing will commence. These tests will verify the manufacturers specified static thrust as well as generate an experimental correlation between engine RPM, thrust and fuel consumption. Note that the JetCat P200-SX ECU comes with a pre-defined, software (calculated) fuel consumption model.

Appendix C contains the results of the bench testing of a JetCat P200 turbine from the AFRL during October, 2009. The results of the bench testing described above will be compared to the results of the AFRL test.

3.3.1.8.2 Installed Turbine Testing (S)

Once bench testing is complete, both JetCat P200-SX turbines will be integrated into the fuselage of the RPV along with the inlet and exhaust ducting. Figure 45 presents a picture of the Mini SensorCraft on a simple static thrust test stand during installed static thrust testing. This picture illustrates a simple version of the static thrust setup that will be used for the Geometrically Scaled RPV.

Figure 45 - Mini SensorCraft on Static Thrust Test Sand

Installed turbine testing will commence with a simple startup, variable throttle run and cool down to ensure that all turbine mounts, ducting and installed JetCat hardware is functioning properly. This will include ensuring that the twin engine setup is functioning properly (i.e. both engines are running at the same RPM throughout the throttle band). Once this initial testing is complete, installed static thrust testing will be completed to ensure that the complex inlet and exhaust ducting used in this aircraft does not interfere with turbine performance.

3.3.1.9 Landing Gear Loads Testing

This test is designed to validate the as-built landing gear. The procedure outlined below is in accordance with MIL-T-6053C and MIL-A-8863C. The landing gear will be mounted to a solid plywood board in the exact configuration required for the Geometrically Scaled RPV. Weights will be added to the board and distributed such that the CG of the system corresponds to the CG of the overall RPV. A total of 5 drops will be completed, and these drops are outlined in Table 13 below.

Table 13 – Landing Gear Loads Test Matrix

Drop Number	Weight (lbs)	Descent Rate (FPS)	Drop Height (ft)	Attitude
1	131.8	10	1.55	Level
2	131.8	10	1.55	Tail Down
3	204.5	6	0.559	Level
4	204.5	6	0.559	Level
5	204.5	6	0.559	Tail Down

The descent rates are specified in MIL-T-6053C, and the drop heights were calculated such that the gear would be at the required descent rate at the point of impact with the ground. The attitudes

specified correspond to the two required test conditions, wheels level and tail down. For the level attitude, the aircraft will be dropped such that all landing gear wheels contact the ground at the same time (this corresponds to the nose strut fully extended). For the tail-down landing, MIL-T-6053 states that, "the airplane pitch angle shall be that angle corresponding to 90 percent of the maximum lift coefficient in level flight using the trimmed lift curve for the power approach configuration in free air at sea level on a tropical day." For the Geometrically Scaled RPV, this corresponds to $C_L = 1.685$ (assuming a flap $\Delta C_L = 0.24$, which is consistent with all other mission performance analysis for this FTP) at an angle of attack of $\alpha = 9.38°$. After each drop, the fully extended height of the strut will be measured along with the height of and width of the rear gear. This will test for any permanent deformation that occurs.

3.3.2 Phase 2 –Flight Readiness Tests

These tests serve to validate the design and fabrication of the complete, flight worthy RPV. The first two tests in this phase (Aircraft Mass and CG Tests) will take place in Victoria, BC prior to shipping the RPV to Foremost. The remainder of the tests will take place in Foremost, prior to Phase 3 Flight Tests. Note that system level ground tests completed during Phase I and II in Victoria, BC will be repeated when the aircraft is re-assembled, prior to flight, in Foremost, AB.

3.3.2.1 Aircraft Mass and CG Tests

These three tests will serve as a primary means of establishing the dry weight of the aircraft, the center of gravity (both longitudinal and vertical) of the dry aircraft, and the movement of the center of gravity with the addition of fuel and trim weights. The tests will be performed in the order described.

3.3.2.1.1 Dry Mass Test (P)

This test will establish the dry (without fuel) mass of the airframe and all required onboard systems.

3.3.2.1.2 Test Point Mass Test (S)

Once the dry mass is established, fuel and trim weights will be used to ballast the aircraft to the test point weight. This will verify the ability of the RPV structure to safely reach the test point mass. Additionally, this will serve to verify that the ballast chambers can hold the appropriate amount of ballast weight to reach the test point.

3.3.2.1.3 Center Of Gravity Tests (P)

A dual balance setup will be used to test for the CG. Two vertical supports will be used to support the RPV, and an electronic balance will be used to measure the mass on each support. Using the mass on each support and the distance between the supports, the longitudinal CG location can be calculated. Once the longitudinal center of gravity has been calculated, the aircraft will be put at an angle of attack. The vertical center of gravity can then be calculated by using the known longitudinal CG location, the angle of attack and the measured mass on each support. This test will be used to test the CG shift as ballast weight is added and as fuel is burned.

3.3.2.2 Static Loading Test (S)

The Geometrically Scaled RPV will be inverted and sand bags will be used to simulate wing loading. The purpose of this test is to validate the structural design of the RPV and ensure that all wing

loadings experienced during flight can be safely sustained. Table 14 below highlights the flight conditions that will be tested during the Static Loading Test. These calculations correlate to a level turn. Note that the Geometrically Scaled RPV has been designed for a maximum load factor of of 3 at the maximum takeoff weight with a factor of safety of 1.5.

Table 14 - Predicted Maximum In Flight Load Factors

Flight Condition	Turn Radius	V (knots)	Load Factor
Minimum Cruise Speed	750 ft	66	1.12
Maximum Cruse Speed	750 ft	125	2.1
Never Exceed Speed	750 ft	152	2.89

3.3.2.3 Bifilar Pendulum Test (P)

A bifilar pendulum test will be used to experimentally determine the moments of inertia about each axis. Tests will include the measurement of the moments of inertia for each configuration in which the RPV will fly. This will include the un-ballasted weight and the full test point weight and with varying amounts of fuel. The trimming weights will be used to match the required scaled moments of inertia. For more information about the required scaled moments of inertia and the trimming masses, see Section 2.6. A primary goal of this test is the investigation of the use of ballast to reach the 204.5 lb test point at the correct scaled moments of inertia. During Phase 3, the Incremental Weight Increase Test (see Section 3.3.3.5) investigates the feasibility of safely flying at the full 204.5 lb test point. This test will lay the groundwork for that flight test.

3.3.3 Phase 3 –Flight Tests

Phase 3 Flight Tests represent the final stage of testing for the Geometrically Scaled RPV. These are the tests that will take place on site in Foremost. These tests have been designed to use a gradual increase in complexity to minimize risk. All instrumentation will be active and taking data for every test, including taxi tests and ground tests. Additionally, *all* tests will be filmed.

3.3.3.1 Low Speed HandlingTest (T)

The pilot will taxi the aircraft with low throttle setting to verify that the Geometrically Scaled RPV is stable while taxiing and ground handling characteristics are acceptable. Ground effect calculations have shown that the aircraft has a stall speed of 48.2 knots (at the maximum takeoff weight of 204.5 lbs) and a stall speed of 38.65 knots (at the un-ballasted takeoff weight of 131.8 lbs). Accordingly, all low speed handling testing will restrict the airspeed of the aircraft to 10 knots or less.

3.3.3.2 High Speed Taxi Test (T)

During High Speed Taxi testing, the pilot will accelerate the aircraft down the runway to the speeds listed below and then reduce throttle to idle. The pilot will demonstrate the ability to control the Geometrically Scaled RPV throughout the takeoff roll. This test will consist of 4 straight line runs down the runway, with the aircraft at 131.8lbs. The maximum speed for each run will be 10 knots, 18 knots, 25 knots and finally 32 knots. The pilot will NOT give the aircraft any pitch input during these runs to eliminate the possibility of unexpected takeoff.

3.3.3.3 Phasing Test

This test is the first flight test, and it is designed to verify the correlation between pilot command, aircraft response and instrumentation measurement. The flight is decomposed into 7 segments to illustrate the flow of this test as well as special considerations during each phase. During each phase of this test, aircraft attitude and control surface deflection data will be compared to pilot input to ensure that the aircraft is responding as expected to pilot input and the resulting control surface deflection. Note that this test is considered a success if the aircraft achieves successful takeoff, climb, trim, descent and landing. The in-flight maneuvering tests will be attempted only after the aircraft is trimmed, if the remaining fuel allows.

3.3.3.3.1 Takeoff (P)

The pilot will accelerate the aircraft down the runway. The ground station operator will communicate current airspeed measurements to the pilot, and once takeoff speed is reached, the pilot will provide pitch up input and the Geometrically Scaled RPV will become airborne. Table 15, presented below, lists the takeoff speeds (120% stall speed) and the ground roll distances for both the unballasted and the 204.5 lb configurations.

Table 15 - Takeoff Speeds and Ground Roll Distances

Takeoff Weight	Takeoff Speed	Ground Roll
131.8 lbs	46.4 kts	268 ft
204.5 lbs	57.8 kts	691 ft

3.3.3.3.2 Climb (P)

The pilot will climb the aircraft as quickly as possible to the test altitude. The nominal test altitude is 550 ft to allow ample time for recovery in the event of unanticipated control response, but stay within comfortable visual range for the pilot. Assuming an airspeed of 93 knots during climb and a climb gradient of 0.088 (climb angle of 5°), it will take approximately 39.8 seconds to reach an altitude of 550 ft; however, the actual climb to 550 ft will most likely take much less time as the pilot will be at full throttle during the early stages of climb and will most likely climb at an angle greater than 5°. The pilot will be free to climb at a comfortable rate of his choosing. The final test altitude will be selected by the pilot during this test as a "comfortable" altitude where visibility and aircraft referencing (assessing aircraft attitude) is acceptable. During the first flight of any radio controlled aircraft, the time immediately after the first takeoff is the riskiest portion of the flight because the aircraft is not trimmed and the pilot is not familiar with the handling qualities. Accordingly, the pilot will gain altitude as quickly as possible to the test altitude to avoid problems caused by unexpected aircraft response at low altitude.

3.3.3.3.3 Trim (P)

The pilot will trim the aircraft at the test altitude. Only after the aircraft is fully trimmed will the maneuvering tests begin.

3.3.3.3.4 Racetrack (S)

The racetrack pattern will consist of the following 4 legs:

1. 1,500 ft straight line*
2. 180°, 750 ft constant radius turn
3. 1,500 ft straight line*
4. 180°, 750 ft constant radius turn

*A 1,500 ft. leg will take approximately 16 seconds at the test point speed of 56 knots and 9.3 seconds at an average cruise speed of 95 knots and 7.1 seconds at a fast cruise speed of 125 knots.

Note that this pattern will be completed in each direction, requiring both right and left turns.

3.3.3.3.5 Figure 8 (S)

The Figure 8 will consist of a 750 ft constant radius turn to the left immediately followed by a 750 ft constant radius turn to the right.

3.3.3.3.6 Landing Configuration Handling Evaluation(S)

The pilot will fly the aircraft on a "mock" approach to test the handling with the flaps extended. This will require the pilot to line up the Geometrically Scaled RPV for landing, reduce power and apply the flaps. Approximately 50% of the way through the approach, the pilot will apply power, retract the flaps and climb back to the test altitude out. At no time during this test will the aircraft come lower than 250 ft above the ground, and earlier tests will take place at higher altitudes. Assuming a maximum increase in lift coefficient of 0.24 due to flap extension, the stall speed of the aircraft (with varying amounts of fuel burn) is presented below in Table 16 along with the calculated landing speed of 1.15 times the stall speed. At no point during the Landing Configuration Handling Evaluation will the aircraft ever slow below 1.3 times the stall speed for the given configuration.

Table 16 - Landing Configuration Handling Evaluation Minimum Test Speeds

MTOW (lbs)	Fuel Burn (lbs)	Stall Speed (kts)	Landing Speed (kts)	Minimum Test Speed (kts)
204.5	10	47.01	54.06	61.11
204.5	20	45.79	52.66	59.53
204.5	30	44.53	51.21	57.89
204.5	40	43.24	49.73	56.21
204.5	50	41.91	48.20	54.48
131.8	10	37.16	42.73	48.31
131.8	20	35.60	40.94	46.28
131.8	30	33.97	39.07	44.16
131.8	40	32.26	37.10	41.94
131.8	50	30.45	35.02	39.59

3.3.3.3.7 Landing (P)

The pilot will safely land the aircraft on the runway. Care will be taken to keep the airspeed well above the stall speed throughout the entire approach and landing to avoid poor handling at low flight speeds. The aircraft is designed with tricycle landing gear with a steerable nose gear which is controlled

via the yaw control channel while on the ground. The aircraft is designed with tricycle landing gear with a steerable nose gear which is controlled via the yaw control channel while on the ground. The brakes will be applied after touchdown to slow the aircraft to a stop.

3.3.3.4 Dynamic Mode Flight Tests (T)

This test will investigate the dynamic stability of the aircraft with the primary focus on the Phugoid Mode and the Dutch Roll Mode. Preliminary vortex lattice analysis has shown that both the Phugoid Mode and the Dutch Roll Mode are marginally stable, and this test will serve to verify these results. This test will include using control doublets to excite the Phugoid Mode and the Dutch Roll mode and measuring the period of the resulting oscillations. The period can then be used to calculate the natural frequency. The Piccolo II has the capability to execute pre-programmed doublets of user-input lag times; however, preliminary tests will use manual doublet inputs for safety. The magnitude of the inputs and the dwell time of the doublets will start with half deflection and a dwell time of 1 second.

3.3.3.5 Incremental Weight Increase Test (S)

This test will demonstrate safe flight at the scaled test point. The actual flight will mirror that of the Phasing Test described in Section 3.3.3.3. Trim weights will be added to the trimming weight bays in the wings and fuselage to gradually increase the weight of the aircraft to the test point. The final goal of this test is to achieve a safe flight at the scaled test point weight. Ballast weight will be added incrementally, while still maintaining the appropriate CG location and moments of inertia. The increments in which the weight will be added will be determined ground testing (CG test and Bifilar Pendulum Test, see Sections 3.3.2.1 and 3.3.2.3). During each flight, the overall performance of the aircraft will be evaluated by the pilot. Prior to adding more ballast weight, the pilot, test director and ground controller will evaluate the performance of the aircraft and determine whether it is safe to continue adding ballast weight. If at any time during these flights the aircraft displays unexpected or undesired flight handling characteristics or is unable to climb at the desired gradient of 0.088 due to the added weight, the pilot will land the aircraft as quickly as safely possible and this test will be discontinued.

3.3.3.6 Aeroelastic Response Preparation Tests (T)

This test represents the final flight test in the Flight Demonstration FTP. This test will lay the groundwork for the Aeroelastic Response Program and the flight test of the Aeroelastically Scaled RPV. The aim of this test is to determine the flight test maneuver (or maneuvers) which achieve the required loading on the aft wing to excite the non-linear aeroelastic response while minimizing risk. This test allows the pilot to try three maneuvers that can generate the required loading: an upwind turn, a push-over pull-up and a windup turn. These maneuvers each present a unique method of reaching the required wing loading. An upwind turn is a simple maneuver where the pilot will fly the aircraft into the wind and then complete a 180° turn. The turn, coupled with the wind speed will produce a high wing loading. This is the simplest maneuver, but it can only be completed once during each flight “lap” and it only accomplishes positive loadings. The push-over pull-up requires the pilot to put the aircraft into a controlled dive and then pull-up, causing the aircraft to encounter positive loading at the bottom of the maneuver and negative loading at the top of the maneuver. The ability to achieve negative loading is useful, but putting the aircraft in a dive at the low altitudes required by a remotely controlled pilot (for

visual reference) is a risky maneuver. Finally, the windup turn is when the pilot maintains constant speed and flys the aircraft through a spiral pattern. As the radius of the turn decreases, the wing loading increases. This approach allows for a gradual increase in wing loading, but again it can only accomplish positive loadings.

Initial testing will take place at the un-ballasted weight of 131.8 lbs. Incremental weight increases will be attempted using the same criteria described in Section 3.3.3.5. It is important to note that if at any time during these flights the aircraft displays unexpected or undesired flight handling characteristics or is unable to climb at the desired gradient of 0.088 due to the added weight, the pilot will land the aircraft as quickly as safely possible and this test will be discontinued.

3.3.4 Overall Test Summary

The following table summarizes all planned tests, the phase of testing that each test falls in to, and the classification (primary objective, secondary objective or tertiary objective) which corresponds to the success criteria mentioned in Section 3.2.

Table 17 - Overall Test Summary

Phase 1 - System Tests	Test Location	Objective Level
System Readiness	Victoria	S
Servo Response	Victoria	S
Control Surface Scheduling	Victoria	S
Backup Control	Victoria	S
Data Collection and Storage	Victoria	S
Data Transmission	Victoria	S
Camera Transmission	Victoria	S
Turbine Tests		
Bench Testing	Victoria	S
Installed Turbine Testing	Victoria	S
Phase 2 - Flight Readiness Tests		
Aircraft Mass and CG		
Dry Mass	Victoria	P
Test Point Mass	Victoria	S
Center of Gravity	Victoria	P
Static Loading	Victoria	S
Bifilar Pendulum	VIctoria	P
Phase 3 - Flight Tests		
Low Speed Handling	Foremost	T
High Speed Taxi	Foremost	T
Phasing Test		
Takeoff	Foremost	P
Climb	Foremost	P
Trim	Foremost	P
Racetrack	Foremost	S
Figure 8	Foremost	S
Landing Configuration Handling	Foremost	S
Landing	Foremost	P
Dynamic Mode Flight Tests	Foremost	T
Incremental Weight Increase	Foremost	S
Aeroelastic Response Preparation	Foremost	T

4 Test Logistics

This section outlines the infrastructure in place to ensure that the fabrication of the Geometrically Scaled RPV, the integration of all onboard systems and the flight testing of the RPV has the highest chance of success. The proposed flight test schedule for the Flight Demonstration Program will be presented, along with the test locations. Test resources, including the ground station and all RPV control systems will then be presented, including a frequency usage chart. Safety requirements, security requirements will follow and a description of all flight test personnel, including each participant's qualifications will close this section.

4.1 Scheduling

Once the FTP has been cleared, Phase 1 tests will take place in Victoria beginning in June, 2011. When Phase 1 and Phase 2 are complete, the RPV will be sent to Foremost for Phase 3 testing.

4.2 Test Locations

This section presents details about each of the two test locations that will be used during this flight test program. These locations are Quaternion Engineering in Victoria, BC and the Foremost Airstrip in Foremost, AB.

4.2.1 Quaternion Engineering, Victoria, BC

Phase 1 and Phase 2 tests will take place in Victoria, BC at Quaternion Engineering, where the Geometrically Scaled RPV has been fabricated. Quaternion Engineering has a full fabrication shop, and is an ideal location to bench test components, assemble the RPV, and do ground testing on the airframe and instrumentation systems. Additionally, the Victoria Flying Club at the Victoria Airport has agreed to provide hanger space to conduct the bifilar pendulum test.

4.2.2 Foremost Airstrip, Foremost, AB

The Canadian Centre for Unmanned Vehicle Services (CCUVS) is a non-profit corporation whose purpose is to "facilitate sustained, profitable growth of the Canadian unmanned systems sector." CCUVS operates small UAV programs at the Foremost airstrip, and provides the required safety support. Foremost, AB is a small town with a population of 524. The Foremost, AB airstrip is a low traffic civilian airstrip off which CCUVS operates small UAV programs. Figure 46 below presents an aerial view of the Foremost, AB airstrip. According to Qwikcast.com, at the time of the planned flights (July), Foremost has an average temperature of 66°F (High 80°F, Low 51°F) and an average rainfall of 1.4 for the month.

Figure 46 - Foremost, AB Airstprip Aerial View

Table 18 – Foremost, AB Location and Elevation

Coordinates	49°29'N 111°29'W
Elevation	2902 ft

The airspace available at this airfield is sufficient for all planned flight tests. Figure 47 presents the allotted airspace.

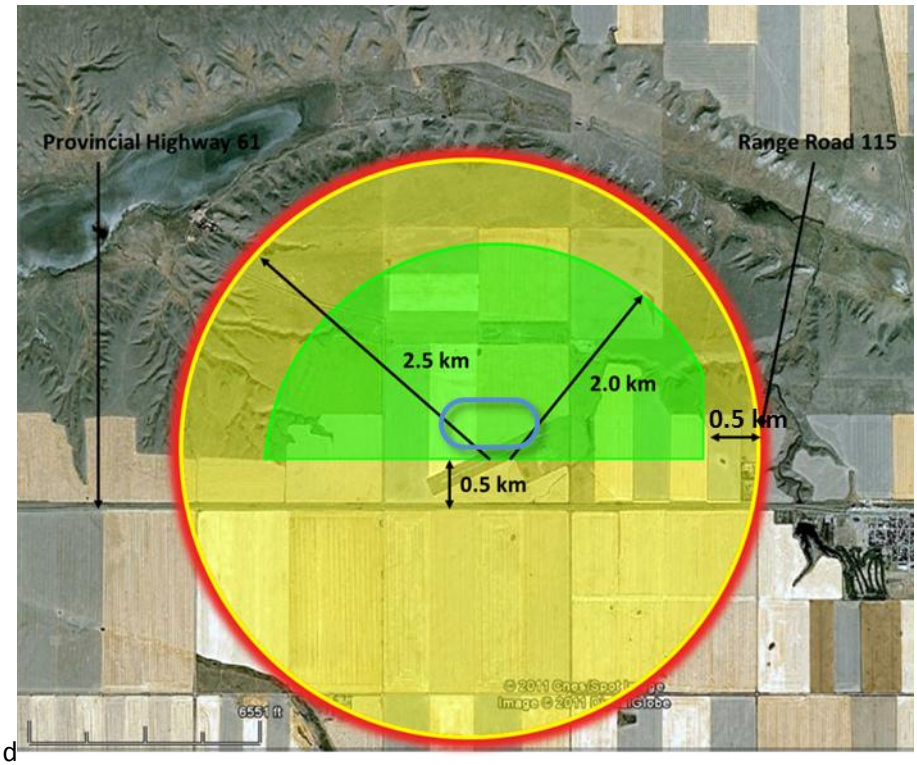

d

Figure 47 - Airspace Requirements (FORMOST AB).

The total approved airspace, shown above, is defined as a 2.5km radius circle centered at Foremost runway. This is the airspace in which Transport Canada has approved for flight operations. The "Safety Template," or the airspace in which all flight operations are allowed to continue uninterrupted, is shown above in green and is a 2.0 km radius circle centered at the runway truncated 0.5 km west of the approved airspace boundary and 0.5 km north of Provincial Highway 61. All planned flight tests will remain well within the Safety Template (as shown by the racetrack flight path presented above); however, should unanticipated flight conditions and/or problems cause the aircraft to leave the safe zone, appropriate measures will be taken. Immediately outside of this safe zone, the rest of the approved airspace, shown in yellow, is known as the Caution Zone. Normal Operations would avoid flight in this region due to its inclusion of Provincial Highway 61 (with very infrequent traffic). The Mayor of Foremost told the flight test crew that no data exists for the frequency of traffic on this road; however, a reasonable estimate is that traffic varies from 0-20 cars per day. To avoid a potentially hazardous situation with traffic on the road, spotters will be placed at either end of the airspace on the road to inform cars of flight operations in the area. Additionally, takeoff and landing will take place to and from the northeast whenever possible (except in emergency landing situations) to de-conflict with traffic on Provincial Highway 61.

Immediately outside of the Caution Zone is the Kill Zone, shown in red. As a requirement of the Special Flight Operations Certificate (see Section 4.2.3), if the Geometrically Scaled exits the approved airspace (which includes the Safety Template and the Caution Zone), failsafe via aerodynamic termination must be automatically executed. In other words, should the aircraft enter the kill zone, the

failsafe will be automatically executed terminating the flight. Note that the Safety Envelope, Caution and Kill zones will be programmed into the ground station computer and overlaid over the real-time vehicle position information.

The maximum permitted flight altitude is 700 ft. The within the airspace is level farmland with no significant terrain elevation change. Immediately outside of the Northern boundary of the airspace is a valley containing a small river. This is an elevation drop, and does not pose a threat to flight operations.

4.2.3 Special Flight Operations Certificate

A Special Flight Operations Certificate (SFOC), dated June 16th 2011, has been provided by Transport Canada for the operation of the Geometrically Scaled RPV at the Foremost test site. This document is provided in Appendix O. All flight operations will abide by the guidelines set forth in this document, including airspace, operational and safety requirements.

4.2.4 Alternate Flying Site: Portuguese Air Force Academy

Details about the flying site at the Portuguese Air Force Academy that was originally identified for use with this project is presented in Appendix M. This is only for reference as this location may be used in future testing.

4.3 Test Resources

4.3.1 Geometrically Scaled RPV

The Geometrically Scaled RPV is the main component to the JWSC Flight Test. Reference Section 2 for a full description of the Geometrically Scaled RPV and supporting systems.

4.3.2 Ground Station

The ground station used for all test operations is shown in Figure 48. The ground station, which is used for real time data monitoring as well as post-flight data download and reduction, has the following features:

1. Built in computer running Windows 7
2. Large, dual monitor display
3. Integration of the Piccolo II Ground Station
4. Gas generator for electrical power
5. Battery backup

Figure 48 - Ground Station[6]

4.3.2.1 Frequency Usage Chart

Radio frequencies are shown in Table 19, and all frequency usage will be coordinated with the test range prior to testing.

Table 19- Frequency Usage

Frequencies Used During the Test	
R/C Communications	2.4 GHz Spread Spectrum (Piccolo II / JR 12x)
Data Transmission	2.4 GHz Spread Spectrum (Piccolo II)
Emergency Navigation Camera	5.8 GHz / 900 MHz (via Oracle Diversity Receiver)
Team Communications	Cell Phone/ 2-Way Radio

4.4 Security Requirements

This program is UNCLASSIFIED and NOT restricted by ITAR regulation. The Piccolo II is ITAR equipment, but Quaternion Engineering has received all required approval to operate with the Piccolo II.

4.5 Test Project Management

This section will outline all personnel who will participate in the tests. At a minimum, the following people are required to be present during Phase 3 testing: Test Director, Ground Controller/Vehicle Technician, Pilot, Backup Pilot and Range Safety Officer. Efforts will be made to have at least 2 additional people on site during flight testing to serve as observers or ground crew. For ground tests (Phases 1 and 2), only the Test Director and the Ground Controller/ Vehicle Technician are required to be present.

Table 20 - Flight Test Personnel

Name	Title	Responsibilities
Dr. Ned Lindsley	AFRL Program Manager	Oversee the administration of the program, including the TRB and SRB. Point of Contact (POC) at AFRL.
Tyler Aarons	Test Director	Plan, coordinate and oversee all tests. Awareness of test area, equipment and procedure. Exercise Go/No Go authority as well as direct pilot during testing (including termination of flight if necessary). Communicates all information to pilot.
Jenner Richards	Ground Controller/ Vehicle Technician	Ground Controller - Operate the ground station. Monitor and oversee data collection and storage. Provide real-time aircraft state and health information to the test director. Additionally, operate the RPV via the tethered transmitter in the event that the aircraft travels outside of visual range. Vehicle Technician – Oversee and direct all on-site test article set-up, maintenance, and tear down.
Kelly Williams	Pilot	Perform flight maneuvers listed on the test cards under direct direction from the test director. The pilot will control the RPV through the primary transmitter.
Jon Harwood	Backup Pilot	The Backup Pilot will be in charge of the backup transmitter. The Backup Pilot will take control of the aircraft if he is directly directed to do so by the primary pilot in the event of a primary link failure or if the pilot becomes incapacitated. The Backup Pilot will also provide assistance to the pilot as required (trim assistance, range assessment, visual orientation, etc.).
Willem Brusson **Ryan Flagg**	Range Safety Officer (RSO)	Intimately aware of the flying site as well as all safety requirements imposed by the flying site. Provides safety briefing at the beginning of each Phase 3 testing day. Authority to call an immediate stop to testing (abort flight) in the event that an unsafe situation arises.

Peter Leu (Quaternion) **Jeff Garno-Royo (VT)** **Others (TBD)**	Observers	Observe test operations and provide assistance as required by other personnel.
TBD (Will be provided by VT, Quaternion Engineering or UVic)	Ground Crew	Observe test operations, help with RPV operations as required and provide assistance as required by other personnel.
Dr. Robert Canfield	Virginia Tech Technical Advisor	Advisor to Tyler Aarons, provide technical guidance and expertise throughout the program.
Dr. Afsal Suleman	University of Victoria Technical Advisor	Advisor to Jenner Richards, provide technical guidance and expertise throughout the program.
Dr. Craig Woolsey	Virginia Tech Technical Advisor	Advisor to Tyler Aarons, provide technical guidance and expertise throughout the program.

4.5.1 Qualifications of Pilots

Kelly Williams is a Mechanical Engineer and has been flying R/C aircraft since 1989, including flying turbine powered R/C jets since 1998. He serves at the Committee Chair on the R/C Jet Committee of The Model Aeronautics Association of Canada. Prior to flying the Geometrically Scaled RPV, Kelly will have logged several hours flying the Mini SensorCraft airframe in preparation for his role. Additionally, he will train on the 6DoF simulator.

Jon Harwood has 15 years' experience as a R/C pilot and holds his private pilot's license. He has served as the primary test pilot during the majority of Quaternion Engineering's Mini SensorCraft. He holds his CCUVS UAS Operator Certificate. Jon will also train on the 6DoF simulator.

A jet aircraft, purchased to serve as a trainer platform from Jon Harwood and to allow for the practicing of flight test maneuvers in Foremost has been purchased by Quaternion. Kelly Williams will use this aircraft to give Jon experience flying turbine powered aircraft. Additionally, this will give the Flight Test Support Team members the opportunity to familiarize themselves with the operation and flight characteristics of a turbine powered aircraft before the first flight of the Geometrically Scaled RPV. A Mini SensorCraft airframe will also be used to rehearse planned flight test maneuvers in Foremost.

4.5.2 Other Qualifications

Willem Brusson, Ryan Flagg, Jenner Richards and Jon Harwood have all taken and passed the CCUVS UAS Operator Certificate Course and the Transport Canada Radio Operator Certificate. The CCUVS UAS Operator Certificate recognizes each as an official CCUVS UAS Operator, and the Transport Canada Radio Operator Certificate gives each the authority to monitor airfield air traffic.

Additionally, Willem, Ryan, Jenner and Jon visited the Foremost Airstrip and met with the Mayor of Foremost, the local Fire Department, the Royal Canadian Mounted Police to discuss JWSC operations.

CCUVS Official Sterling Cripps traveled to Foremost, met with the team, and gave approval to operate the Geometrically Scaled RPV at the Foremost Airstrip.

4.5.3 Operations NOTAM

Prior to flight operations, the JWSC Flight Crew has been given the authority to post a Transport Canada NOTAM, a notice to all pilots, alerting them to JWSC flight operations in the area of the Foremost Airstrip. Additionally, flight test personnel will monitor NOTAMs in order to identify potential conflicts.

5 Test Procedures

On each test day, the specific testing procedure will consist of the following steps:

Prior to the first test:

1. Test Day Overview Briefing
    a. Test Briefing
    b. Safety Briefing
2. AFRL SUAS Test Ops ORM Assessment

Procedure for each test:

1. Pre-Test Briefing
2. Pre-flight checklists:
    a. Airframe
    b. JetCat P200-SX turbines
    c. Piccolo II
    d. Ground Station
    e. Instrumentation
3. Comply with SFOC Requirements
    a. Notify Nac Canada, Edminton FIC at 866-514-4102 prior to each flight.
    b. Monitor the Foremost UNICOM VHF frequency on 123.2 commencing 15 minutes prior to and during all flights.
    c. Make an Advisory call to “All Traffic in the Foremost Area” prior to all flights warning aircraft of location, altitude and duration of proposed flight.
    d. Cell phone or radio contact will be available with the nearest Air Traffic Control Agency (Medicine Hat Municipal Airport - MHMA)
    e. Aerodrome operator must be notified of all intended UAS operation and have no objections.
4. Go/No-go Decision
5. ***Test execution***
6. Post-Flight Checklists
7. Post-Test Briefing

5.1 Test Day Overview Briefing

This briefing will be completed at the beginning of each test day and will consist of two parts, the test briefing and the safety briefing.

5.1.1 Test Briefing

The test briefing will be conducted by the Test Director and will consist of an overview of all tests planned for the current test day. All personnel present for the days testing will be required to attend. The briefing will serve to allow everyone on site to unify their understanding of the goals for that particular day. The test briefing may also consist of:

1. A review of results of the previous days test
2. Proposed schedule for the days test
3. Weather report
4. Any security issues

5.1.2 Safety Briefing

The safety briefing will be conducted by the Range Safety Officer and will include the following:

1. Test boundaries for the day (this may change day to day by sharing airspace on base or other factors)
2. Safety concerns for any of the planned tests
3. Review of THA's

5.2 Pre-Test Briefing

The Pre-Test Briefing will be conducted by the Test Director prior to each test. The Pre-Test Briefing will consist of:

1. Brief description of the test item configuration (if any changes have been made since any previous tests)
2. Overview of the test objective(s) and procedure
3. Review of Test Cards (Test Card Template shown in Appendix H)
4. Weather report (visibility, wind direction and strength, precipitation forecast)
5. Complete the AFRL SUAS ORM form and brief participants on ORM level (AFRL SUAS ORM Form shown in Appendix C).

5.3 Pre-Flight Checklists

Pre-Flight Checklists will be completed prior the start of each test. All pre-flight checklists are located in Appendix D. There are separate pre-flight checklists for:

1. Airframe
2. JetCat P200-SX Turbines
3. Piccolo II
4. Ground Station
5. Instrumentation

5.4 Go/No-go Decision

The Go/No-go decision will be made by the Test Director. The Range Safety Officer has the authorization to terminate testing at any time should a safety concern arise. The following are the required conditions:

1. Weather
    a. Daylight VFR conditions
    b. No current precipitation with favorable forecast
    c. No lightning within a 10 mile radius
    d. Visibility: >3 miles
    e. Ceiling: >1700 feet (AGL)
    f. Wind: Calm, gusting to no more than 10 kts
    g. Sustained Maximum Crosswind: 4 kts
2. AFRL SUAS Test Ops ORM Assessment must be complete.
3. All pre-flight checklists must be complete with no concerns.

5.5 Post-Flight Checklists

Post-Flight Checklists will be completed after the completion of all planned test points. All post-flight checklists are located in Appendix E.

5.6 Post-Test Briefing

The Post-Test briefing will be conducted by the Test Director and will consist of (but is not limited to):

1. System Status
2. System Performance
3. Overall Review of the Test
4. Lessons Learned
5. Action Items
6. Brief Overview of Tests for the Next Day

6 Safety Considerations and Risk Minimization

All testing, both ground testing and flight testing, will be conducted in accordance with this approved test plan. If any changes are necessary, the test team will contact the Safety Review Board for approval prior to completing the test. If, at any point during the test, a conflict between technical and safety issues should arise, safety concerns will always take precedence.

The following sections will outline safety considerations and risk minimizing procedures for several key risks during flight operations.

6.1 Required Test Conditions

All ground tests will be conducted indoors when possible. All outdoor tests, both ground tests and flight tests, during which the Geometrically Scaled RPV is in motion, will take place during in daylight, VFR conditions. The following weather conditions must exist at all times for testing to continue:

1. No current precipitation with favorable forecast
2. No lightning within a 10 mile radius
3. Visibility: >3 miles
4. Ceiling: >1700 feet (AGL)
5. Wind: Calm, gusting to no more than 10 kts
6. Sustained Maximum Crosswind: 4 kts

The weather will be evaluated at the beginning of each test to satisfy the Go/No-Go determination, and the test director will monitor the weather throughout the test. The Test Director will confirm his assessment of the weather with the Pilot prior to all flights. If at any time the Pilot, Test Director or Range Safety Officer raises any concerns about current conditions, testing will be immediately suspended until all 3 parties agree it is safe to continue. If these conditions are exceeded during a flight test, the pilot will be asked to land the RPV as safely and quickly as possible.

6.1.1 Personnel Locations During Testing

During all flight tests, all personnel will be positioned behind the pilot (behind a horizontal line parallel to the runway, at the pilot's distance from the runway) to ensure that the pilot has an unobstructed view of the runway and all personnel are accounted for. A rope barrier will be used to mark this line during all flight operations. During taxi, takeoff and landing, all personnel will be required to remain around the ground station. Once the RPV has reached a safe altitude, spotters may move to other locations in the field, as required, but they will return to the ground station for landing. The desired location or each person involved in the testing will be communicated prior to beginning testing. The final positions of all personnel will be decided once the test group reaches the flight facility in Foremost.

6.1.1.1 Safe Zone

A pre-defined safe zone will be established at the flying site to serve as a gathering point in the event that the aircraft is in danger of impacting on or near personnel. This safe zone will be placed behind the truck and trailer used to transport the aircraft, and these objects will serve as a protective barrier. The safe zone will be away from batteries and fuel, and will be kept unobstructed during all flight operations.

6.2 Airspace

All flights will take place at the Foremost Airstrip in Foremost, AB. All flights will take place in the approved airspace. For more details about the airspace, see Section 6.11.2. Additionally, for a description of the airspace in the backup location in Ota, Portugal, see Appendix M.

6.2.1 Midair Collision

The pilot will remain in manual control of the aircraft at all times, and in the event of a midair collision (bird strike, FOD ingestion in flight), the pilot will land the aircraft as quickly and safely as possible. Spotters will be used to help locate possible collision risks, and inform the pilot if necessary.

6.3 Hazardous Materials

The Geometrically Scaled RPV is powered by twin JetCat P200-SX turbines, and as such, the RPV will carry an onboard fuel supply consisting of Jet A1 or 1-K Kerosene and turbine oil. In order to minimize the risk, all operation of the JetCat turbines will follow the JetCat Safety Protocol (see Appendix J for more information) and fuel will be stored in approved containers. Additionally, a fire extinguisher will be located at the ground station at all times. Finally, all flight crew members will be giving hearing protection for use when operating the JetCat P200SX turbine engines.

The Geometrically Scaled RPV will also have electrical power provided by lithium polymer (LiPo) batteries. Only LiPo approved chargers will be used, and all batteries will never be charged at a rate greater than 1C. LiPo batteries will also be stored carefully, away from fuel and other combustibles.

6.4 Loss of Link

The use of the Acroname RxMUX allows for the incorporation of an independent backup control system. For more information about this control system, see Section 2.8.

6.4.1 Backup Communications Hierarchy

The hierarchy of communications is as follows:

Piccolo II Primary Controller→ RC Rx Backup Control → Piccolo II Tethered Controller → Failsafe

In all communications failures, the Piccolo II will flash a warning on the ground station and the GSO will relay this information to the TD and pilot. In the event of primary communications link loss a warning is given on the ground station display. Should this happen during the flight of the Geometrically Scaled RPV, the backup pilot will immediately take control. The Piccolo II does not allow for automatic switch of control to the backup transmitter, so the backup pilot will need to manually take control via a toggle switch on the backup transmitter. In the event that that the aircraft is within visual range but neither the primary nor the backup pilot can comfortably fly the aircraft, the Ground Station Operator will take control of the RPV using the Piccolo II Tethered Controller. The Ground Station Operator will return the aircraft to a location where the primary pilot can assess the attitude of the aircraft and take control. In the event that the RPV leaves visual range, the last effort to control the aircraft will be using the Piccolo II tethered controller. Using the Emergency Navigation Nose Camera as well as the Piccolo II telemetry (which includes an artificial horizon), the Ground Station Operator will steer the aircraft back into visual range at which point the Primary Pilot will take control. Flying the aircraft using the nose camera is the last option, and should this prove unsuccessful, the failsafe protocol will be executed.

In the event of total communication loss with the RPV (primary and RC backup controls all fail), a failsafe procedure will automatically be executed. For more information about the failsafe procedure,

see Section 6.8.2. This automatic failsafe procedure will be tested *at full range* at the Foremost Airfield prior to commencing flight operations.

6.4.2 RF Masking/ Shielding

The use of carbon fiber composite materials and the unique shape of the JWSC creates a situation where RF masking and/or shielding is a concern. To combat these issues, remote receivers are placed with the antennas outside of the fuselage to avoid masking. Additionally, the placement of these receivers allows communication to be maintained with the RPV in any attitude. All servo extension wires will be braided to avoid EMI issues. Note that all onboard systems will be rigorously tested for interference/masking/shielding issues during Phase 1 tests.

The Piccolo II ground station contains a 2.4GHz spectrum analyzer. Through the user interface on the ground station, the Ground Station Operator can generate a spectrum analysis table that provides an indication of other RF users and potential sources of interference across the 2.4GHz band. The spectrum analyzer will be used survey the spectrum before all flight operations and during range/EMI testing.

6.4.3 Automatic Turbine Shutdown

In the event of total loss of signal, the JetCat ECU will automatically take the turbines to idle, or shut them down if necessary. The default parameters in the JetCat ECU take the turbines to idle after 0.1 seconds of total signal loss. If the signal loss persists for 3 seconds, the turbines are shut down.

6.5 Loss of Vehicle Position Information

Since the Geometrically Scaled RPV will be under manual control at all times, a loss of vehicle position information (GPS) while the vehicle is flying within visual contact represents a loss of telemetry, and not a hazardous situation. At all times during the flight, the pilot and backup pilot will keep visual reference on the aircraft. The ground station operator will monitor the telemetry feeds from the aircraft and the spotters will assist in visual referencing of the aircraft.

If the Geometrically Scaled RPV inadvertently travels outside of visual contact, but remains within the allotted airspace, the Ground Station Operator will take control of the aircraft using the live feed from the nose camera to navigate the aircraft back into visual contact. The camera feed will be placed next to the artificial horizon (from the Piccolo II) on the ground station to assist with maintaining constant altitude while flying using the nose camera. In the event that the nose camera fails, the artificial horizon and GPS information available in real time on the Piccolo II ground station display can be used to navigate the aircraft. In the event that the nose camera feed fails and either the GPS or artificial horizon fails, the failsafe procedure will be executed.

6.6 Loss of Flight Reference Data

The Piccolo II provides the GSO with real time GPS position, GPS altitude, barometric altitude, attitude and airspeed information. Since the Geometrically Scaled RPV will be under manual control at all times, a loss of flight reference information while the vehicle is flying within visual range represents a loss of telemetry, and not a hazardous situation. In the event that the Geometrically Scaled RPV inadvertently travels outside of visual range and the primary means of non-visual control (the nose

camera) fails, the artificial horizon and GPS position information will be used to navigate the aircraft. In the event that the nose camera feed fails and either the GPS or artificial horizon fails, the failsafe procedure will be executed.

6.7 Unresponsive Flight Controls

In the event that flight controls are unresponsive, the backup controller will be activated and the backup pilot will take control of the aircraft. If the backup controller is unable to control the aircraft due to a total loss in link, the failsafe procedure will automatically execute.

6.8 Flight Termination System

The flight termination system (FTS) consists of a failsafe procedure that will be executed manually (commanded kill) in the event that the RPV is uncontrollable or if it travels outside of visual range and the backup navigation systems fail. The failsafe procedure will be executed automatically in the event of a total loss in link (loss in link with the backup transmitter), or in the event that the RPV travels outside of approved airspace.

6.8.1 Flight Termination Criteria

The following list consists of situations in which the failsafe procedure would be executed:

1. Unresponsive flight controls
2. Total loss of link
3. Geometrically Scaled RPV travels outside of the approved airspace boundary
4. Complete visual contact is lost and the backup navigation systems (GPS, nose camera, artificial horizon) fail

6.8.2 Failsafe Procedure

The failsafe condition is executed during full loss of link, and corresponds to a controlled crash: full up elevator, full right rudder, full right aileron, turbines shutdown. The failsafe condition is designed to minimize residual damage and results in the aircraft experiencing a tip stall on the right wing and entering a tight, downward spiral until impact.

There is no documentation of the total time delay before failsafe is initiated; however, there is a manufacturer specified time delay of less than 4 ms for the JR-12x to regain control in SmartSafe mode. SmartSafe mode is a failsafe mode in which, if signal is regained, the failsafe condition will be removed and manual control is resumed. If the JR-12x is able to regain control in 4 ms, then it is a reasonable assumption that it is also able to detect a loss of signal in 4 ms.

6.8.3 Commanded Kill

In the event that the RPV is uncontrollable or travels outside of visual range and the backup navigation systems fail a Commanded Kill command will be executed. A Commanded Kill corresponds to a manually executed failsafe condition. The commanded kill can be executed via both the backup controller and the ground station.

6.8.4 Automatic Failsafe Procedure

In the event of a total loss of link (the RPV is unresponsive to input from either the primary or backup transmitter) the failsafe procedure will execute automatically. The Piccolo II features a loss of link failsafe that defaults the aircraft to a pre-programmed autonomous flight path, a fixed radius, fixed altitude circle above the ground station, in the event that primary link is lost. The pilot will realize that loss of control has occurred and call for the backup pilot to take control. The backup pilot will take control with the backup transmitter and attempt to fly the aircraft. In the event that link is lost with the backup transmitter, the aircraft will automatically execute the failsafe procedure.

The automatic failsafe procedure is accomplished via the default control hierarchy contained within the Acroname RxMUX. The RxMUX contains two inputs: the default input A and the secondary input B, as shown in Figure 49.

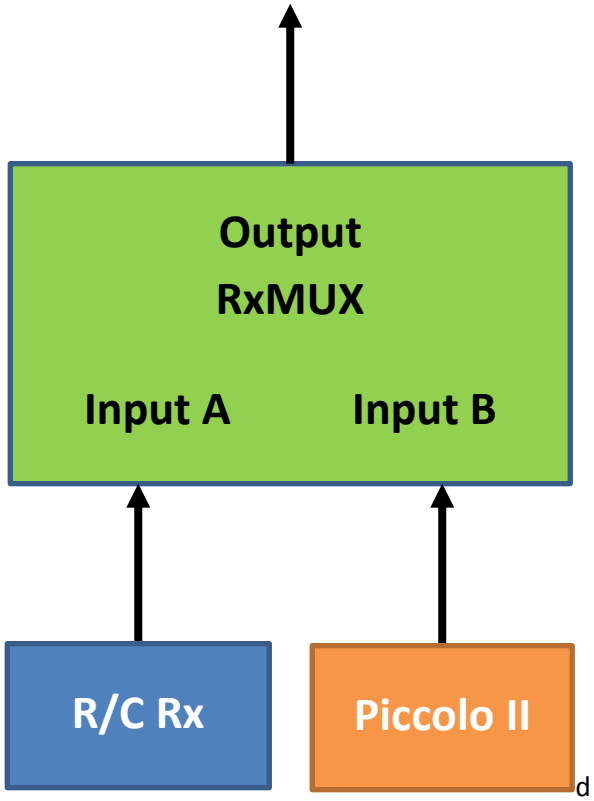

Figure 49 - RxMUX Control Schematic

In this setup, the backup receiver will be attached to Input A and the Piccolo II will be attached to Input B. The RxMUX is designed such that in the event that Input B is lost, the RxMUX will default to Input A; however, the reverse process is not permitted. This means that if the backup pilot takes control of the RPV, and in doing such switches the RxMUX to Input A, and there is a loss of link with the backup R/C system, the R/C system will realize total loss of link and enter failsafe as programmed into the R/C system. The RxMUX, which prevents default switch of command from Input A to Input B, will allow the failsafe procedure to be executed automatically.

6.9 General Safety Mitigating Considerations

This section will elaborate on several topics relating to general safety.

6.9.1 Malfunction/Failure Ground Operations

A malfunction or failure of the aircraft or related systems during ground operations could be caused by mishandling of the aircraft by ground crew, equipment failure or by not following all pre-flight checklists and procedures. The effects of a malfunction or failure during ground operations could include damage to or loss of the vehicle as well as property damage, personal injury or death.

In order to minimize the risk of a malfunction or failure during ground operations, all personnel who will be in contact with the aircraft at any time during the test procedures will be trained by either the Test Director or Ground Station Operator before arriving at the test site. This training will include an overview of all systems on board of the aircraft as well as general safety guidelines. Additionally, the Geometrically Scaled RPV will be disassembled, packed and transported in protective containers to the test site to avoid damage during travel. Finally, the Test Director will ensure that all checklists and procedures are completed as required and the Range Safety Officer and Test Director will be present at all Phase 3 tests to observe pre-flight preparations.

In the event that a malfunction or failure occurs, the primary pilot will shut down the JetCat P200-SX turbines immediately. Once the turbines are shut down, a single member of the ground grew will approach the aircraft from the nose of the aircraft, with a fire extinguisher in hand, and shut down power. JetCat specifies that the recommended minimum safe distances are 15 ft in front of the turbine, 25 ft on either side and 15 ft behind the turbine. These distances will be enforced at all times during turbine operation.

Remaining personnel are free to approach the aircraft only after Test Director and Range Safety Officer confirm that the aircraft is powered down and call “all clear.” Flight testing will resume only after the Test Director, Ground Controller/Vehicle Technician and Pilot approve any/all repairs.

6.9.2 Malfunction/ Failure During Takeoff

A malfunction/ failure during takeoff could be caused by a loss of control during, taxi, takeoff roll, or climb out, a total Loss of link with the aircraft, pilot error during takeoff or FOD ingestion. . The effects of a malfunction or failure during ground operations could include damage to or loss of the vehicle as well as property damage, personal injury or death.

In order to minimize the risk of a malfunction or failure during takeoff, both the primary and backup pilot have trained on several reduced complexity flight models in preparation for their roles in this project. Additionally, the Test Director will ensure that all checklists and procedures are complete as described in this flight test plan and the runway will be examined for FOD prior to each flight. The backup controller will be tested prior to each flight for reliable link with the aircraft as well as the ability to take control of the aircraft at any time and the backup pilot will have the backup transmitter in his hands at all times during test operations, ready to take control if a loss of primary link situation arises. Finally, the primary pilot will be ready at all times to re-direct the aircraft away from people or property.

In the event that a malfunction or failure occurs, the pilot will perform evasive maneuvers if required to avoid personnel and property damage and landing the aircraft as quickly as safely possible and shut down the JetCat P200-SX turbines immediately. Once the turbines are shut down, a single member of the ground grew will approach the aircraft from the nose of the aircraft and shut down power. Remaining personnel are free to approach the aircraft only after Test Director and Range Safety Officer confirm that the aircraft is powered down and call "all clear." Any available personnel will perform first aid if needed and inform proper facilities personnel as necessary.

6.9.3 JetCat P200-SX Turbine Malfunction During Flight

A failure of one or both turbines during flight could be caused by FOD ingestion,fuel pump failure, ECU battery failure, fuel tubing coming loose or turbine mechanical failure. The effects of such a failure may include a forced deadstick landing, damage to the turbines, loss of the vehicle, property damage, personal injury or death.

In order to minimize the risk of turbine failure during flight, FOD screens will be checked during preflight and the runway will be cleared of any noticeable FOD before each flight. A fuel filter will be used on all fuel containers. All batteries, including flight packs, transmitter batteries ground station backup batteries will be fully charged according to manufacturer specifications, and voltage checked before each flight and zip ties will be used to secure all fuel tubing connections. The manufacturer's specified 25 hour maintenance interval will be strictly adhered to, and the total turbine run time will be checked prior to each flight. Finally, the pilot and backup pilot will have trained on a simulator for degraded modes of flight, including both single and double turbine failure.

In the event that a single turbine malfunctions or shuts down, the primary pilot will attempt to land the aircraft as quickly as safely possible under the power of the remaining turbine. In the event that single engine operations results in an uncontrollable yawing moment or undesired handling characteristics, the second turbine will be shut down and a power off landing will be attempted. In the event that both turbines fail, a power off landing will be attempted as quickly as safely possible. dIf failure occurs during ground operations, all personnel will wait until turbines have completely stopped spinning to approach aircraft. If failure occurs during flight, the pilot will call "DEADSTICK" and begin an emergency approach. All personnel will clear the landing surface and keep eyes on the aircraft at all times. After landing/impact, a single member of the ground crew will approach aircraft carefully *with a fire extinguisher in hand.* In the event of a fire, the Test Director will contact the local fire department.

6.9.4 Fire

A fire could be caused by faulty/malfunctioning electronics, improper charging of batteries or a fuel spill. The effects of a fire could include damage to or loss of the vehicle, property damage or personal injury or death.

In order to minimize the risk of a fire, all batteries charged according to manufacturer specifications. Electrical connections will be checked for frayed wires and possible short circuits before flight. Fuel will be stored in approved containers only, away from the flight line, test equipment, test personnel and the flight test article. The Test Director will ensure that all checklists and procedures are

complete as described in this flight test plan and a fire extinguisher will be present at the test site at all times.

In the event that a fire occurs, the local fire department will be contacted immediately. If the fire is small enough, a single member of the ground crew will carefully approach the aircraft and attempt to put out the fire with the fire extinguisher. If in doubt, wait and let the fire patrol take care of the fire. Additionally, the following lists will be followed, depending on the location and/or cause of the fire.

1. If the fire is inside of the aircraft:
    a. The primary pilot will immediately shut down both turbines.
    b. A single member of the ground crew will carefully approach the aircraft use the fire extinguisher to put out the fire.
    c. After the fire is extinguished, the ground crew member will power down the RPV, if it is safe to do so.
    d. All remaining personnel will wait 15 minutes after the flames are extinguished to approach the aircraft.
2. In the event that a LiPo battery begins to show signs of swelling during charging:
    a. The person charging the battery will immediately disconnect battery from charger.
    b. Wait for swelling to stop increasing
    c. DO NOT attempt to start charging the battery again
    d. Place the battery in a location away from the ground station away from any combustible material.
    e. Dispose of LiPo battery according to manufacturer's specifications as soon as safely possible.

6.9.5 Structural Damage

Structural damage could be caused by loss of control and resulting dive causes pilot to fly outside of safe flight speed range, failure of one or more structural components during flight, a hard impact on landing, a mid-air collision or mishandling of vehicle. The effects of structural damage could include loss of the vehicle, property damage or personal injury or death.

In order to minimize the risk of a fire, the primary and backup pilots will have extensive simulator training before flying the Geometrically Scaled RPV, including training for degraded modes of flight, including structural failure. To prevent a mid-air collision, spotters will actively search the airspace for collision hazards, and inform the pilot if necessary. In order to prevent mishandling of the vehicle, all personnel who will be in contact with the aircraft at any time during the test procedures will be trained by either the Test Director or Ground Station Operator/Vehicle Technician before arriving at the test site and the vehicle will be disassembled and transported in protective containers. During flight, the pilot will be prepared for inadvertent flight maneuvers due to loss of link, stuck control surfaces, or other degraded modes of flight and the backup pilot will be prepared to take control in the event that the primary pilot loses control. Finally, the aircraft structure will be checked for wear and tear before each flight.

In the event that structural damage occurs during shipping or ground operations, the appropriate repairs will be made and checked before testing is resumed. If damage occurs in flight, the pilot will perform an

emergency landing (if possible) as quickly as possible to minimize collateral damage. In the event that the structural damage renders the aircraft uncontrollable, all personnel will clear the landing surface and keep eyes on the aircraft at all times.

6.9.6 Malfunction/ Failure during Landing

A malfunction or failure during landing could be cause by a loss of control during approach or landing, heavy crosswind or adverse weather conditions, landing gear failure, pilot error during approach or landing or a total loss of link. The effects of such a failure include damage to or loss of the vehicle, property damage and personal injury or death.

In order to minimize the risk of such a malfunction or failure, the Test Director will ensure that all checklists and procedures are complete as described in this flight test plan. Both pilots will have had extensive training on both reduced complexity flight models. Additionally, the primary pilot will be ready at all times to re-direct the aircraft away from people or property and the Backup Pilot will have the backup transmitter in his hands at all times during test operations, ready to take control if a loss of primary link situation arises. The backup controller will be tested prior to each flight for reliable link with the aircraft as well as the ability to take control of the aircraft at any time.

In the event that a malfunction or failure occurs during landing, the primary pilot will shut down the turbines as quickly as possible. If airborne, the pilot will perform evasive maneuvers if required to avoid personnel and property damage. If possible, a "go around" maneuver will be performed to avoid a hard landing and give the pilot more time to assess the situation and the pilot will land aircraft as soon as safely possible. After landing, a single member of the ground crew will carefully approach and power down the aircraft. Remaining personnel are free to approach the aircraft only after Test Director and Range Safety Officer confirm that the aircraft is powered down and call "all clear." Flight testing will resume only after the Test Director, Ground Controller/Vehicle Technician and Pilot approve any/all repairs.

6.10 Test Hazard Analysis

A detailed test hazard analysis is provided in Appendix F.

6.11 Mishaps

For the purposes of this test, a mishap will be defined as:

> ***Mishap:*** An event that results in damage to the aircraft (outside of normal wear and tear from operations), injury to personnel, damage to private property and/or damage to airfield property at the flight location in Foremost.

In the event of a mishap, the Test Director will contact the AFRL Flight Test and Evaluation Office as well as AFRL Flight Safety POC Maj Stew Eyer as soon as possible (within 8 hours) to inform them of the event. The decision to continue, postpone or cancel testing will be made in collaboration with the Test Director, Pilot, Ground Station Operator, Range Safety Officer and CCUVS Officials in charge of the airfield during testing and AFRL Safety Review Board. Immediately after the RPV is recovered and damage is assessed, AFRL Form 29 – AFRL Test Safety Mishap Form will be completed. A partially completed copy is located in Appendix G. Efforts will be made to be as detailed and descriptive as

possible about the cause and effects (both short and long term) of the mishap, as well as its implications on future testing.

A copy of the Certificate of Liability Insurance is located in Appendix I. A copy of the Mishap Investigation letter, signed by CCUVS POC Sterling Cripps, is located in Appendix P.

6.11.1 Emergency Personnel

Emergency Personnel, including the fire department, will be local to the Foremost, AB and available by phone during all flight operations.

Appendix A. Reduced Complexity Flight Models

This appendix was adapted from Reference 6.

Flight Testing of the Geometrically Scaled RPV presents two unique but interlinked goals. The first goal is that both the RPV is flown safely and successfully through all required flight test maneuvers. The unconventional configuration and control surface layout of the JWSC, coupled with the large scale and complexity of the RPV, make this a significant challenge. The second goal is that all required flight test data to validate the scaling, further the understanding of the flight characteristics of the RPV, and pave the way for the Aeroelastic Response Program is successfully gathered. The design and testing of an instrumentation system for each FTP as well as the incorporation of these systems into each RPV present another challenge.

At the onset of this program, it was decided to initially address each of the above mentioned goals individually through the use of reduced complexity flight tests. These tests, which include the fabrication and flying of sub-scale JWSC models for configuration testing as well the use of conventional "trainer" style, high wing aircraft for instrumentation testing, allow for an incremental increase in complexity. The overall aim is to merge the lessons learned from both the configuration and instrumentation and data collection testing into the Geometrically Scaled RPV, thereby increasing the chances of a safe and successful FTP. In addition, preliminary flight testing allows for the pilot's perspective to be included in the design and optimization of the RPV.

This appendix serves as a reference on each of the four reduced complexity flight models used for preliminary flight testing of the JWSC configuration and the flight test instrumentation. Photographs (or CAD renderings) of each aircraft are presented along with design specifications and a description of key design features.

A. Senior Telemaster

Figure A-1. Senior Telemaster Used For Development of Autopilot and Instrumentation Systems

Figure A-2. Senior Telemaster During Autonomous Flight

Figure A-3. Mobile Command Center

Description

Due to the unconventional configuration and unknown flying qualities of the JWSC, provisions for an autopilot are included to allow for stability augmentation. In addition, the autopilot allows for safety features such as an electronic fence, return to home and the ability to release a parachute etc. In addition, the autopilot offers a convenient way to both log and send telemetry of the aircraft states in real time as well as offering 16 analog to digital inputs for items such as rpm sensors, strain gauges etc.

Before integrating and operating the autopilot within the JWSC, it was decided to test the setup using a commercially available trainer. The Senior Telemaster exhibits docile flying characteristics while offering sufficient cargo space and payload carrying capabilities.

Flights have been performed under both manual and autonomous modes and a basic flight test program performed in order to characterize the aircraft and tune the PID control loops. Future tests will include the testing of instrumentation systems that are slated for the *Geometrically Scaled RPV* and *Aeroelastically Scaled RPV* flight test programs.

***Senior Telemaster* Specifications**	
General	
Span	94 in
Length	64 in
Wing Area	1330 in^2
TOGW	19 lbs
Construction	
Airframe	Balsa/Monokote
Stiffeners	Carbon Fiber reinforcements
Propulsion	
Engine	Saito 1.8 ci 4-stroke
Propeller	APC 16 x 8
Thrust	14 lbs
Other	
Stability Augmentation	Piccolo II Autopilot
Telemetry	Aircraft states
Other	Onboard video with telemetry overlay, stabilized camera gimbal

B. Flat Plate Foamie

Figure A-4. Flat Plate Foamie

Figure A-5. Underside of Aircraft Highlighting Carbon Fiber Stiffeners

Figure A-6. Flat Plate Foamie in Flight

Description

The Flat Plate Foamie, shown in in Fig. A-4, represents the lowest complexity model of the JWSC used in this program, and also the first to be designed and flown. When designing the model, a balance was struck between the simplicity and operability of the model and the desired accuracy of the representation of the flight dynamics of the full scale RPV. The Flat Plate Foamie features a flat plate, extruded polystyrene airframe stiffened with carbon fiber arrow shafts, as shown in Fig. A-5. Dihedral, anhedral and sweep angles match full scale geometry; however, the complex spanwise twist distribution present in fore and aft wings was omitted as this was impossible to replicate with commercially available fanfold foam without the inclusion of custom, composite stiffeners. Additionally, the turbine propulsion system was replaced with a simplified, high thrust to weight ratio propeller setup for ease of operation and maintenance. Figure A-6 shows the Flat Plate Foamie in flight during a flight test.

***Flat Plate Foamie* Specifications**	
General	
Length	42.25 in
Span	66 in
TOGW	2.2 lbs
Construction	
Airframe	0.25 inch extruded polystyrene
Stiffeners	Carbon Fiber arrow shafts
Control	
Transmitter	Futaba T10CAP
Reciever	Futaba R319DPS
Servos	7 x Hextronik HXT 900
Propulsion	
Motor	TowerPro BM2409-18T
ESC	TowerPro MAG8 25 Amp
Propeller	GWS 10 x 4.7
Battery	Turnigy 1000mAh 3 Cell LiPo

C. EDF Twist Corrected Foamie

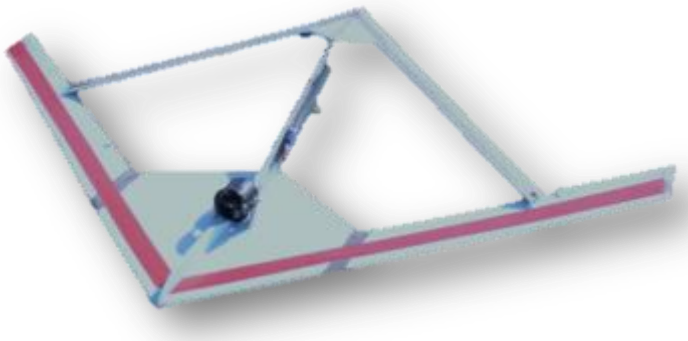

Figure A-7. ***EDF Twist Corrected Foamie***

Figure A-8. Aft Wing in Jig Under Vaccum to Create Spanwise Twist Distribution

Figure A-9. ***EDF Twist Corrected Foamie*** **in Flight**

Description

The EDF Twist Corrected Foamie, shown in Fig. A-7, represents a marked improvement over the Flat Plate Foamie. As with the Flat Plate Foamie, dihedral, anhedral and sweep angles are representative of the full scale geometry; however, for the EDF Twist Corrected Foamie the airframe is fabricated using extruded polystyrene wrapped in a fiberglass/ expoxy composite with unicarbon strips are used as stiffeners in the lifting surfaces and tail boom. Wing jigs, such as the one shown in Fig. A-8 and Fig. A-9, were used to create the complex spanwise twist distribution present in fore and aft wings. A 2800 kV brushless outrunner motor spinning a 6 blade, 2.75 in diameter EDF was used to power this model. Figure B-4 presents the EDF Twist Corrected Foamie in flight.

EDF Twist Corrected Foamie **Spec.**	
General	
Length	42.25 in
Span	66 in
TOGW	2.6 lbs
Construction	
Airframe	0.28 inch extruded polystyrene 3.2 oz/in2 fiberglass/epoxy composite
Stiffeners	Unicarbon strips
Control	
Transmitter	JR 1221
Reciever	JR 12X
Servos	7 x Hextronik HXT 900
Propulsion	
Motor	2800 kV Brushless Outrunner
ESC	45 Amp
Propeller	6 Blade, 2.75 in diameter
Battery	Turnigy 2450 mAh 4 cell LiPo

D. Mini Sensorcraft

Figure A-10. Mini Sensorcraft

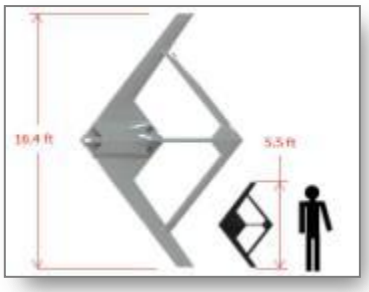

Figure A-11. Relative Size of *Mini Sensorcraft* Compared to *Geometrically Scaled RPV*

Figure A-12. Assembly of *Mini Sensorcraft* Used for Glide Tests

Description

The Mini Sensorcraft is similar in size to both the Foamie Sensorcraft and the Twist Corrected Foamie but employs the exact outer mould line of the full scale aircraft, including accurate airfoils and twist distribution. This variant will be the most accurate reduced complexity model before the final Geometrically Scaled RPV and Aeroelastically Scaled RPV.

The aircraft was fabricated using CNC machined female moulds. The outer skin consists of carbon/epoxy composites and two part polyurethane foam will be expanded within the fuselage and wings. The aircraft will use two 2800 kV brushless outrunner motors spinning 6 blade, 2.75 in diameter EDFs in order to more accurately reproduce the scaled thrust to weight of the given test point.

Additional testing of landing gear configurations was completed and control surface scheduling, stall characteristics and aircraft trim were investigated through flight testing.

At present, over 20 hours of successful flight testing has been completed on MiniSensorCraft airframes.

***Mini SensorCraft* Specifications**	
General	
Length	42.25 in
Span	72.8 in
TOGW	3.6 lbs (Estimated)
Test Point	10.8 lbs
Construction	
Airframe	2 part PU foam core expanded into 3.2 oz/in2 fiberglass/epoxy composite skins
Stiffeners	Unicarbon
Control	
Transmitter	JR 1221
Reciever	JR 12X
Servos	7 x Hextronik HXT 900
Propulsion	
Motor	**2 x** 2800 kV Brushless Outrunner
ESC	**2 x** 45 Amp
Propeller	**2 x** 6 Blade, 2.75 in diameter
Battery	**2 x** 2450 mAh 4 cell LiPo

Appendix B. Results from AFRL Bench Testing of a JetCat P200

The following plots are the results from the bench testing of a JetCat P200 turbine at the AFRL on October 26th, 2009 and October 29th, 2009. These results will be used as a benchmark for comparison with the experimental data generated during the static thrust tests completed for the JWSC. For more information about these tests, see Section 3.3.1.8.

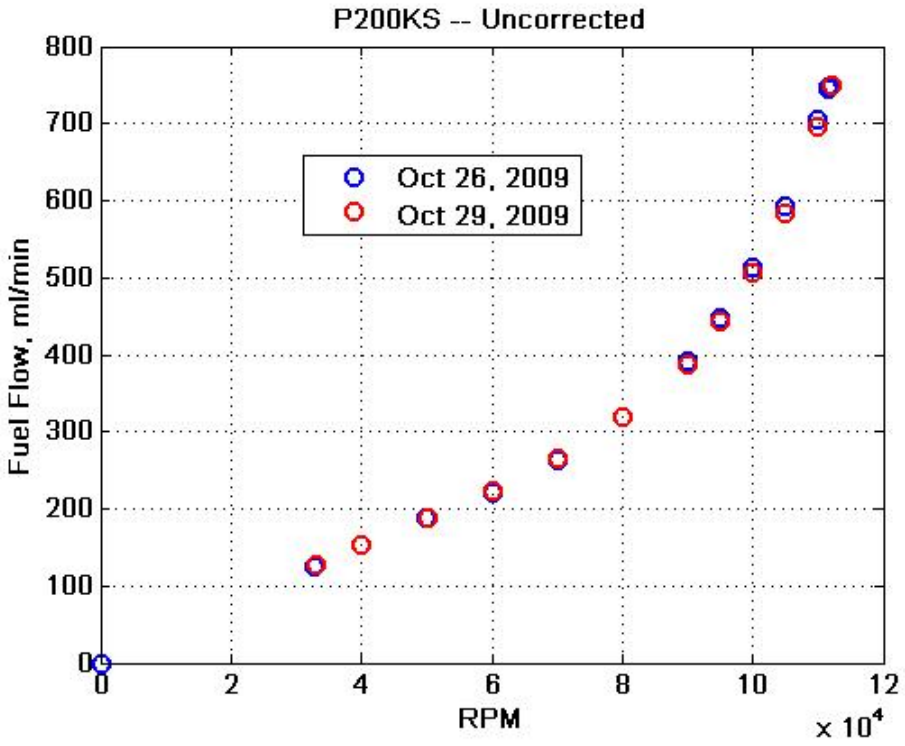

Figure B-1 - Fuel Flow vs. RPM

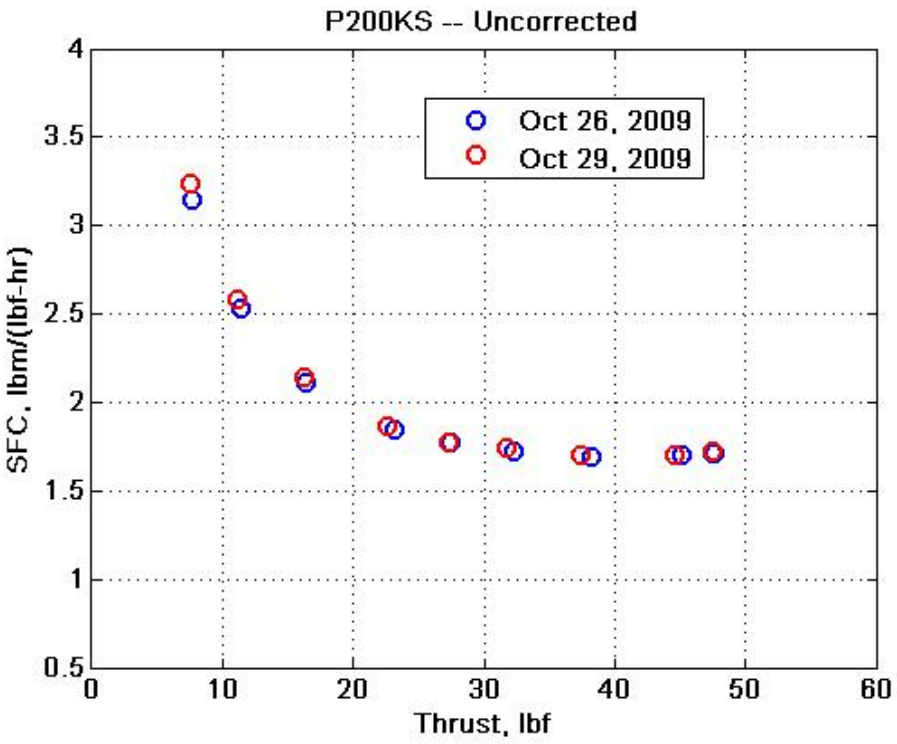

Figure B-2 - Specific Fuel Consumption vs. Thrust

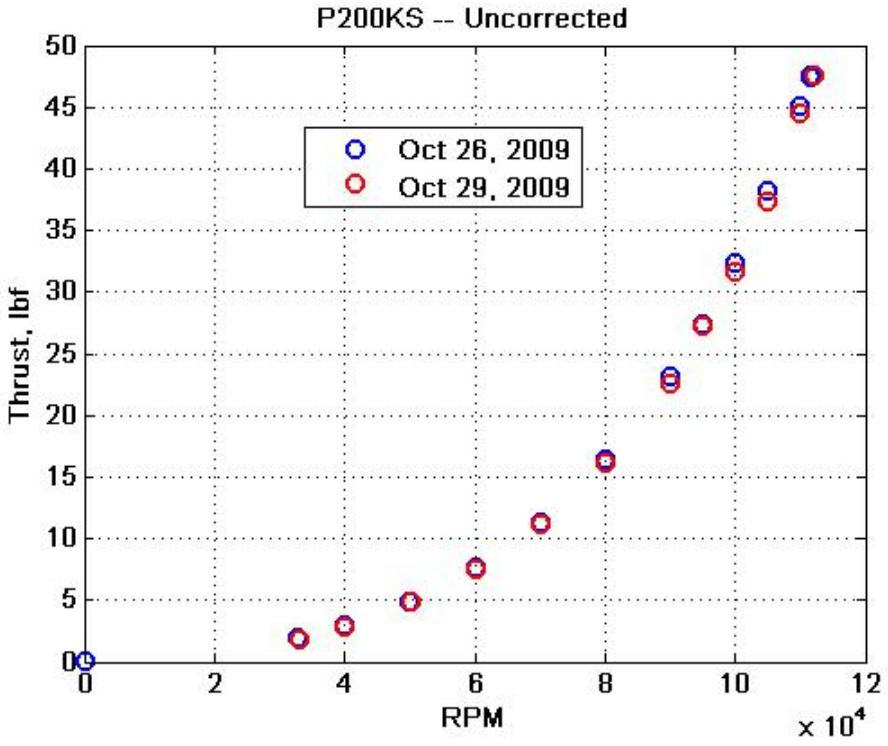

Figure B-3 - Thrust vs. RPM

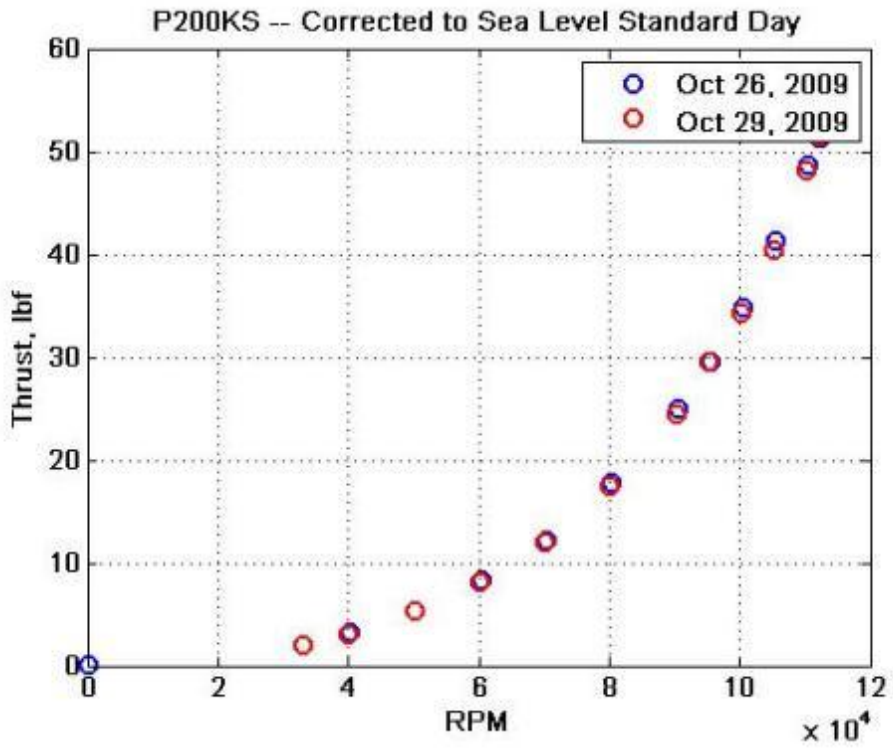

Figure B-4 - Thrust vs. RPM (Corrected to a Sea Level Standard Day)

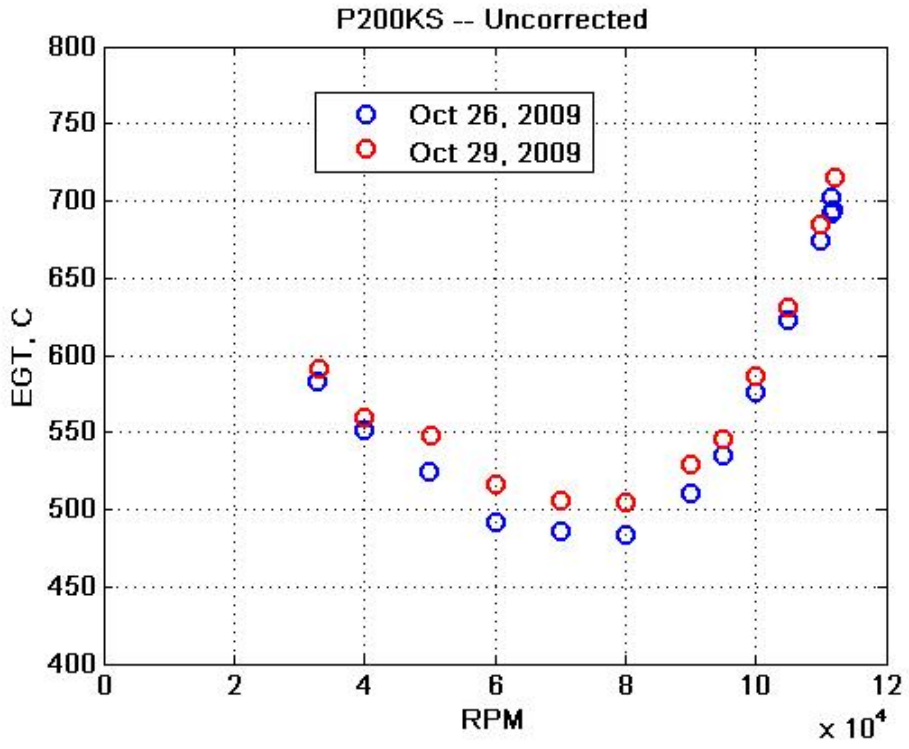

Figure B-5 - Exhaust Gas Temperature vs. RPM

Appendix C. AFRL SUAS ORM Assessment Form – Preliminary First Flight Form

Date: 5/1/2011 Program: JWSC GSRPV Flight Test Vehicle: GSRPV Flight # 1

	GREEN		YELLOW		RED	
HUMAN	Place "X" in appropriate box					
Vehicle Operator						
Qualified *		Fully Qualified	X	In-Training		No Training at All
Currency (this vehicle) *	X	< 30 Days		30-60 Days		> 60 Days
Sleep (Crew Rest)	X	≥ 8 Hours		6 – 8 Hours		≤ 6 Hours
Ground Control Station (GCS) Operator						
Qualified	X	Fully Qualified		In-Training		No Training at All
Currency (this GCS/vehicle)	X	< 30 Days		30-60 Days		> 60 Days
Sleep (Crew Rest)	X	≥ 8 Hours		6 – 8 Hours		≤ 6 Hours
Payload Operator						
Qualified	X	Fully Qualified		In-Training		No Training at All
Currency (this payload/vehicle)	X	< 30 Days		30-60 Days		> 60 Days
Sleep (Crew Rest)	X	≥ 8 Hours		6 – 8 Hours		≤ 6 Hours
Launch Crew						
Qualified		Fully Qualified		In-Training		No Training at All
Currency (this launch system/vehicle)		< 30 Days		30-60 Days		> 60 Days
Sleep (Crew Rest)		≥ 8 Hours		6 – 8 Hours		≤ 6 Hours
Observers						
Qualified (if flying in the National Airspace	X	Fully Qualified		In-Training		No Training at All
Sleep (Crew Rest)	X	≥ 8 Hours		6 – 8 Hours		≤ 6 Hours
Crew/Personal Concerns	X	None		Minor		Major
MISSION/OPS	Place "X" in appropriate box					
Test Location Familiarity	X	> 3 Previous Tests at this Location		1 - 3 Previous Tests at this Location		First Time at this Location
Test Location Weather	X	All Criteria Acceptable		1-2 Criteria Within 30% of Limits		1-2 Criteria Within 10% of Limits or > 2 Criteria Within 30% of Limits
Mission Duration	X	< 30 minutes		30-120 minutes		> 120 minutes
Takeoff Times	X	Between Sunrise & Sunset		All Other Times		At Night
Landing Times	X	Between Sunrise & Sunset		All Other Times		At Night
Bird Activity (check US Avian Hazard Advisory System at www.usahas.com, verify on-site, prior to start of testing)	X	Low		Moderate		Severe
Duration of Duty Day	X	< 8 Hours		8 - 12 Hours		> 12 Hours
Mission Complexity	X	Low/Normal		Demanding		Extremely Demanding
Safety Risk	X	Low		Medium		High
Check AFRL Flight Crew Information Folder (Flight Crew Information Folder)	X	0 Notices pertaining to systems under test or all relevant issues have been satisfactorily addressed				Relevant notices exist and not yet complied with
VEHICLE/GCS/LAUNCH SYSTEM/RECOVERY SYSTEM	Place "X" in appropriate box					
Config Changes (hardware/software)		None		Minor or first flight after down time > 30 days	X	Major modifications or Functional Check Flight or down time > 90 days
Maintenance Write-ups	X	0 Write-ups outstanding		≤ 3 Minor Write-ups outstanding – no impact on meeting test objectives and/or compromising safety		≥ 1 Major Write-up(s) outstanding impacting meeting test objectives and/or compromising safety or > 3 Minor Write-ups outstanding
Service Bulletins/Safety Supplements **	X	0 New Bulletins / Supplements outstanding; all existing complied with and reviewed/approved by SRB and TAA				Bulletin/Supplement exists, applicable to system under test, and not yet complied with
TOTAL ORM LEVEL	X	**GREEN** (< 3 Total Yellows/Reds, with no more than 1 Red)		**YELLOW** (≥ Total 3 Yellows/Reds, with no more than 1 Red)		**RED** (2 or More Reds)

AFRL Form 33A DRAFT 4 Aug 10
Prescribing Directive AFRLI 61-103, Volume 1

*** Review FAA Interim Operational Approval Guidance 08-01, dated 13 Mar 08, Section 9.0 Personnel Qualifications, for specific requirements.**

**** Mandatory for all commercial products used in test (vehicle, ground control station, launch system, and recovery system). If using an in-house system designed and developed by another organization, check with that organization for any cautions and warnings. Assessment only needs to be completed prior to first flight of each week's testing.**

Test Director: Discuss How ORM Which Shows Up as Yellow or Red Was Addressed/Mitigated/Who Was Notified (use continuation page as needed)

This is a preliminary form filled out in anticipation of the first flight of the Geometrically Scaled RPV. The pilots will have both flown at the test site prior to the first flight of the RPV, and the Virginia Tech/Quaternion Engineering crew will have performed ground operations at the test site (as part of this test plan) before the aircraft goes wheels up. The only yellow ORM level comes from the fact that this is the first flight of a new aircraft. The pilots will have both flown reduced scale models of this aircraft prior to flying the full 1/9th scale RPV.

Mission Completed (y/n): _____

If Not, Why:

Initials _____

GREEN ORM: If any specific area is Red, look at ways to lower risk in that area. Test Director or Test Safety Officer discretion to continue test.

YELLOW ORM: Try to mitigate to Green ORM. Work with Test Director, Vehicle Operator, and Test Safety Officer to lower ORM risk. If unable to lower risk, AFRL Branch Chief must be notified and approve test start.

RED ORM: Try to mitigate to Green or Yellow ORM. Work with Test Director, Vehicle Operator, and Test Safety Officer to lower ORM risk. If unable to lower risk, AFRL Division Chief must be notified and approve test start.

INSTRUCTIONS:

1. Complete this assessment prior to each flight or like series of consecutive sorties.
2. Maintain completed forms in test log book.
3. If Total ORM level is Yellow or Red, notify AFRL/SEF and AFRL/RBCT that approval to continue with testing was sought/garnered by the appropriate level of authority. Notification should be made within 4 hours of the start of the test. Preferred method of notification is by e-mailing the completed form to Afrl.se.workflow@wpafb.af.mil and AFRLDL.flighttestandevaluation@wpafb.af.mil
4. Provide copy of completed forms to AFRL/SEF and AFRL/RBCT upon the completion of the test program.

AFRL Form 33A DRAFT Aug 10
Prescribing Directive AFRLI 61-103, Volume 1

Appendix D. Draft Pre-Flight Checklist

This appendix will contain the pre-flight checklists for the aircraft, turbines, Piccolo II and Instrumentation systems. Modifications and changes to this list are expected since this a new prototype aircraft. The following list is an example, and the true pre-flight checklist will be more detailed as the required checks for all onboard systems are more fully understood.

Aircraft Configuration:	**Date:**
Signatures:	
Test Director: **Ground Station Operator:** **Pilot:** **Backup Pilot:**	
Aircraft	**Acceptable?**
1. All batteries, including flight packs, transmitter batteries and ground station backup batteries are fully charged according to manufacturer specifications, and voltage has been checked.	
2. Check FOD screens for security. Clear lodged FOD.	
3. Check controls surfaces for loose hinges.	
4. Check control horns and push rods for loose connections.	
5. Check fasteners for tightness on all exterior doors (hatch, trimming weight bays).	
6. Inspect Landing Gear.	
7. Verify Fuel Level.	
Piccolo II	
1. Check and record initial battery voltage and current **Piccolo Battery Pack_____ (3s, 1800mAh)**	
2. Power on Piccolo II and wait for GS and AP to initialize.	
3. Configure map page as required for mission	
4. Verify and/or load flight plans	
5. Verify correct controller settings	
6. Verify mission limits, including deadman status and lost comm waypoint. **Mission Limits:** **Deadman Status:**	

7. Verify working aircraft GPS	
8. Check number of satellites and PDOP **Satellites:** Indicates the number of satellites used in the GPS solution, and the total number of visible satellites. Usually there at least six to ten satellites visible. In some cases there are no satellites visible. This occurs if the GPS receiver does not have a complete GPS constellation almanac. Once the almanac download is complete this value is corrected. **PDOP:** The Position Dilution Of Precision value is a number calculated based upon the geometry of the current satellite constellation. Typical values should be less than three. If you are seeing high PDOP values or too few satellites that indicate the GPS is not performing well, there could be problems with the antenna configuration. **Number of Satellites**_____ (6-10 Optimal) **PDOP**_____ (< 3 Optimal)	
9. Set altimeter to local base pressure	
10. Verify Backup Control Hierarchy (Test for the ability to pass between: stability augmentation ←→ manual ←→ RxMUX backup	
11. Verify failsafe settings for lost comm with backup transmitter.	
12. Match trim settings for all flight modes	
13. Verify the reported control surfaces match the actual control positions for all transmitters	
14. Check air data readings and zero them if needed. Complete in *MANUAL MODE* so the AP will not assume it is flying.	
15. Check the correct operation of the gyros and accelerometers by physically rotating the aircraft and verifying the sensor outputs.	
16. Verify that the pitot tube is clear by blowing into it and seeing the airspeed response.	
17. Set the initial fuel weight or battery charge state of the vehicle.	
18. Configure the autopilot loops as needed, typically in auto, with the waypoint set for the launch plan.	
19. Start the engine and verify correct operation throughout the entire RPM range. Check sensor readings for signs of excessive noise due to engine vibration at different RPMs.	
20. Check communications at the far end of the runway strip. RSSI signal should indicate close to the maximum reading (-71 dBm). ➢ **–71 is the maximum reading.** ➢ **Communications performance will begin to degrade when the RSSI reaches –101 or lower.** ➢ **The receiver sensitivity is about -105 dB so if RSSI reads close to -105 you are pushing the receiver about as far as it can go.**	

RSSI Reading_____ **-71 = Perfect** **-101 = degraded** **-105 threat of receiver dropout**	
21. Check Communication AckRatio (acknowledgement ratio) aka"Link" AckRatio (Link number) is an indication of bidirectional communications performance. Since the system operates via polled communications, the ground station requests data from the aircraft, and then responds. The ground station keeps track of the acknowledgements from the aircraft. If communications are **solid the link number will typically be 95 to 100. Anything less than 85 could be cause for concern particularly for manual control.** **Link_____**	
22. Check for aircraft traffic and make any radio calls mandated by air traffic control.	
Instrumentation	
1. All instrumentation components and wires are securely fastened	
2. Onboard cameras are on a transmitting data to the ground station	
a. The ground station is receiving video feed from the cameras	
3. Power on the strain gage/accelerometer system	
4. LED Indicators from microcontrollers are flashing synchronously	
5. Start instrumentation timer as soon as LED indicators flash	
6. LED Indicators from data loggers are flashing	
JetCat P200-SX Turbines	
This checklist come directly from JetCat, and is specified in the user's manual[7].	
1. Check total engine runtime hours, verify <25.	
2. Charge ECU Battery	
3. Prepare fire extinguisher	
4. Check fuel lines and filter. Make sure they are clean with no restrictions	
5. Check that the fuel tank vent is unobstructed	
6. Verify fuel mix of 5% turbine oil in fuel (i.e.: 1 quart per 5 gal of kerosene)	
7. Fill fuel tank(s). Make sure the main and header tanks are full	
8. Turn on receiver switch	
9. Place the model with nose into the wind	
Final Preparations	
1. Notify Nav Canada, Edminton FIC at 866-514-4102	
2. Monitor the Foremost UNICOM VHF frequency on 123.2	

3. Make an advisory call to "All Traffic in the Foremost Area" warning all aircraft of aircraft location, altitude, and duration of proposed flights.	
4. Verify Go/No-Go Minimums: **Weather:** Daylight VFR conditions No current precipitation with favorable forecast No lightning within a 10 mile radius **Visibility:** >3 miles **Ceiling:** >1700 feet (AGL) **Wind:** **Calm, gusting to no more than 10 kts** **Sustained Maximum Crosswind: 4 kts**	
5. Clear runway of any noticeable FOD	
6. Verify Backup Control Hierarchy (Test for the ability to pass between: **stability augmentation ←→ manual ←→ RxMUX backup**	
7. Confirm wind direction, direction of taxi and takeoff and location of all personnel.	
8. All personnel are located behind the pilot (a horizontal line parallel to the runway)	
9. Manually push aircraft to center of runway	
10. Apply brakes	
11. Start turbines, allow both turbines to stabilize	
23. Final Piccolo II check: If any of the below rated no-go values are reached, the mission is aborted until the problem is corrected. **Battery Voltage_____ No-Go =** **RSSI_____ No-Go = -102** **Link_____ No-Go = 90** **Number of Satellites_____ No-Go = 5** **PDOP_____ No-Go = 3**	
12. Range Safety Officer clears RPV for takeoff	
13. Ground Station Operator clears RPV for takeoff	
14. Test Director clears RPV for takeoff	
15. Pilot clears RPV for takeoff	
16. ***Takeoff***	

Appendix E. Draft Post-Flight Checklist

Aircraft Configuration:	**Date:**
Signatures:	
Test Director: **Ground Station Operator:** **Pilot:** **Backup Pilot:**	
Aircraft	Acceptable
1. Wait until the aircraft has come to a complete stop, and then shut down the turbines.	
2. Wheel aircraft back to staging area near ground station	
3. Turn model into the wind, allowing the JetCat turbine cooling process to finish	
4. Remove the forward hatch and power down the instrumentation system.	
5. Download flight data from the accelerometers and strain gages.	
6. Power down the RPV and remove all batteries	
7. Power down the primary and backup transmitters	
8. Check the RPV for damage and/or wear and document all findings	
9. **Document any significant events that occurred during the flight immediately (positive or negative):**	

Appendix F. Test Hazard Analysis

This appendix documents the test specific hazards associated with the flight operations of the JWSC Geometrically Scaled RPV. A list of these hazards is presented below in Table F-1. Additional, non-test specific hazards are discussed in Section 6.9.

Table F-1 – JWSC Geometrically Scaled RPV Hazard List

Hazard Number	Hazard Title
1	Loss of Control

In the following sections, each of these hazards will be analyzed individually. The causes and effects will be examined, along with the minimizing procedures that will be followed to avoid the negative effects of these hazards as well as corrective action that will be taken should the hazard be encountered. Additionally, each hazard will be assigned a risk level (1-20) based on the Risk Assessment Matrix shown in Figure F-1 below.

	HAZARD SEVERITY CATEGORY			
	Catastrophic	*Critical*	*Marginal*	*Negligible*
HAZARD PROBABILITY	May cause death, system loss	May cause severe injury, severe occupational illness, or major system/facility damage	May cause minor injury, minor occupational illness, or minor system/facility damage	May cause less than minor injury occupational illness or system/facility damage
FREQUENT Likely to occur frequently during the test	1	3	7	13
PROBABLE Will occur several times during the test	2	5	9	16
OCCASIONAL Likely to occur sometime during the test	4	6	11	18
REMOTE Unlikely, but possible to occur during the test	8	10	14	19
IMPROBABLE Highly unlikely to occur during the test	12	15	17	20

Figure F-1 – JWSC Geometrically Scaled RPV Risk Assessment Matrix

The numbers in the Risk Assessment Matrix (1-20) are correlated to an overall hazard risk level based on the combined hazard probability and the hazard severity category. The designations, known as the Hazard Risk Levels, are presented below in Table F-2.

Table F-2 – Hazard Risk Levels

Risk Level	Definition	Risk Assessment Matrix Numbers
Low	Hazards which present no greater risk than normal operations, assuming all operational and safety protocol are followed.	10,11,12,13,14, 15,16,17,18,19,20
Medium	Hazards which present a greater risk to personnel, equipment or property than normal operations. These hazards are caused by a malfunction, failure or personal error.	5,6,7,8,9
High	Hazards which present a significant risk to personnel, equipment or property. These hazards are caused by a malfunction, failure or personal error.	1,2,3,4

TEST HAZARD ANALYSIS (THA)		PAGE 2	
PROGRAM TITLE: Joined Wing SensorCraft Flight Demonstration Program		TEST PLAN # Version 10	
PROGRAM MANAGER: Ned Lindsley	PHONE NUMBER:	HAZARD CATEGORY:	DATE: 6 July 2011
PREPARED BY: Tyler Aarons	PHONE NUMBER 484-269-7894	OFFICE SYMBOL:	

TEST HAZARD:
Loss of Control

Location: Foremost, AB Platform: Geometrically Scaled RPV

CAUSE:
1. Flutter
2. Structural Damage
3. Inadequate Stability and Control Margins

EFFECT:
1. Damage to vehicle
2. Loss of vehicle
3. Possible injury or death
4. Possible property damage

MINIMIZING PROCEDURES:
1. (1,E1,E2) The Ground Station Operator will ensure that flight speeds are available to the pilot during flight to avoid overspeed.
2. (1) Each control surface is designed with multiple (at minimum 2) servos to provide two points of contact.
3. (1) A flutter analysis has been completed for the vehicle.
4. (2) The vehicle will be disassembled and transported in protective containers.
5. (2,E1) The aircraft structure will be checked for wear and ear before each flight.
6. (3) A buildup approach to testing has been taken, wing 3 flight models of increasing complexity being used to test stability, control and flying qualities.
7. (1,2,3) The pilot will have trained on a simulator for degraded modes of flight.
8. (1,2,3,E1,E2,E3,E4) The Backup Pilot will have the backup transmitter in his hands at all times during test operations, ready to take control if a loss of primary link situation arises.

CORRECTIVE ACTIONS:
1. In the event that flutter occurs, the Primary Pilot will slow the aircraft to control the instability.
2. Structural Damage:
   a.) If damage occurs during shipping or during ground operations, the appropriate repairs will be made and checked before testing is resumed.
   b.) If damage occurs in flight, the pilot will perform an emergency landing (if possible) as quickly as safely possible to minimize collateral damage.
   c.) In the event that the structural damage renders the aircraft uncontrollable, all personnel will clear the landing surface and keep eyes on the aircraft at all times.
3. If the aircraft is uncontrollable due to inadequate stability and control margins, aerodynamic termination will be used to create a controlled crash in a safe area away from all personnel.

SRB CHAIRMAN:	SIGNATURE:	DATE:

Appendix G. AFRL Form 29 – AFRL Test Safety Mishap Worksheet

AFRL Test Safety Mishap Worksheet

Complete General Information and Mishap Notification Contacts in advance.
Mishap to be reported within 8 hours of occurrence.

General Information

	AFRL Costs	Non-AFRL Costs
Program Title: Joined Wing SensorCraft Flight Demonstration	Vehicle:	$100,000
Program Manager/Symbol/Phone: Dr. Ned Lindsley	Non-Vehicle:	$60,000
	Total System:	$160,000

Mishap Notification Contacts/Record

Name/Office	Phone/Cell	Email	Date/Time Notified
AFRL Det Safety:	Brian Rhodes 937-255-0049/937-313-5558	Brian.rhodes@wpafb.af.mil	
Branch Chief:	Denis Mrozinski, AFRL/RBSD (937) 255-2123	Denis.Mrozinski@wpafb.af.mil	
Division Chief:	James Kocher, AFRL/RBS (937) 255-3031	James.Kocher@wpafb.af.mil	
SRB Chair:	Gary Hellmann, AFRL/RBCT (937) 255-9742	Gary.Hellmann@wpafb.af.mil	
AFRL Flight Safety:	Maj Stew Eyer 937-255-8639/(24/7 safety cell)937-626-3513	stewart.eyer@wpafb.af.mil	
Host Safety Office:	CCUVS POC Sterling Cripps, (410) 488-7208	sterling@ccuvs.com	

==========

For use only in the case of a Class A, B, or C mishap.

TD Executive Officer: _____

Tech Director: _____

Mishap Information: Class A, B, or C? (See instructions on Page 2) ☐ Yes ☐ No

Location of Mishap: _____ Date of Mishap: _____

Brief Narrative: _____ Time of Mishap: _____

Personnel

Injuries? ☐ Yes ☐ No If Yes: ☐ Military ☐ Gov't ☐ Civilian ☐ Contractor ☐ Non Gov't

How many people were injured? _____ Hospitalization Required? _____

Extent of Injuries (be as specific as possible):

Name of responding emergency organization:

Point of contact at organization (name & number):

Name of clinic or hospital where injured was taken:

Property

Property Damage? ☐ Yes ☐ No If Yes: ☐ Gov't ☐ Contractor ☐ Non Gov't

Approx dollar cost:

Extent of Damage:

Additional Notes:

FOR OFFICAL USE ONLY (FOUO) When Form is Completed

AFRL Form 29, Previous Editions Obsolete

Prescribing Directive: AFRLI 61-103, Volume 1

As a reminder, in case a mishap occurs the test team should follow the initial responses listed below:

- Ensure everyone is safe and contact emergency services, if needed.
- Minimize fire damage to wreckage, if applicable.
- Do not disturb the accident scene – preserve all wreckage and surrounding areas in their original state.
- Only move or change things at the scene in the interest of safety. Photograph the site before and after anything is disturbed. Take lots of pictures so an investigator can easily retrace the situation before it was changed.
- Gather pertinent personal information from everyone at the scene (name, duty, title, office symbol, contact information).
- Gather witness statements as soon as possible to ensure clarity and freshness of memory. Write down exactly what was personally witnessed.
- Follow the contact procedures on the front of the AFRL Form 29. Report mishap to identified contacts as soon as possible but no later than 8 hours after occurrence.
- **For Class A, B, or C mishaps, notify the Tech Directorate's Executive Officer or Tech Director to initiate OPREP-3 reporting procedures IAW AFI10-206 AFMCSUP 1.** (See below for additional information on OPREP reporting.)
- Wait for guidance from range safety, a trained safety investigator, or HQ safety personnel before removing, cleaning, or disturbing a crash site.

If in doubt, wait and ask AFRL Safety. Remember that all safety investigations are non-retributional in nature and are conducted for mishap prevention purposes only.

OPREP-3 Reporting Matrix

Event/Incident	Submit Report When (Description)	Type Report
Aircraft Mishap	Any AF aircraft mishap involving civilian causalities or damage to civilian property	PINNACLE
Aircraft Mishap Class A	A. aircraft destroyed, B. damage of $2,000,000 or more, C. mishap resulting in an AF fatality	BEELINE
Aircraft Mishap Class B	A. damage of $500,000 but less than $2,000,000, B. aircraft mishap resulting in a permanent partial disability, C. aircraft mishap resulting in inpatient hospitalization of three or more personnel	BEELINE
Aircraft Mishap Class C	Damage of $50,000 or more but less than $500,000 not reportable under BEELINE criteria	HOMELINE
Civil Aircraft Mishap	Any civil aircraft mishap that occurs on AF property or under the control of/in airspace controlled by an AF air traffic control facility	HOMELINE

For Determining Vehicle and Non-vehicle Costs:

For "Vehicle" cost consider providing quantity and cost of each vehicle, chase aircraft, or unmanned aerial vehicle.

For "Non-vehicle" cost consider infrastructure, ground control station, trailers, ground equipment, etc.

Note 1: Vehicle and Non-vehicle costs shall be mutually exclusive.
Note 2: Non-AFRL and AFRL costs shall be mutually exclusive.

Appendix H. Test Card Template

Medium Risk

Medium Risk

SENSORCRAFT VT - Uvic - Quaternion	Flight Demonstration Program TEST TITLE		
Pilot:	**FTE:** Tyler Aarons	**GSO:** J. Richards	**Date:**
Aircraft: Geom. Scaled RPV	**GTOW:** kg (lbs batt)	**Location:**	

Restrictions

VIAS:	Range: visual	Ceiling:	Deck:	Max Time: s

Test Summary

#	Event	Condition

Test Boundaries

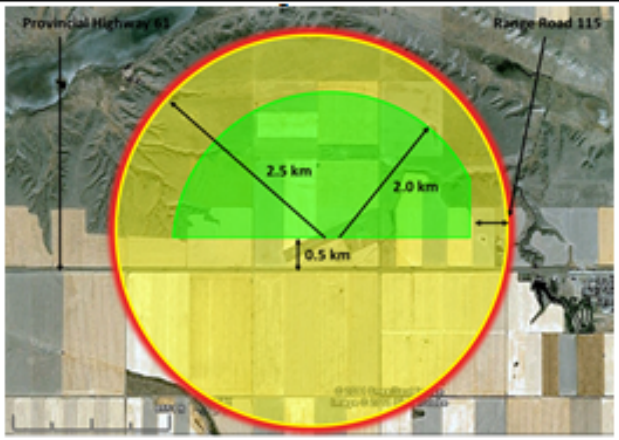

Go/No-Go Conditions	Satisfied?
Weather: Daylight VFR conditions	
No current precip with favorable forecast	
No lightinging within 10 miles	
Visibility: > 3 miles	
Ceiling: > 1700 ft (AGL)	
Wind: Calm, gusting < 10 kts	
Crosswing < 4 kts	
AFRL SUAS Test Ops ORM Assessment Complete	
If all satisfied, proceed to pre-flight checklist	

Medium Risk
TDAarons 7/6/2011

Medium Risk
TDAarons 7/6/11

Pre-Flight Checklist

Complete Pre-Flight Checklist as outlined in document. List any relevant notes below.

Notes

Test Point 1.0

Test Point 2.0

Appendix I. Certificate of Insurance

VirginiaTech

Risk Management
130 Southgate Center (0310)
Blacksburg, Virginia 24061
540/231-7439 Fax: 540/231-5064
www.co.vt.edu/risk

1 of 3 pages

May 5, 2011

Department of the Air Force
Air Force Research Laboratory
c/o Robert Canfield
Aerospace & Ocean Engineering
Virginia Tech

FAX: 1-9632

RE: General Liability Insurance Certificate

Dear Air Force Research Laboratory;

Enclosed is the general liability certificate of insurance requested. This certificate verifies Virginia Polytechnic Institute and State University's (a/k/a Virginia Tech) insurance coverage for the activities outlined on the enclosed certificate.

Once you have had an opportunity to review the enclosed certificate, should you have questions, do not hesitate to contact me.

Sincerely,

John H. Urquhart, ARM
Claims Manager

Enclosure

CERTIFICATE OF LIABILITY INSURANCE

DATE (MM/DD/YYYY): 05/05/2011

THIS CERTIFICATE IS ISSUED AS A MATTER OF INFORMATION ONLY AND CONFERS NO RIGHTS UPON THE CERTIFICATE HOLDER. THIS CERTIFICATE DOES NOT AFFIRMATIVELY OR NEGATIVELY AMEND, EXTEND OR ALTER THE COVERAGE AFFORDED BY THE POLICIES BELOW. THIS CERTIFICATE OF INSURANCE DOES NOT CONSTITUTE A CONTRACT BETWEEN THE ISSUING INSURER(S), AUTHORIZED REPRESENTATIVE OR PRODUCER, AND THE CERTIFICATE HOLDER.

IMPORTANT: If the certificate holder is an ADDITIONAL INSURED, the policy(ies) must be endorsed. If SUBROGATION IS WAIVED, subject to the terms and conditions of the policy, certain policies may require an endorsement. A statement on this certificate does not confer rights to the certificate holder in lieu of such endorsement(s).

PRODUCER
Risk Management Plan of the Commonwealth of Virginia - Self Insured

CONTACT NAME: John Urquhart
PHONE (A/C, No, Ext): 540-231-7459 FAX (A/C, No): 540-231-5064
E-MAIL ADDRESS: johnu84@vt.edu

INSURER(S) AFFORDING COVERAGE	NAIC #
INSURER A: State Insurance Reserve Trust Fund created in	
INSURER B: Section 2.5-526.5 of the Code of Virginia	
INSURER C: State Property Risk Management Plan created in	
INSURER D: Section 2.1-526.3 of the Code of Virginia	
INSURER E:	
INSURER F:	

INSURED
Commonwealth of Virginia and all of its agencies,
including Virginia Tech,
Mail Code 0310
Blacksburg VA 24061

COVERAGES CERTIFICATE NUMBER: REVISION NUMBER:

THIS IS TO CERTIFY THAT THE POLICIES OF INSURANCE LISTED BELOW HAVE BEEN ISSUED TO THE INSURED NAMED ABOVE FOR THE POLICY PERIOD INDICATED. NOTWITHSTANDING ANY REQUIREMENT, TERM OR CONDITION OF ANY CONTRACT OR OTHER DOCUMENT WITH RESPECT TO WHICH THIS CERTIFICATE MAY BE ISSUED OR MAY PERTAIN, THE INSURANCE AFFORDED BY THE POLICIES DESCRIBED HEREIN IS SUBJECT TO ALL THE TERMS, EXCLUSIONS AND CONDITIONS OF SUCH POLICIES. LIMITS SHOWN MAY HAVE BEEN REDUCED BY PAID CLAIMS.

INSR LTR	TYPE OF INSURANCE	ADDL INSR	SUBR WVD	POLICY NUMBER	POLICY EFF (MM/DD/YYYY)	POLICY EXP (MM/DD/YYYY)	LIMITS	
A	GENERAL LIABILITY ☑ COMMERCIAL GENERAL LIABILITY ☐ CLAIMS-MADE ☑ OCCUR GEN'L AGGREGATE LIMIT APPLIES PER: ☐ POLICY ☐ PROJECT ☐ LOC	N		See Additional Remarks Sch.	07/01/2010	06/31/2012	EACH OCCURRENCE	$ 2,000,000
							DAMAGE TO RENTED PREMISES (Ea occurrence)	$
							MED EXP (Any one person)	$
							PERSONAL & ADV INJURY	$
							GENERAL AGGREGATE	$
							PRODUCTS - COMP/OP AGG	$
								$
A	AUTOMOBILE LIABILITY ☐ ANY AUTO ☐ ALL OWNED AUTOS ☐ SCHEDULED AUTOS ☐ HIRED AUTOS ☐ NON-OWNED AUTOS						COMBINED SINGLE LIMIT (Ea accident)	$
							BODILY INJURY (Per person)	$
							BODILY INJURY (Per accident)	$
							PROPERTY DAMAGE (Per accident)	$
								$
	☐ UMBRELLA LIAB ☐ OCCUR ☐ EXCESS LIAB ☐ CLAIMS-MADE ☐ DED ☐ RETENTION $						EACH OCCURRENCE	$
							AGGREGATE	$
								$
A	WORKERS COMPENSATION AND EMPLOYERS' LIABILITY Y / N ANY PROPRIETOR/PARTNER/EXECUTIVE OFFICER/MEMBER EXCLUDED? ☐ (Mandatory in NH) If yes, describe under DESCRIPTION OF OPERATIONS below	N/A					WC STATU-TORY LIMITS ☐ OTH-ER	
							E.L. EACH ACCIDENT	$
							E.L. DISEASE - EA EMPLOYEE	$
							E.L. DISEASE - POLICY LIMIT	$
C								

DESCRIPTION OF OPERATIONS / LOCATIONS / VEHICLES (Attach ACORD 101, Additional Remarks Schedule, if more space is required)

Activities of Virginia Tech employees and volunteers, while acting within the scope of their duties and responsibilities as representatives of Virginia Tech while participating in Virginia Tech Aerospace and Ocean Engineering Department Flight Test Program for an Un-manned Aircraft activities to be held at Foremost Air Base in Alberta, Calgary, Canada and the Portuguese Air Force facilities located in Sintra and Ota, Portugal during the period beginning July 1, 2010 and ending on August 31, 2012.

CERTIFICATE HOLDER

Department of the Air Force
Air Force Research Laboratory
Aerospace & Ocean Engineering Department
Virginia Tech

CANCELLATION

SHOULD ANY OF THE ABOVE DESCRIBED POLICIES BE CANCELLED BEFORE THE EXPIRATION DATE THEREOF, NOTICE WILL BE DELIVERED IN ACCORDANCE WITH THE POLICY PROVISIONS.

AUTHORIZED REPRESENTATIVE
John H Urquhart

AGENCY CUSTOMER ID: _____

LOC #: _____

ACORD

ADDITIONAL REMARKS SCHEDULE

AGENCY	NAMED INSURED
Risk Management Plan of the Commonwealth of Virginia - Self Insured	Commonwealth of Virginia and all of its agencies, including Virginia Tech Mail Code 0310 Blacksburg, VA 24061
POLICY NUMBER	
CARRIER / NAIC CODE	EFFECTIVE DATE: 07/01/2010

ADDITIONAL REMARKS

THIS ADDITIONAL REMARKS FORM IS A SCHEDULE TO ACORD FORM,

FORM NUMBER: 25 FORM TITLE: Certificate of Liability Insurance

The Commonwealth of Virginia and all of its Agencies and institutions are covered by a self insurance program as authorized by section 2.2-1832 to 2.2-1843, 8.01-581.1 to 8.01-581.20 and 8.01-195.1 to 8.01-195.9 of the Code of Virginia which is based upon a comprehensive general liability manuscript policy form. Claims against the Commonwealth (not employees) are subject to Virginia Tort Claims Act, Sections 8.01-195.1 through 8.01-195.9 of the Code of Virginia.

ACORD 101 (2008/01)

Appendix J. JetCat P200-SX Operational Protocol

The following is taken directly from the *JetCat Instruction Manual, V6.0J2 ECU*. The full document is available online at the JetCat USA website: http://www.jetcatusa.com/PDFFiles/Instruction%20manual%20V6.0J2.pdf.

Safety Precautions

If other persons or animals are present while operating the *JetCat ENGINE*, **ALWAYS ENFORCE THE PROPER MINIMUM SAFE DISTANCES FROM** THE TURBINE! The recommended minimum safe distances are:

In front of the turbine = 15 feet
On the side of the turbine = 25 feet
Behind the turbine = 15 feet

In case of a mishap, fire extinguishers should be on hand at all times. *JETCAT USA* recommends the CO/2 variety. Powdered extinguishers will contaminate the precision components, upsetting the integrity of the turbine.

To the avoid hearing damage, always use hearing protection when you are near a running turbine engine!

When the turbine is running, never place your hands closer than six inches into the area of the intake. **An extreme suction** - which can grasp a hand, fingers or other objects in a flash - prevails in this area. Be aware of this source of danger, always!

Prevent foreign materials from entering the intake or exhaust when working with the turbine. Before operation, make sure there are no lose parts or debris near the turbine. Objects being sucked in can cause severe damage.

Always exercise caution around the hot parts of the turbine, to avoid burns. The outer case at the turbine stage and nozzle reaches 450-500° (Celsius), while the exhaust gas may exceed 720 °C.

Assure that the fuel is mixed with approximately 5% synthetic oil. Use only synthetic turbine oils available at local airport fuel suppliers or from *JETCAT USA*. Synthetic turbine oils are dangerous and should only be handled per the manufactures MDS sheets

Never run the turbine in a closed room, or an area near any kind of flammable matter. Do not fly turbine-powered aircraft near flammable materials, nor in forested tracts or areas experiencing drought or dryness. Obey all forest fire regulations and warnings by refraining from operating the *JetCat ENGINE* in restricted fire zones. Never operate model turbine jet aircraft in or around residential or heavily populated areas.

Installation of unauthorized parts from another manufacturing source may also result in engine failure. Do not introduce engine or electronic components other than those delivered by *JETCAT USA*, unless you are willing to risk destroying your turbine! *JETCAT USA's* parts are designed and engineered specifically for the *JetCat P80/ P120/P160*. Accept no substitutes, unless you are prepared to sacrifice your aircraft.

Appendix K. Portuguese Air Force Academy Letter or Approval

Air Force Academy
Research Centre

Virginia Tech
Virgina, USA
Dr. Kolonay and Professor Kapania

Sintra, 27 January 2011

The Portuguese Air Force agrees to make available the flight test site at the Air Force Base in Ota, Portugal for the experimental flight tests of the Joined Wing Program.

The Scaled Joined Wing flight testing at Ota will be performed under the guidance of the PoAFA Research Centre Unmanned Aerial Systems team in accordance with the technical advice and scientific coordination of Professor Afzal Suleman at the University of Victoria and Professor Robert Canfield at Virginia Tech.

The Portuguese Air Force Point of Contact for all matters concerning the flight testing at Ota is Capt. Carlos Silva from the Air Force Academy Research Centre.

Sincerely,

The Director of the Air Force Academy Research Centre

António Pedro Fernandes Costa

António Pedro Fernandes Costa, PhD
Cor/Engaer 076442-G

Academia da Força Aérea, Granja do Marquês, 2710 000 Sintra tlf 219678951 fax 219678945

Appendix L. MicroPilot2128^{LRC}

The MicroPilot 2128^{LRC} dual modem system is a backup autopilot option for follow on SensorCraft RPV flight test efforts. Aircraft altitude, attitude, airspeed, groundspeed and servo commands (which can be correlated to estimate control surface deflections) are all recorded and transmitted to the ground station in real time during the flight. Note that the Geometrically Scaled RPV will be under ***manual control*** at all times, with a backup pilot in place for all tests in which the RPV will be moving. The MicroPilot 2128^{LRC} is used primarily as a data acquisition system and as a means of establishing reliable, redundant manual control of the RPV.

The MicroPilot 2128^{LRC} is MicroPilot's premium autopilot package providing redundant control through the use of two RF links (900 MHz and 2.4 GHz). Primary control of the RPV is provided through a JR 11X 2.4 GHz transmitter connected to the MicroPilot Ground Station. Control signals are then sent to the RPV via both the 900MHz and 2.4 GHz RF links providing redundant control. A backup transmitter, a JR 12X, provides an entirely independent backup system in the event of total link loss with the ground station. The JR 12X provides link to a separate remote control (RC) receiver on board of the RPV, and this backup link can be activated at any time during the flight by simply flipping a switch on the backup transmitter. The JR 12X signal is passed through a 1 W signal booster to boost the effective range. For a Frequency Usage Chart see Section 4.3.2.1. A schematic of the control system used for the Geometrically Scaled RPV is shown in Figure 50.

It is important to note that stability augmentation provided by the autopilot will be used to help with yaw stability issues and control surface coupling; however, the RPV will always be under manual control. The JWSC exhibits strong roll-yaw coupling and preliminary flight tests with reduced complexity models have shown that stability augmentation can greatly assist in removing pilot workload during the flight by improving undesired coupling and reducing pilot workload. Stability augmentation does not take any control authority away from the pilot, it simply uses the built in instrumentation in the autopilot to correct undesired control surface coupling. The stability augmentation provided by the autopilot can be switched off via a switch on the transmitter at any point during the flight.

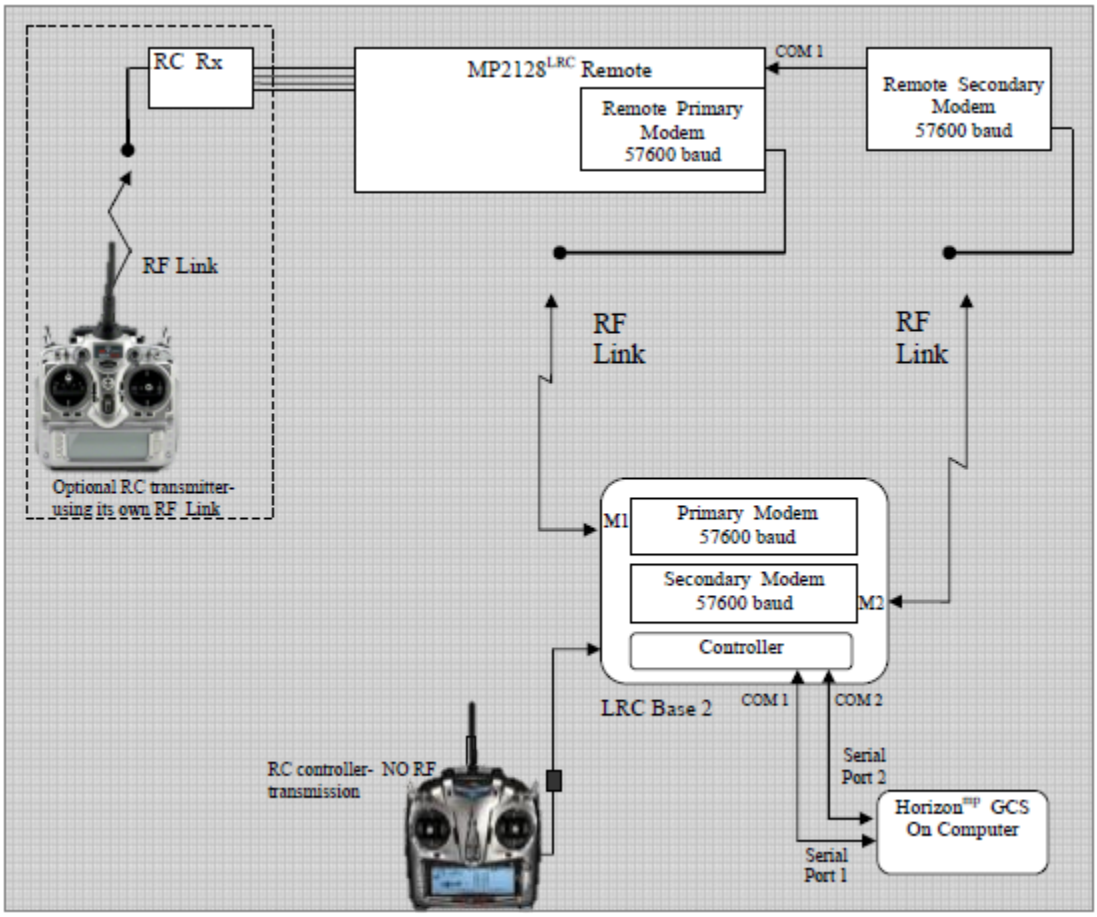

Figure 50 - MicroPilot 2128[LRC] System Concept[12]

Appendix M. Portuguese Air Force Academy Alternate Flying Site

This appendix contains details about the alternate flying site in Portugal.

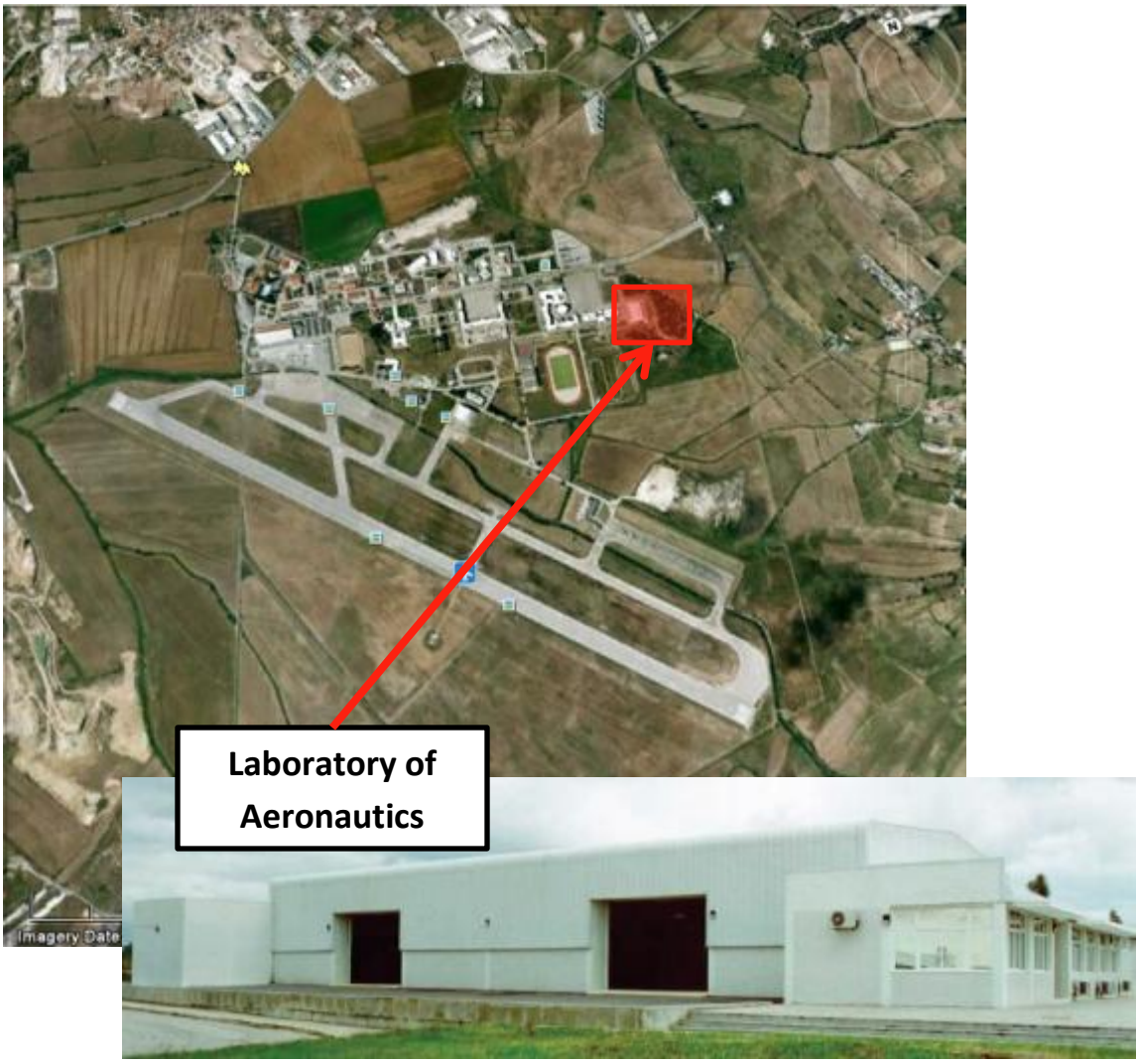

Figure 51 – Portuguese Air Force Academy, Sintra, Portugal

Table 21 - POAFA Location and Elevation

Coordinates	38° 49' N 9° 20' W
Elevation	440 ft

POAFA is an active base for the Portuguese Air Force (POAF) and home to the Portuguese Air Force Academy. The Laboratory of Aeronautics, highlighted above in

Figure 51 will be the location for the Bifilar Pendulum Test as well as all other integration, assembly and bench tests in Portugal.

6.11.2 Portuguese Air Force Military and Technical Center School (Ota, Portugal)

Figure 52 - CFMTFA, Ota, Portugal

Table 22 - CFMTFA Location and Elevation

Coordinates	39° 5' N
	8° 57' W
Elevation	140 ft

CFMTFA is a decommissioned base for the POAF, and it is currently used for all POAF UAV operations and testing. CFMTFA will be the location for all Phase 3 tests (Flight Tests). CFMTFA is a POAF sectured and certified test site and it features an on site weather station and an asphalt runway

surface (8202 ft x 147 ft). CFMTFA also features a small building near the flight line, and a tent is provided by the POAF for all UAV Flight operations.

UAV flight tests are allowed up to an altitude of 2000ft and within a 3nm radius from the runway. The airspace for CFMTFA UAV flight testing is shown below in Figure 53, with the racetrack flight pattern highlighted to show the relative amount of the airspace used.

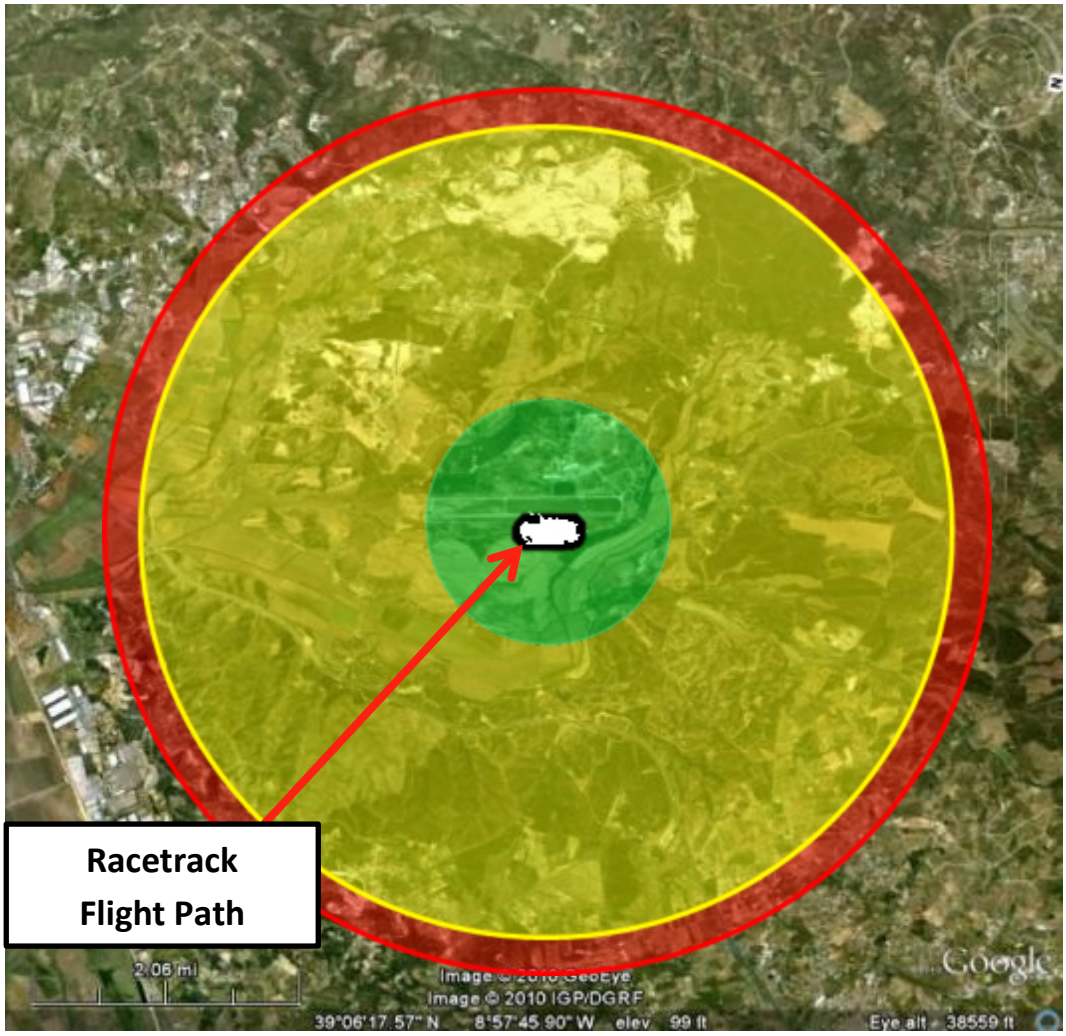

Figure 53 - 3nm radius airspace at CFMTFA

The airspace allotted for this test has been divided into three regions. The region shown in green corresponds to the "safe zone" where all flight operations are allowed to continue uninterrupted. The safe zone is 0.82 nautical miles in radius (5,000 ft). All planned flight tests will remain well within the safe zone (as shown by the racetrack flight path presented above); however, should unanticipated flight conditions and/or problems cause the aircraft to leave the safe zone, appropriate measures will be taken. Immediately Outside of this safe zone up to 1,500 ft from the border of the airspace is designated the "caution zone." This is shown above in yellow. If the aircraft enters the caution zone, the pilot will immediately turn the aircraft around and return into the safe zone. The last 1,500 ft in the

cleared airspace, shown above in red, is known as the “kill zone.” Should the aircraft enter the kill zone, the failsafe will be manually executed terminating the flight. This hierarchy is designed to prevent the aircraft from ever leaving the cleared airspace. Note that the safe, caution and kill zones will be programmed into the ground station computer and overlaid over the real-time vehicle position information.

Appendix N. Control Surface Derivatives

The following table shows the control surface derivatives (given per degree of deflection). The coordinate system corresponds to x-axis out the nose of the aircraft, y-axis out the right wing and z-axis downward. Positive deflection of the control surfaces is given with trailing edge down.

Reference Area/ Lengths:

Wing area = 1.390 m^2 Wingspan = 5 m c_bar = 0.576 m

Right Flap

AoA	CL	CY	CD	Cl	Cm	Cn
-2	0.00663	-0.001	0.00014	-0.0011	0.00187	0.00012
0	0.00655	-0.0009	0.00021	-0.0011	0.00185	9.3E-05
2	0.00646	-0.0009	0.00027	-0.0011	0.00182	6.6E-05
4	0.00635	-0.0008	0.00032	-0.0011	0.00179	3.9E-05
6	0.00622	-0.0008	0.00038	-0.0011	0.00175	1.3E-05
8	0.00608	-0.0007	0.00043	-0.001	0.00172	-2E-05
10	0.00592	-0.0006	0.00048	-0.001	0.00169	-2E-05

Left Flap

AoA	CL	CY	CD	Cl	Cm	Cn
-2	0.00663	0.00101	0.00014	0.00113	0.00187	-0.0001
0	0.00655	0.00094	0.00021	0.00111	0.00185	-9E-05
2	0.00646	0.00088	0.00027	0.0011	0.00182	-7E-05
4	0.00635	0.00082	0.00032	0.00107	0.00179	-4E-05
6	0.00622	0.00075	0.00038	0.00105	0.00175	-1E-05
8	0.00608	0.00069	0.00043	0.00103	0.00171	1.6E-05
10	0.00592	0.00062	0.00048	0.001	0.00169	1.8E-05

Right Inboard Aileron

AoA	CL	CY	CD	Cl	Cm	Cn
-2	0.00437	-0.0008	6.6E-05	-0.0012	-0.0029	0.00012
0	0.00432	-0.0007	0.00011	-0.0012	-0.0028	9.5E-05
2	0.00426	-0.0007	0.00015	-0.0012	-0.0028	6.7E-05
4	0.00419	-0.0006	0.00019	-0.0012	-0.0028	0.00004
6	0.00411	-0.0005	0.00022	-0.0012	-0.0027	1.3E-05
8	0.00402	-0.0005	0.00026	-0.0011	-0.0027	-1E-05
10	0.00392	-0.0004	0.00029	-0.0011	-0.0026	-4E-05

Left Inboard Aileron

AoA	CL	CY	CD	Cl	Cm	Cn
-2	0.00437	0.00079	6.6E-05	0.00124	-0.0029	-0.0001
0	0.00432	0.00073	0.00011	0.00122	-0.0028	-1E-04
2	0.00426	0.00066	0.00015	0.0012	-0.0028	-7E-05
4	0.00419	0.0006	0.00019	0.00118	-0.0028	-4E-05
6	0.00411	0.00054	0.00022	0.00115	-0.0027	-1E-05
8	0.00402	0.00047	0.00026	0.00113	-0.0027	1.3E-05
10	0.00392	0.00041	0.00029	0.0011	-0.0026	3.8E-05

Right Inner Outboard Aileron

AoA	CL	CY	CD	Cl	Cm	Cn
-2	0.0032	-0.0002	1.1E-05	-0.0011	-0.0042	4.1E-05
0	0.00317	-0.0002	4.2E-05	-0.0011	-0.0042	2.3E-05
2	0.00314	-0.0002	7.2E-05	-0.0011	-0.0042	7E-06
4	0.0031	-0.0002	0.0001	-0.0011	-0.0041	-1E-05
6	0.00305	-0.0002	0.00013	-0.0011	-0.0041	-3E-05
8	0.00299	-0.0001	0.00016	-0.001	-0.004	-4E-05
10	0.00293	-0.0001	0.00019	-0.001	-0.0039	-6E-05

Left Inner Outboard Aileron

AoA	CL	CY	CD	Cl	Cm	Cn
-2	0.0032	0.00025	1.1E-05	0.00112	-0.0042	-4E-05
0	0.00317	0.00023	4.2E-05	0.00111	-0.0042	-2E-05
2	0.00314	0.0002	7.2E-05	0.0011	-0.0042	-7E-06
4	0.0031	0.00018	0.0001	0.00108	-0.0041	0.00001
6	0.00305	0.00015	0.00013	0.00106	-0.0041	2.6E-05
8	0.00299	0.00013	0.00016	0.00104	-0.004	4.2E-05
10	0.00293	0.00011	0.00019	0.00102	-0.0039	5.7E-05

Right Outer Outboard Aileron

AoA	CL	CY	CD	Cl	Cm	Cn
-2	0.00211	-0.0002	-6E-05	-0.0009	-0.0035	2E-06
0	0.0021	-0.0001	-2E-05	-0.0009	-0.0034	-5E-06
2	0.00209	-0.0001	2.4E-05	-0.0009	-0.0034	-1E-05
4	0.00207	-0.0001	6.4E-05	-0.0008	-0.0034	-2E-05
6	0.00205	-0.0001	0.00011	-0.0008	-0.0034	-2E-05
8	0.00202	-0.0001	0.00014	-0.0008	-0.0033	-3E-05
10	0.00198	-9E-05	0.00018	-0.0008	-0.0033	-3E-05

Left Outer Outboard Aileron

AoA	CL	CY	CD	Cl	Cm	Cn
-2	0.00211	0.00016	-6E-05	0.00086	-0.0035	-2E-06
0	0.0021	0.00015	-2E-05	0.00086	-0.0034	5E-06
2	0.00209	0.00014	2.4E-05	0.00085	-0.0034	1.1E-05
4	0.00207	0.00013	6.4E-05	0.00084	-0.0034	1.6E-05
6	0.00205	0.00012	0.00011	0.00083	-0.0034	2.1E-05
8	0.00202	0.0001	0.00014	0.00082	-0.0033	2.6E-05
10	0.00198	9.4E-05	0.00018	0.00081	-0.0033	0.00003

Right Inboard Elevator						
AoA	CL	CY	CD	Cl	Cm	Cn
-2	0.00391	0.0004	-3E-05	-0.0002	-0.011	-0.0001
0	0.0039	0.00038	3.5E-05	-0.0002	-0.011	-0.0001
2	0.00387	0.00035	0.0001	-0.0002	-0.011	-0.0001
4	0.00384	0.00032	0.00017	-0.0002	-0.0109	-0.0001
6	0.00379	0.00029	0.00024	-0.0002	-0.0108	-0.0001
8	0.00374	0.00026	0.0003	-0.0002	-0.0107	-9E-05
10	0.00367	0.00023	0.00036	-0.0002	-0.0105	-8E-05

Left Inboard Elevator						
AoA	CL	CY	CD	Cl	Cm	Cn
-2	0.00391	-0.0004	-3E-05	0.00024	-0.011	0.00014
0	0.0039	-0.0004	3.5E-05	0.00024	-0.011	0.00013
2	0.00387	-0.0003	0.0001	0.00024	-0.011	0.00012
4	0.00384	-0.0003	0.00017	0.00024	-0.0109	0.00011
6	0.00379	-0.0003	0.00024	0.00024	-0.0108	0.0001
8	0.00374	-0.0003	0.0003	0.00024	-0.0107	9.2E-05
10	0.00367	-0.0002	0.00036	0.00024	-0.0105	8.2E-05

Right Middle Elevator						
AoA	CL	CY	CD	Cl	Cm	Cn
-2	0.00395	0.00048	3.7E-05	-0.0005	-0.0093	-0.0001
0	0.00392	0.00045	8.4E-05	-0.0005	-0.0092	-0.0001
2	0.00389	0.00042	0.00013	-0.0005	-0.0092	-0.0001
4	0.00384	0.00039	0.00018	-0.0005	-0.0091	-0.0001
6	0.00378	0.00036	0.00022	-0.0005	-0.009	-0.0001
8	0.00371	0.00033	0.00026	-0.0005	-0.0088	-0.0001
10	0.00363	0.0003	0.00031	-0.0005	-0.0087	-9E-05

Left Middle Elevator						
AoA	CL	CY	CD	Cl	Cm	Cn
-2	0.00395	-0.0005	3.7E-05	0.00054	-0.0093	0.00013
0	0.00392	-0.0005	8.4E-05	0.00053	-0.0092	0.00013
2	0.00389	-0.0004	0.00013	0.00053	-0.0092	0.00012
4	0.00384	-0.0004	0.00018	0.00053	-0.0091	0.00011
6	0.00378	-0.0004	0.00022	0.00052	-0.009	0.00011
8	0.00371	-0.0003	0.00026	0.00052	-0.0088	0.0001
10	0.00363	-0.0003	0.00031	0.00051	-0.0087	9.3E-05

Right Outboard Elevator						
AoA	CL	CY	CD	Cl	Cm	Cn
-2	0.00384	0.0005	7.8E-05	-0.0008	-0.007	-9E-05
0	0.00381	0.00047	0.00013	-0.0008	-0.0069	-9E-05
2	0.00377	0.00045	0.00017	-0.0008	-0.0069	-9E-05
4	0.00371	0.00043	0.00022	-0.0008	-0.0068	-9E-05
6	0.00365	0.0004	0.00026	-0.0008	-0.0067	-9E-05
8	0.00357	0.00038	0.0003	-0.0008	-0.0066	-9E-05
10	0.00349	0.00035	0.00035	-0.0008	-0.0065	-9E-05

Left Outboard Elevator						
AoA	CL	CY	CD	Cl	Cm	Cn
-2	0.00384	-0.0005	7.8E-05	0.00081	-0.007	9.4E-05
0	0.00381	-0.0005	0.00013	0.00081	-0.0069	9.4E-05
2	0.00377	-0.0005	0.00017	0.0008	-0.0069	9.4E-05
4	0.00371	-0.0004	0.00022	0.00079	-0.0068	9.4E-05
6	0.00365	-0.0004	0.00026	0.00078	-0.0067	9.4E-05
8	0.00357	-0.0004	0.0003	0.00077	-0.0066	9.4E-05
10	0.00349	-0.0003	0.00035	0.00075	-0.0065	9.4E-05

Appendix O. Special Flight Operations Certificate

Transport Canada
Civil Aviation
Prairie and Northern Region

Transports Canada
Aviation Civile
Région des Prairies et du Nord

344 Edmonton Street
Winnipeg, MB
R3C 0P6

June 16, 2011

5812-11-0811
RDIMS: 6717804

University of Victoria - UVic
Department of Mechanical Engineering
PO Box 3055, Stn CSC
Victoria, BC
V8W 3P6

Dear: Mr. Richards:

Pursuant to section 603.67 of the *Canadian Aviation Regulations*, this constitutes your **Special Flight Operations Certificate (SFOC)** for the operation of the **5m Joined Wing Unmanned Aerial System (UAS) and RC model aircraft** as described in your SFOC applications dated **May 10, 2011** for the purpose of training and testing. Issued under the authority of the Minister pursuant to the ***Aeronautics Act***, this document certifies that the Certificate holder is adequately equipped and able to conduct a safe operation, subject to the observance and performance by the Certificate holder of the conditions set out in this Certificate, or any part thereof:

1. This Certificate:

   a) is issued to **Jenner Richards on behalf of the University of Victoria (UVic)**

   b) may be suspended or cancelled at any time by the Minister for cause, including failure on the part of the Certificate holder, its servants or agents to comply with the provisions of the ***Aeronautics Act*** and the *Canadian Aviation Regulations* (CARs);

   c) is not transferable and is valid **July 17, 2011 to August 18 , 2011** or until it is suspended or cancelled;

   d) is valid for the operation of the **5m Joined Wing UAS** within **2.5 kilometers** of the Foremost, Alberta Airport (N49 28' 59" W111 29' 40"): Normal flight operations shall remain .5 KM north of provincial highway 61 (unless blocked to public traffic) and west of Range Road 115 , as described in the SFOC application dated May 10, 2011 and associated documents.

2. Nothing in this Certificate shall be held to relieve the Certificate holder from the requirement to comply with the provisions of such Canadian Aviation Documents as may have been issued to him pursuant to the *Aeronautics Act* or the *Canadian Aviation Regulations* (CARs).

I

3. This Certificate is issued for the operation of the **5m Joined Wing UAS** without a transponder, aircraft markings, aircraft registration or a flight authority.

4. The Certificate holder shall maintain an adequate management organization that is capable of exercising supervision and operational control over persons participating in the UAS operations. The Trained UAS pilot/operator will be responsible for flight and operational decisions.

5. The management organization, the facilities, the normal operations plan, the emergency operating procedures, the operating limitations, the flying areas to be used, the Security and Emergency contingency plans for the **5m Joined Wing UAS,** shall be in accordance with data provided in the SFOC application dated **May 10, 2011** or as otherwise agreed upon between UVic and Transport Canada.

6. The Certificate holder shall conduct the operation of the **5m Joined Wing UAS** in a safe manner.

7. Only one (1) **UAS** shall be operated in-flight, by an operator at any one time.

8. All **5m Joined Wing UAS** operations shall be limited to a maximum altitude of 700 feet above ground level(AGL).

9. All **5m Joined Wing UAS** operations shall be during day light hours.

9. The **5m Joined Wing UAS** operations shall give way to manned aircraft.

10. The **5m Joined Wing UAS** shall be operated or supervised by personnel who are fully trained in all aspects of its flight planning, operation and recovery.

11. Throughout the flight operation, the Certificate holder shall ensure that the **5m Joined Wing UAS** are flown over areas that would permit a safe landing on the surface without hazard to persons or property in the event of any emergency or system failure requiring or resulting in an immediate descent.

12. For any **5m Joined Wing UAS** operated under the authority of this SFOC, **UVic** shall have subscribed for liability insurance covering risks of public liability in the amount described in subsection 606.02(8) of the *Canadian Aviation Regulations*.

13. The **5m Joined Wing UAS** shall only be operated when weather conditions in the area of operation are such that the minimum cloud ceiling shall be at least 1000 feet above the planned flight altitude and visibility shall exceed 3 SM. The UAS must remain within the Pilot's visual line of sight and clear of cloud during flight operations.

14. The Certificate holder is responsible for ensuring that property owners, over which flights of the **5m Joined Wing UAS** will take place; have been advised of the proposed operation and have no objections.

15. The Certificate holder shall locate an observer in the area. This observer must advise the **5m Joined Wing UAS** operator if; there appears to be a conflict with aircraft, or it appears that the **5m Joined Wing UAS** is violating any conditions of this SFOC.

16. For all operations the certificate holder shall ensure that the **5m Joined Wing UAS** is operated at a distance of not less than 500 feet away from members of the public, inhabited structures such as buildings and vehicles without the owner's consent.

17. Flight over spectators is prohibited.

18. Due to the operations of the **5m Joined Wing UAS** being at an uncontrolled airport the following conditions apply:

    a) Nav Canada, Edmonton FIC they shall be contacted at 866-514-4102 and notified prior to and after each flight, unless they advise otherwise. All instructions from the FIC shall be complied with.
    b) Monitor the Foremost UNICOM VHF frequency on 123.2 commencing 15 minutes prior to and during all flights.
    c) Make an Advisory call to "All Traffic in the Foremost Area" prior to all flights warning aircraft of the location, altitude and duration of the proposed flight.
    d) Cellular phone or radio contact must be available with the nearest Air Traffic Control Agency during all UAS operation.
    e) The aerodrome operator must be notified of all intended UAS operation and have no objections.

19. Certificate holder shall report to Transport Canada, General Aviation on the first working day following any of the following occurrences, with details of any of the occurrences:

    a) The **5m Joined Wing UAS** fly's outside of planned bounds of operation; or
    b) Any person being injured as a result of the operation; or
    c) Any unintended contact between the **5m Joined Wing UAS** and person(s), livestock, vehicle(s) or structure(s).

20. The Certificate holder shall not operate the, UAV following any of the occurrences listed in condition 19 (a) (b) and (c), until Transport Canada, General Aviation, approves its further operation in writing.

21. All persons involved with these operations (flight crew, ground station crew, and spotters) shall be familiar with the contents of this SFOC, and the contents of the application dated **May 10, 2011.**

22. A copy of this SFOC and a copy of the application dated **May 10, 2011**, shall be on site any time the **5m Joined Wing UAS** is in operation.

23. Transport Canada shall be notified 2 business days in advance of any operation of the **5m Joined Wing UAS.**

24. The Certificate holder shall:

a) Document their flight planning and procedures for each location and flight.
b) Document a post flight report on performance and any deviations from the plan.

Documentation shall be kept and made available for inspection for 1 calendar year following the date of the flight.

25. The certificate holder shall; Prior to the commencement of the **5m Joined Wing UAS** flights ground test and establish that the " Aircraft Breaks Geo Fence" Autopilot Aerodynamic termination and Loss of All Communications Safety protocols are functioning.

Yours truly,

Doug Tomalin
Acting Superintendent Safety Oversight - Certification
General Aviation
Prairie and Northern Region
For Minister of Transport

Appendix P. Mishap Investigation Letter

Canadian Centre for Unmanned Vehicle Systems
Centre Canadien des Systèmes de Véhicules Télépilotés
Facilitating sustained, profitable growth in the Canadian unmanned systems sector

4, 49 Viscount Avenue, Medicine Hat, Alberta, T1A 5G4, Canada
t: +1 403 488 7208; e: ccuvsoffice@ccuvs.com: w: www.ccuvs.com

27 June 2011

MISHAP INVESTIGATION

The Geometrically Scaled RPV flight testing will be conducted in Foremost, Alberta under the guidance and scientific coordination of Professor Afzal Suleman of the University of Victoria and Professors Robert Canfield and Craig Woolsey at Virginia Tech. The flight operations are scheduled from 17 July, 2011 – 18 August, 2011

For the purposes of the flight test of the Geometrically Scaled RPV, a *MISHAP* will be defined as:

> ***Mishap:*** *An event that results in damage to the aircraft (outside of normal wear and tear from operations), injury to personnel, damage to private property and/or damage to airfield property at the flight location in Foremost.*

In the event of a mishap, the CCUVS will assist the University of Victoria by conducting a formal mishap investigation.

Sterling Cripps
Chief Operating Officer
CCUVS

Flight Test Plan References

[1]Blair, M., Canfield, R. A., and Roberts Jr., W., "Joined-Wing Aeroelastic Design with Geometric Nonlinearity," Journal of Aircraft, Vol.42, No.4, 2005, pp. 832-848.

[2]Bond, V., "Flexible Twist for Pitch Control in a High Altitude Long Endurance Aircraft with Nonlinear Response," Ph.D. Dissertation Prospectus, Department of the Air Force, Air Force Institute of Technology, Wright-Patterson AFB, Dayton, OH, 2007.

[3] The Boeing Company. "Selected Results from Test of Model on Sting", Presentation Excerpts, NASA Langley, Hampton VA, slides 2-5.

[4] Lucia, David J., "The SensorCraft Configurations: A Non-Linear AeroServoElastic Challenge for Aviation," AIAA Paper 2005-1943, 2005.

[5]Roberts, R. W., Jr., Canfield, R. A., and Blair, M., "Sensor-Craft Structural Optimization and Analytical Certification," AIAA Paper 2003-1458, April 2003.

[6]Richards, J., Suleman, A., Aarons, T. and Canfield, R.A., "Multidisciplinary Design for Flight Test of a Scaled Joined Wing SensorCraft," AIAA Paper 2010-9351, Sep. 2010.

[7]Richards, J., Aarons, T., Suleman, A., Canfield, R.A., Woolsey, C., Lindsley, N. and Blair, M., "Design for Flight Test of a Scaled Joined Wing SensorCraft," AIAA Paper 2011-2011, Apr. 2011.

[8]Piccolo II Manual.

[9]http://www.jetcatusa.com/p200.html

[10]Roskar, Jan. *Airplane Design: Part II: Preliminary Configuration Design and Integration of the Propulsion System*. Lawrence, KS: DAR Corporation, 2004. Print.

[11]Roskar, Jan. *Airplane Design: Part IV: Layout of the Landing Gear and Systems*. Lawrence, KS: DAR Corporation, 2004. Print.

[12]MicroPilot2128^{LRC} Manual

[13]CAD work completed by Jenner Richards of Quaternion Engineering/ University of Victoria

B. Military Flight Release

Air Force Research Laboratory

MILITARY FLIGHT RELEASE No. MFR-0711-002

1. Program Name: Joined Wing SensorCraft (JWSC)	5. Aircraft Type/Serial/Tail Number: Geometrically Scaled, Joined Wing Sensorcraft (16.4 foot span)
2. Program Office Symbol: AFRL/RBSD	
3. Issue Date: 29 July 2011	
4. Expiration: 18 Aug 2011	

6. Terms and Conditions: as specified in Transport Canada issued Special Flight Operations Certificate (SFOC) # 5812-11-0811, dated 16 Jun 2011.

Specific limitations: as specified in Transport Canada issued SFOC # 5812-11-0811, dated 16 Jun 2011.

7. Supporting Documentation:	Date:
JWSC Test Plan (version 10)	06 Jul 2011
AFRL Technical Review Board (TRB) Minutes	24 Mar 2011
AFRL Safety review Board (SRB) Minutes	06 Jul 2011
Memo for Record; Airworthiness Statement, University of Victoria, BC Canada	27 Jul 2011
AFRL Form 19a	05 Jul 2011
AFRL Form 19b	08 Jul 2011

8. Signature (Name/Title)

Kenneth Barker, PhD, AFRL Designated Technical Authority

References

[1]Kimberlin, Ralph D. Flight Testing of Fixed-Wing Aircraft. American Institute of Aeronautics and Astronautics, Inc., Reston, VA, 2003.

[2]Gallagher, Gerald L., Higgins, Larry B., Khinoo, Leroy A. and Peter W. Pierce. Fixed Wing Performance. U.S. Navy Test Pilot School Flight Test Manual. USNTPS-FM-NO.108. 30 Sept 1992.

[3]Fixed Wing Stability and Control: Theory and Flight Test Techniques. U.S. Navy Test Pilot School Flight Test Manual. Naval Air Warfare Center, Aircraft Division. Patuxent River, MD. USNTPS-FM-NO.103. Jan 1997.

[4]Lucia, David J., "The SensorCraft Configurations: A Non-Linear AeroServoElastic Challenge for Aviation," AIAA Paper 2005-1943, 2005.

[5]Richards, J., Aarons, T., Suleman, A., Canfield, R.A., Woolsey, C., Lindsley, N. and Blair, M., "Design for Flight Test of a Scaled Joined Wing SensorCraft," AIAA Paper 2011-2011, Apr. 2011.

[6]Martinez, Juan R., Flick, Peter, Perdzock, John, Dale, Gary and Myron B. Davis. "An Overview of SensorCraft Capabilities and Key Enabling Technologies," AIAA Paper 2008-7185, 2008.

[7]Blair, M. and Canfield, R. A. "A Joined-Wing Structural Weight Modeling Study," AIAA Paper 2002-1337, April 2002.

[8]Roberts, R. W., Jr., Canfield, R. A., and Blair, M., "Sensor-Craft Structural Optimization and Analytical Certification," AIAA Paper 2005-2015, April 2005.

[9]Blair, M., Canfield, R. A., and Roberts Jr., W., "Joined-Wing Aeroelastic Design with Geometric Nonlinearity," Journal of Aircraft, Vol.42, No.4, 2005, pp. 832-848.

[10]Wolkovitch, J., "The Joined Wing: An Overview," *Journal of Aircraft*, Vol. 23, No. 3, 1986, pp. 161-178

[11]Bond, V., "Flexible Twist for Pitch Control in a High Altitude Long Endurance Aircraft with Nonlinear Response," Ph.D. Dissertation Prospectus, Department of the Air Force, Air Force Institute of Technology, Wright-Patterson AFB, Dayton, OH, 2007.

[12]The Boeing Company. "Selected Results from Test of Model on Sting", Presentation Excerpts, NASA Langley, Hampton VA, slides 2-5, 2010.

[13]Richards, J., Suleman, A., Canfield, R., and Blair, M., "Design of a Scaled RPV for Investigation of Gust Response of Joined-Wing SensorCraft," AIAA Paper 2009-2218, May 2009.

[14]Richards, J., Suleman, A., Aarons, T. and Canfield, R.A., "Multidisciplinary Design for Flight Test of a Scaled Joined Wing SensorCraft," AIAA Paper 2010-9351, Sep. 2010.

[15]Garnand-Royo, Jeffrey, "Strain Gage Instrumentation Design for a Scaled Joined Wing SensorCraft," Undergraduate Research Final Report. Virginia Polytechnic Institute and State University, Aerospace and Ocean Engineering Department, Blacksburg, VA. May 2011.

[16]"Introduction to Strain & Strain Measurement," Technical Reference 8600-699-A02G000. Acromag Incorporated, Wixom, MI, 2001.
<http://www.acromag.com/sites/default/files/White%20Paper%20Introduction%20to%20Strain%20699A.pdf>

[17] "INA125: Instrumentation Amplifier with Precision Voltage Reference". Texas Instruments Online Data Sheet. Dallas, Texas, 2009. <http://www.ti.com/lit/ds/symlink/ina125.pdf>.

[18]Ziemer, J.K., Cubbin, E.A., Choueiri, E.Y., Oraevsky, V. and Dokukin, V., "Pulsed Plasma Propulsion for a Small Satellite: Mission COMPASS P^3OINT," AIAA Paper 1996-3292, July 1996.

[19]Jardin, Matt R., and Mueller, Eric R., "Optimized Measurements of UAV Mass Moment of Inertia with a Bifilar Pendulum," AIAA Paper 2007-6822, Aug. 2007.

[20] "AFRL Flight Test and Evaluation." AFRL MAN 99-103. 21 May 2007.

[21] "Unmanned Aerieal Vehicle – UAV." Transport Canada. 13 April 2011.
<http://www.tc.gc.ca/eng/civilaviation/standards/general-recavi-uav-2265.htm>.

[22] "0.7m Subsonic Open Jet Wind Tunnel." Virginia Polytechnic Institute and State University, Aerospace and Ocean Engineering Department, Blacksburg, VA, 2011.
<http://www.aoe.vt.edu/research/facilities/openjet.html>.

[23]Parrish, Grant. "Design, Fabrication, and Calibration of a Cost Effective Miniature Air Data Unit." Master's Non-Thesis Option Final Report. Virginia Polytechnic Institute and State University, Aerospace and Ocean Engineering Department, Blacksburg, VA. 11 May 2011.

[24]"Digital Protractor Series 950 –Pro 360, Pro 3600: Product Overview." Mitutoyo U.S.A. 2011.
<http://www.mitutoyo.com/TerminalMerchandisingGroup.aspx?group=1438>.

[25]Canadian Centre for Unmanned Vehicle Systems Website. <http://www.ccuvs.com/index.php>.

[26]Gallman, J. W., and Kroo, I. M., "Structural Optimization for Joined-Wing Synthesis," Journal of Aircraft, Vol. 33, No. 1, 1996, pp. 214–223.

[27]Livne, E., "Aeroelasticity of Joined-Wing Airplane Configurations: Past Work and Future Challenges—A Survey," AIAA Paper 2001-1370, April 2001

[28]Blair, Maxwell, Robinson, Jason, McClelland, William A., and Bowman, Jason C. "A Joined-Wing Flight Experiment." AFRL Design and Analysis Methods Branch, Structures Division. AFRL-RB-WP-TR-2008-3101. Februaru 2008.

[29]McClelland, William A., "Inertia Measurement and Dynamic Stability Analysis of a Radio-Controlled Joined-Wing Aircraft," MS Thesis, Department of Aeronautical Engineering, Graduate School of Engineering and Management, Air Force Institute of Technology, Wright-Patterson AFB, Dayton, OH, March 2006.

[30]Pereira, P., Almeida, L., Suleman, A., Bond, V., Canfield, R. A., and Blair, Maxwell, "Aeroelastic Scaling and Optimization of a Joined-Wing Aircraft Concept," AIAA Paper 2007-1889, April 2007.

[31]Blair, Maxwell; Garmann, Daniel, Canfield, Robert A.; Bond, Vanessa; Pereira, Pedro; and Suleman, Afzal, "Non-Linear Aeroelastic Scaling of a Joined- Wing Concept," AIAA Paper 2007-1887, April 2007.